Influence of Atlantic Meridional Overturning Circulation changes on deglacial deep-water ecosystems off NW-Africa

DISSERTATION submitted in fulfillment of the requirements for the Doctoral degree in Natural Sciences (Dr. rer. nat.) at the Department of Geosciences (FB5) at the University of Bremen

presented by Sofía Barragán-Montilla

Bremen, April 2024

marum
Center for Marine Environmental Sciences
University of Bremen

University of Bremen

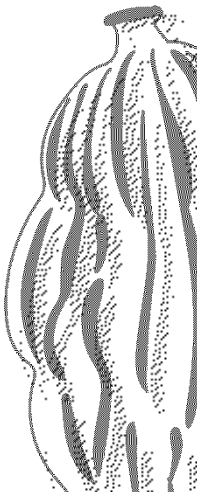

Tout ce qui, dans la nature, n'est pas appréciable à la vue simple, non seulement reste inconnu de la masse des populations, mais encore échappe, des siècles entiers, à l'observation des hommes spéciaux qui cherchent à dévoiler les beautés de la création. Combien de myriades d'êtres nous restent encore à connaître! Combien d'années s'écouleront encore avant que nous ayons acquis une juste idée de l'ensemble de la zoologie!

Alcide d'Orbigny, 1839

Reviewers:

Prof. Dr. Heiko Pälike
MARUM - Center for Marine Environmental Sciences,
University of Bremen, Germany

Prof. Dr. Gerhard Schmiedl
Fachbereich Erdsystemwissenschaften
Universität Hamburg

Date of Colloquium: June 13th, 2024

PhD. Thesis Committee and Supervisors:

Prof. Dr. Heiko Pälike
MARUM - Center for Marine Environmental Sciences,
University of Bremen, Germany

Dr. Stefan Mulitza
MARUM - Center for Marine Environmental Sciences,
University of Bremen, Germany

Dr. Heather J. Johnstone
MARUM - Center for Marine Environmental Sciences,
University of Bremen, Germany

Dr. Tilmann Schwenk
University of Bremen, Faculty of Geosciences,
University of Bremen, Germany

Dr. Enno Schefuß
MARUM - Center for Marine Environmental Sciences,
University of Bremen, Germany

Affirmation in lieu of an oath

according to § 5 (5) of the Doctoral Degree Rules and Regulations of 28 April 2021

I, Sofía Barragán Montilla,

With my signature I affirm in lieu of an oath that I prepared the submitted dissertation independently and without illicit assistance from third parties, that I appropriately referenced any text or content from other sources, that I used only literature and resources listed in the dissertation, and that the electronic (PDF) and printed versions of the dissertation are identical.

I affirm in lieu of an oath that the information provided herein to the best of my knowledge is true and complete.

I am aware that a false affidavit is a criminal offence which is punishable by law in accordance with § 156 of the German Criminal Code (StGB) with up to three years imprisonment or a fine in case of intention, or in accordance with § 161 (1) of the German Criminal Code with up to one year imprisonment or a fine in case of negligence.

Bremen, April 29th 2024
_____
Place, Date

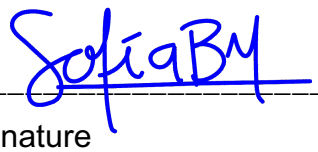
_____
Signature

Note from the author

The present manuscript summarizes the findings of the author's doctoral research taken place from January 2021 to April 2024. The initial project "*Methane seepage activity of NW Africa during the last deglaciation and its relation with global climate change; paleoenvironmental multiproxy analysis using foraminifera*" was planned to investigate methane seepage activity off NW Africa during the last 30,000 years, with special focus on bottom water temperature changes as a potential driver. The doctoral research was projected to use cores from the Mauritanian shelf initially planned to be retrieved on October 2021, however due to the COVID pandemic the expedition was postponed and later cancelled.

The first phase of this research focused on analyzing the benthic foraminifera taxonomy and distribution, in addition to the trace element concentrations and stable isotope measurements on benthic foraminifera species from core GeoB9512-5. This site is located near the area of the original proposed study, and at a similar depth where methane seepage is known to occur off NW Africa, and the anlyses was started before the cancellation of the research cruise. The unavailability of the samples from the original target seep site, led to the joint decision (of the doctoral candidate and supervisors) to take the project in a slightly different direction, aiming to increase the coverage of temperature reconstructions based on benthic foraminifera Mg/Ca measurements. To this end, records from GeoB9506-1, GeoB9508-5 and GeoB9512-5 provide information of the temperature profile in the eastern North Atlantic off NW Africa during times of major climatic shifts in the last 30,000 years. In addition, the use of duplicate species for benthic Mg/Ca in this investigation, confirms that there are other potential environmental controls on benthic foraminifera Magnesium uptake besides temperature, making a critical evaluation for past and future paleotemperature records ever more necessary.

In addition to the normal challenges usually faced in any research, the global pandemic changed the course of this and many other research projects in the last years, deeply affecting early career researchers. However, it also offered an opportunity to take new approaches, for instance using the unexploited potential of

existing material that still holds very valuable information (for example in the GeoB Core repository) key for climate change studies. In this regard, the oxygen reconstructions presented here were unanticipated in the original proposal but have provided important records and contributed significatively to the outcomes of this doctoral dissertation. The author hopes the forced change of this research focus still contributes to MARUM's objectives as the initial proposed was meant to do.

Outline and research questions

This manuscript contains the results of the doctoral thesis “Atlantic Meridional Overturning Circulation slowdown effects on deglacial tropical eastern Atlantic paleoceanography recorded by benthic foraminifera”. The **foreword** is a summary about benthic foraminifera, and why and how they are used in paleoceanographic studies. This short article was published in Nature Reviews Earth and Environment as joint effort between the GeoLatinas organization and Nature Reviews Earth and Environment to publish multilingual peer-reviewed content increasing science accessibility for Spanish-speaking individuals. The **introduction** presents a summary of the modern oceanographic configuration of the tropical eastern Atlantic area studied here. A condensed **methodology** section summarizes the analyzed material, including the preparation and extraction of microfossil content, as well as the taxonomical and geochemical analyses carried out.

The **first chapter** *(in preparation for submission)* gives an overview of the benthic foraminifera taxonomy study of the eastern Atlantic, to show ***how benthic foraminifera are distributed in the NE Atlantic and what are the main environmental parameters influencing their diversity.*** This chapter summarizes previous benthic foraminifera studies in the area and contrasts the available information with the benthic foraminifera extracted from surface sediment analyzed for this research.

On **chapter two** (in review at *Nature Communications*), we explore research question 2: ***what are the effects of AMOC slowdown in the Eastern tropical North Atlantic Oxygen Minimum Zone (ETNA - OMZ)?*** From detailed taxonomical and quantitative analyses of GeoB9512-5 (793 m water depth, 15.33°N, 17.36°W) benthic foraminifera, we found that in times of deglacial AMOC decline ETNA-OMZ became better ventilated and oxygenated due to an intensification of the subtropical cell.

This bottom water oxygen decline during AMOC slowdown influenced benthic foraminifera Mg/Ca, therefore introducing additional uncertainties in paleotemperature reconstructions. This led to the research question 3: ***does oxygen availability affect***

Mg uptake in Melonis barleeanus? and if so, ***can this effect be removed from our temperature calculations?*** In **chapter three** *(in preparation for submission)*, I present a revised temperature calibration for *M. barleeanus* Mg/Ca and provide evidence of potential oxygen effects on this species Mg/Ca ratios. Applying the new calibration to reconstruct the deglacial paleotemperature changes of site GeoB9512-5, an earlier LGM warming is observed, incompatible with the *Uvigerina* paleotemperature record of the same site. This suggests additional controls to the Mg/Ca signal of *M. barleeanus* (like microhabitat changes) and prevents a composite paleotemperature record in our site, exploring vital effects in benthic foraminifera Mg/Ca paleothermometry.

Chapter four was published in *Paleoceanography and Paleoclimatology and* contains the results of benthic foraminifera Magnesium/Calcium (Mg/Ca) ratios from site GeoB9508-5 (2,384 m water depth, 15.49°N, 17.94°W). In this chapter, we explore research question 4: ***how the Atlantic Meridional Overturning Circulation (AMOC) changes in the last 30,000 years influenced deep ocean heat uptake in the eastern North Atlantic?*** Based on these new records, we provide evidence of heat uptake stagnation in the deep eastern North Atlantic in times of AMOC slowdown.

Finally, in **chapter five** *(in preparation for submission)*, I present an integrated analysis of the paleotemperature records based on *Uvigerina* Mg/Ca of sites GeoB9506-1, GeoB9508-5 and GeoB9512-5 also concerning research question 4 considering the upper Atlantic. Our data shows that during the last deglaciation, heat storage shifted from a shallow mode during the Last Glacial Maximum to a deep mode in the Holocene. These findings are in line with the results from chapter two and contribute valuable information to the understanding of AMOC slowdown effects on ocean heat uptake and storage and oxygen changes in the eastern part of the Atlantic.

Own Contributions to manuscripts

The research questions and methodologies were formulated by the doctoral candidate and author of this thesis Sofía Barragán-Monitlla (SBM) with significant contributions from advisors Dr Stefan Mulitza (SM), Dr Heather Johnstone (HJ) and Prof. Dr Heiko Pälike (HP). The foreword was entirely written and submitted by SBM.

The processed samples form surface sediments used in chapter 1 and chapter 4 were selected by SBM in close consultation with SM. The washing and sediment analyses, including microfossil extraction and taxonomy was made by SBM. The results from chapter one was summarized and interpreted by SBM.

The records from gravity core GeoB9508-5 (chapter two) were obtained by SM and HJ, and the data analyses, interpretation, and discussion of the results, including the age model was made by SBM in close consultation with SM, HJ and HP.

The results from chapter three and four came from core GeoB9512-5, sampled, washed, and analyzed entirely by SBM including the microfossil extraction and taxonomy. HJ contributed significatively in the element to calcium ratios laboratory cleaning protocols, measurements, and interpretation. Analysis and interpretation of this chapter was made by SBM with key contributions from the SM, HJ, HP. and collaborator Dharma Reyes Macaya from the Lyell Centre (Heriot-Watt University).

Chapter five analyses and results were carried out by SBM with significant contributions from HJ in the element to calcium ratios laboratory and data interpretation, while the analysis and interpretation were closely supported by SM and HP.

Core samples, including samples from gravity cores and surface samples mentioned here were kindly provided by the GeoB Core repository at MARUM. Surface samples from retrieved by the RV Tyro used in Chapter one and four, were provided by Dr. Enno Schefuß. Stable isotope analyses presented here were made at MARUM-Center for Marine Environmental Sciences of the University of Bremen. Radiocarbon

ages from site GeoB9512-5 and GeoB9506 were measured at the MICADAS - Mini Carbon Dating System of the Alfred Wegener Institute in Bremerhaven.

Graphic designs, including figures here and graphic abstracts were made by SBM. All data produced and/or used during this study is published or in the review process at the PANGAEA database. Code availability for chapter 3 analysis was documented in the Github Repository https://github.com/SophieBM93/Tropical-eastern-Atlantic-Benthic-Foraminifera-analyses

Data produced during this research

Barragán-Montilla, Sofía; Johnstone, Heather J H; Mulitza, Stefan; Pälike, Heiko (2023a): Bottom water temperatures (raw and processed including confidence intervals) calculated using Mg/Ca ratios of endobenthic Uvigerina spp. from the last 50.000 years from site GeoB9508-5 off NW Africa. PANGAEA, https://doi.org/10.1594/PANGAEA.950494

Barragán-Montilla, Sofía; Johnstone, Heather J H; Mulitza, Stefan; Pälike, Heiko (2023b): Processed stable isotope (carbon and oxygen) data from epibenthic Cibicidoides spp., including confidence intervals from the last 50.000 years from site GeoB9508-5 off NW Africa. PANGAEA, https://doi.org/10.1594/PANGAEA.950502

Barragán-Montilla, Sofía; Mulitza, Stefan (in review a): Radiocarbon ages of sediment core GeoB9506-1. PANGAEA, https://doi./10.1594/PANGAEA.962888

Barragán-Montilla, Sofía; Mulitza, Stefan (in review b): Radiocarbon ages of sediment core GeoB GeoB9512-5 -1. PANGAEA, https://doi.org/10.1594/PANGAEA.962899

Barragán-Montilla, Sofía (in review a): Benthic Foraminifera counts off NW Africa during the last deglaciation. PANGAEA, https://doi.org/10.1594/PANGAEA.962951

Barragán-Montilla, Sofía (in review b): Benthic foraminifera stable isotopes (d18O and d13C) of sediment core GeoB9512-5. PANGAEA, https://doi.org/10.1594/PANGAEA.962968

Barragán-Montilla, Sofía (in review c): δ18O and δ13C stable isotopes of benthic foraminifera Melonis barleeanus from sediment core GeoB9506-1. PANGAEA, https://doi.org/10.1594/PANGAEA.962975

Barragán-Montilla, Sofía (in review d): δ18O and δ13C stable isotopes of benthic foraminifera Cibicidoides wuellerstorfi from sediment core GeoB9506-1. PANGAEA, https://doi.org/10.1594/PANGAEA.962981

Barragán-Montilla, Sofía (in review e): δ18O and δ13C stable isotopes of benthic foraminifera Uvigerina peregrina from sediment core GeoB9506-1. PANGAEA, https://doi.org/10.1594/PANGAEA.962982

Barragán-Montilla, Sofía; Johnstone, Heather J H (in review a): Benthic foraminifera minor element to calcium ratios for core-tops from the eastern Tropical Atlantic. PANGAEA, https://doi.pangaea.de/10.1594/PANGAEA.964299

Barragán-Montilla, Sofía; Johnstone, Heather J H (in review b): Benthic Foraminifera trace elements to calcium ratios and bottom water temperatures from the last 27,000 years of sediment core GeoB9512-5. PANGAEA, https://doi.pangaea.de/10.1594/PANGAEA.964318

Barragán-Montilla, Sofía; Johnstone, Heather J H (in review c): Benthic foraminifera element to calcium ratios and bottom water temperatures of sediment core GeoB9506-1. PANGAEA, https://doi.pangaea.de/10.1594/PANGAEA.964374

Contents

Affirmation in lieu of an oath 4

Note from the author 5

Outline and research questions 7

Own Contributions to manuscripts 9

Contents 12

List of Figures 1

List of Tables 3

Foreword: Filling the deep-ocean data gap with benthic foraminifera 1

Abstract 4

Zusammenfassung 6

Resumen 8

Introduction 10

Methods 15

Chapter 1: North Atlantic Recent Benthic Foraminifera distribution patterns and environmental controls: a review 21

Chapter 2: Enhanced ventilation of Eastern North Atlantic Oxygen Minimum Zone with deglacial slowdown of Meridional Overturning 35

Chapter 3: New insights on infaunal foraminifera paleothermometry: environmental effects on *Melonis barleeanus* Mg/Ca from the tropical eastern Atlantic 52

Chapter 4: Stagnant North Atlantic Deep Water heat uptake with reduced Atlantic Meridional Overturning Circulation during the last deglaciation 84

Supplementary Information for Chapter 4 102

Chapter 5: Eastern Tropical North Atlantic shallow mode heat storage in the Last Glacial Maximum shifted to deep mode in the Holocene 108

Final conclusions and Outlook 128

Acknowledgements 134

References 136

Appendix 1 – Congress Abstracts 194

Appendix 1.1 – Recent Benthic from surface samples of the eastern tropical Atlantic 211

Appendix 2.1 – Benthic Foraminifera interpretation Chapter 2 223

Appendix 2.2 – GeoB9512-5 Benthic foraminifera digital microscope images 233

Appendix 3.1 – Supplementary Information Chapter 3 239

Appendix 6 – Eastern tropical North Atlantic Benthic Foraminifera response to paleoceanographic changes during the last deglaciation 242

Supplementary Information 6.1 – Benthic Foraminifera Digital Microscope Images from site GeoB9506-1 271

Additional Supplementary Information 277

List of Figures

Figure I1. *Geographic Location of the studied surface sediments and gravity cores GeoB9512-5, GeoB9508-5, and GeoB9506-1.* 11

Figure M1. Uncalibrated Fe/Ca records from Gravity Cores GeoB9512-5, GeoB9508-5, and GeoB9506-1. 18

Figure 1.1 *Compilation of eastern Atlantic recent Foraminifera data published in PANGAEA (https://www.pangaea.de/).* 23
Figure 1.2 Idealized microhabitats of common eastern North Atlantic benthic foraminifera species 26
Figure 1.3 Core location and water masses at the eastern North Atlantic off NW Africa 28
Figure 1.4 Digital microscope images from the most representative benthic foraminifera in the Eastern Atlantic 30
Figure 1.5 Eastern North Atlantic recent benthic foraminifera diversity, group distribution and environmental parameters. 31
Figure1.6 Non-metrical multidimensional scaling of the most abundant benthic foraminifera of the Eastern North Atlantic. 32

Figure 2.1 GeoB9512-5 location in the Eastern Tropical Atlantic Oxygen Minimum Zone. 38
Figure 2.2 GeoB9512-5 deglacial paleo-oxygenation record and Atlantic circulation proxies. 42
Figure 2.3 GeoB9512-5 benthic foraminifera distribution and diversity, paleo-oxygenation record and Atlantic circulation proxies. 44
Figure 2.4 GeoB9512-5 age model with the key climatic events in the last 27,000 years. 46
Figure 2.5 Central and Intermediate water masses in the studied site GeoB9512-5 47
Figure 2.6 GeoB9512-5 downcore relative abundances of the most relevant benthic foraminifera species and other paleoenvironmental indicators 49

Figure 3.1 Core tops and GeoB9512-5 (15°20'13.20''N/17°22'1.20''W, 793 m water depth) location 58
Figure 3.2 Principal Component Analyses (PCA) of *M. barleeanus* trace elements and modern bottom water conditions of the tropical eastern Atlantic (this study). 66
Figure 3.3 Location of the *Melonis barleeanus* sites from the eastern North Atlantic used for the revised calibration. 67
Figure 3.4 ΔBWT using *Melonis barleeanus* Mg/Ca – temperature calibrations from previous and the present studies in 55 coretops from the tropical eastern Atlantic. . 68
Figure 3.5 *Uvigerina mediterranea* and *Melonis barleeanus* Mg/Ca ratios and Bottom Water Temperatures from site GeoB9512-5 during the last 27 kyrs. 70
Figure 3.6 Interspecific Bottom Water Temperature offset (ΔBWToffset) in this study. ΔBWT_{offset} between different *Melonis barleeanus* calibrations and *Uvigerina mediterranea* BWTs from site GeoB9512-5 73
Figure 3.7 Deglacial Bottom Water Temperatures from site GeoB9512-5. Bottom Water Temperatures (BWTs) calculated with 73
Figure 3.8 *Uvigerina mediterranea* and *Melonis barleeanus* Mg/Ca and Mn/Ca ratios and deglacial Bottom Water Temperatures from site GeoB9512-5. 76
Figure 3.9 GeoB9512-5 benthic foraminifera infaunal content (from Barragán-Montilla et al., in review), and $\delta^{13}C$, $\delta^{18}O$, Mg/Ca, Mn/Ca and bottom water temperatures (this study). 80

Figure 4.1 *GeoB9508-5 Location* 88
Figure 4.2 *GeoB9508-5 Age Model showing key climatic events of the last 50 kyrs*. 89
Figure 4.3 Benthic foraminifera proxies from core GeoB9508-5 showing the deglacial evolution of the eastern North Atlantic in the last 45 kyrs. 92
Figure 4.4 *Bottom water temperatures and trace element concentrations measured in Uvigerina spp. from Core GeoB9508-5* 95
Figure 4.5 $^{231}Pa/^{230}Th$ records from the North Atlantic, Global CO_2 fluctuations, Global Mean Surface Temperature (GMST) and benthic foraminifera proxies from core GeoB9508-5 (this study) spanning the last 25 kyrs. 97

Figure 5.1 Oceanographic and geographical situation of sites GeoB9512-5, GeoB9506-1 and GeoB9508-5. 112

Figure 5.2 Age model from site GeoB9506-1 113
Figure 5.3 Downcore $\delta^{18}O_{sw}$, Mg/Ca, and paleotemperature and salinity calculations for sites GeoB9512-5, GeoB9506-1 and GeoB9508-5 118
Figure 5.4 T-S diagram showing the average BWTs and salinities for each climatic period in the studied cores. 123
Figure 5.5 Western Atlantic $^{231}Pa/^{230}Th$ and benthic Foraminifer paleotemperature and $\delta^{13}C$ from sites GeoB9512-5, GeoB9506-1 and GeoB9508-5 125

Figure C.1 Distribution of core top samples in relation to water depth in the eastern tropical Atlantic. Modified from Chapter 1. Groups correspond to samples with similar benthic foraminifera assemblages as described in Chapter 1 – Section 3. 128
Figure C.2 Graphic Abstract summarizing the findings of Chapter 2. 129
Figure C.3 Graphic Abstract summarizing the findings of Chapter 3. 130
Figure C.4 Global AMOC proxy and benthic foraminifera paleotemperature and $\delta^{13}C$ from sites GeoB9512-5, GeoB9506-1 and GeoB9508-5 modified from Chapter 5. 132

List of Tables

Table M1 Stable isotopes sample data used produced during this research 16
Table M2 Element-calcium ratios data produced during this research 16
Table M3 Planktic foraminifera for AMS radiocarbon dating and benthic foraminifera for taxonomy and paleoenvironmental interpretation 16

Table 1.1 Average relative abundances (Avg.) of the most abundant benthic foraminifera species off NW Africa. 29

Table 3.1 Pearson correlation coefficients (r) for element to calcium ratios against bottom water parameters, n=22. 65

Foreword: Filling the deep-ocean data gap with benthic foraminifera

Published in Nature Reviews Earth and Environment, formatted to fit the manuscript style
https://doi.org/10.1038/s43017-022-00332-6

S. Barragán-Montilla[1]

[1] MARUM – Center for Marine Environmental Sciences and Department of Geosciences, University of Bremen, Bremen, Germany

Oceans trap around 90% of the excess heat and sequester ~30% of the CO_2 released by anthropogenic activity. However, insufficient information on historic deep-water temperature still limits the understanding of ocean–climate interactions. To understand previous ocean conditions and improve future predictions, benthic foraminifera (BF) are used to reconstruct past changes in bottom waters.

BF are unicellular marine microorganisms that live on the seafloor and produce a hard shell (test) in chemical equilibrium with the surrounding water. The distribution of BF is controlled by changes in deep-ocean parameters, which can be tracked using diversity patterns, species distribution and the chemical compositions of BF tests. To track these changes, seafloor sediments that contain BF microfossils are washed, dried, sieved, and analyzed under a microscope in the lab to observe the microfossils content. For each sample, around 300 BF are taxonomically classified, and some tests are separated to measure $\delta^{18}O$ and/or $\delta^{13}C$ stable isotopes and elements concentrations (such as Al, Ca, Mg, Mn, and Sr). Changes in BF distribution usually indicate fluctuations in bottom water oxygenation and organic matter content, while bottom water can be reconstructed from $\delta^{13}C$. BF geochemistry can also be used to estimate bottom water salinity (based on a combination of $\delta^{18}O$ with Mg/Ca) and paleotemperatures (based on Mg/Ca ratios).

Multiproxy studies that integrate BF taxonomical and quantitative analyses with geochemical proxies enable deeper understanding of paleoceanographic changes. This multiproxy approach sheds light on how changes in Atlantic circulation have affected the capacity of this ocean to store excess heat, or the impact of primary productivity changes on ocean CO_2 sequestration. BF research will improve the

understanding of how ocean processes can influence global temperatures and add context for changes predicted for the future.

Spanish official translation: *Descubriendo las profundidades del océano con foraminíferos bentónicos*

Los océanos capturan alrededor del 90% del exceso de calor de nuestro planeta, y secuestran ~30% del CO_2 liberado por actividad antropogénica. Sin embargo, la falta de información histórica acerca de las temperaturas del fondo oceánico sigue limitando nuestro entendimiento sobre las interacciones entre el océano y el clima. Para entender los cambios del océano en el pasado y mejorar las predicciones del futuro, se usan los foraminíferos bentónicos (FB) para reconstruir las condiciones del fondo oceánico en el pasado geológico.

Los FB son organismos marinos unicelulares que habitan en el suelo oceánico y producen una concha (caparazón) en equilibrio químico con el agua donde viven. Su distribución, depende de los cambios en los parámetros ambientales del fondo oceánico, los cuales se pueden analizar mediante patrones de diversidad de los FB, distribución de las especies y composición química de los caparazones. Con este fin, se lavan, tamizan y analizan muestras de sedimento del suelo oceánico con alto contenido microfósil. El análisis se realiza usando un microscopio para extraer y clasificar taxonómicamente alrededor de 300 FB por muestra. Adicionalmente, algunos caparazones se separan para medir isótopos estables (como el $\delta^{18}O$ y $\delta^{13}C$) y concentraciones de elementos químicos (como Al, Ca, Mg, Mn, y Sr). Los cambios en la distribución de FB responden principalmente a variaciones en la oxigenación y concentración de materia orgánica en las aguas de fondo, mientras que parámetros como la ventilación pueden reconstruirse analizando el $\delta^{13}C$. Además, mediante la geoquímica de FB, se pueden estimar otros parámetros del fondo oceánico como la salinidad (combinando $\delta^{18}O$ con Mg/Ca) y las paleo-temperaturas (con base en los radios Mg/Ca).

Los estudios multiproxy que integran análisis taxonómicos y cuantitativos de FB con proxies geoquímicas, permiten entender en detalle cambios paleoceanográficos. Este planteamiento multiproxy ayuda a explicar cómo los cambios en la circulación del

Atlántico afectaron su capacidad de absorber el exceso de calor de la tierra, o cuál es el impacto de las variaciones en la productividad primaria en la extracción de CO_2. La investigación de FB mejorará el entendimiento de cómo los procesos oceánicos influyen en las temperaturas globales y aportan un contexto clave para las predicciones del futuro de nuestro planeta.

Abstract

The Atlantic Ocean is an important component of the global climate system. In this ocean basin, the Atlantic Meridional Overturning Circulation (AMOC), partially driven by the formation of North Atlantic Deep Water (NADW) in the northern hemisphere, uptakes an important percentage of the anthropogenically induced excess heat of our planet and distributes it around the globe through a complex ocean circulation system that influences global warming rate (e.g. Cummins et al., 2016; Levitus et al., 2000). As described in Chapter 2 and Chapter 4, the instrumental record of AMOC strength provides evidence of a potential decrease or weakening also known as "AMOC slowdown" in the 19th and 20th centuries, synchronous with the increasing trend of CO_2 in the atmosphere, as well as greenhouse gases concentrations (Caesar et al., 2021; Dima et al., 2021; IPCC, 2022; Rahmstorf et al., 2015). Furthermore, AMOC will very likely decrease in the 21st century (IPCC, 2023). However, the instrumental AMOC record is still too short to fully understand the effects of such slowdown in the climate system, therefore our knowledge must rely on paleoceanographic proxies. Although controversial, AMOC slowdown has been recorded by different proxies in the last 30,000 years, offering the opportunity to observe the effects of this slowdown in the deep ocean through the marine fossil record. This is discussed in detail in the Introduction of Chapter 4.

The last deglaciation period in the Eastern North Atlantic (NE Atlantic) starts after the end of the Last Glacial Maximum (LGM, ~ 19 kyrs BP). Temporary returns to cold periods occurred during the Heinrich Stadial 1 (HS1, ~18.3 – 15.4 Kyr BP) and Younger Dryas (YD, ~12.9 – 11.7 Kyr BP), and between these two cold periods, the Bølling–Allerød warming (B-A) was a transient warming time in the northern hemisphere. The record of AMOC, includes kinematic proxies like $^{231}Pa/^{230Th}$ (Böhm et al., 2015; Gherardi et al., 2005; McManus et al., 2004), paleo-circulation proxies like the radiogenic neodymium (Nd) isotope composition (Böhm et al., 2015; Du et al., 2020; Roberts et al., 2010) and bottom water ventilation proxies like the benthic foraminifera $\delta^{13}C$ (e.g., Oppo et al., 2015), that show a consistent AMOC decline during the HS1 and YD, alternated by a short B-A resumption period.

In this research, deglacial sedimentary records of gravity cores GeoB9512-5 (15.34 °N, 17.37 °W, 793 m water depth), GeoB9508-5 (15.50 °N, 17.95 °W, 2,384 m WD) and GeoB9506-1 (15.61 °N, 18.35 °W, 2,956 m WD) were analyzed to extract and investigate the benthic foraminifera content, and reconstruct the bottom water changes in the NE Atlantic during the last 27,000 years. Three components of bottom waters were investigated; (1) bottom water oxygenation reconstructed from the detailed taxonomic and quantitative analyses of benthic foraminifera (GeoB9512-5 and GeoB9506-1); (2) bottom water temperatures (BWTs) reconstructed from benthic foraminifera Magnesium-Calcium (Mg/Ca) ratios (GeoB9512-5, GeoB9508-5 and GeoB9506-1); and (3) changes in ventilation and salinity inferred from benthic foraminifera $\delta^{13}C$ and $\delta^{18}O$ respectively (GeoB9512-5, GeoB9508-5 and GeoB9506-1). The key outcomes of this research are: (1) deep-ocean heat uptake stagnation in times of reduced AMOC in the NE Atlantic, suggesting AMOC strength sets the oceanic heat storage depth; (2) a better ventilated and oxygenated deglacial Eastern Tropical North Atlantic Oxygen Minimum Zone, related to an intensified subtropical cell due to AMOC slowdown; than in turn (3) affected calcification processes of some benthic foraminifera at intermediate depths introducing uncertainties on Mg/Ca-based paleotemperature reconstructions at intermediate depths in the eastern North Atlantic. Finally, the integrated paleotemperature records show that during the LGM and most of the last deglacial period, heat storage took place in the intermediate waters in the tropical eastern Atlantic, and shift to a deep mode in the Holocene as AMOC strength is restored.

Zusammenfassung

Der Atlantische Ozean ist ein wichtiger Bestandteil des globalen Klimasystems. In diesem Ozeanbecken nimmt die Atlantische Meridionale Umwälzbewegung (AMOC), die teilweise durch die Bildung des Nordatlantischen Tiefenwassers (NADW) in der nördlichen Hemisphäre angetrieben wird, einen bedeutenden Prozentsatz der anthropogen verursachten überschüssigen Wärme unseres Planeten auf und verteilt sie über ein komplexes Ozeanzirkulationssystem, das die globale Erwärmungsrate beeinflusst, rund um den Globus (z. B. Cummins et al., 2016; Levitus et al., 2000). Wie in Kapitel 2 und Kapitel 4 beschrieben, liefert die instrumentelle Aufzeichnung der AMOC-Intensität Beweise für eine mögliche Abnahme oder Abschwächung, auch bekannt als "AMOC-Verlangsamung" im 19. und 20. Jahrhundert, synchron mit der Steigerung von CO_2 in der Atmosphäre sowie den Konzentrationen von Treibhausgas (Caesar et al., 2021; Dima et al., 2021; IPCC, 2022; Rahmstorf et al., 2015). Tatsächlich wird die AMOC im 21. Jahrhundert sehr wahrscheinlich abnehmen (IPCC, 2023). Der Zeitraum der instrumentellen AMOC-Aufzeichnung ist jedoch noch zu kurz, um die Auswirkungen einer solchen Verlangsamung im Klimasystem vollständig zu verstehen. Die Verlangsamung der AMOC ist zwar umstritten, wurde aber in den letzten 30 000 Jahren durch verschiedene proxies aufgezeichnet und bietet die Möglichkeit, die Auswirkungen dieser Verlangsamung in der Tiefsee anhand der aufgezeichneten Daten von Meeresfossilien zu beobachten. Dies wird in der Einleitung von Kapitel 4 ausführlich erörtert.

Die letzte Deglazialperiode im Nordostatlantik (NE-Atlantik) beginnt nach dem Ende des letzten glazialen Maximums (LGM, ~ 19 kyrs BP). Während des Heinrich Stadial 1 (HS1, ~18,3 - 15,4 Kyr BP) und der Jüngeren Dryas (YD, ~12,9 - 11,7 Kyr BP) kam es zu einer vorübergehenden Umkehr zu kalten Perioden, und zwischen diesen beiden kalten Perioden war die Bølling-Allerød-Erwärmung (B-A) eine vorübergehende Erwärmung der nördlichen Hemisphäre. Die Aufzeichnung der AMOC umfasst kinematische Proxies wie 231Pa/230Th (Böhm et al., 2015; Gherardi et al., 2005; McManus et al., 2004), Paläo-Zirkulationsproxies wie die radiogene Neodym (Nd)-Isotopenzusammensetzung (Böhm et al., 2015; Du et al, 2020; Roberts et al., 2010) und Bodenwasser-Ventilations proxies wie die benthischen Foraminiferen δ13C (z. B.

Oppo et al., 2015), die einen konsistenten AMOC-Rückgang während der HS1 und YD zeigen, der von einer kurzen B-A-Wiederaufnahmeperiode abglöst wird.

In dieser Forschung, wurden deglaziale Sedimentproben von Schwereloten GeoB9512-5 (15,34 °N, 17,37 °W, 793 m Wassertiefe), GeoB9508-5 (15,50 °N, 17,95 °W, 2.384 m WD) und GeoB9506-1 (15. 61 °N, 18,35 °W, 2.956 m WD) analysiert, um den Gehalt an benthischen Foraminiferen zu extrahieren und zu untersuchen und damit die Veränderungen des Bodenwassers im Nordostatlantik während der letzten 27.000 Jahre zu rekonstruieren.

Drei Komponenten des Bodenwassers wurden untersucht: (1) Sauerstoffgehalt des Bodenwassers, rekonstruiert aus den detaillierten taxonomischen und quantitativen Analysen benthischer Foraminiferen (GeoB9512-5 und GeoB9506-1); (2) Bodenwassertemperaturen, die aus dem Magnesium-Calcium-Verhältnis (Mg/Ca) benthischer Foraminiferen rekonstruiert wurden (GeoB9512-5, GeoB9508-5 und GeoB9506-1); und (3) Veränderungen der Ventilation des Bodenwassers und des Salzgehalts, die aus $\delta^{13}C$ bzw. $\delta^{18}O$ benthischer Foraminiferen abgeleitet wurden (GeoB9512-5, GeoB9508-5 und GeoB9506-1). Die wichtigsten Ergebnisse dieser Forschung sind: (1) Stagnation der Wärmeabsorption in der Tiefsee in Zeiten reduzierter AMOC im Nordostatlantik, was darauf hindeutet, dass die Stärke der AMOC die ozeanische Wärmeinhaltstiefe bestimmt; (2) eine besser belüftete und mit Sauerstoff angereicherte deglaziale Sauerstoffminimumzone im östlichen tropischen Nordatlantik, die mit einer verstärkten subtropischen Zelle aufgrund der AMOC-Verlangsamung zusammenhängt; und (3) beeinträchtigte Kalzifizierungsprozesse einiger benthischer Foraminiferen in mittleren Tiefen, was zu Unsicherheiten bei Mg/Ca-basierten Paläo-Temperaturrekonstruktionen in mittleren Tiefen im östlichen Nordatlantik führt. Schließlich zeigen die integrierten Paläotemperaturaufzeichnungen, dass während des LGM und des größten Teils der letzten Deglazialperiode die Wärmespeicherung in den mittleren Gewässern des tropischen Ostatlantiks stattfand und sich im Holozän mit der Wiederherstellung der AMOC-Intensität in eine größere Tiefe verlagerte.

Resumen

El Océano Atlántico es un componente importante del clima global. En esta cuenca oceánica, la Circulación de Retorno Longitudinal (por sus siglas en inglés *AMOC* de *Atlantic Meridional Overturning Circulation*), influenciada en gran parte por la formación de las aguas profundas del Atlántico norte (por sus siglas en inglés *NADW* de *North Atlantic Deep Water*) en el hemisferio norte, absorbe un porcentaje importante del exceso de calor de nuestro planeta (en parte inducido por el forzamiento antropogénico) y lo distribuye globalmente a través de un sistema de circulación complejo que influencia a su vez las tasas de calentamiento global. (e.g. Cummins et al., 2016; Levitus et al., 2000). Como se describe en los capítulos 2 y 4, el registro instrumental de la fuerza de la AMOC muestra evidencias de un debilitamiento conocido como "desaceleración de la AMOC" durante los siglos 19 y 20, que coinciden temporalmente con el aumento de CO_2 atmosférico y de las concentraciones de gases de efecto invernadero (Caesar et al., 2021; Dima et al., 2021; IPCC, 2022; Rahmstorf et al., 2015). De hecho, una potencial desaceleración de la AMOC es muy probable en el siglo 21 (IPCC, 2023). Sin embargo, el registro moderno de la AMOC es todavía muy corto para entender por completo los efectos de dicha desaceleración en el sistema climático, por lo que nuestro conocimiento depende en gran parte del estudio del registro fósil, particularmente de los últimos 30,000 años cuando una desaceleración de la AMOC ha sido registrada por diferentes *proxies*. Esto de discute en mayor detalle en la introducción del Capítulo 4.

La última deglaciación en el Atlántico Norte Oriental comenzó con la culminación del Último Máximo Glacial (por sus siglas en inglés *LGM,* de *Last Glacial Maximum*, hace aproximadamente 19,000 años). Retornos temporales a periodos fríos ocurrieron durante el evento Heinrich 1 (por sus siglas en inglés *HS1*, de *Heinrich Stadial 1*, hace ~18,300 – 15,400 años) y el Dryas Reciente (por sus siglas en inglés *YD,* de *Younger Dryas*, hace ~12,900 – 11,700 años), interrumpidos por el calentamiento del Bølling–Allerød (por sus siglas en inglés *B-A*) en el hemisferio norte. En el pasado geológico, la fuerza de la AMOC se mide con *proxies* cinemáticas como los radios $^{231}Pa/^{230}Th$ (Böhm et al., 2015; Gherardi et al., 2005; McManus et al., 2004), *proxies* de paleo-circulación como la composición isotópica del Neodimio radiogénico (ξNd) (Böhm et

al., 2015; Du et al., 2020; Roberts et al., 2010), y *proxies* de ventilación de las aguas de fondo como los radios isotópicos de carbono ($\delta^{13}C$) en foraminíferos (e.g., Oppo et al., 2015). Todas estas *proxies* coinciden con una disminución de la AMOC durante el HS1 and YD, interrumpidos por un corto periodo de aceleración durante el B-A.

En esta investigación, se analizaron los registros sedimentarios de la última deglaciación, provenientes de los núcleos de gravedad GeoB9512-5 (15,34 °N, 17,37 °W, 793 m de profundidad), GeoB9508-5 (15,50 °N, 17,95 °W, 2384 m de profundidad) y GeoB9506-1 (15,61 °N, 18,35 °W, 2.956 m de profundidad), para extraer e investigar el contenido y geoquímica de foraminíferos bentónicos con el fin de reconstruir los cambios en las aguas de fondo del Atlántico nororiental durante los últimos 27,000 años. Se investigaron tres aspectos (1) la paleo-oxigenación reconstruida usando análisis taxonómicos y cuantitativos detallados (GeoB9512-5 y GeoB9506-1); (2) las paleo-temperaturas reconstruidas a partir de los radios magnesio-calcio (Mg/Ca) de las conchas (GeoB9512-5, GeoB9508-5 y GeoB9506-1); y (3) los cambios en la ventilación y la salinidad inferidos de los radios isotópicos de carbono ($\delta^{13}C$) y oxígeno ($\delta^{18}O$) de estos microfósiles (GeoB9512-5, GeoB9508-5 y GeoB9506-1). Los resultados más importantes de esta investigación incluyen: (1) un estancamiento de la absorción de calor del océano profundo durante los periodos de desaceleración AMOC en el Atlántico nororiental, lo que sugiere que la fuerza de AMOC determina la profundidad de almacenamiento de calor; (2) aumento en la ventilación y oxigenación en la Zona Mínima de Oxígeno del Atlántico Norte Tropical Oriental durante la última deglaciación, debido a una intensificación de la célula subtropical relacionada a la desaceleración de AMOC; que a su vez (3) afectó los procesos de calcificación de algunos foraminíferos bentónicos a profundidades intermedias, introduciendo incertidumbres en las reconstrucciones de paleo-temperatura basadas en Mg/Ca. Finalmente, los registros integrados de paleo-temperatura muestran que, durante el LGM y la mayor parte de la última deglaciación, el almacenamiento de calor tuvo lugar principalmente en las aguas intermedias del Atlántico oriental tropical, migrando a mayores profundidades durante el Holoceno a medida que se restablecía la fuerza de la AMOC.

Introduction

Modern Oceanography – Hydrography of the studied area

Upwelling and Subtropical Circulation in the Eastern North Atlantic

The Canary and Benguela upwelling systems are one of the four eastern boundary upwelling systems that currently sustain major fisheries in the tropical eastern Atlantic. The Canary Current Upwelling System extends between 43°N and 8°N, and from 10°N and 36°N with seasonal variations. Its features are controlled by wind forcing and the shape of the coastline (Cropper et al., 2014). Along the coast off NW Africa, wind blowing moves surface waters offshore and subsurface waters ascend (upwell) bringing nutrients that enhance biological activity and reduced CO_2 at surface waters (Lefèvre et al., 2023). Although these upwelling systems are seasonal, the areas between the Canary Islands through the Strait of Gibraltar, as well as between 21°N and 26°N, experience upwelling all year around, that intensifies during summer due to the seasonal migration of trade winds (Cropper et al., 2014). These upwelling systems can be tracked using remote sensing data like average year-round chlorophyll concentration (e.g. Lefèvre et al., 2023).

Water masses in the area include the Eastern North Atlantic Central Water (ENACW) and Eastern South Atlantic Central Water (ESACW) that feed the nutrient rich ecosystems of NW Africa. The ENACW forms during winter subduction between 39 and 48°N (Poole and Tomczak, 1999; Liu and Tanhua, 2021), and the ESACW, originates southwest of South Africa where Indian Ocean waters are introduced by the Agulhas Current and are mixed with the western South Atlantic Current (Liu and Tanhua, 2021) that flows northward form the South Atlantic Subtropical Gyre. These central water masses are described in the oceanographic setting of Chapter 2.

Subtropical circulation in the eastern Atlantic is mainly driven by wind stress, related to the meridional temperature gradients controlled by energy distribution between the subtropical and subpolar gyres (Poole and Tomczak, 1999). Our area of study, specifically site GeoB9512-5 is located between the North and South Atlantic Subtropical Gyres, where older water masses form shadow zones, poorly ventilated

areas (Poole and Tomczak, 1999) that forms the Eastern Tropical North Atlantic Oxygen Minimum Zone (ETNA).

The Eastern North Atlantic upwelling systems and subtropical circulation play a key role in sustaining the unique and rich ecosystems off the coast of NW Africa. In fact, Marine Protected Areas (MPA) ecosystems that depend on these upwelling systems, are in the Atlantic Oxygen Minimum Zones. These ecosystems host a wide range of marine biodiversity, relevant for fisheries resources and other species that support ecosystems (e.g. seagrass, corals and other invertebrates). Here, different MPAs have been delineated to protect not only marine diversity, but also fisheries resources that are vital for human subsistence (Assis et al., 2021). However, ocean warming, and deoxygenation has already led to a decline in the diversity and size of these ecosystems in MPAs (Bruno et al., 2018), as well as in large fishes within nekton ecosystems, limiting the accessibility of commercially fished species (Stramma et al., 2012; Gilly et al., 2013).

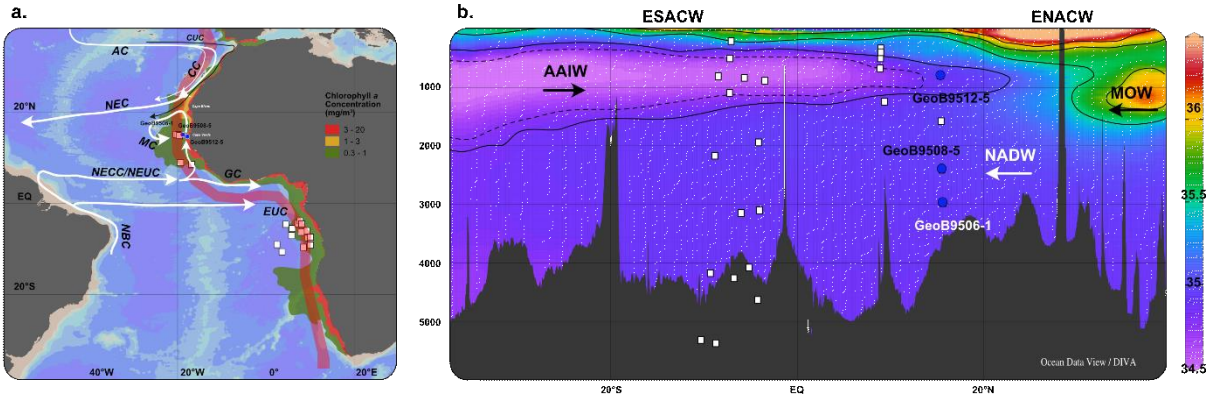

Figure I1. ***Geographic Location of the studied surface sediments and gravity cores GeoB9512-5, GeoB9508-5, and GeoB9506-1.*** **a.** Surface currents were modified from Talley (2011), Brandt et al. (2015) and Pelegrí and Peña-Izquierdo (2015). Approximate Chlorophyll a concentration (mg/m^3) zones were sketched based on the Aqua-Modis data set consulted for November 2019 with a 4 km resolution (https://oceancolor.gsfc.nasa.gov/, consulted November 2023). Surface currents: North Brazil Current (NBC), North Equatorial Counter Current / Under Current (NECC/NEUC), Equatorial Under Current (EUC), Guinea Current (GC), Mauritania Current (MC), North Equatorial Current (NEC), Canary Current (CC), Azores Current (AC), and Canary Upwelling Current (CUC); **b.** Salinity profile of the studied area, showing the water depth of the studied cores. Deep-water masses are approximately delineated. Antarctic Intermediate Water (AAIW), North Atlantic Deep Water (NADW), Mediterranean Outflow Water (MOW), Eastern North Atlantic Central Water (ENACW), and Eastern South Atlantic Central Water (ESACW). The salinity section was plotted using Ocean Data View (Schlitzer, 2023) with data from WOA 2018 (Boyer et al., 2018; García et al., 2019).

The North Atlantic Oxygen Minimum Zones (OMZs) have been expanding in the last decades (Stramma and Schmidtko, 2021; Schmidtko et al., 2017) due to the increased coastal eutrophication (Malone and Newton, 2020) and ocean warming (Stramma et

al., 2008). However, the effect of ocean circulation changes in de-oxygenation trends is not clear, and a potential decline of Atlantic Meridional Overturning Circulation (AMOC) strength by the end of this century (e.g. IPCC, 2022; Liu et al., 2020; Weijer et al., 2020; Zhang et al., 2019) makes it necessary to understand how AMOC strength can influence Eastern Atlantic OMZs. This research question is explored in Chapter 2.

Deep ocean circulation: Atlantic Meridional Overturning Circulation lower limb

At North Atlantic intermediate depths, the South Atlantic Antarctic Intermediate Water (AAIW) is a high oxic (> 260 µmol/kg), low temperature (~ 3.5°C) water mass formed in the Southern Ocean east of the Drake Passage extending as far north as 30°N (Liu and Tanhua, 2021). Also found at intermediate depths to the North, the Mediterranean Overflow Water (MOW) flows into the eastern north Atlantic through the Strait of Gibraltar, bringing warm high salinity waters that rapidly mix with the ENACW (Figure xb).

The upper North Atlantic Deep Water (uNADW) originates from the mixing of high oxic - low salinity Labrador Sea Water (LSW) -formed by winter deep convection in the Labrador Sea Region- and low oxic-nutrient rich Iceland–Scotland Overflow Water (ISOW) (Liu and Tanhua, 2021). These water masses make the uNADW a relatively warm, low oxic – nutrient-rich water mass. The lower portion of the NADW (lNADW), is regarded as a mixing of the ISOW and the Denmark Strait Overflow Water (DSOW), the coldest and densest water mass in the North Atlantic, that results from intense mixing of water masses from the Arctic Ocean and Nordic Seas flowing through the Denmark Strait (Liu and Tanhua, 2021).

The formation of NADW is a main component of the overturning cell in the Atlantic that transports energy away from the sea surface and distributes heat to the south in the ocean interior as part of the lower limb of the AMOC, potentially influencing the rate of global warming (e.g., Muschitiello et al., 2019; Talley et al., 2003; Talley, 2013; Zhang et al., 2019). The limited instrumental record of AMOC hinders our understanding of its influence on deep ocean heat uptake, therefore limiting our understanding of potential effects on global warming rates. A view of ocean heat uptake changes related

to AMOC strength variability is presented in Chapter 4 to contribute to this research question.

Atlantic Meridional Overturning Circulation strength variability during the last deglaciation

The AMOC is an important part of global climate, it transports a significant amount of heat, salt, nutrients, and CO_2 globally (e.g. Nürnberg et al., 2021. For this reason, changes in the strength of this global circulation are critical in climate dynamics, that are still not fully understood. According to the latest IPCC reports (e.g. IPCC, 2023) and available research (e.g. Liu et al., 2020; Zhang et al., 2019), AMOC is projected to slowdown in the future, making it relevant to improve our understanding of the effects of such slowdown in the Atlantic Ocean and in global climate. Since the instrumental record of AMOC strength remains limited to constrain such effects, interpretation must rely for now in paleoceanographic records, specifically from time periods where AMOC strength changes are relatively well recorded. This is the case of the sedimentary record of the last deglaciation in the Atlantic Ocean during the last 30,000 years. During this time, AMOC changes are registered by the kinematic proxy $^{231}Pa/^{230}Th$ (e.g. McManus et al., 2004; Böhm et al., 2015), one of the best tools to reconstruct AMOC strength changes. Other evidence supporting such changes are provided by northern-southern hemisphere bipolar seesaw pattern (Marino et al., 2015), or partially by the registered southern meridional shift of the Intertropical Convergence Zone that is also predicted by climate models (e.g. Broccoli et al., 2006; Dupont et al., 2010, Mulitza et al. 2017). Evidence of AMOC strength variability, and current controversies around this are further discussed in the Introduction of Chapter 4.

From the available proxy data, a significant AMOC decline is consistently recorded during the Heinrich Stadial 1 (HS1, 18.3 -15.4 kyrs BP). Subsequently, during the Bølling–Allerød (B-A), records show a period of temporary AMOC reinvigoration, that was followed by a less pronounced slowdown in the Younger Dryas (12.9 - 11.7 kyrs BP). For the Holocene, a restored AMOC is inferred from the $^{231}Pa/^{230}Th$ (e.g. McManus et al., 2004; Böhm et al., 2015). Another proxy of AMOC decline, can be benthic foraminifera $\delta^{13}C$, particularly drop of the carbon isotopes of epifaunal

foraminifera from deep-ocean records have been seen in the western North Atlantic during HS1 and YD. These drops are interpreted as ventilation decrease compatible with a slowdown of AMOC (e.g., Oppo et al., 2015), and can therefore be used to observed ventilation changes in our eastern North Atlantic record (Chapter 4, section 4.1).

During this research, a study of deep-ocean (GeoB9508-5 Chapter 4; GeoB9506-1 Chapter 5) and intermediate waters (GeoB9512-5, Chapter 2, Chapter 3, Chapter 4 and Chapter 5) sedimentary deglacial records was carried out to reconstruct paleoceanographic changes in times of AMOC slowdown. This research focused on the benthic foraminifera taxonomy and distribution to observe oxygenation changes, and benthic ecosystems response; stable isotopes to infer changes in bottom water ventilation $\delta^{13}C$ and salinity $\delta^{18}O$; and Mg/Ca to reconstruct paleotemperature changes. This record provided the opportunity to study the effects of AMOC variations in (1) North Atlantic deep water heat uptake (Chapter 4 and Chapter 5), (2) ETNA OMZ changes related to subtropical subsurface circulation (Chapter 2), and (3) benthic foraminifera Mg/Ca palaeothermometry at the eastern North Atlantic at intermediate waters (Chapter 3).

Methods

Core materials and location

The material used for this research came from surface sediment samples of 32 core tops from the eastern North Atlantic, and 16 core tops of the eastern South Atlantic (Figure I1a and b). Three gravity cores (GeoB9506-1, GeoB9508-5, and GeoB9512-5) from off the Northwestern African Margin were analyzed (Figure I1a and b). Gravity core GeoB9512-5 (15.34 °N, 17.37 °W, 793 m water depth) is in the mixing zone of the SACWs and the NACW (Figure I1b). Here, bottom water temperature (BWT) is approximately 7.1°C and has low oxic conditions (dissolved oxygen concentrations ~ 78 µmol/kg) (Lauvset et al., 2022). Gravity cores GeoB9508-5 (15.50 °N, 17.95 °W, 2,384 m WD) and GeoB9506-1 (15.61 °N, 18.35 °W, 2,956 m WD) correspond to the NADW, that at the studied sites, has temperatures of ~ 3.8°C and ~ 2.7°C respectively, and oxygen concentrations of ~ 227 and ~ 237 µmol/kg (Lauvset et al., 2022).

Samples from cores GeoB9506-1 and GeoB9512-5, were recovered from working and in some cases archive halves at the GeoB Core Collection at the MARUM – Center for Marine Environmental Sciences, University of Bremen. A total of 110 samples from core GeoB9512-5 and 104 samples of core GeoB9506-1 were washed and dry sieved in the UFT laboratories. The samples were initially washed with deionized water through a 63 µm sieve to remove mud content and then dried for less than 24 hours at 45°C. The remaining material was dry sieved through 63 µm, 125 µm, 150 µm and 250 µm. Washed and dry sediment from the fraction >150 µm was analyzed to extract at least 250 specimens of benthic foraminifera for taxonomical analyses and geochemical measurements. The remaining number of analyzed samples from the gravity core GeoB9506-1 and core tops included in this research were provided by the GeoB Core Repository collection and consisted of washed sediments >150 µm. Stable isotopes and Mg/Ca data from site GeoB9508-5 was available and were obtained by the coauthors of Chapter 4. Additional data from GeoB9506-1 was taken from Multiza et al. (2021). A detailed summary of the number of samples analyzed is included in tables M1 -M3.

Table M1 Stable isotopes sample data used produced during this research

	Stable Isotopes			
Sites	*Uvigerina* spp.	Interval (cm)	*Cibicidoides* spp.	Interval (cm)
GeoB9506-1	142	17.5 - 978	76	2.5 - 260
GeoB9508-5	-	-	345	5.5 – 955.5
GeoB9512-5	27	12.5 - 547.5	208	2.5 - 547.5
Total	**169**		**284**	

Table M2 Element-calcium ratios data produced during this research

	Trace Elements			
Sites	*Uvigerina* spp.	Interval (cm)	*Melonis barleeanus*	Interval (cm)
GeoB9506-1	95	5 - 260	-	-
GeoB9508-5	92	3 - 793	-	-
GeoB9512-5	78	2.5 – 547.5	35	52.5 467.5
Surface samples NE Atlantic	-	-	27	-
Surface samples SE Atlantic	-	-	5	-
Total	265		67	

Table M3 Planktic foraminifera for AMS radiocarbon dating and benthic foraminifera for taxonomy and paleoenvironmental interpretation

	Planktic Foraminifera	Benthic Foraminifera Taxonomy			
Sites	C14	Samples	Interval (cm)		No. Specimens
GeoB9506-1	12	64	2.5	260	15,587
GeoB9508-5	Mulitza et al., 2008	-	-	-	-
GeoB9512-5	16	100	2.5	547.5	24,340
Surface samples NE Atlantic	0	10	-	-	3,639
Surface samples SE Atlantic	0	17	-	-	5,036
Total	**28**	**191**			**48,602**

Deglacial Chronology

Downcore ages and uncertainty were modelled using the R-Package Bacon (Blaauw and Christen, 2011) on RStudio version 2.5. and the MarineCal20 calibration curve (Heaton et al., 2020). The AMS radiocarbon ages used in this model were measured on *G. sacculifer* and *G. bulloides* from 16 samples from core GeoB9512-5 and 12 samples from core GeoB9506-1, for site GeoB9508-5 the available radiocarbon dates were employed (Mulitza et al., 2008). The measurements were carried out at the MICADAS laboratory from the Alfred Wegener Institute (AWI)-Bremerhaven (Mollenhauer et al., 2021). In addition, the uncalibrated XRF Fe/Ca ratios of the three gravity cores were visually correlated with the resulting age models (Mulitza and Zabel, 2009; Völpel et al., 2019; Itambi, 2010;) allowing to calibrate the timing of Heinrich stadial events. Elemental ratios like Fe/Ca, are useful for this as they are synchronous in areas restricted geographically and are mostly driven by dust deposition changes related to continental aridity (e.g. Völpel et al., 2019). The resulting age models from sites GeoB9512-5, GeoB9508-5 and GeoB9506-1 show a deglacial sedimentary sequence with no apparent reversals deposited in the last ~27.000 years (Figure 2). The studied intervals then include the Last Glacial Maximum interval (LGM), Heinrich Stadial 2 (HS2), Heinrich Stadial 1 (HS1), the Bølling–Allerød warming (B-A) and the Younger Dryas (YD). Data from older sediments was also obtained for GeoB9506-1 and GeoB9508-5 deployed in the PANGAEA database, however this research focused on the last 27.000 years of the record.

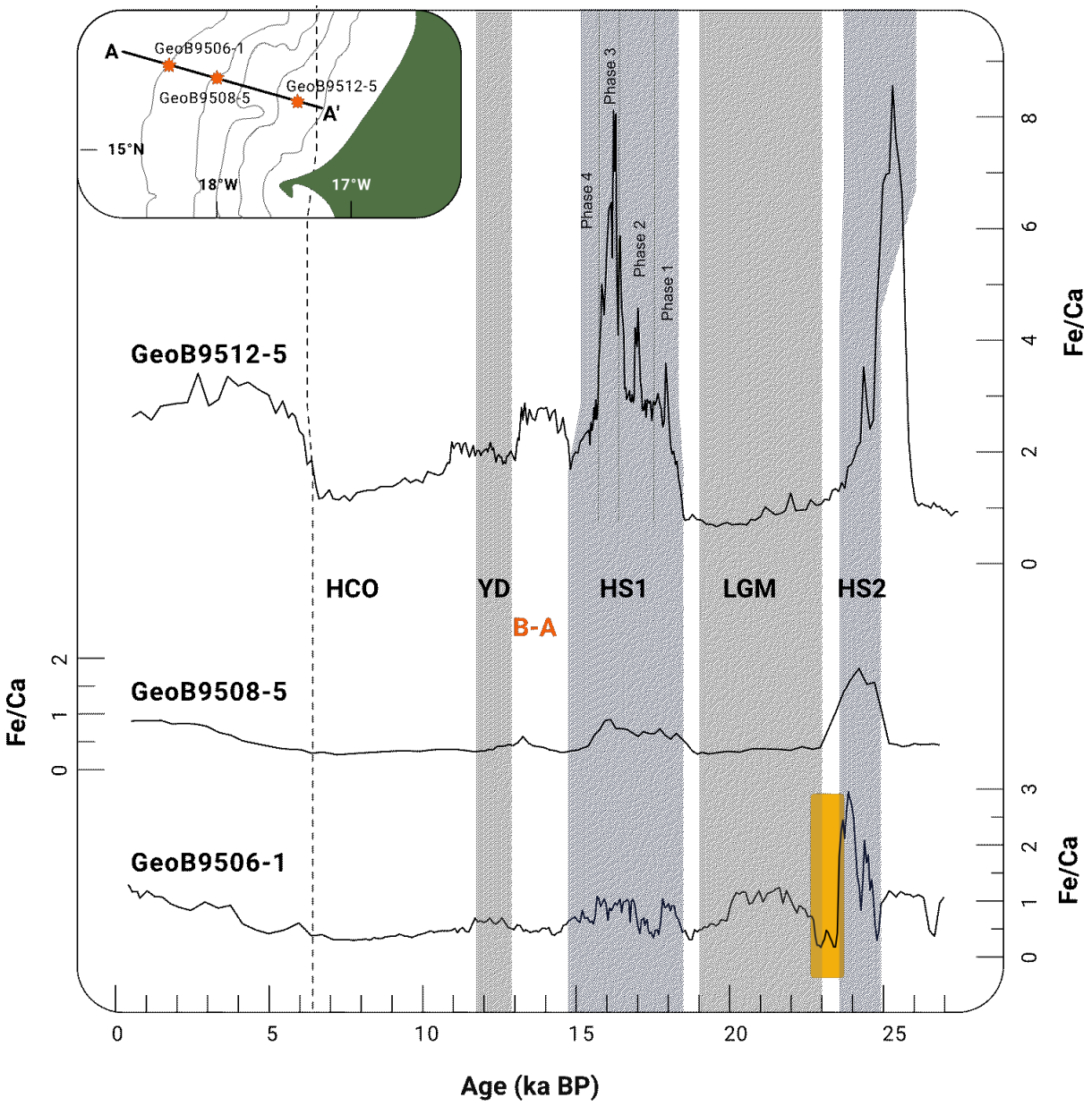

Figure M1. Uncalibrated Fe/Ca records from Gravity Cores GeoB9512-5, GeoB9508-5, and GeoB9506-1. Upper panel showing the geographic position of the studied cores. Uncalibrated XRF Fe/Ca ratios from GeoB9508-5 (Mulitza and Zabel, 2009), GeoB9506-1 (Itambi, 2010), and GeoB9512-5 (Völpel et al., 2019) with the updated age models, used to calibrate Heinrich Stadials periods.

Benthic Foraminifera: deglacial paleoenvironmental and paleoceanographic changes of the NE Atlantic

Benthic foraminifera are single celled organisms that live on the ocean floor (epifaunal) or buried in the first centimeters of the sediment (infaunal). These microorganisms produce a hard test around their cell in relative chemical equilibrium with the surrounding waters (e.g. Murray, 2006). This allows paleoceanographers to use this abundant microfossil group to reconstruct paleoceanographic and paleoenvironmental

changes of bottom waters in the geological record, improving our understanding of the ocean-atmosphere dynamics that shape global climate.

Taxonomical and quantitative analyses of benthic foraminifera are also a valuable tool for paleoenvironmental reconstructions. Their diversity and distribution are highly sensitive to changes in bottom water conditions like oxygenation, organic matter (food) content, and bathymetry. This means that by investigating the changes in their distribution, we can reliably reconstruct these environmental conditions in the past (e.g. Alegret et al., 2021; Murray, 1991; Murray 2006). Furthermore, this allows a better understanding of the effect of global and regional phenomena on benthic ecosystems and the implications of climate change in this part of the biosphere.

During this research, 100 samples of core GeoB9512-5, 64 samples of GeoB9506-1, 9 samples for core tops of the NE Atlantic and 19 core top samples of the SE Atlantic were analyzed to extract the benthic foraminifera content. The size fraction used was >150 μm, and for each sample at least 250 specimens of benthic foraminifera were recovered. Over 50,000 benthic foraminifera were recovered for taxonomic and geochemistry analyses. All specimens were taxonomically classified in most cases to a species level, and a total of 236 taxonomical units were identified, including 115 genus and 194 species.

Stable Isotopes: deglacial paleoceanography of the NE Atlantic

Stable isotope measurements, including $\delta^{13}C$ and $\delta^{18}O$ were made on benthic foraminifera tests to infer changes in bottom water ventilation, and salinity in the NE Atlantic. This analysis relied primarily in the recovery and preservation state of some species of *Uvigerina* and *Cibicidoides. Cibicidoides wuellerstorfi* was extracted for stable isotopes in cores GeoB9508-5 and GeoB9506-1, while specimens from *Cibicidoides pachyderma, Cibicidoides robertsonianus* and *Lobatula lobatula* were used in GeoB9512-5 for $\delta^{13}C$ and $\delta^{18}O$ measurements. Additional tests from *Uvigerina peregrina* were analyzed on site GeoB9506-1 integrated with previous data (Multiza et al., 2022). In addition, stable isotope measurements were made for surface sediments of *C. pachyderma, C. robertsonianus*, *M. barleeanus, U. peregrina* and *Uvigerina mediterranea*.

The measurements were made using a ThermoFisher Scientific 253 plus gas isotope ratio mass spectrometer, with a Kiel IV automated carbonate preparation device, at MARUM- Center for Marine Environmental Sciences of the University of Bremen. The instruments were calibrated against the house standard (ground Solnhofen limestone), also calibrated against the NBS 19 calcite. The house standard deviation over the measurement period is reported in each chapter, and data is reported in the delta-notations versus V-PDB. A detailed assessment of stable isotope corrections and uncertainty is included in each chapter accordingly.

Benthic foraminifera Mg/Ca ratios: paleothermometry of bottom waters

Paleothermometry using foraminifera Mg/Ca is a very widely used tool to reconstruct changes in surface (using planktic foraminifera) and bottom water (using benthic foraminifera) temperatures. Here, we reconstructed bottom water temperatures during the last deglaciation in the NE Atlantic using benthic foraminifera Mg/Ca of intermediate (GeoB9512-5 -5) and deep waters (GeoB9508-5 and GeoB9506-1). On site GeoB9512-5 we integrated this proxy with other paleoenvironmental reconstructions obtained from benthic foraminifera taxonomy, to identify potential external (environmental) and internal (vital effects) parameters affecting Mg uptake (Chapter 3). The data comes from: (1) tests of shallow infaunal *U. peregrina* from GeoB9508-5 and GeoB9506-1, and of *U. mediterranea* of coreGeoB9512-5; and (2) intermediate infaunal *M. barleeanus* of GeoB9506-1 and GeoB9512-5. Additionally, *M. barleeanus* and *Uvigerina spp.* from surface sediment samples of the NE Atlantic was also measured to revise *M. barleeanus* temperature calibrations.

Trace element concentrations were measured with an Inductively Coupled Plasma Optical Emission Spectrometer (ICP-OES)—Agilent Technologies 700 Series with Cetac ASX-520 autosampler. The spectral lines and calibration standards used are described accordingly in each chapter, and linear regressions were used to calibrate the measurements in all cases. Uncertainties of the geochemical proxies used in this study are described in each chapter.

Chapter 1: North Atlantic Recent Benthic Foraminifera distribution patterns and environmental controls: a review

In preparation for submission

S. Barragán-Montilla[1,2]

[1] MARUM – Center for Marine Environmental Sciences and Department of Geosciences, University of Bremen, Bremen, Germany
[2] Faculty of Geosciences, University of Bremen, Bremen, Germany

1. Introduction

Benthic foraminifera are one of the most abundant soft bodied meiofauna on the seafloor (e.g. Gooday, 2001). Their striking abundance and diversity have become a key tool in reconstructing past environmental changes of bottom waters, utilizing our knowledge of their distribution in modern seas (Gooday, 2001; Murray, 2006). The in-depth study of this extant-fossil microscopic group goes back to the early 17th century, with the extensive studies of d'Orbigny (e.g. d'Orbigny, 1839 in Webb et al., 1836) whose definition of several benthic foraminifera species has held up until modern times (Vénec-Peyré, 2002).

Recent benthic foraminifera of the eastern North Atlantic: earlier studies

In the Atlantic Ocean, benthic foraminifera have been extensively and a vast record of benthic foraminifera taxonomy and distribution (Cushman, 1923; Cushman, 1931; Tikhonova et al., 2019) has shaped our knowledge of their distribution in recent times. A robust compilation of the occurrence of benthic foraminifera species in the Atlantic Ocean by Murray (1991), documented marginal marine associations from marshes and mangrove swamps to deeper settings from shelves, slope and deep seas. However, significant gaps in the knowledge of extant benthic foraminifera in large areas of the eastern North Atlantic and South Atlantic (particularly in shallow areas, Figure 1.1b), still limited our understanding of the ocean dynamics of bottom waters that are key in palaeoceanographic studies.

From the early studies, Lutze and Coulbourn (1980) defined four major faunal provinces in the eastern North Atlantic off NW Africa. The main control on such provinces is related to water depth, conditioning the occurrence of species like *Cibicides lobatulus* (today accepted as *Lobatula lobatula), Trifarina foranisinii, Planulina ariminensis, Uvigerina finisterrenses* and *Cibidoides wuellerstorfi*. This study found that other environmental parameters like coarse subtrate (*Cancris auriculus*), oxygen decrease (*Bolivina subaenariensis*) and/or low organic carbon concentration (*Hoeglundina elegans* and *Cibicidoides kullenbergi* – accepted as *C. mundulus*), also influence benthic foraminifera distribution. Additionally, the well-known palaeoceanographic tool *Uvigerina peregrina* is found confined to the continental slope of Cape Blanc probably due to the high organic carbon concentration and fine grain size sediment. The provinces reported were (1) shelf – upper slope *C. auriculus – L. lobutula*; (2) northern mid slope *U. finisterrensis*; (3) southern mid – lower slope restricted south of 22°N *U. peregrina* (4) lower slope and rise province below 1,000 m *C. mundulus – wuellerstorfi*.

This depth dependence was also observed by Haake (1980), in gravity cores off Senegal/Gambia in NW Africa. They identified five zones based on the benthic foraminifera content: (1) Upper Shelf Zone between 30 – 300 m; (2) Lower Shelf Zone between 80 and 300 m; (3) Upper Shelf and Slope Zone between 80 and > 2,000 m; (4) Upper Slope Zone between 200 and > 2,000 m; and (5) Lower Slope Zone between 900 and > 2,000 m. The assemblage of zone 1 is made up of Textulariids, Miliolids, *Nouria polymorphinoides, Bulimina gibba, Rectuvigerina phlegeri* and *Nonionella cordiformis*; zone 2 of *Cribrostomoides* cff. *triangularis, Bolivina striatula, Globobulimina* cff. *glabra* and *Trifarina fornasinii*: zone 3 *Reophax scorpiurus, Bolivina dilitata dilitatissima*, and *Uvigerina* sp.; zone 4 *Eggerella arctica, Bulimina aculeata, Uvigerina peregrina dirupta* and *Trifarina elongatastriata*; and zone 5 by *Reophax aduncus, Ammobaculites agglutinans, Globobulimina turgida, Cibicidoides wuellerstorfi* and *Melonis barleeanus.*

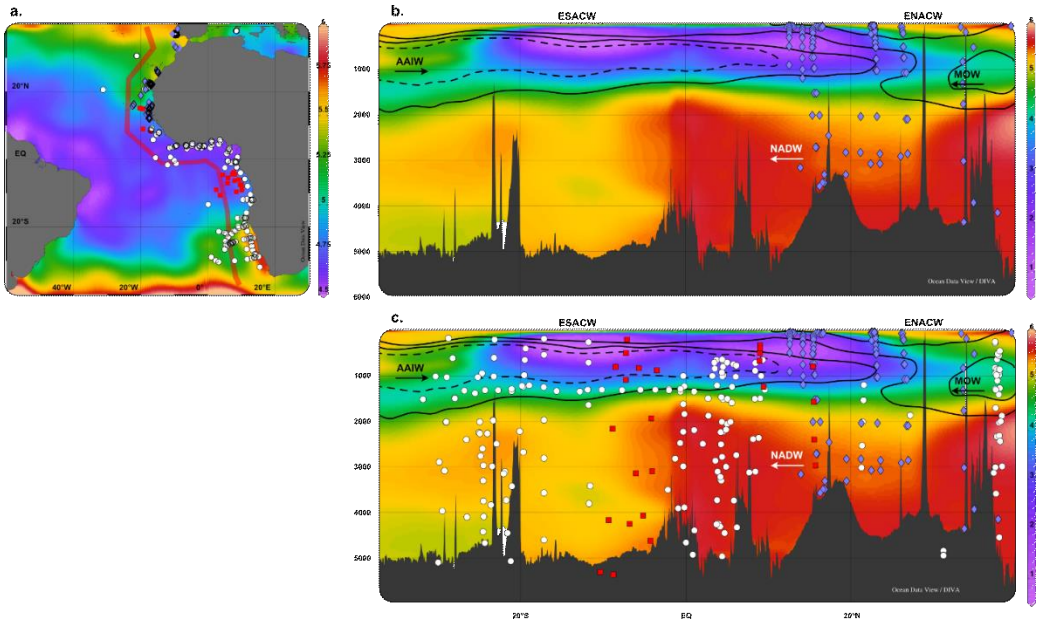

Figure 1.1 ***Compilation of eastern Atlantic recent Foraminifera data published in PANGAEA (https://www.pangaea.de/).*** **a.** Geographic location of sites reporting living and dead benthic foraminifera recent occurrences; **b.** Data published before 1992 (purple diamonds); **c.** Living and dead benthic foraminifera recent occurrences published after 1992 (white circles), including the dead benthic foraminifera data reported in this study (red squares).

Studies after 1992: an improved understanding of benthic foraminifera distribution environmental controls in the NE Atlantic

Since 1992, numerous research studies have focused on the recent benthic foraminifera distribution off NW Africa and its controls (Figure 1.1c), making significant contributions to the afore mentioned research and filling significant gaps. This has provided evidence of organic matter quantity/quality control on benthic foraminifera distribution, in addition to the clear depth dependence of certain species observed (Haake, 1980; Lutze and Coulbourn, 1980). In the eastern North Atlantic, benthic foraminifera densities were found to reflect surface primary productivity, and abundant *Epistominella exigua* was found dominating areas with abundant phytodetrital organic matter at the Porcupine Abyssal plain (48°N, 16°W, Gooday, 1996). Further south (around 21.5°N) benthic foraminifera assemblages' evidence that benthic ecosystems at a station at 1200 m WD are permanently influenced by upwelling, while at deeper settings (stations at 3010 and 2530 m WD) ocean bottom experiences significant organic matter fluxes exclusively in summer (Jorissen et al., 1998).

In the South Atlantic, research suggests that deep sea foraminifera distribution is controlled by factors like bottom water ventilation, primary productivity and organic matter content, carbonate corrosiveness and benthic boundary level energetic state (Mackensen et al., 1995). A strong control of productivity regimes on benthic foraminifera assemblages was also clearly observed between 2°N and 12°S off NW Africa in an area heavily influenced by coastal and ocean upwelling. Licari et al. (2003), found that (1) epifaunal and shallow infauna benthic foraminifera colonized oxygenated sediments with labile organic matter; (2) intermediate infauna like *M. barleeanus* was related to nitrate reduction sediments, feeding probably off bacterial biomass or on particles from bacterial degradation of refractory organic matter; and (3) deep infauna is most abundant in anoxic sediments with complex metabolizable organic matter.

This preference on the type/quality of organic matter is also inferred in the north Atlantic. Bartels-Jónsdóttir et al. (2006) observed that in the Tagus Prodelta and Estuary in Portugal, epifaunal – shallow infaunal like *Rectuvigerina phlegeri* and *Stainforthia fusiformis* prefer fresh phytodetritus or labile organic matter; while infaunal living down to 10 cm like *Bulimina marginata, Globobulimina auriculata* and *Nonionella turgida* that live in the low oxic to anoxic sediment feed selectively and use refractory organic matter or bacterial stocks. Furthermore, these authors found a strong relation between the foraminifera concentrations and the organic matter distribution.

In addition to organic matter content, another important parameter influencing benthic foraminifera distribution in the eastern North Atlantic is oxygen. Jorissen et al. (1998), showed that the vertical zonation of benthic foraminifera is controlled by the depth distribution of dissolved oxygen. Some species prefer low oxygen conditions, while others, for instance *M. barleeanus* have adaptation strategies for nitrate respiration in the absence of oxygen.

Benthic Foraminifera microhabitats and adaptation strategies recorded in the NE Atlantic

The observed preferences of benthic foraminifera species to specific environmental conditions allowed researchers to define “microhabitats”, closely spaced habitats

within the sediment, that are characterized by a series of physical, chemical, and symbiotic conditions including (but not limited to) oxygen, food, toxic substances, and biological relations (Jorissen et al., 1999). In benthic foraminifera, microhabitats are vertically distributed in the sediment and can be shallow, intermediate, or deep. Furthermore, a species microhabitat is not necessarily static through time, as its defining conditions can vary, therefore influencing the occurrence of benthic foraminifera.

In the Bay of Biscay (eastern North Atlantic above 30°N), benthic foraminifera microhabitats are seen to be controlled by export productivity of organic matter and oxygen concentration is not that relevant (Fontanier et al., 2002). These studies provide valuable information about benthic foraminifera preferences, like *Nonion scaphum* and *Chilostomella oolina* that feed on labile organic matter in dysoxic – anoxic environments; *Melonis barleeanus* and *Globobulimina affinis* thrive in lower quality organic matter settings; and *Uvigerina mediterranea* and *Cibicidoides pachyderma* are more commonly found in the water-sediment interface (Fontanier et al., 2002; Fontanier et al., 2005).

Another important aspect is that microhabitat depth is particularly variable for highly adapting species. This is the case of *Melonis barleeanus* and *Globobulimina affinis* who migrate vertically within the sediment looking for their preferred living conditions and food (Linke and Lutze, 1993). This behaviour has also been registered by culture studies using *Globobulimina turgida* (Koho et al., 2011) as erratic movements in the sediment looking for their preferred microhabitat in changing conditions. Benthic foraminifera species like U*. mediterranea, U. peregrina* and *G. affinis* also have a well recorded vertical migration behavior related to changes in oxygen availability (Geslin et al., 2004). Average living depths (ALD) on benthic foraminifera have been determined for several species (Figure 1.2) in areas like the Bay of Biscay, North Atlantic and Pacific Oceans, and in ideal oxic – food conditions show consistent distribution patterns. *U. peregrina* and *U. mediterranea* are commonly found in shallow infaunal microhabitats (Corliss and Emerson, 1990; Fontanier et al., 2002; Fontanier et al., 2006; Geslin et al., 2004; Griveaud et al. 2010), with ALD from 0 to 2 cm in the sediment. *M. barleeanus,* preferably lives deeper in the sediment, and is commonly

regarded as an intermediate infaunal species with ALDs between 1 to 6 cm (Corliss, 1985; Corliss and Emerson, 1990; Fontanier et al., 2002; Fontanier et al., 2006; Geslin et al., 2004; Griveaud et al. 2010). Deeper in the sediment, deep infaunal *Globobulimina affinis* is found at ALDs from 4 to 12 cm.

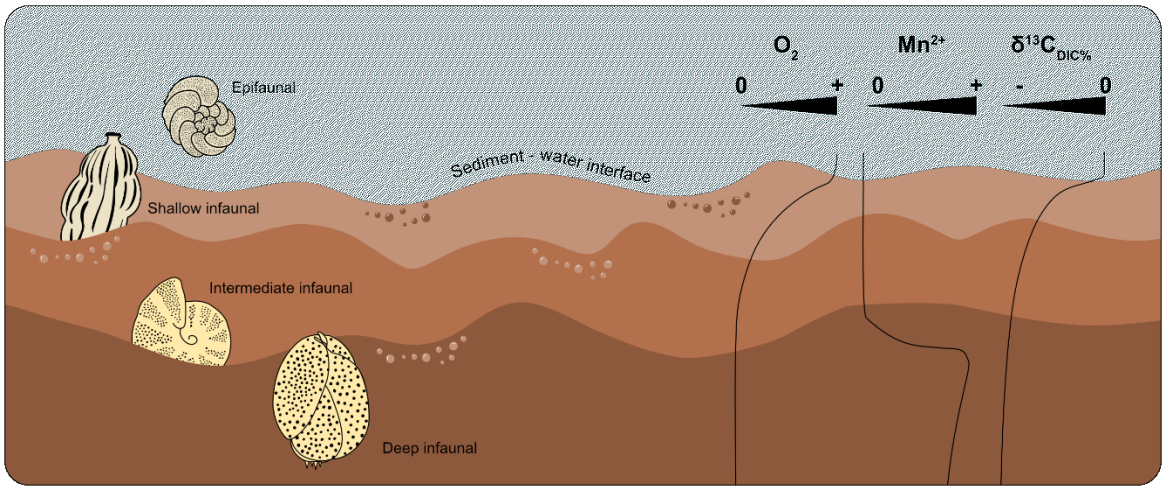

Figure 1.2 Idealized microhabitats of common eastern North Atlantic benthic foraminifera species *(e.g. Linke & Lutze, 1993) and In-sediment chemical composition taken from Koho & Piña-Ochoa in Altenbach, 2012)*. Epifaunal *Cibicidoides wuellerstorfi* / *pachyderma*, shallow infaunal *Uvigerina mediterranea* / *peregrina*, intermediate infaunal *Melonis barleeanus* and deep infaunal *Globobulimina turigda* / *affinis.*

Benthic Foraminifera: investigating the present to understand the past

Well-recorded benthic foraminifera microhabitat preferences, linked to the environmental parameters (water depth, organic matter type, quantity and quality, and oxygen concentration), make these microorganisms excellent tools to study the changes in bottom waters / benthic ecosystems environmental parameters in the fossil record. Furthermore, reconstructing the variability of this parameters in the past, enable us to understand its relation to regional hydrographic processes like upwelling, and to global changes like for example Atlantic Meridional Overturning Circulation (AMOC) variability.

More precisely, detailed taxonomic/quantitative analyses can be used to estimate dissolved oxygen concentration (BWOx) at bottom waters (Kaiho, 1994; Kranner et al., 2022), an ecologically and climatically relevant element that strongly controls benthic diversity in modern oceans (Vaquer-Sunyer and Duarte, 2008), and depends

on global factors like ventilation of the deep-ocean, deep-water circulation, and regional carbon consumption (e.g. Brandt et al., 2015). Also important, and in addition to the abundance of certain species, benthic foraminifera who live buried in the sediment (infauna) are powerful tools to understand variations in the quantity/type of food in benthic ecosystems (Gooday et al., 1992; Jorissen et al., 1995; Sweetman et al., 2009), that along with oxygen consumption, are relevant to the carbon pump that sequesters carbon preventing it to be released to the atmosphere (Volk and Hoffert, 1985).

This knowledge is also important to identify discrepancies in geochemical proxies based on benthic foraminifera. Adaptive strategies leading to changes in microhabitat depths and potentially during calcification, can impact the geochemical signal of the tests used by paleoceanographers introducing critical bias in this data and in any inferences made from these (e.g. Bryan and Marchitto, 2008). A complete understanding of the benthic foraminifera distribution, and its controls notably improves our knowledge of the ocean-atmosphere dynamics that shape global climate, and also allows for more accurate interpretations of the geochemical records we obtain from this microfossil group.

2. Methods

2.1 Core Location and materials

Surface sediment samples (25) from the tropical eastern Atlantic were used to extract the benthic foraminifera dead assemblages (Figure 1.3). Northern sites multicore samples were collected during Meteor Cruise M65/1 (Mulitza et al., 2005) and the southern samples were retrieved by the RV Tyro cruise (Jansen et al., 1990). The studied M65/1 sediment samples come from previously dried sieved sediment provided by the GeoB Core repository from MARUM institute, while the samples from the RV Tyro Cruise correspond to sediment studied by Schefuß et al. (2004).

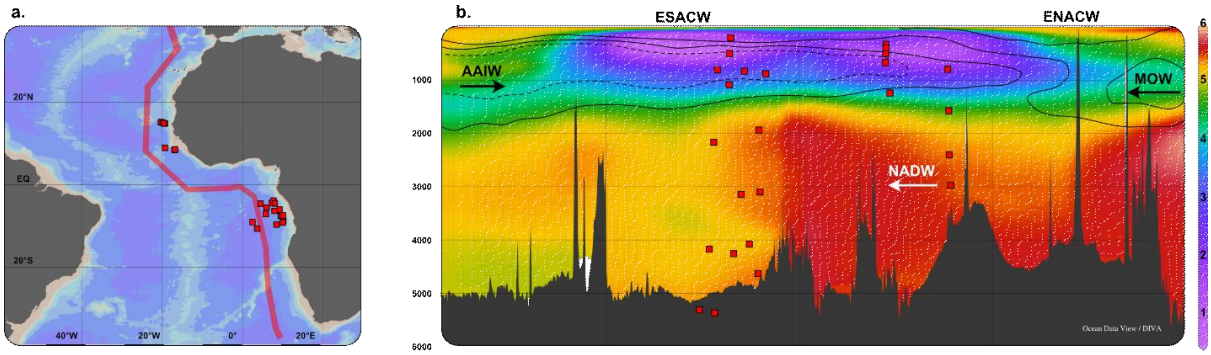

Figure 1.3 Core location and water masses at the eastern North Atlantic off NW Africa; a. Geographic location of the studied sites, including the core tops of the NE Atlantic and SE Atlantic; **b.** Oceanographic situation of the studied sites colour scheme showing the dissolved oxygen concentration with water depth (scale on the right-side ml/l), modern oceanographic water masses in the study area obtained from the modern salinity. Images were obtained and modified from Ocen Data View (Schlitzer, Reiner, Ocean Data View, https://odv.awi.de, 2022) with data from GLODAP version 2 (Lauvset et al., 2022).

2.2 Benthic foraminifera taxonomy

At least 200 - 250 benthic foraminifera were handpicked from 25 samples of eastern Atlantic surface sediment using the fraction > 150 µm. The extracted benthic foraminifera were not stained, therefore inferred as dead assemblages, and were morphologically separated for taxonomical identification made to a specific level when possible. Genera determinations are based on Loeblich and Tappan (1987), and species were identified using multiple references (e.g. Jones and Brady, 1994; Holbourn et al., 2013; van Morkhoven et al., 1986). Taxonomy was revised with the online database WoRMS to ensure updated nomenclature. Benthic foraminifera were digitally photographed with a Keyence VHX 6000 digital microscope with a motorized stage at the Microscopy Laboratory at the MARUM Institute (Appendix 1.1). Quantitative analyses based on benthic foraminifera counts, were made on RStudio using a data frame grouping similar taxonomical units (Supplementary Information 1.1). Non-metric Multidimensional Scaling (NMDS) analyses were made using taxonomic units with relative abundances greater than 5 %.

Bottom water oxygenation was calculated using an Enhanced Benthic Foraminifera Oxygen Index (EBFOI) to estimate Dissolve Oxygen Concentration (BWOx) in past marine deposits (Kranner et al., 2022). These values were then compared to modern conditions based on GLODAPv2 data (Lauvset et al., 2022), to evaluate the accuracy of this approach in the studied area. This was also compared with the distribution of stress species (species better adapted to oxygen depleted environments e.g.

Southward et al., 2003). Organic matter content was inferred using the TROX model (Jorissen et al. 1995).

3. Results

For this study, the modern distribution of benthic foraminifera and its environmental controls in the eastern Atlantic was inferred from 9 core top samples of the NE Atlantic and 17 of the SE Atlantic. Data from cores T89-13 and T89-19 were not considered in the environmental analysis due to low benthic foraminifera recovery. From the taxonomical analysis, 134 genus and 91 species of benthic foraminifera were recognized. In the NE Atlantic, abundant species included *Uvigerina peregrina, Melonis barleeanus* and *Bulimina aculeata* (Table 1.1), while for the SE Atlantic agglutinated foraminifera like *Recurvoides turbinatus, Rhizammina* spp. and *Eratidus foliaceus* are more representative (Figure 2).

Table 1.1 Average relative abundances (Avg.) of the most abundant benthic foraminifera species off NW Africa.

NE Atlantic	Average relative abundance (%)	SE Atlantic	Average relative abundance (%)
Uvigerina peregrina	10.9	*Recurvoides turbinatus*	5.96
Melonis barleeanus	8.7	*Rhizammina* spp.	4.86
Bulimina aculeata	7.1	*Eratidus foliaceus*	4.33
Uvigerina mediterranea	4.7	*Bolivina* sp. 1	4.19
Cassidulina teretis/laevigata	4.11	*Uvigerina peregrina*	4.02

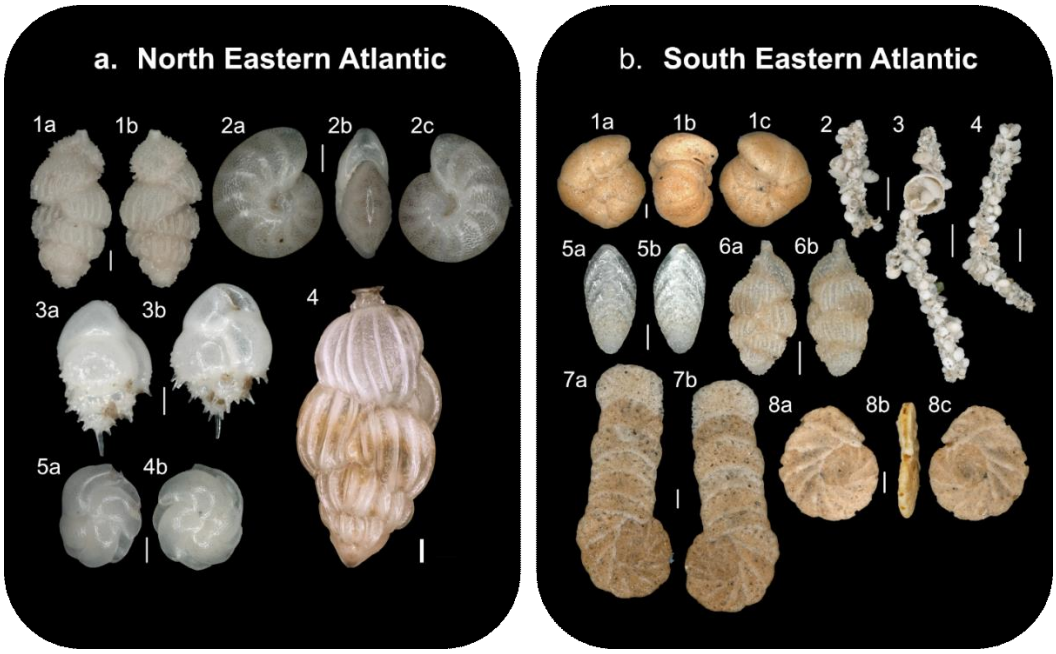

Figure 1.4 Digital microscope images from the most representative benthic foraminifera in the Eastern Atlantic a. Most abundant benthic foraminifera in the NE Atlantic 1. *Uvigerina peregrina*, 2. *Melonis barleeanus*, 3. *Bulimina aculeata*, 4. *Uvigerna mediterranea*, 5. *Cassidulina teretis/laevigata;* **b.** Most abundant foraminifera in the SE Atlantic: 1. *Recurvoides turbinatus*, 2-4. *Rhizammina* sp., 5. *Bolivina* sp. 1, 6. *Uvigerina peregrina*, 7-8. *Eratidus foliaceus.*

Benthic foraminifera diversity in the eastern north Atlantic is generally moderate (Figure 1.5b), with an average Fisher Alpha index (black bars in Figure 1.5b) of 10.4. For the SE Atlantic average diversity (black bars in Figure 1.5a) is around 8.5. More importantly for the southern part of the studied area, diversity in core tops recovered at water depths < 1200 m is higher (average Fisher Alpha index 9.4) than those from core tops deeper than 1200 (average Fisher Alpha index 7.9). Assemblages' homogeneity in the eastern Atlantic was measured with the Shannon index (purple bars in Figure 1.5a and 1.5b) and shows benthic foraminifera assemblages are heterogeneous (Shannon Index on average 2.7, standard deviation SD=0.3). Only the deeper sites studied (T89-28 and T89-47) present more homogeneous content (Shannon Index 2.3 and 2.2 respectively).

Bottom water environmental conditions in the NE Atlantic are characterized by high organic matter content as seen by the infaunal percentages (Figure 1.5f) and vary from low oxic at depths shallower than 1200 m and become high oxic (Figure 1.5d) in deeper settings (1500 to 3000 m water depth). For the SE Atlantic three types of environments are recognized: (1) high organic matter – low oxic (2) moderate organic matter content – high oxic; and (3) low organic matter content – high oxic. These

environments are distributed in depth: (1) for core tops < 1200 m water depth; (2) for core tops from 1900 – 4600 m water depth; and (3) at around 5300 m water depth (Figure 1.5c and 1.5e).

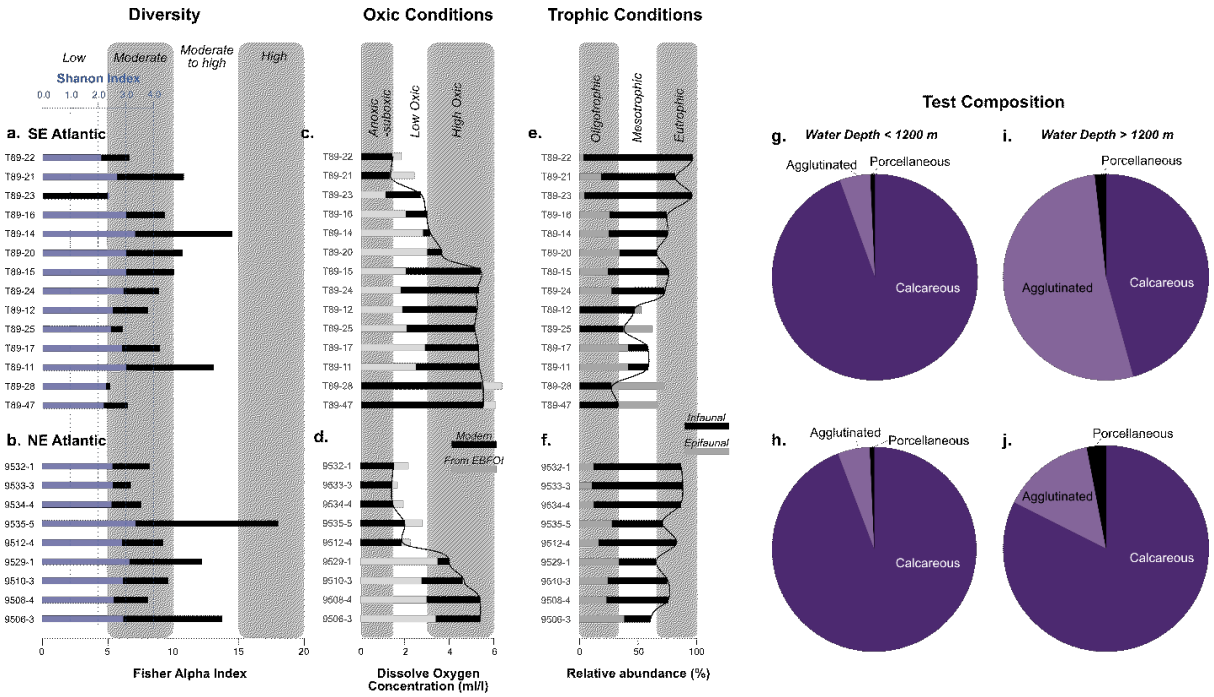

Figure 1.5 Eastern North Atlantic recent benthic foraminifera diversity, group distribution and environmental parameters. a. SE Atlantic and **b.** NE Atlantic Diversity measured with the Fisher Alpha Index (black bars) and homogeneity measured with the Shannon Index (purple bars); **c.** SE Atlantic and **d.** NE Atlantic Oxic Conditions taken from nearby locations modern measurements (World Ocean Atlas 2018) (black bars), and calculated using the EBFOI (gray bars); **e.** SE Atlantic and **f.** NE Atlantic Trophic Conditions inferred from infaunal foraminifera relative abundances (black bars), epifaunal content (gray bars); **g.** SE Atlantic and **h.** NE Atlantic test composition predominance in shallow core tops (<1200 m water depth); **i.** SE Atlantic and **j.** NE Atlantic test composition predominance in deep core tops (>1200 m water depth).

NE Atlantic core top samples contain predominantly calcareous assemblages (Figure 1.5h and 1.5j, on average higher than 90 %), in contrast to higher agglutinated foraminifera content in the SE Atlantic (Figure 1.5g and 1.5i, on average higher than 37 %) which are dominant in core tops deeper than 1,200 m water depth (Figure 1.5i) reaching relative abundances up to 89 %.

Non-Metrical Multidimensional Scaling (NMDS) was made with species with relative abundances higher than 5% in at least 1 sample, including samples from cores T89-13 and T89-19 (Figure 1.6). This allowed us to observe how the studied sites are distributed according to their benthic foraminifera content, and subsequently infer the dominant environmental conditions influencing such distribution. The used data frame contained 43 taxonomical units and shows three main groups (Figure 1.6a), the first

one divided into two subgroups (1a – blue triangles and 1b – white triangles in Figure 1.6a-b). Groups are distributed following water depth differences (Figure 1.6b). The first group contains the deepest core tops from the SE Atlantic, 1b groups the deepest sites (T89-12, T89-13, T89-19, T89-25), and 1a groups cores between 3,092 and 4,164 m. Group 2, clusters sites from the NE and SE Atlantic between 1,080 to 2,964 m and Group 3 contains sites from 200 to 868 m water depth. Sites differentiation observed in the NMDS analysis, is also related to specific environmental conditions: Group 3 is characterized by low oxic and eutrophic conditions (see infaunal foraminifera percentages contribution in NMDS1 axis); Group 2 by eutrophic and higher oxygen levels; and Group 1, by high oxic and mesotrophic environments (1a), and mesotrophic to oligotrophic conditions (1b).

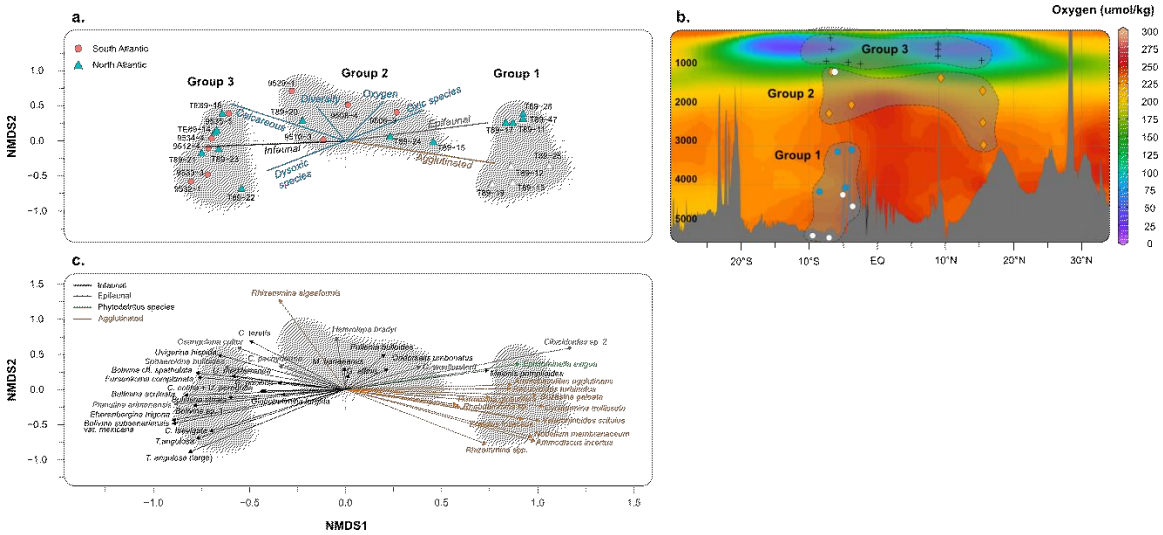

Figure1.6 Non-metrical multidimensional scaling of the most abundant benthic foraminifera of the Eastern North Atlantic. a. NMDS showing the distribution of the studied sites, along with the related environmental parameters (in blue); **b.** NMDS Groups distribution in depth in the eastern Atlantic showing modern dissolved oxygen concentration conditions, hydrographic data plotted using Ocen Data View (Schlitzer, Reiner, Ocean Data View, https://odv.awi.de, 2022) with data from GLODAP version 2 (Lauvset et al., 2022); **c.** NMDS showing the distribution of the benthic foraminifera species for each assigned group, differentiating infaunal (black), epifaunal (gray), phitodetritus feeders (green) and agglutinated (orange) foraminifera.

These environmental variations in depth have provided the conditions for different foraminiferal assemblages to thrive in benthic ecosystems (Figure 1.6c). Group 3 is represented by a predominantly calcareous association, dominated by infaunal *Uvigerina peregrina, Bulimina aculeata, Bolivina* sp. 1, *Cassidulina laevigata, Bulimina striata, Uvigerina mediterranea* (average relative abundances between 5 – 8.8 %). Group 2 is also calcareous, and dominated by *Melonis barleeanus* (average 11.1 %), and *U. peregrina, G. affinis* and *U. mediterranea* (average between 5.5 – 9.6%). Group

1 is characterized by higher agglutinated foraminifera, especially in subgroup 1a with *Rhizammina* spp., *Eratidus foliaceus, Cyclammina trullissata* (average relative abundances from 10.7 – 19.5 %). Subgroup 1b is dominated by calcareous *Cibicidoides* sp. 2c (average 17.4%) and agglutinated *Recurvoides turbinatus* (average 11.7%). Also important in subgroup 1 is the high abundance of phytodetritus feeder *Epistominella exigua* (average 7.9%).

4. Discussion and Conclusions

Our results show that benthic foraminifera distribution in the eastern North Atlantic is heavily influenced by water depth, as previously observed with the studies of Lutze and Coulbourn (1980) and Haake (1980). From the identified assemblages, the southern mid – lower slope *U. peregrina* province of Lutze and Coulbourn (1980) could partially coincide to this study's Group 3. The zones observed by Haake (1980) were not seen in the dead assemblages of this study. However, these studies were made on samples collected around 1971, while our southern site samples were recovered during 1989 and the northern sites samples during 2005. This 18- and 34-year difference could imply shifts in the benthic foraminifera distribution off the NW African Margin, but more detailed studies would be necessary to confirm this hypothesis. In addition, this could also bias our own data as the southern samples were collected 16 years earlier, however, the groups identified here are relatively consistent in the NMDS analyses.

A significant shift in the benthic foraminifera assemblages in our data is observed at 1,200 m water depth. The predominant calcareous assemblage at water depths below 1,200 m in both areas, shift to a more agglutinated benthic foraminifera assemblage especially in the SE Atlantic at water depths > 1,200 m. This coincides with a shift from low oxic to suboxic – high organic matter bottom water conditions (< 1,200 WD) to high oxic – moderate organic matter concentrations at deeper settings (>1,200 m WD). Such differentiation was noted by Jorissen et al. (1998) who suggested that at water depths above 1,200 m benthic foraminifera are controlled by organic matter from the upwelling areas. This is compatible with our findings, showing that at sites with water depths shallower than 1,200 m infaunal benthic foraminifera are more abundant

(eutrophic conditions), while at deeper conditions they decrease (mesotrophic and oligotrophic conditions).

Bottom water environmental conditions in the NE Atlantic are predominantly eutrophic (Figure 1.5f) and vary from low oxic at depths shallower than 1200 m and become high oxic (Figure 1.5d) in deeper settings (1,500 to 3,000 m water depth). For the SE Atlantic three types of environments are recognized: (1) eutrophic – low oxic (2) mesotrophic – high oxic; and (3) oligotrophic – high oxic. These environments are distributed in depth: (1) for core tops < 1200 m water depth; (2) for core tops from 1900 – 4600 m water depth; and (3) at around 5300 m water depth (Figure 3c and 3e). An additional control in the oxic conditions in the eastern Atlantic off NW Africa is set by the eastern Atlantic Oxygen Minimum Zones (e.g. Stramma and Schmidtko, 2021), and shallower sites located near these zones (Group 3 in Figure 1.6b) in low oxic conditions (< 130 µmol/kg – 2.9 ml/l), are represented by abundant stress species *Uvigerina peregrina, Bulimina aculeata, Bolivina* sp. 1, *Cassidulina laevigata, Bulimina striata, Uvigerina mediterranea*.

The large amount of available information about Atlantic benthic foraminifera environmental preferences, as well as the marked differences observed in their distribution, shows the potential of paleoceanographic studies based on detailed taxonomic and quantitative analyses of existing sedimentary archives. These studies will provide new relevant information to fill the gaps in our knowledge about unexplored questions like how tropical subsurface circulation is related to Atlantic Meridional Overturning Circulation (AMOC) changes, or what are the impact of AMOC slowdown is on benthic ecosystems.

Chapter 2: Enhanced ventilation of Eastern North Atlantic Oxygen Minimum Zone with deglacial slowdown of Meridional Overturning

In review at *Nature Communications.* Adjusted to fit the format style.

https://dx.doi.org/10.21203/rs.3.rs-4083170/v1

Sofía Barragán-Montilla[1], Heather J. H. Johnstone[1], Stefan Mulitza[1], Dharma A. Reyes Macaya[1,2,3], Heiko Pälike[1]

[1]MARUM – Center for Marine Environmental Sciences and Department of Geosciences, University of Bremen, Bremen, 28359, Germany
[2]Lyell Centre, Heriot-Watt University, Edinburgh, UK
[3] Millennium Nucleus UPWELL, Concepcion, Chile

Abstract

The eastern Tropical North Atlantic Oxygen Minimum Zone (ETNA OMZ) sustains unique marine ecosystems off northwestern Africa. One of the key controls of the ETNA OMZ is ventilation driven by the subsurface ocean circulation of the Atlantic subtropical gyres. However, how this shallow circulation interacts with changes in the strength of the Atlantic Meridional Overturning Circulation (AMOC) remains unclear. Here, we present a new deglacial and high-resolution paleo-oxygenation record (GeoB9512-5, 793 m water depth) from the low oxic waters of the margin of ETNA OMZ, that registers more strongly oxygenated periods during the Last Glacial Maximum (LGM), two parts of the Heinrich Stadial 1 (HS1), and the latter part of the Younger Dryas (YD). We show that steeper meridional temperature gradients during HS1 and YD with AMOC slowdown intensified the subsurface subtropical gyre circulation and the oxygen supply to the ETNA.

Graphic Abstract

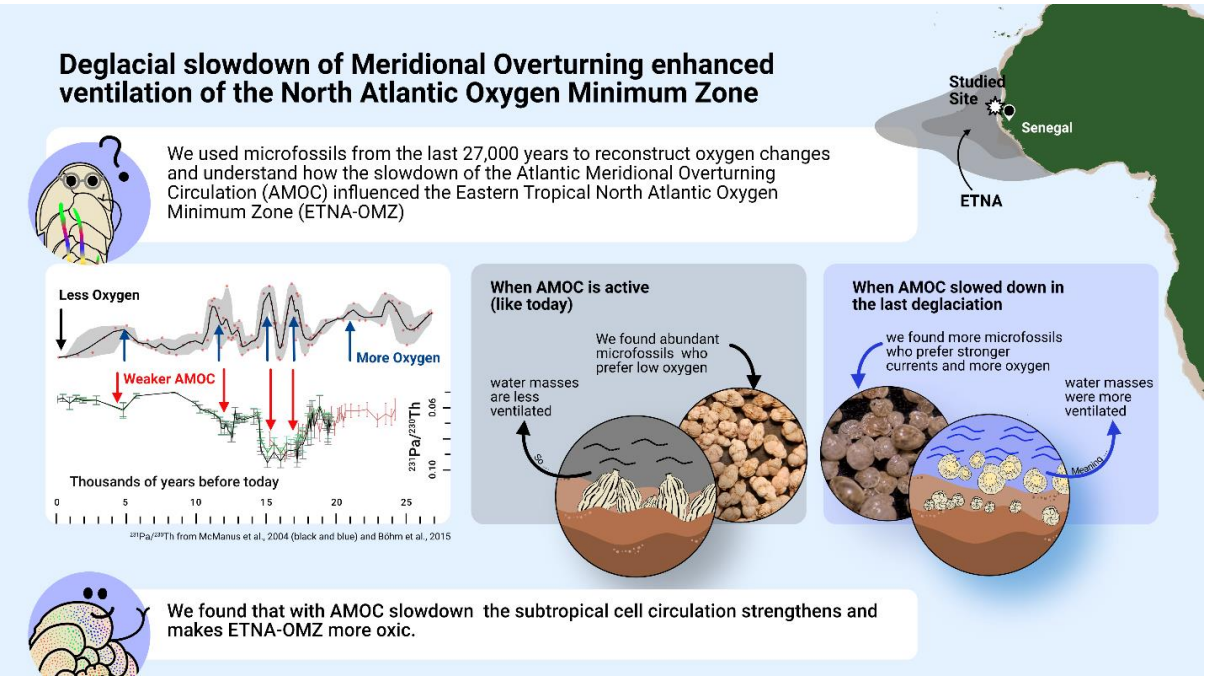

1 Introduction

Oxygen Minimum Zones (OMZ) are found beneath highly productive upwelling systems that sustain unique marine ecosystems (e.g., Zhang et al., 2010; Pauly and Dimarchopoulou, 2022) in the world oceans (Bruno et al., 2018, Stramma et al., 2008; Stramma et al., 2012; Gilly et al., 2013). The diversity of these ecosystems depends, among other factors, on the oxygen supply, which has decreased in the last decades partly due to global ocean warming associated with anthropogenic greenhouse gas emissions (Schmidtko et al., 2017; Gilbert, 2017). Another concern in a warming world are projections that the large-scale deep circulation of the ocean, the Atlantic Meridional Overturning Circulation (AMOC), could slow down in the foreseeable future (e.g. IPCC, 2013; Liu et al., 2020; Zhang et al., 2019; Caesar et al., 2018), as shown consistently in all Phase 6 models from the Coupled Model Intercomparison Project (CMIP6) (Weijer et al., 2020). However, the relationship between AMOC strength and subsurface ventilation has not been studied so far.

Since the available instrumental oxygen records at any ocean depth date only from the 1970s (Moore, 1984), our knowledge must rely on marine paleo-oxygenation records. One approach comes from detailed benthic foraminifera taxonomic analyses

used to infer changes in ocean oxygen concentrations (Kaiho, 1994; Kranner et al., 2022). Changes in this parameter actively modify benthic organisms' physiological responses and are registered as shifts in biodiversity and distribution patterns of benthic foraminifera (e.g., Zhang et al., 2010; Gilly et al., 2013; Portner et al., 2017; Hanz et al., 2019). Benthic foraminifera are a microfossil and extant group that makes up around 50% of the eukaryotic biomass in modern oceans (Gooday et al., 1992), and are one of the most diverse hard-shelled microorganisms in the ocean (Sen Gupta, 1999). Their distribution mostly depends on seafloor food and oxygenation (Altenbach et al., 2012; Bernhard and Sen Gupta, 1999; Jorissen et al., 1995; Murray, 2006, 1991; Southward et al., 2003), and since the environmental preferences of several species are well documented, environmental models based on benthic foraminifera assemblages hold promise to investigate oceanic oxygen variability, particularly in OMZs (Erdem et al., 2020; Moffit et al., 2014; Tetard et al. 2017; Sharon et al., 2021).

In this study we reconstructed the deglacial paleo-oxygenation trends of the suboxic (< 1.5 ml/l) middle depth (300 - 700 m water depth) OMZ (Brandt et al., 2010; Brandt et al., 2015; Karstensen et al., 2008) of the eastern tropical North Atlantic (ETNA). We used the sedimentary record of gravity core GeoB9512-5, retrieved off the coast of Senegal in northwestern Africa (15°20'13.20''N, 17°22'1.20''W, 793 m water depth, Figure 1) (Mulitza et al., 2005). This site is located in low oxic conditions at the margin of the OMZ (Figure 1b), making it a sensitive record of oxygen changes during the last deglaciation when AMOC strength changed. These changes included periods of AMOC decline, consistently registered in the sedimentary records of the Atlantic Ocean during the Heinrich Stadial 1 (HS1, ~ 17.6 – 14.7 ka BP) and Younger Dryas (YD, ~ 12.6 – 11.8 ka BP) (e.g. Böhm et al., 2015; Gherardi et al., 2005; McManus et al., 2004; Ng et al., 2018). These weak AMOC periods are also synchronous with meridional shifts in the position of the southern and northern Atlantic subtropical gyres (Portilho-Ramos et al., 2017; Pinho et al., 2021; Reißig et al., 2019) that influence subsurface circulation and central water masses in the tropical Atlantic. For this reason, the last deglaciation in the eastern North Atlantic provides the opportunity to investigate how AMOC strength changes are related to the subtropical cell.

The new paleo-oxygenation record presented here, is based on a stratigraphic framework modelled with 16 Accelerator Mass Spectrometry radiocarbon dating of planktic foraminifera (Figure 4), and on a detailed taxonomic and quantitative analyses of the benthic foraminifera content in this site. Using the Enhanced Benthic Foraminifera Oxygen Index (EBFOI, Kranner et al., 2022), that allows to quantitatively estimate the dissolved oxygen concentration of the sea floor-habitat, we reconstructed the oxygen changes at our site during the last 27,000 years. We show changes in ETNA oxygenation during times of documented AMOC slowdown (HS1 and YD) and provide new insights into the relationship between subtropical cells circulation and AMOC changes in the tropical Eastern North Atlantic.

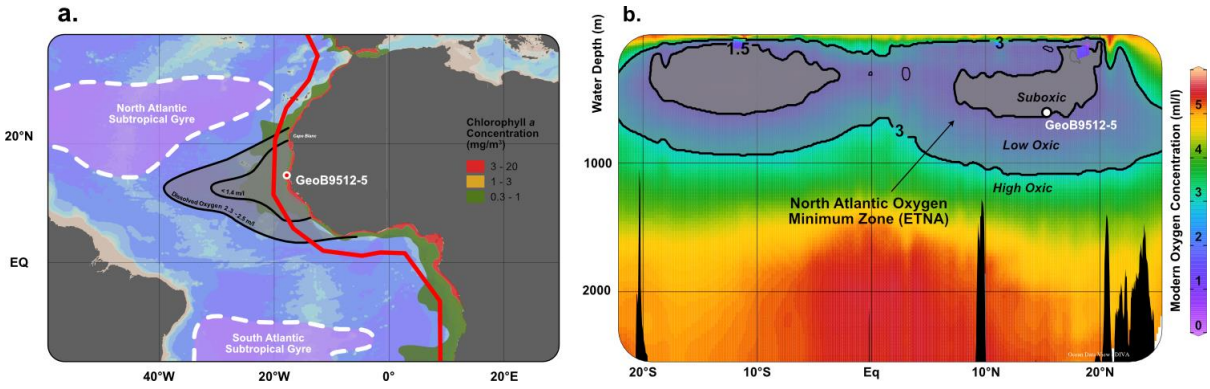

Figure 2.1 GeoB9512-5 location in the Eastern Tropical Atlantic Oxygen Minimum Zone. a. Geographic location of gravity core GeoB9512-5 (15°20'13.20''N/17°22'1.20''W, 793 m water depth), Atlantic subtropical gyres and the Eastern Tropical Atlantic Oxygen Minimum Zone (gray shadowed) (Brandt et al., 2015; Pelegrí and Peña-Izquierdo, 2015 and Poole and Tomczak, 1999). Upwelling areas indicated with the Approximate Chlorophyll a concentration (mg/m3) zones based on the Aqua-Modis data (4 km resolution, in November 2019) (https://oceancolor.gsfc.nasa.gov/); b. GeoB9512-5 location and modern configuration of the Tropical Eastern North Atlantic Oxygen Minimum Zone in depth (shadowed). Plotted with Ocean Data View (Schlitzer, 2023), data from WOA 2018 (Boyer et al., 2018; García et al., 2019).

2 Results and Discussion

Our record shows dissolved oxygen concentrations (BWOx in Figure 2d) of between 1.7 and 4.8 ml/l (EBFOI between 6 and 78, Figure 2d). The record is characterized by an alternation of low oxic and high oxic conditions (Figure 2d), as seen by the variations of the proportions of oxic, suboxic and dysoxic species used in the EBFOI calculations (Figure 2c). The relative abundance of stress species (Figure 6), which

are foraminifera species better adapted to environments of reduced oxygen (e.g. Bernhard and Sen Gupta, 1999), are consistent with these interpretations as they are present in average percentages over 50 % in low oxic intervals, and under 50 % in high oxic intervals.

Oxygen reconstruction shows high oxic conditions (dissolved oxygen concentrations >3 ml/l) at our site at the ETNA OMZ margin from the onset of the record (~ 27 ka BP), through most of the last glacial (Figure 2d) until 18.9 ka BP. This period was interrupted only by one low oxic interval centered on 25.1 ka BP. Even higher values (average 4.2 ml/l) were recorded between 24 - 23.5 ka BP (Supplementary Information 1). The deglaciation was characterized by abrupt transitions between high oxic and low oxic (< 3 ml/l) conditions. Low oxic conditions after 18.9 ka BP were followed by a rapid increase in oxygen during Heinrich Stadial 1 (HS1), with two transient oxygen peaks (1) of 4.4 ml/l around 17.3 - 17.2 ka BP and (2) of 4.8 ml/l at 16.8 ka BP, which represents the highest oxygen values of the record. Between 16.2 and 15.8 ka BP there was a return to low oxic conditions within HS1, followed by another high oxic period (4.6 ml/l) between 15.2 - 14.8 ka BP marking the end of HS1.

Oxygen dropped below 3 ml/l at 14.4 ka BP at the start of the Bølling–Allerød (B-A) and these low oxic conditions continued through this period. A transient return to high oxic levels (3.3 ml/l) was recorded at 13.1 ka BP, and between 12.2 ka and 11.9 ka BP (average 3.7 ml/l) during the YD. High oxic conditions were recorded at the onset of the Holocene when the final peak of 4.2 ml/l is registered between 11.3 and 11.1 ka BP. The last high oxic period (on average 3.1 ml/l) occurred between 5 and 4.2 ka BP, and was followed by the lowest oxygen concentrations in the record of 1.8 ml/ between 0.7 and 0.2 ka BP. This compares well with modern measured values of 2.01 ml/l at the site (Lauvset et al., 2016; Key et al., 2015).

The low oxic conditions are linked to a high abundance infaunal benthic foraminifera (Figure 6a) and stress species (Figure 6b), indicating eutrophic and mesotrophic (moderate to high organic matter) and low oxygen conditions respectively (Supplementary Information 3.1), as seen in this area today. While opposing trends in oxygen and organic matter would be consistent with productivity induced changes in

remineralization (Wyrtki, 1962; Kurian et al., 2006) this does not explain the oxygen changes at our site. Periods of extremely high productivity recorded off NW Africa during the AMOC slowdowns of HS2, HS1 and the YD (Bradtmiller et al., 2016; Zarriess and Mackensen, 2010) coincide with high oxic periods in the GeoB9512-5 record. Furthermore, good calcite preservation throughout the core also suggests no periods of enhanced remineralization, at least at the seafloor. Therefore, we infer that the main control on the observed oxygen variability is a response to deglacial ventilation changes driven by ocean circulation.

The association between oxic intervals at our site and AMOC perturbations (e.g. McManus et al., 2004) aligns with observations that the major shifts in ocean circulation are reflected in altered ventilation throughout the global ocean (Schmittner et al. 2007). Although the spatial extent of the OMZ in the east Atlantic cannot be inferred from a single site, our data supports findings of enhanced ventilation in the upper ocean (< 1 km), synchronous with diminished ventilation of deepwater masses during periods of reduced AMOC (Oliver et al., 2010; Skinner et al., 2021).

During cold periods, reduced northward heat transport by AMOC results in a higher pole to equatorial temperature gradient due to cold Atlantic SSTs, strengthening the Hadley cell and the subtropical cell (McGee et al., 2018; Shakun and Carlson 2010). Changes in wind stress were even more intense during the deglaciation. In the HS1 and YD the deep AMOC cell was weakened, while active AMOC is recorded during the B-A and Holocene (Figure 2a; Böhm et al., 2015; McManus et al., 2004). A weaker AMOC during the HS1 and YD, supposed a limited transport of warm waters from the subtropical to the subpolar gyre of the North Atlantic, leading to a steeper meridional surface temperature gradient estimated here from the sea surface temperature difference between North Atlantic Site SU81-18 (Bard et al., 2000) and South Atlantic site M35003-4 (Rühlemann et al., 1999) (Figure 2b and Figure 3e). Such steepening enhanced easterly winds strength (Mulitza et al., 2008), and accelerated wind circulation over NW Africa strengthening the North Atlantic subtropical cell circulation, where more water pumped into the thermocline increased ventilation at intermediate depths. A stronger and more southern North Atlantic subtropical gyre (Reißig et al., 2019), allowed better ventilated NACW to penetrate further south into the NW African

margin during the HS1 (Huang et al., 2012) and to a lesser extent during the YD. This higher NACW contribution and the intensified ventilation at the subtropical Atlantic, is compatible with our paleo-oxygenation record that shows high oxic and well-ventilated waters during most part of the HS1 and YD, contrasting the low oxic - poorly ventilated conditions of the B-A and Holocene (Figure 2e). Perhaps most relevant to future projections of AMOC strength (e.g. IPCC, 2013; Liu et al., 2020; Zhang et al., 2019; Caesar et al., 2018), is that the slight decrease in AMOC strength between 5.5 - 3 ka (Figure 2) is also associated with a brief oxic interval.

Increased oxygen concentrations between 15.7 and 14.8 ka BP in HS1, high oxic conditions (3.3 ml/l) at 13.1 ka BP, and another peak from 11.3 to 10.9 ka BP at the end of the YD, are temporarily close to transient appearances of subpolar foraminifera species at 14.7, 13.1 and 11.5 ka BP at 38°N, at what is now the northern boundary of the subtropical gyre (Repschläger et al., 2015). These are explained as the presence of subpolar water encroaching south during intense cold intervals. This water mass is one component of Subpolar Mode Water (SPMW), which forms today ~50-63 °N, from a mix of subpolar water and North Atlantic Current water from the subtropical gyre, the proportions of each being controlled by subpolar gyre dynamics (McCartney and Talley, 1982). SPMW is entrained to ENACW which flows southwards along the NW African coastline (Keffer, 1985). Oxygen pulses in our record at these times may reflect increased oxygen content in subpolar water during cold intervals as well as an increase in the proportion of subpolar water contributed to ENACW.

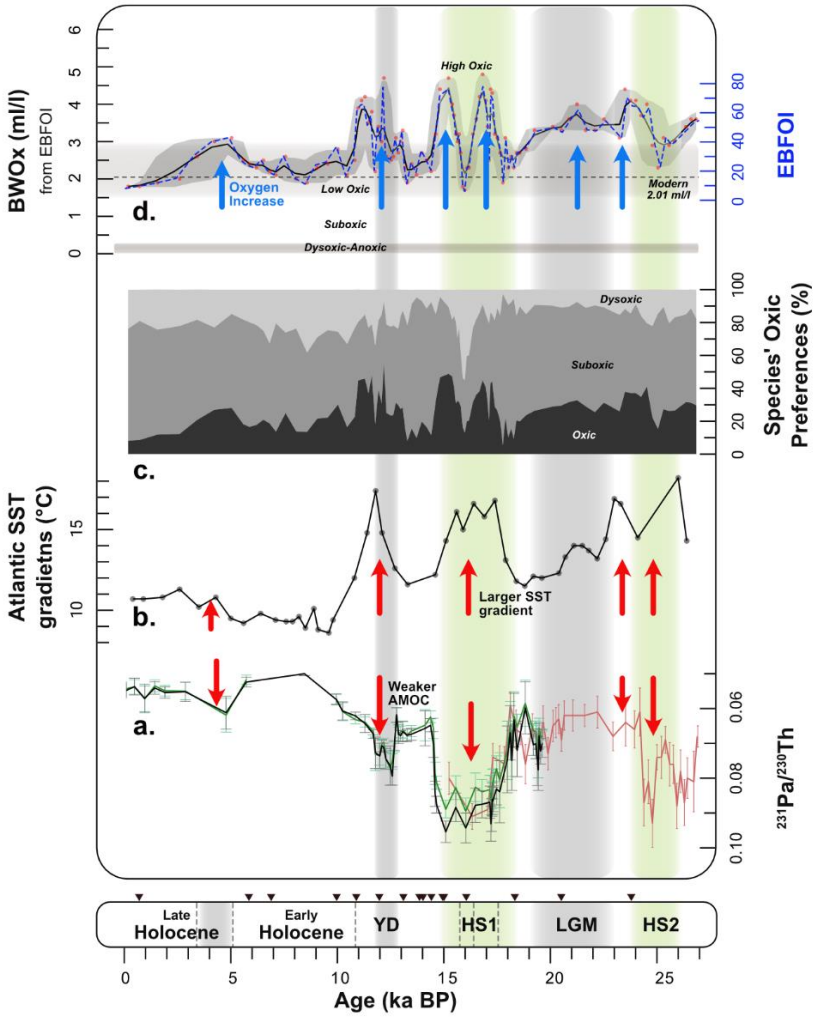

Figure 2.2 GeoB9512-5 deglacial paleo-oxygenation record and Atlantic circulation proxies. a. Sedimentary $^{231}Pa/^{230}Th$ taken from McManus et al., 2004 (Bermuda Rise, black and green curves), and Böhm et al., 2015 (deep western North Atlantic, red curve); **b.** Atlantic Sea Surface Temperature (SST) gradient estimated by extracting the SST of North Atlantic Site SU8118 (37.76 N, 10.18 W; Bard et al, 2000) to the SSTs South Atlantic site M35003-4 (12.09 N, 61.243 w; Rühlemann et al., 1999); **c.** GeoB9512-5 relative abundances of oxic, suboxic and dysoxic benthic foraminifera species; **d.** GeoB9512-5 bottom water dissolved oxygen concentration record (BWOx – ml/l) calculated using the Enhanced Benthic Foraminifera Oxygen Index (EBFOI in blue), shaded area corresponds to the 95% envelope and red dots is the raw data. **Key Climate events:** Heinrich Stadial 2 (HS2); Last Glacial Maximum (LGM); Heinrich Stadial 1 (HS1); Bølling–Allerød (B-A); Younger Dryas (YD). Triangles in age axis indicate radiocarbon ages.

Another interesting aspect of our record is the four phases of HS1 (Figure 3, Age axis). These are defined from transient changes in oxygen concentrations (Figure 3a) are consistent with rapid changes in benthic foraminifera distribution and diversity, hinting

at rapid adaptations to the unstable conditions of the HS1. These changes are characterized by a high oxic double-peak pattern (Figure 3a) centered around 16.8 and 15.2 ka BP respectively, and seem to be (within dating uncertainty) temporarily related to the changes in AMOC strength (Figure 3b-c and 3d) during HS1 registered by Ice-rafted Debris (IRD) and Magnetic Susceptibility (MS) (Figure 3b and 3c) and by other proxy records in the Atlantic (e.g. Huang et al., 2019; Novello et al., 2017; Qiu et al., 2022). These AMOC changes during HS1 events are also recorded as a double-peak pattern and suggests there were two distinct meltwater pulses during the HS1 related to different stages of AMOC slowdown (e.g. Bard et al., 2000; Hodell et al., 2017). The double-peaked structure resembles the HS1 double-peak of high oxic conditions identified in our record (Figure 3a, blue arrows) and suggests that these two oxygen peaks are potentially related to episodes (Figure 3b-c) of AMOC decline (Figure 3d).

During the B-A and Holocene times, as AMOC strengthens, the subtropical gyres moved north similar to their modern position (Portilho-Ramos et al., 2017; Pinho et al., 2021; Reißig et al., 2019), in a modern - like oceanographic configuration compatible with the low oxic conditions registered by benthic foraminifera in our site.

Our data show that a decline in AMOC strength increases ventilation of the Eastern Tropical Atlantic Oxygen Minimum Zone, due to steeper latitudinal temperature gradients that intensify the Northeast trade winds and the subtropical cell of the North Atlantic. This implies that the future of the eastern North Atlantic OMZ is critically dependent on the state of the AMOC and that the projected future decline of the AMOC might counteract the current de-oxygenation trend due to global warming. The eastern South Atlantic OMZ, however, might respond differently as South Atlantic warming due to the bipolar seesaw can weaken the South Atlantic gyre circulation with AMOC slowdown.

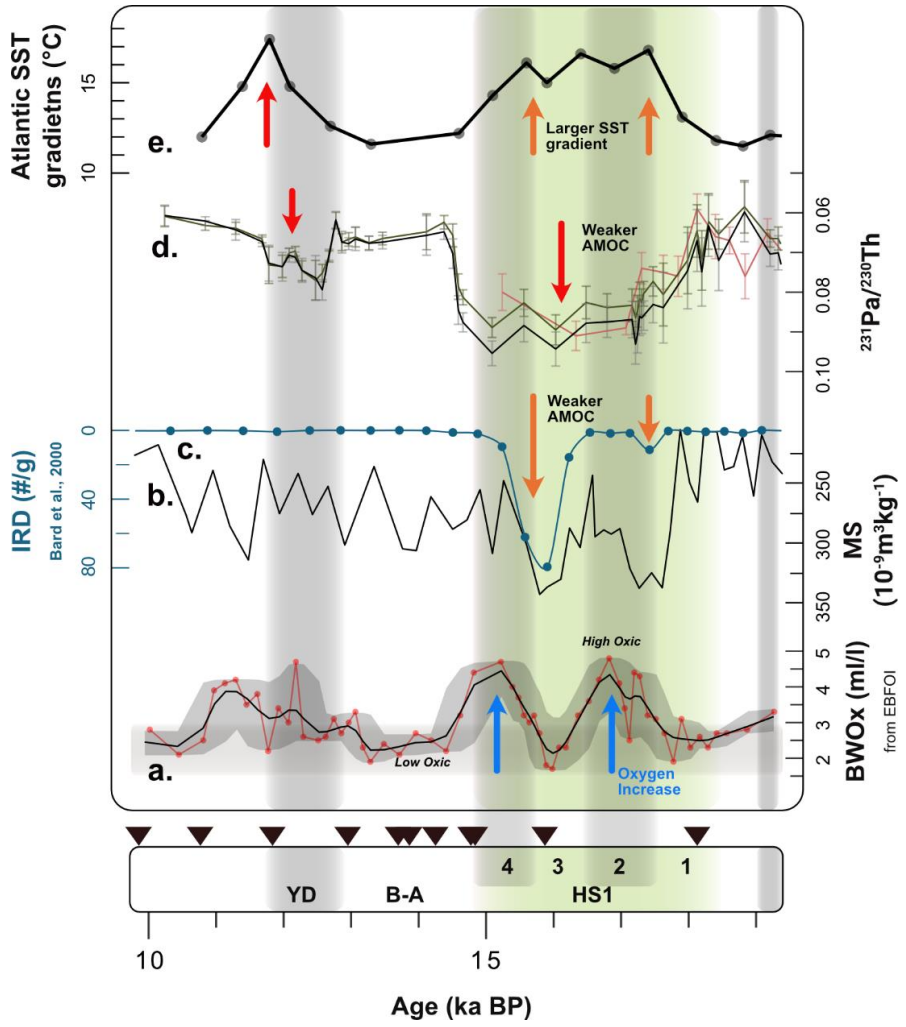

Figure 2.3 GeoB9512-5 benthic foraminifera distribution and diversity, paleo-oxygenation record and Atlantic circulation proxies. a. GeoB9512-5 Relative abundances of most abundant benthic foraminifera species during HS1**; b.** GeoB9512-5 benthic foraminifera diversity measured by the Fisher Alpha Index; **c.** GeoB9512-5 bottom water dissolved oxygen concentration record (BWOx – ml/l) calculated using the EBFOI, ; shaded are is 95% uncertainty envelope and red dots is the raw data; **d.** Magnetic Susceptibility (MS) and **e.** Ice-rafted detritus (IRD) from site SU8118 (37.76 N, 10.18 W; Bard et al., 2000); **f.** Sedimentary $^{231}Pa/^{230}Th$ taken from McManus et al., 2004 (Bermuda Rise, black and green curves); and Böhm et al., 2015 (deep western North Atlantic, red curve); **g.** Atlantic Sea Surface Temperature (SST) gradient estimated by extracting the SST of North Atlantic Site SU8118 (37.76 N, 10.18 W; Bard et al., 2000) to the SSTs South Atlantic site M35003-4 (12.09 N, 61.243 w; Rühlemann et al., 1999). **Key Climate events:** Heinrich Stadial 2 (HS2); Last Glacial Maximum (LGM); Heinrich Stadial 1 (HS1); Bølling–Allerød (B-A); Younger Dryas (YD). Triangles in age axis indicate radiocarbon ages.

3 Methods

3.1 Chronology and Age model

The downcore ages from site GeoB9512-5 (Figure 5) were modelled using 16 AMS radiocarbon ages from planktic foraminifera (G. sacculifer-G. bulloides) samples (Barragán-Montilla and Mulitza, in review, Barragán-Montilla, 2024). The samples were measured at the MICADAS laboratory at the Alfred Wegener Institute (AWI)-Bremerhaven (Mollenhauer et al., 2021). A continuous age model was calculated with the R script BACON (Blaauw and Christen, 2011) version 2.5.5 and the Marine20 calibration curve (Heaton et al., 2020), to obtain a median calendar age and uncertainty for each sampled depth. Median calendar ages were also calculated for sedimentary and uncalibrated Fe/Ca and Ti/Ca from XRF analysis (Völpel et al., 2019). Peaks in these ratios are used as an indicator of continental aridity that occur synchronously in geographically restricted areas (Völpel et al., 2019) like those which occurred during Heinrich Stadials (HS) and Younger Dryas (YD). In this study, we used Fe/Ca and Ti/Ca to calibrate the timing of HS2, HS1 and YD in our site (Figure 4). The resulting age model shows a deglacial sequence deposited in the last 27,000 years with no age reversals. The GeoB9512-5 record, includes a continuous and undisturbed sequence of the key climatic periods (Figure 4) Heinrich Stadial 2 (HS2), Last Glacial Maximum (LGM), Heinrich Stadial 1 (HS1), Bølling–Allerød warming (B-A), Younger Dryas (YD), and the Holocene Climatic Optimum (HCO), that divides the early Holocene from the Late Holocene.

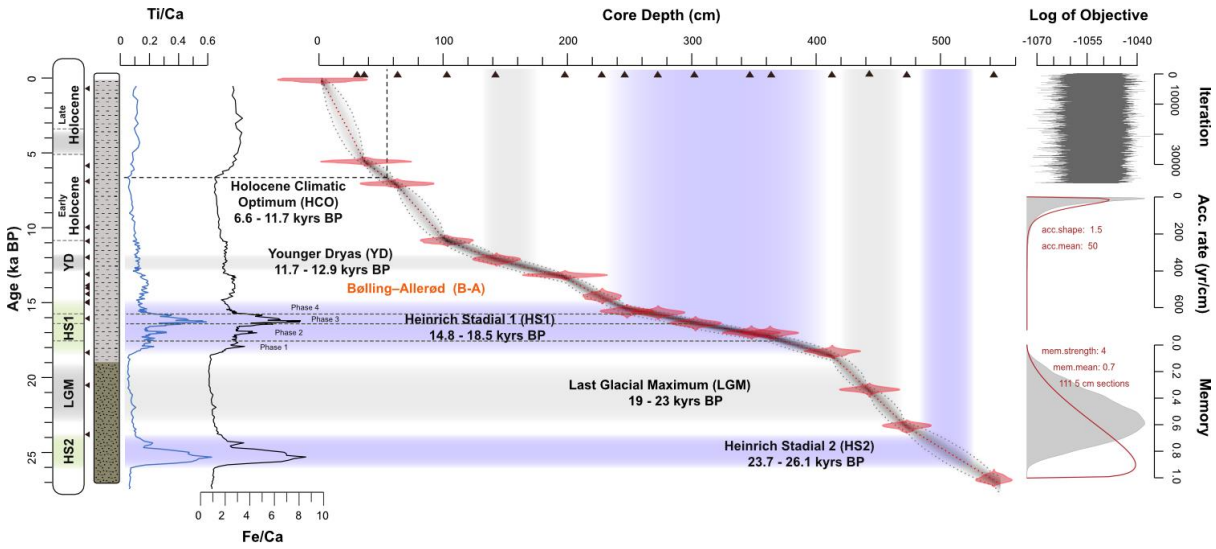

Figure 2.4 GeoB9512-5 age model with the key climatic events in the last 27,000 years. Downcore median calendar ages modelled using 16 radiocarbon ages (triangles in the Core Depth axis) in the Bacon Package (Blaaw and Christen, 2011) with the Marine20 calibration (Heaton et al., 2020). Heinrich Events and Younger Dryas were visually calibrated using Fe/Ca and Ti/Ca (Völpel et al., 2019), with the new modelled ages.

3.2 Oceanographic setting

To identify the water masses in our site, we used a T-S diagram showing GeoB9512-5 situation (Supplementary Figure 3.5a), along with the existing available references. The studied gravity core GeoB9512-5 (15°20'13.20'N, 17°22'1.20'W, 793 m water depth, Figure 1) (Mulitza et al., 2005). The site is situated in the "shadow zone" between the north and south Atlantic subtropical gyres (Figure 1a), where older water masses with lower renewal rates (Poole and Tomczak, 1999) lead to poorly ventilated regions that make up ETNA (gray area in Figure 1a). At our site, modern low oxygen values of 2.01 ml/l are typical of the OMZ margin (Figure 1b), and bottom water temperatures and salinities are approximately 6.9°C, and ~ 34.8 (Figure 5a) respectively (Lauvset et al., 2016; Key et al., 2015). Such conditions position GeoB9512-5 in the mixing area of of the North Atlantic Central Water (NACW) and Eastern South Atlantic Central Water (ESACW) (Figure 5) (Poole and Tomzak, 1999).

The South Atlantic Central Water flows northward from the south Atlantic subtropical gyre (Liu and Tanhua, 2021), where coincidence of wind-driven downwelling and seasonal buoyancy drives waters into the thermocline (Slowey and Currey, 1992). In the Cape Verde area, this water mass is present as Western and Eastern South Atlantic Central Waters (Figure 5b, WSACW and ESACW respectively). The WSACW is differentiated by its formation area in the western South Atlantic, and even though it is mainly concentrated in the western Atlantic it reaches the eastern North Atlantic to some extent (Liu and Tanhua, 2021). The ESACW is a nutrient rich and poorly oxygenated water mass formed at the mixing area of the Agulhas Current and the South Atlantic Current south of Africa (Poole and Tomczak, 1999; Liu and Tanhua, 2021).

Above the SACW masses, the North Atlantic Central Water (NACW) flows southward and is represented in our area by the Eastern North Atlantic Central Water (ENACW, Figure 6b and c), bringing more oxic - better ventilated waters. The ENACW is formed

in the inter-gyre region (between 39-48°N) and its core is located at around 500 m water depth (Liu and Tanhua, 2021). At the Eastern Tropical North Atlantic Oxygen Minimum Zone, the low oxic - suboxic conditions are set by the northward flow of poorly ventilated ESACW waters and the southward flow of better ventilated ENACW (Brandt et al., 2015; Liu and Tanhua, 2021), and site GeoB9512-5 is located in the low oxic lower end of this OMZ.

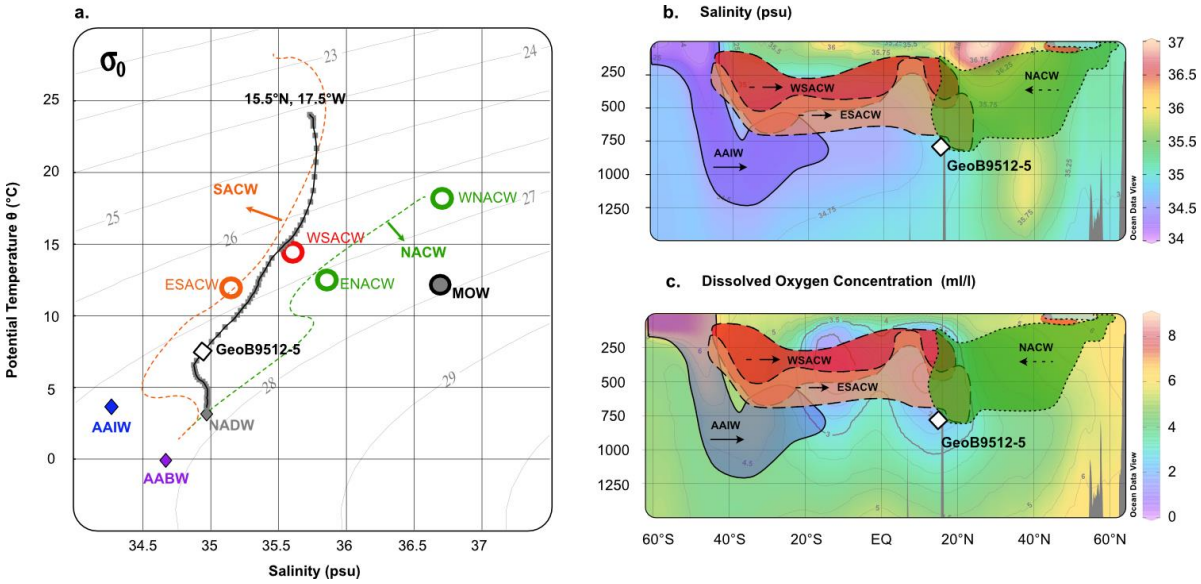

Figure 2.5 Central and Intermediate water masses in the studied site GeoB9512-5 - white diamond- (15°20'13.20'N, 17°22'1.20''W, 793 m water depth). **a.** Temperature-Salinity diagram showing the water masses sources in the eastern North Atlantic (adapted from Poole and Tomczak, 1999; and Liu and Tanhua, 2021), dashed lines represent the transition of North and South Atlantic Central Waters (NACW and SACW respectively in the eastern North Atlantic) (Tomczak and Godfrey, 1994); **b.** Salinity (Schlitzer, 2023; Boyer et al., 2018; Zweng et al., 2019) showing the eastern north Atlantic central water Masses distribution in the studied area (following Poole and Tomczak, 1999); **c.** Dissolved oxygen concentration (ml/l) (Schlitzer, 2023; Boyer et al., 2018; García et al., 2019) and modern extension in depth of the North Atlantic Oxygen Minimum Zone (ETNA).

3.3 Benthic foraminifera taxonomy and quantitative analyses

Sediments samples were (1) washed through a 63 µm sieve with deionized water; (2) dried in an oven at temperatures ~ 45°C for no more than 24 hours; and (3) dry sieved through 63, 125, 150 and 250 µm stored and labelled in glass vials. The >150 um was analyzed to extract benthic foraminifera (for taxonomic, quantitative, and geochemical analyses) and planktic foraminifera (for radiocarbon dating).

Paleoenvironmental and paleo-oxygenation results and interpretation are based on the taxonomical identification and the quantitative analyses of at least 200 -250 benthic foraminifera from 100 samples from core GeoB9512-5 (Barragán-Montilla, in review). Benthic foraminifera were morphologically separated, and the taxonomical identification was made to a specific level in most cases. Genera were determined following Loeblich and Tappan (1987), and species were identified based on multiple references (Jones and Brady, 1994; Holbourn et al., 2013; Morkhoven et al., 1986). The updated taxonomy was finally revised using the online database WoRMS (Supplementary Information 3.2). Digital images of the benthic foraminifera extracted during this study were taken at the Microscopy Laboratory at MARUM, using a Keyence VHX 6000 digital microscope with a motorized stage (Supplementary Information 3.3, here as Appendix 2.2).

3.4 Paleo-Oxygenation reconstruction and uncertainties

The paleo-oxygenation record presented here was inferred using the Enhanced Benthic Foraminifera Oxygen Index (EBFOI) that offers the best approximation to dissolved paleo-oxygen concentrations in marine deposits (Kranner et al., 2022). The terms high oxic (> 3 ml/l), low oxic (1.5 – 3 ml/l), suboxic (0.3 – 1.5 ml/l), dysoxic (0.1 – 0.3 ml/l) and anoxic (0 ml/l) are used here as described by Kranner et al. (2022). In our record, EBFOI relies in multiple species, and of the 156 taxonomic units identified on our site, 129 (including all abundant species) have information about their oxygen preference (Supplementary Information 3.2). We also assessed the accuracy of our reconstruction comparing our paleo-oxygenation record with downcore relative abundances of stress species (Figure 6b), that are better adapted to oxygen depleted environments (Bulimina, Bolivina, Cassidulina, Melonis, Fissurina, Globobobulimna; e.g. Southward et al., 2003).

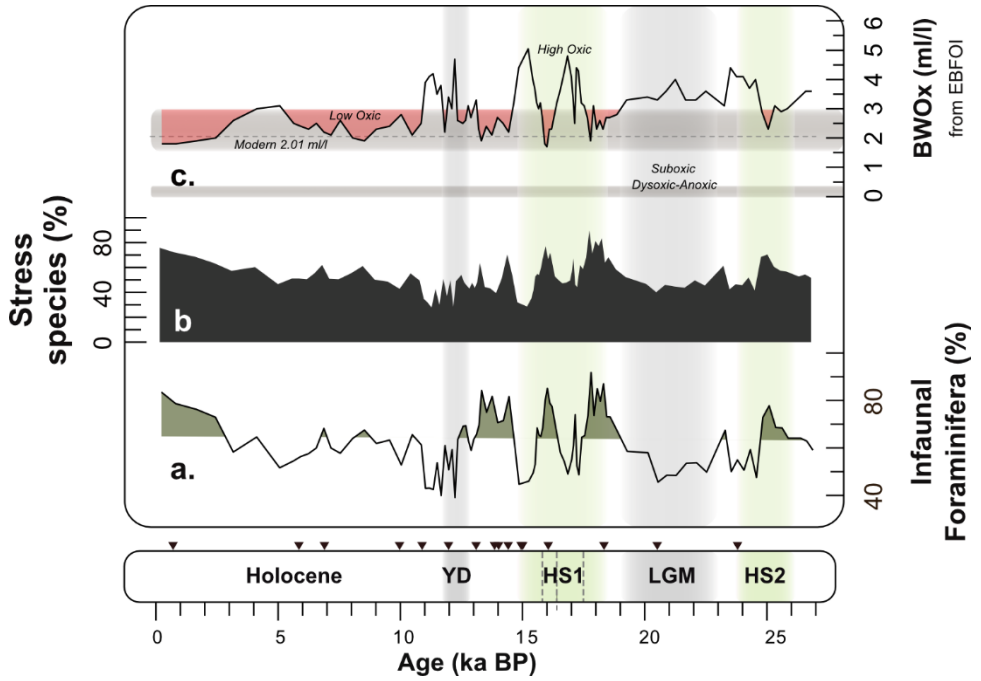

Figure 2.6 GeoB9512-5 downcore relative abundances of the most relevant benthic foraminifera species and other paleoenvironmental indicators. a. Relative abundances of infaunal benthic foraminifera, and b. Stress Species; c. Dissolved Oxygen Concentration (ml/l) from Enhanced Benthic Foraminifera Oxygen Index (EBFOI). Key Climate events: Heinrich Stadial 2 (HS2); Last Glacial Maximum (LGM); Heinrich Stadial 1 (HS1); Bølling–Allerød (B-A); Younger Dryas (YD). Triangles in the age axis indicate radiocarbon ages.

To estimate the uncertainty associated with our dissolved oxygen reconstruction, we assumed that oceanographic conditions during the late Holocene were relatively stable and used samples younger than 2.6 ka BP (n=6) to estimate reproducibility. Dissolved oxygen calculated from EBFOI for four samples (between 2.5 and 17.5 cm) in gravity core GeoB9512-5 and two samples (2 cm, 8 cm) from nearby multicore GeoB9512-4 (Mulitza et al., 2005) (Supplementary Information 3.2) gave a mean value of 2.2 ml/l, and standard deviation of 0.17 ml/l. However, given that the distribution of our data is not normal (p-value = 0.015 using the Shapiro test), the 95% confidence interval was estimated only considering the age uncertainty (Fig 2, Fig 3d), combined with 10,000 downcore proxy series produced with the Bacon script for R (Blaauw and Christen, 2011).

Acknowledgements

This research was funded by the “Deutsche Forschungsgemeinschaft” (DFG) through the Cluster of Excellence EXC 2077 “The Ocean Floor – Earth’s Uncharted Interface”. The sample material used here was provided by the GeoB Core Repository at

MARUM. The authors thank Jakob Quabeck who produced some of the microfossil images and Ishani Rathnayake who helped with sample preparation. This research is also supported by GLOMAR – Bremen International Graduate School for Marine Sciences, University of Bremen. The first author thanks Babette Hogakker for the valuable feedback in the latest versions of the manuscript, and GeoLatinas members for their support and feedback, especially Giulia Molina, Mónica Alejandra Gómez Correa and Rocío Caballero-Gill who provided insights on the benthic foraminifera analyses and manuscript state.

Author Contributions

S.B.M contributed with the conceptualization, core sampling, sample preparation, benthic foraminifera extraction, taxonomy and quantitative analyses, data interpretation and manuscript; H.J.H.J. contributed with the conceptualization, data interpretation and discussion; S.M. contributed with the core sampling, conceptualization, age model, and discussion; D.A.R.M. contributed with the quantitative analyses, introduction and discussion; H.P. contributed with the conceptualization and discussion.

Competing Interest

The authors declare no competing interests.

Code availability

The code used to process and visualize the benthic foraminifera data can be found at Barragán-Montilla (2024). The script for the age model is based on Blaauw and Christen (2011) and processing and visualization of the data is available in the same repository.

Data availability

Sofía Barragán-Montilla. (2024). SophieBM93/Tropical-eastern-Atlantic-Benthic-Foraminifera-analyses: GeoB9512-5 Deglacial Paleo-Oxygenation Reconstruction (Version v2). Zenodo. https://doi.org/10.5281/zenodo.10806183

Barragán-Montilla, S. (dataset in review). Benthic Foraminifera counts off NW Africa during the last deglaciation. PANGAEA, https://doi.pangaea.de/10.1594/PANGAEA.962951

Barragán-Montilla, S. and Mulitza, S. (dataset in review). Mulitza, Stefan: Radiocarbon ages of sediment core GeoB9512-1. PANGAEA, https://doi.pangaea.de/10.1594/PANGAEA.962899

Chapter 3: New insights on infaunal foraminifera paleothermometry: environmental effects on *Melonis barleeanus* Mg/Ca from the tropical eastern Atlantic

In preparation for submission

Sofía Barragán-Montilla[1,2], Heather J. H. Johnstone[1], Dharma Andrea Reyes Macaya[1,3], Stefan Mulitza[1], Heiko Pälike[1]

[1] MARUM – Center for Marine Environmental Sciences and Department of Geosciences, University of Bremen, Bremen, Germany
[2] Faculty of Geosciences, University of Bremen, Bremen, Germany
[3] Lyell Centre, Heriot-Watt University, Edinburgh, UK

Abstract

Deep-sea foraminifera *Uvigerina* Mg/Ca is widely used for bottom water temperature (BWT) reconstructions, with multiple calibrations available for a wide range of temperatures. However, low recovery/poor preservation of *Uvigerina* at intermediate and shallower depths and sometimes in deep settings, makes necessary to explore other species, like intermediate infaunal Melonis *barleeanus*, commonly used in BWT reconstructions of the Arctic North Atlantic. As calibrations for this species in the tropical eastern Atlantic (tropical eastern Atlantic) are limited, we revised *M. barleeanus* Mg/Ca temperature calibrations integrating new and existing data and propose two new calibrations, including coretop data from sites with varying oxygen content, and propose two new calibrations for this species. The first calibration describes a Mg/Ca - BWT exponential relationship (Mg/Ca [mmol/mol] = 0.817 * exp (0.0815*BWT [°C]), r^2=0.8, n=140); and a second calibration aiming to reduce paleotemperature uncertainties introduced by bottom water dissolved oxygen (BWOx) effects (Mg/Ca [mmol/mol] = 0.22*BWT [°C] + 0.13*BWOx [ml/l] - 0.44 , r^2=0.9, n=22) decreases temperature uncertainties in modern samples by ~ 50% compared to previous calibrations. In a second part of this study, we attempted to use a species-composite record, to produce a high resolution BWT reconstruction from site GeoB9512-5 (794m water depth) located in the eastern Tropical North Atlantic Oxygen Minimum Zone during the last deglaciation. These records are based on Mg/Ca of *Uvigerina mediterranea* (BWT_{Uvig}) and *M. barleeanus* (BWT_{Mel}), the latter corrected by

BWOx effects using an available high-resolution paleo-oxygenation record from sediments deposited in the last 27,000 years in our site. However, a composite record was not possible, as both species show some contrasting BWT trends during the Last Glacial Maximum – Heinrich Stadial 1 and show no constant offset. We conclude that our BWT_{Mel} is most likely biased by microhabitat changes of this species. From our data we found that the BWT_{Uvig} remains as one of the most reliable intermediate bottom water temperature proxies for the eastern tropical North Atlantic.

Graphic Abstract

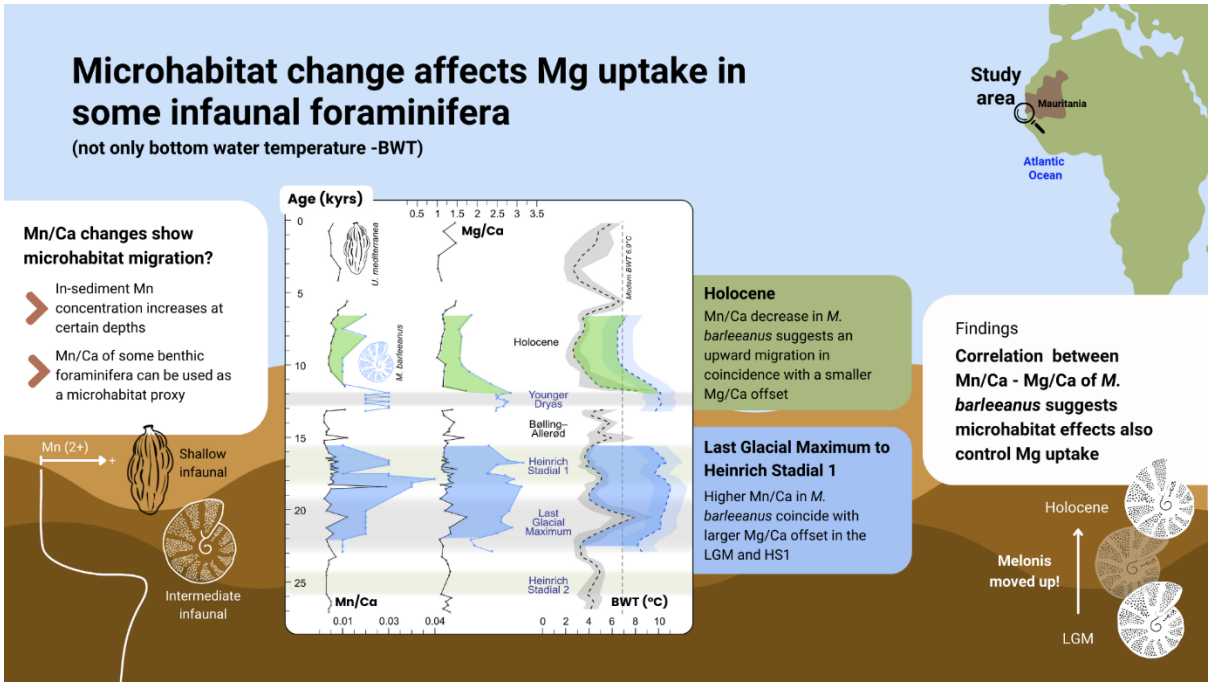

1 Introduction

Benthic foraminifera geochemistry is widely used to reconstruct bottom water conditions changes, as species calcify their tests in relative chemical equilibrium with the surrounding water (e.g. Lear et al., 2002; Schmittner et al., 2017). Stable isotopes are used to interpret paleoceanographic changes like bottom water ventilation and/or nutrient content (e.g. Oppo et al., 2015), while trace element to Calcium ratios are useful to estimate bottom water paleotemperatures (BWT) (Mg/Ca, e.g. Lear et al., 2002; Elderfield et al., 2010), paleo-oxygenation (Mn/Ca e.g. Groenveld and Filipsson, 2013), and in some cases paleoproductivity (Ba/Ca, e.g. Mojtajid et al., 2019) or water depth (WD) (Sr/Ca, e.g. Sælen et al., 2009). These proxies rely on global/regional

calibrations to account for all possible effects, constructed from modern samples with known environmental and geochemical variables. This is important, as benthic foraminifera calcification depends on the ambient water geochemistry, vital (like internal metabolism and calcification rates) and environmental/geochemical effects (i.e. carbonate ion concentration or salinity), and in some cases dissolution/recrystallization (taphonomy effects), all of which impact geochemical-based paleoceanographic reconstructions.

Although some research has successfully reconstructed paleotemperature changes in the deep Atlantic (e.g. Barragán-Montilla et al., 2022; Roberts et al., 2016; Skinner et al., 2003), the knowledge about the response of subsurface and intermediate waters to weakened AMOC in the equatorial Atlantic is limited. The BWTs reconstructions from benthic foraminifera Mg/Ca from the tropical western Atlantic suggest regional subsurface water warming during the HS1 (Oppo et al., 2023; Rühlemann et al., 2004), as do other records in other parts of the Atlantic above 1,500 m (Poggemann et al., 2018, Weldeab et al., 2016) and in the subpolar Atlantic (Marcott et al., 2011).

Such unresolved issues in benthic foraminifera Mg/Ca paleothermometry introduce considerable uncertainties on paleotemperature reconstructions. Oppo et al. (2023) found that carbonate ion saturation ($\Delta[CO_3^{2-}]$) influence benthic foraminifera Mg uptake, as previously hypothesized by Elderfield et al. (2010). Effects of $\Delta[CO_3^{2-}]$ on Mg/Ca have been confirmed for epifaunal foraminifera (Yu and Elderfield, 2008), and deep infaunal *Globobulimina* (Weldeab et al., 2016), but have not been seen in other infaunal foraminifera. Stirpe et al. (2021), found that anomalously high *Uvigerina* Mg/Ca (between 0.6 to 2.1 mmol/mol, average Mg/Ca = 1.4 mmol/mol, SD= 0.36) from the Southwest Pacific cannot be explained by BWT gradients only, but other effects could not be constrained with the available data. In the eastern equatorial Atlantic, Weldeab et al. (2016) found evidence of a $\Delta[CO_3^{2-}]$ effect on *Globobulimina* Mg/Ca from Gulf of Guinea core tops and propose a temperature calibration correction using Ba/Ca ratios. A clear Mg/Ca - $\Delta[CO_3^{2-}]$ relation for *Uvigerina* and *Melonis barleeanus* has not been recorded. Instead, North Atlantic core top data suggests no correlation between $\Delta[CO_3^{2-}]$ and *Melonis* Mg/Ca, although a potential salinity effect cannot be ruled out for the eastern tropical Atlantic (Hasenfratz et al., 2017).

Another unexplored confounding factor on Mg/Ca paleothermometry using benthic foraminifera is their known migration behavior within the sediment. Such microhabitat changes could potentially influence benthic foraminifera Mg/Ca. Benthic foraminifera microhabitats are closely spaced habitats within the sediment, characterized by a series of physical, chemical, and biological conditions including (but not limited to) oxygen, food, toxic substances, and symbiotic relations with other organisms (Jorissen et al., 1999). In benthic foraminifera, microhabitats are vertically distributed and can be shallow, intermediate, or deep. Furthermore, a species microhabitat is not necessarily static through time, and has been found to be particularly variable for highly adapting species like *M. barleeanus* or *Globobulimina affinis*, who migrate vertically looking for their preferred living conditions (Linke and Lutze, 1993). This behavior is seen in culture studies using *Globobulimina turgida* (Koho et al., 2011), and species like *U. mediterranea*, *U. peregrina* and *G. affinis* have a well recorded vertical migration related to oxygen availability (Geslin et al., 2004). In addition, some studies suggest food availability/quality determine benthic foraminifera microhabitat preference (e.g. Jorissen et al., 1995; Jorissen, 1999), as is the case of *M. barleeanus* (Linke and Lutze, 1993). Recorded average living depths (ALD) on benthic foraminifera from the Bay of Biscay, North Atlantic and Pacific Oceans, show consistent distribution patterns in ideal oxic-food conditions. *U. peregrina* and *U. mediterranea* are found in shallow infaunal microhabitats (Corliss and Emerson, 1990; Fontanier et al., 2002; Fontanier et al., 2005; Geslin et al., 2004; Griveaud et al. 2010), with ALD from 0 to 2 cm; and *M. barleeanus* usually lives deeper as an intermediate infaunal species with ALDs between 1 to 6 cm (Corliss, 1985; Corliss and Emerson, 1990; Fontanier et al., 2002; Fontanier et al., 2005; Geslin et al., 2004; Griveaud et al. 2010).

Ní Fhlaithearta et al. (2018) and Koho et al. (2017) found that Mn concentrations and Mn/Ca ratios decrease in pore waters from shallower to deeper settings in the NW Mediterranean (350 - 1987 m WD) in sites with constant BWT and salinity. These studies showed that during the calcification of some benthic foraminifera (*U. mediterranea* - *U. peregrina* and *M. barleeanus*) Mn/Ca ratios reflect pore water geochemistry and possibly changes with microhabitat depth, as usyally Mn

concentration increases with sediment depth. Furthermore, *M. barleeanus* showed higher Mn/Ca variability than *Uvigerina* (Ní Fhlaithearta et al., 2018), potentially linked to Bottom Water Oxygenation (BWOx), organic matter availability and deeper microhabitats.

To date, oxygen sensitivity and microhabitat changes have not been considered as a factor influencing Mg/Ca. In this research, we used a set of existing and new core top data (297 – 4,297 m water depth) with BWTs between -0.9 – 15.6°C, salinity from 34.55 to 36.28, $\Delta[CO_3^{2-}]$ from -1.9 to 121.5, and BWOx between 1 and 5.52 ml/l to try to constrain the effects of these factors on benthic foraminifera Mg/Ca in the eastern tropical North Atlantic.

We found that although Mg/Ca ratios of *M. barleeanus* are highly sensitive to BWTs changes according to our revised calibration in the tropical eastern North Atlantic, other bottom water parameters like BWOx, and even microhabitat changes seem to influence Mg/Ca ratios and therefore paleotemperature estimations. Integrating our core top *M. barleeanus* Mg/Ca measurements with previously published data, we propose two updated calibrations for the tropical eastern North Atlantic to correct for possible additional effects (1) an exponential regression calibration between new and previous Mg/Ca and modern BWTs; (2) based on the linear regression between Mg/Ca against BWT and BWOx. With this new approach, BWT uncertainties can be reduced by more than 50% compared to previous calibrations, with BWT uncertainties of ±0.76°C (1) and ±0.58°C (2) respectively. Although corrections for microhabitat effects were not possible with our data, we provide new evidence showing other environmental (oxygen) and vital (microhabitat) parameters possibly introduce large uncertainties in paleotemperature reconstructions based on benthic foraminifera Mg/Ca, particularly in areas with changing oxygen and organic matter content like in Oxygen Minimum Zones and upwelling areas.

In order to test our new calibrations and findings we compared Mg/Ca for two species of benthic foraminifera in downcore record GeoB9512-5 (15°20’13.20’’N, 17°22’1.20’’W, 793 m water depth). The Mg/Ca ratios were measured in shallow infaunal *Uvigerina mediterranea* and intermediate infaunal *Melonis barleenus.*

Temperature calibrations for both species are available, however *Uvigerina* calibration is one of the best stablished and widely used (e.g. Elderfield et al., 2010). For *M. barleeanus* temperature calibrations have been less studied and come from Atlantic higher latitudes of the Atlantic Ocean (Kristjándóttir et al., 2007) and from the tropical Atlantic (Hasenfratz et al., 2017). However, the sites used for Kristjándóttir et al. (2007) were made on high oxic (dissolved oxygen >6) sites with low variability, while the sites studied here and by Hasenfratz et al. (2017) are in the eastern tropical North Atlantic Oxygen Minimum Zone (ETNA-OMZ) and cover a wider range of oxygen conditions from suboxic (0.3 – 1.5 ml/l), low oxic (1.5 – 3 ml/l) and high oxic (> 3 ml/l).

Site GeoB9512-5 is also located in the ETNA-OMZ low oxic margin and has a high-resolution paleo-oxygenation record available based on benthic foraminifera taxonomy and quantitative analyses (Barragán-Montilla et al., in review – Chapter 2) that shows large changes in BWOx over the last deglaciation. This site is also located in the seasonal upwelling area off NW Africa (Pelegrí and Peña-Izquierdo, 2015), and during the last 27,000 years is characterized by abundant organic matter content (Appendix 2.1). The situation of site GeoB9512-5, therefore, allows us to test the new calibrations proposed here, as well as to understand the effects of BWOx and microhabitat changes in benthic foraminifera Mg/Ca in the fossil record.

2 Methods

2.1 Core Location and materials

Benthic foraminifera were extracted from 29 core top samples of the tropical eastern Atlantic, collected at water depths (WD) from 200 to 5,362 m and BWTs ranging from 2.4 to 14.2°C. Northern sites multicore samples were collected during Meteor Cuise M65/1 (Mulitza et al., 2005) and the southern samples were retrieved by the RV Tyro cruise (Jansen et al., 1990). *Melonis barleeanus* (mostly rose stained, Barragán-Montilla and Johnstone, in review) were used to measure trace element concentrations (Mg/Ca, Mn/Ca, Sr/Ca, Ba/Ca, Al/Ca and Fe/Ca) to calibrate the Mg/Ca-based temperature equations. Core top sediments from the northern sites were provided by the GeoB Core repository, and were first washed with deionized water through a 63 µm sieve to remove mud content, and then dried in an oven at temperatures lower than 45°C. The dry sediment was separated using 63, 150 and

250 µm sieves and the latter fraction was used to extract benthic foraminifera for geochemical analysis. Specimens retrieved from the southern sites come from already washed and dry sieved sediment (Schefuss et al., 2004).

Downcore reconstructions were made from marine sediment core GeoB9512-5 (793 m water depth) off the coast of Senegal, North-western Africa (Figure 4.1) (Multiza et al., 2005). The core is in the mixing zone of the North Atlantic Central Water (NACW) and the South Atlantic Central Water (SACW), with a modern BWT of 7.1°C and dissolved oxygen concentration of 2.01 ml/l (Lauvset et al., 2022). The studied interval corresponds to the top 548.5 cm of the core sampled every 5 cm with an average age resolution of 0.2 kyrs (Barragán-Montilla et al., in review). Samples come from an unconsolidated dark grey to brownish mud interval with abundant microfossil content (Mulitza et al., 2005). Samples were washed as described for the core tops, with the difference that during dry sieving was made using 63 and 150 µm sieves (Barragán-Montilla et al., in review). Benthic foraminifera for geochemical measurements were hand-picked from the 150 µm fraction.

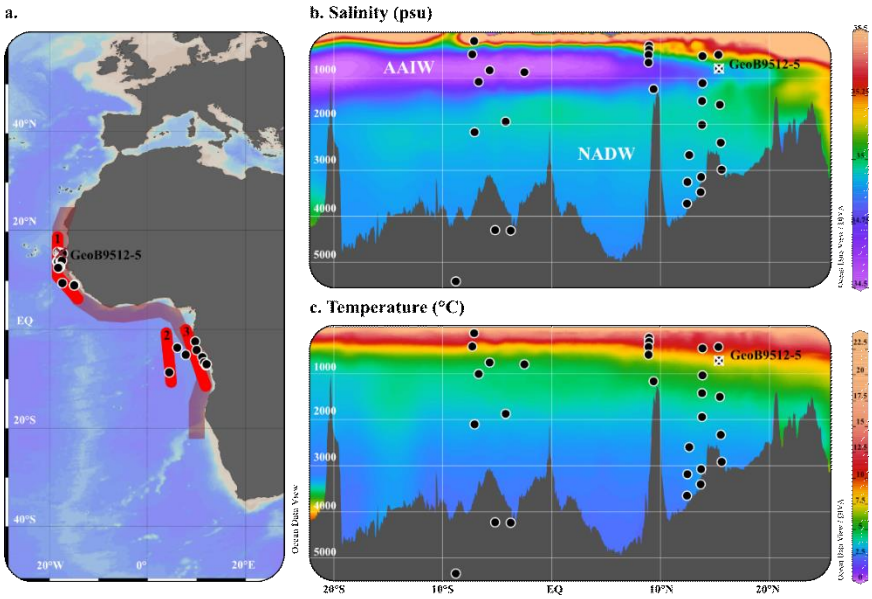

Figure 3.1 Core tops and GeoB9512-5 (15°20'13.20''N/17°22'1.20''W, 793 m water depth) location a. Geographic location of the studied sites in the Northeastern Atlantic, red lines with numeration 1-3 indicate the sections used to estimate core top - hydrographic parameters; **b.** Modern dissolved Oxygen concentrations (ml/l) and water depth/latitude distribution of the studied sites; **c.** Modern sea water temperatures in the studied area. Plotted using ODV -Schlitzer, Reiner, Ocean Data View, https://odv.awi.de, 2022; GLODAP version 2 of Lauvset et al., 2022; and World Ocean Data of Boyer et al., 2018.

2.2 GeoB9512-5 age model

The ages used here correspond to those calculated by Barragán-Montilla et al. (in review, Chapter 2). The model was calculated using planktic foraminifera AMS dating from 16 planktic foraminifera samples of GeoB9512-5 measured at the MICADAS laboratory at the Alfred Wegener Institute (AWI)-Bremerhaven (Mollenhauer et al., 2021). The median ages and corresponding uncertainties were modelled with the Bayesian age modelling script BACON version 2.5.5 (Blaauw and Christen, 2011) and the Marine20 calibration curve (Heaton et al., 2020). Heinrich Stadials were visually correlated with uncalibrated XRF Fe/Ca ratios (Völpel et al., 2019). This resulted in an age model showing a deglacial sedimentary sequence deposited in the last 27,000 years with no reversals. This includes the key climatic periods Heinrich Stadial 2 (HS2, 25.9 - 24.2 ka BP), Last Glacial Maximum interval (LGM, 23 - 19 ka BP), Heinrich Stadial 1 (HS1, 18.3 - 15.4 ka BP), the Bølling–Allerød warming (B-A, 15.4 - 13 ka BP) and the Younger Dryas (YD, 12.9 - 11.7 ka BP). An Holocene Fe/Ca minima was found at 6.6 kyrs, putting the African Humid Period between 11.7 and 6.6 kyrs.

2.3 Benthic foraminifera geochemistry and Palaeoceanography

For core GeoB9512-5, 110 samples were used for benthic foraminifera stable isotopes and trace element measurements. Paleoceanographic proxies have been measured on epifaunal foraminifera *Cibicidoides pachyderma*, and *Lobatula lobatula* stable isotopes, including $\delta^{13}C$ and $\delta^{18}O$ measurements (Barragán-Montilla, in review). These analyses were made using a ThermoFisher Scientific 253 plus gas isotope ratio mass spectrometer, with a Kiel IV automated carbonate preparation device, at MARUM- Center for Marine Environmental Sciences of the University of Bremen. The data is reported in the delta-notations versus V-PDB. Instruments were calibrated against the house standard (ground Solnhofen limestone), and against the NBS-19 calcite. Over the measurement period the house standard deviation was 0.03 ‰ for $\delta^{13}C$ and 0.06 ‰ for $\delta^{18}O$.

Element concentrations in GeoB9512-5 were measured on shallow infaunal foraminifera *Uvigerina mediterranea* and intermediate infaunal *Melonis barleeanus* (Barragán-Montilla and Johnstone, 2024b). *M. barleeanus* tests were also picked from 29 core top samples to investigate other potential effects on Mg/Ca ratios in modern

conditions in the tropical eastern Atlantic (Barragán-Montilla and Johnstone, 2024a). Foraminifera were crushed and cleaned with MiliQ water, methanol, and hot hydrogen peroxide solution (no reductive cleaning step) using a pipette robot programmed to follow the protocol of Barker et al. (2003) (Johnstone et al, 2016).

Trace element concentrations were measured with an Inductively Coupled Plasma Optical Emission Spectrometer (ICP-OES)—Agilent Technologies 700 Series with Cetac ASX-520 autosampler. Measurements follow the spectral lines: Mg (279.6 nm), Ca (315.9 nm), Sr (421.6), Al (167.0 nm), Fe (238.2 nm), and Mn (257.6 nm), and were calibrated with linear regressions. Standards of calibration consisted of a blank and five multi-element standards (Mg, Sr, Al, Fe, Mn) between 20 and 100 ppm Ca. We monitored the instrumental precision using a commercial multi-element standard solution (SCP, France), and commercial powder sample ECRM752-1. Theoretical value (measured value, σ standard deviation, standard error) in mmol/mol for the SCP standard during these runs were: Mg/Ca, 2.955 (2.959, σ 0.030, 0.0029), Sr/Ca, 1.402 (1.402, 0. σ 016, 0.0015), Mn/Ca 0.3234 (0.3291, σ 0.0019, 0.00019), Fe/Ca, 0.3312 (0.3228, σ 0.0034, 0.00033), Ba/Ca, 0.00832 (0.00840, σ 0.00034, 0.000033) and Al/Ca 0.678 (0.695, σ 0.018, 0.0018), n=108. Mg/Ca of dissolved, centrifuged, ECRM 752-1 (measured at 3.750 σ 0.015, 0.0014 by Greaves et al. (2005)) was 3.735 σ 0.031, 0.0057 (Barragán-Montilla and Johnstone, in review b). Long term standard deviation is better than 2% during the measurement runs reported here. The Al/Ca ratios were used to monitor contamination (Barker et al., 2003; Johnstone et al., 2016).

2.3.1 Core top hydrographic data

The hydrographic data used in this study was obtained using Ocen Data View (Schlitzer, Reiner, Ocean Data View, https://odv.awi.de, 2022) and GLODAP version 2 (Lauvset et al., 2022). Average bottom water temperature, salinity, dissolved oxygen, alkalinity, and pH were extracted with (https://github.com/Paleobiogeochemistry/BWC) based in three different sections of 200 km width (figure 4.1a, red lines 1-3). We used Diva gridding excluding outliners and hiding bad estimates with maximum interpolation of 15X and 10Y. The resulting data was then used to estimate carbonate ion saturation state with version 1.3.0 of CO2calc (Robbins et al., 2010), using total alkalinity and the pH total scale for each

core top, and with K1 and K2 constants after Luecker et al. (2020). These variables are summarized in the Supplementary information 4.3.

Principal Component Analysis (PCA) including the trace elements and environmental parameters was used to better visualize the impact of bottom water conditions on *Melonis* tests composition and identify the largest variations in our core top data. Variables were used the element to calcium ratios (Mg/Ca, Mn/Ca, Sr/Ca and Ba/Ca) and the environmental parameters extracted here (WD, BWT, BWOx, and salinity). Data was normalized by scaling the values to zero mean and unit variance using the decostand function from the vegan package (Okansen et al., 2022) in RStudio.

2.3.2 Benthic Foraminifera existing and revised temperature callibrations

During this study we included core top trace element measurements to calibrate Mg/Ca-temperature equations of *Melonis barleeanus*. The revised calibrations were calculated using correlation tests combining our eastern tropical North Atlantic *M. barleeanus* Mg/Ca data with those reported by Hasenfratz et al. (2017) and the hydrographic data (BWT and BWOx). Data from other areas was excluded as we are aiming to make a local correlation for the eastern tropical Atlantic. We compared our revised *M. barleeanus* temperature calibrations with those provided by Hasenfratz et al. (2017, equation 1), estimated from core top measurements from 50 to 4,305 m WD and BWTs from -1 to 16°C in the NE Atlantic. The calibration of Kristjánsdóttir et al. (2007, equation 2) from core tops retrieved from 165 to 656 m WD and BWTs between 0 and 7°C in the Arctic continental shelf, was also considered.

$$\frac{Mg}{Ca}\left[\frac{mmol}{mol}\right] = 0.113 * BWT_{Mel}[°C] + 0.792, r^2 = 0.81, n = 120 \quad \textbf{(1)}$$

$$\frac{Mg}{Ca}\left[\frac{mmol}{mol}\right] = 0.658 * \exp(0.137 * BWT_{Mel}[°C]),\ r^2 = 0.81, n = 31 \quad \textbf{(2)}$$

$$\frac{Mg}{Ca}\left[\frac{mmol}{mol}\right] = 0.0915 * BWT_{Uvig}[°C] + 0.843,\ r^2 = 0.92 \quad \textbf{(3)}$$

2.3.3 GeoB9512-5 downcore BWT record

Downcore BWTs for the intermediate site GeoB9512-5, were calculated from the Mg/Ca measurements of *U. mediterranea* (BWT_{Uvig}) using the calibration of Roberts

et al. (2016 – Equation 3); while bottom water temperatures based on Mg/Ca *M. barleeanus* (BWT_{Mel}) were used in the calibration of Kristjánsdóttir et al. (2007 – Equation 2) and the proposed in this study.

Seawater $\delta^{18}O$ ($\delta^{18}Osw$) of site GeoB9512-5 was obtained by extracting the temperature effect from BWT_{Uvig} to the $\delta^{18}Oc$ of *Cibicidoides* spp. (corrected by a species-specific offset of +0.64 ‰) using the equation by Shackleton (1974) (Supplementary Information 4.1). An additional $\delta^{18}O_{sw}$ was obtained extracting a temperature effect based on our BWT_{Mel} (Supplementary Information 4.2). This record was also obtained using the equation of Shackleton (1974), considering no species-specific based on a $\delta^{18}O$ *Cibicidoides wuellerstorfi* – $\delta^{18}O$ *M. barleeanus* from core top measurements. *Cibicidoides* spp. $\delta^{13}C$ in core GeoB9512-5 was taken from (Barragán-Montilla, in review; Völpel et al., 2019).

Ages and proxies uncertainties were obtained with the Bacon R-package (Blaauw and Christen, 2011). Ensembles of 10,000 possible time series were produced for the studied proxies. Then, the 10,000 age-depth relations were used to produce 10,000 normal-distributed values randomly for the studied depths and integrated with the 10,000 downcore proxy records. The standard deviation (SD) considered were 0.7 °C for BWT_{Uvig} (Roberts et al. 2016), 1°C for BWT_{Mel} calculated with equation 1 (equation 1, Hasenfratz et al., 2017), and 1.10°C for BWT_{Mel} calculated with equation 2 (Kristjánsdóttir et al., 2007). Standard deviations for the stable isotopes were 0.06 ‰ and 0.03 ‰ for $\delta^{18}O$ and $\delta^{13}C$ respectively. The final proxy reconstructions were reported from the median value with the corresponding 95 % uncertainty envelope at the estimated median age of each observation.

3 Results and discussion

3.1 Quality control

Clay contamination and Mn-rich coatings visibly affect Mg/Ca measurements (Barker et al., 2003), even after careful cleaning methods, they can still be present and influence Mg/Ca ratios. Here we use Al/Ca and Mn/Ca to identify samples with potential clay contamination, removing samples with Al/Ca > 0.5 mmol/mol and/or Mn/Ca > 0.25 mmol/mol (Hasenfratz et al., 2017).

Core top data of *M. barleeanus* with high Al/Ca and/or Mn/Ca (Barragán-Montilla and Johnstone, in review a) showed 3 samples with potential contamination. From the retained samples, average Al/Ca was 0.06 mmol/mol, and average Mn/Ca 0.03 mmol/mol. Low correlation between Mg/Ca and Al/Ca (r^2=0.12, n=33) and Mn/Ca (r^2=0.02, n=33) suggests no contamination in the remaining samples.

U. mediterranea measurements from site GeoB9512-5 (Barragán-Montilla and Johnstone, in review b), show average Al/Ca of 0.06 mmol/mol, and 4 samples with Al/Ca > 0.5 mmol/mol were not retained. Low correlation between remaining Al/Ca and Mg/Ca of the remaining samples (r^2 = 0.02, n=81) suggest no clay contamination. Duplicates of 2 samples were measured showing good accordance between element concentrations (average standard deviations in Mg/Ca was 0.13 mmol/mol).

Element concentrations from GeoB9512-5 *M. barleeanus*, come from 35 samples and 4 duplicates. Al/Ca was on average 0.11 mmol/mol, and ranged from 0.05 and 0.24 mmol/mol, higher than *U. mediterranea*. However, Al/Ca did not exceed 0.5 mmol/mol, and low correlation with Mg/Ca (r^2= 0.03, n=35), suggest no critical clay contamination, as does low Mg/Ca – Mn/Ca correlation (r^2= 0.02, n=35). Between duplicates, variation was higher ranging between 0.12 and 0.55 mmol/mol (standard deviations on average 0.16 mmol/mol). Highest differences were encountered in the samples collected at 177.5 cm (0.55 mmol/mol), and samples from 52.5 cm and 192.5 cm in core depth show differences of 0.22 and 0.37 mmol/mol respectively. The larger differences may be related to the sample size from duplicates which differed significantly (at 177.5 cm, original measurement was made in 9 tests, while duplicates were made on 3).

3.2 Trace elements on modern benthic foraminifera: parameters controlling Melonis chemical composition in the tropical eastern Atlantic

The Mg/Ca ratios of core top *M. barleeanus* (SD=0.46, n=33) ranged between 0.78 and 2.81 mmol/mol while Mn/Ca was measured from 0.006 to 0.121 mmol/mol.

3.3.1 Carbonate ion saturation controls on infaunal benthic foraminifera trace elements to calcium ratios

Carbonate ion saturation (ΔCO_3^{2-}) has been observed to affect Mg uptake in epifaunal foraminifera like *Cibicidoides wuellerstorfi* (Yu and Elderfield, 2008), deep infaunal *Globobulimina* (Weldeab et al., 2016) and aragonitic *Hoeglundina elegans* (Rosenthal et al., 2006). During this study we compared the ΔCO_3^{2-} obtained as described by Hasenfratz et al. (2017), with the measured Mg/Ca ratios of *M. barleeanus* in the eastern tropical Atlantic. From our data, we can corroborate no correlation is observed between ΔCO_3^{2-} and Mg/Ca of *M. barleeanus* (r^2=0.005, n=25). These results agree with the low correlation between $\Omega_{calcite}$ and Mg/Ca in our data set (r^2=0.116, n=25). Furthermore, when integrating our core top measurements with the reported by Hasenfratz et al. (2017), the lack of correlation between ΔCO_3^{2-} and Mg/Ca of *M. barleeanus* is sustained (r^2=0.0065, n=60). These results provide stronger evidence that carbonate ion saturation seemingly does not affect Mg/Ca of *Melonis*, at least in the tropical eastern Atlantic.

3.3.2 Bottom water parameters controlling M. barleeanus test composition

Although no carbonate ion saturation effects were observed on the Mg/Ca ratios of both *Melonis* species in our study, other bottom water parameters could impact their calcification. To keep consistency of the data, and to eliminate a possible microhabitat effect bias, when possible, only sites of intermediate in-sediment depths (of 6-9 cm) were considered (in line with *M. barleeanus* intermediate infaunal microhabitat preference – Supplementary Information 1). This left a total of 22 samples for the correlation and statistical tests for *M. barleeanus*.

Possible links between Mg/Ca, Sr/Ca, Mn/Ca and Ba/Ca ratios measured in *M. barleeanus* and bottom water parameters were assessed by running linear correlation tests. In our study, parameters with r^2 >0.5 were considered to show some correlation, and $r^2 \geq 0.8$ are considered as strongly correlated. *M. barleeanus* Mg/Ca shows a negative correlation with BWOx (r^2=0.7, n=22, p=4.2 × $^{-06}$) and BWT (r^2=0.8, n=22, p=3.7 × $^{-07}$). Strong negative linear correlations were also seen for Sr/Ca and BWOx (r^2=0.8, n=22, p=1.9 × $^{-06}$). Mg/Ca correlation with modern BWT shows this species is highly sensitive to temperature changes, as BWTs correlation is also seen with Sr/Ca

and to a lesser extent with Ba/Ca. Additionally, another striking correlation observed in our data is present between water depth and Sr/Ca (r^2=0.9, n=22, p=5.0 × $^{-07}$) as previously noted by (Sælen et al., 2010). In addition, Mn/Ca of *M. barleeanus* shows no correlation with any of the considered bottom water parameters, including BWOx (r^2=0.1, n=22, p=3.5 × $^{-10}$).

Table 3.1 Pearson correlation coefficients (r) for element to calcium ratios against bottom water parameters, n=22. Abbreviations: bottom water temperature (BWT) and oxygen (BWOx), carbonate ion saturation (ΔCO_3^{2-})

Pearson (r)	Mg/Ca (mmol/mol)	p-value	Sr/Ca (mmol/mol)	p-value	Mn/Ca (mmol/mol)	p-value	Ba/Ca (mmol/mol)	p-value
BWT	0.91	3.7E-07	0.92	1.88E-06	-0.34	7.72E-08	-0.44	6.9E-08
Salinity	0.64	5.6E-42	0.39	2.24E-51	-0.17	3.62E-51	-0.10	1.7E-51
BWOx	-0.84	4.2E-06	-0.93	3.55E-07	0.34	3.46E-10	0.51	3.2E-10
dco3	-0.05	7.3E-10	0.12	6.62E-10	-0.26	2.9E-10	0.16	2.8E-10

A PCA analysis including the trace elements and environmental parameters was used to better visualize the impact of bottom water conditions on *Melonis* tests composition. The PCA1(figure 4.2a) shows that Dim1 and Dim2 explain 74.1% of our data variation. Dim1 includes positive contributions of BWT and Salinity, and negative of BWOx. These parameters are also correlated with each other, therefore making more difficult to separate their effect in the geochemical signatures considered here.

Dim2 is mainly described by ΔCO_3^{2-}. Positive association to Dim1 are shown by Mg/Ca and Sr/Ca. Ba/Ca is represented by higher Dim2 and Mn/Ca with lower Dim2 values. This suggest that both Sr/Ca and Mg/Ca of *M. barleeanus* are strongly influenced by BWT and BWOx, with a positive association to BWT and a negative association to BWOx. Results also show that to a lesser extent Mg/Ca also responds to salinity changes (Table 4.1), similar to the reported r^2=0.4 (p=4.8 × $^{-5}$, n=35) by Hasenfratz et al. (2017). Furthermore, ΔCO_3^{2-} effects are not seen as values in Dim2 for Mg/Ca are close to 0 (Figure 4.2).

One aspect to consider is that the main groups identified by the PCA correspond to water depth interval, with the shallowest (300 – 787 m) towards positive Dim1, and deeper (2,648 – 4,267 m) towards negative Dim1 values. As factors like temperature (BWT), oxygenation (BWOx) and salinity are also depth-dependent, the effects of these variables cannot be easily separated.

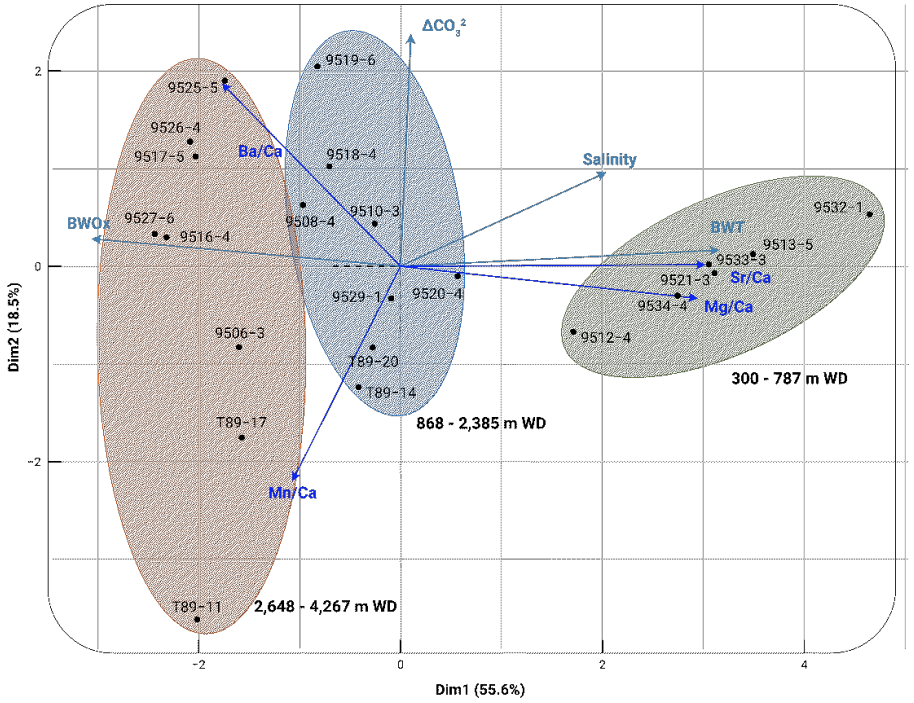

Figure 3.2 Principal Component Analyses (PCA) of *M. barleeanus* trace elements and modern bottom water conditions of the tropical eastern Atlantic (this study). Data was standardized using the decostand function (Okansen et al., 2022) in RStudio by scaling the values to zero mean and unit variance. Green group, corresponds to coretops between 300 -787 m water depth; blue group between 868 – 2,385 m water depth; and orange group between 2,648 – 4,267 m water depth.

3.3.3 Revised temperature calibration for M. barleeanus Mg/Ca in the eastern tropical Atlantic

Our results show trace element-based paleotemperature reconstructions, specifically for *M. barleeanus* in the tropical eastern Atlantic are not exclusively temperature dependent. The effects of other bottom water conditions on Mg/Ca and therefore on BWT reconstructions and can be seen when applying our revised calibration to our core top data (Figure 4.3 c), and comparing the results with the BWTs obtained using to the existing calibrations for this species of Hasenfratz et al. (2017, equation 1 in Figure 4.3c) and of Kristjánsdóttir et al. (2007, equation 2 in Figure 4.3c). Our first revised calibration combines Mg/Ca data from this study with the eastern tropical

Atlantic *M. barleeanus* Mg/Ca reported by Hasenfratz et al. (2017). The regression analysis using *M. barleeanus* Mg/Ca and modern BWT shows a better fit described by the exponential equation 4 (Figure 4.3c). A linear approach (like the one proposed by Hasenfratz et al., 2017, equation 2 in Figure 4.3c) is not considered in this study as it leads to unrealistically high temperatures (Section 3.3.2), and BWT differences (ΔBWT = $BWT_{Modern} - BWT_{Calculated}$) on average over ±1.99°C (SD=1.33, n=22) showing large BWT uncertainties (Figure 4.4a).

$$Mg/Ca\ [mmol/mol] = 0.817 * \exp(0.0815 * BWT_{Mel}[°C]),\ r^2 = 0.8, n = 140 \qquad \textbf{(4)}$$

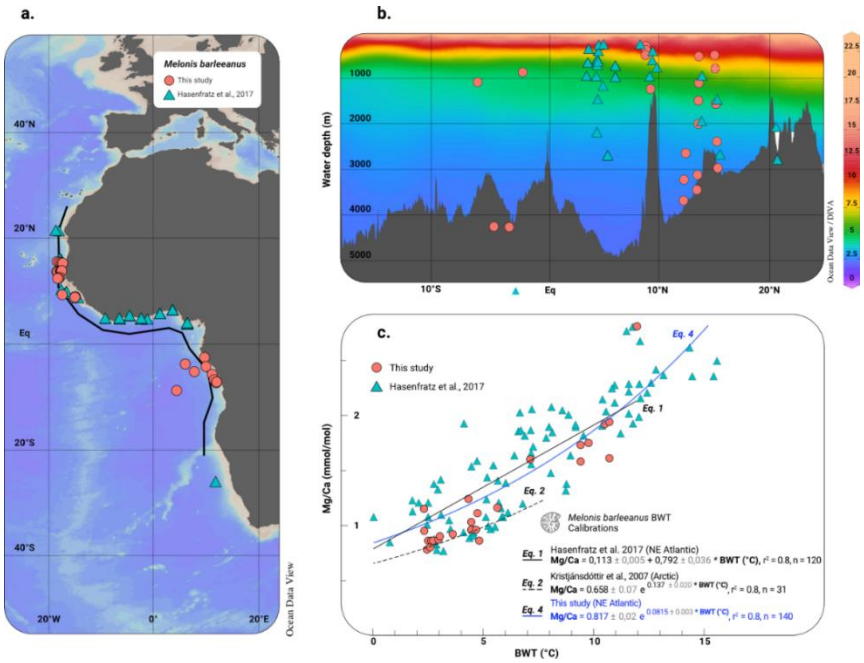

Figure 3.3 Location of the *Melonis barleeanus* sites from the eastern North Atlantic used for the revised calibration. a. Geographic location of the sites used for the revised calibrations presented in this study; **b.** Hydrographic section showing the modern water temperatures and the location in depth of the studied sites; **c.** *Melonis barleeanus* Mg/Ca BWT calibration for the NE Atlantic, including for reference the calibrations by Hasenfratz et al. (2017, black line), Kristjándóttir et al. (2007, dashed black line), and the proposed here (blue line).

BWTs estimated with equation 2 (Kristjánsdóttir et al., 2007), for our core top Mg/Ca ratios are in general higher than modern values, with average ΔBWT (Figure 4.4b) of ±1.9°C (SD=1.20, n=185). We also applied our revised calibration (equation 4), which shows an average ΔBWT of ±2.22 (SD=1.65, n=185, Figure 4.4c). As seen in section 3.2.2, Mg/Ca of *M. barleeanus* in this area is affected by other bottom water parameters like BWOx. Using the Mg/Ca and dissolved oxygenation concentration data from the sites studied here and the reported by Hasenfratz et al. (2017), we performed a multivariate regression analysis to describe the relationship between

Mg/Ca against BWT and BWOx simultaneously. We did not include the sites of Kristjánsdóttir et al. (2007) because all sites are in high oxygen conditions and come from a different region. The resulting equation 5, offers an improved approximation with an average ΔBWT of ±0.91°C (SD=0.8, n=85, Figure 4d), giving so far, the best results for temperature Mg/Ca-based reconstructions in the tropical eastern Atlantic, and reducing temperature uncertainties by more than 50% (Figure 4d) compared to previous calibrations.

$$\frac{\boldsymbol{Mg}}{\boldsymbol{Ca}}\left[\frac{mmol}{mol}\right] = 0.22\,\boldsymbol{BWT_{Mel}}[°C] + 0.131\,\boldsymbol{BWOx}\left[\frac{ml}{l}\right] - 0.438,\ r^2 = 0.88, n = 22 \qquad \textbf{(5)}$$

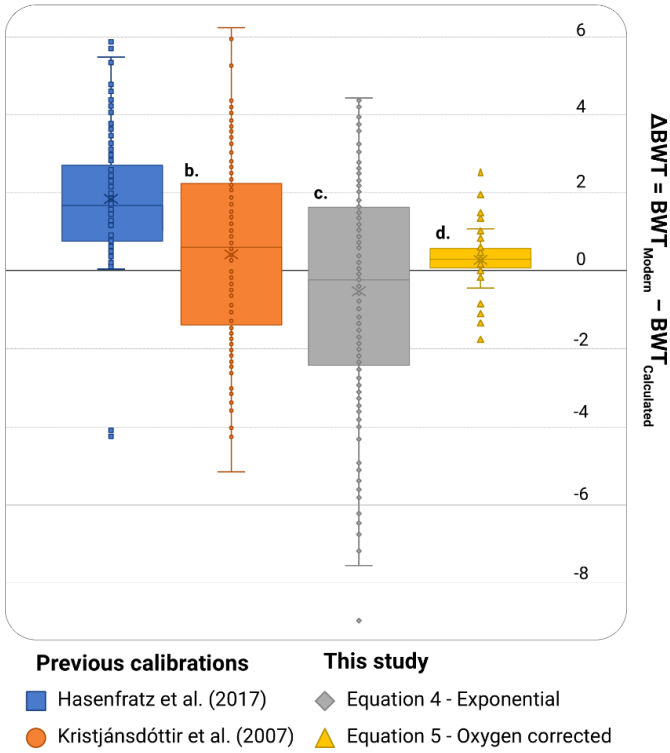

Figure 3.4 ΔBWT using *Melonis barleeanus* Mg/Ca – temperature calibrations from previous and the present studies in 55 coretops from the tropical eastern Atlantic. The boxplot shows the ΔBWT for each calibration calculated as $BWT_{Modern} - BWT_{Calculated}$ Using the equation of **a.** Hazenfratz et al. (2017); **b.** Kristjánsdóttir et al. (2007); **c.** Equation 4 in this study (exponential); and **d.** Equation 6 in this study (corrected by oxygen effect).

3.3 GeoB9512-5 downcore deglacial bottom water temperatures and stable isotopes based on benthic foraminifera

3.3.1 Benthic Foraminifera Stable Isotopes

Cibicidoides pachyderma $\delta^{18}O$ ranged between 1.9 and 3.6 ‰ and show a consistent declining trend from the end of the LGM into modern times, compatible with the ice effect-related global $\delta^{18}O$ (Waelbrock et al., 2001, Figure 4.8 e-f). The record shows average 3.5 ‰ from ca. 27 ka BP throughout the LGM until 18.9 ka BP (SD=0.08, n= 42). During the deglaciation, average values dropped to 3.3 ‰ at the onset of the HS1 (18.6 – 17.5, SD=0.03, n=13), followed by an additional decrease to average 3.0 ‰ between 17.4 and 14.8 ka BP (SD=0.2, n= 39). In the YD, $\delta^{18}O$ rapidly dropped to values under 2.5 ‰ at 12.9 ka BP and average 2.3 ‰ continued during this period (SD=0.1, n=12). Average 2.3 ‰ persisted in the early Holocene (11.6 – 11.2 ka BP, SD=0.02, n=10), and decrease to average 2.2 ‰ (SD=0.1, n=26) between 11 and 6.5 ka BP, into average 2.1 ‰ at the end of the record (6.2 – 1.5 ka BP, SD=0.1).

The *Cibicidoides pachyderma* carbon isotope record was not used here as it seems to be influenced by bottom water ventilation and nutrient content changes, making interpretation more difficult. A detailed description of this record is included in Chapter 5.

3.3.2 GeoB9512-5 Uvigerina mediterranea Mg/Ca and BWT record

Mg/Ca of *U. mediterranea* in core GeoB9512-5 (Figure 4.5a) was measured between 1 to 1.76 mmol/mol (average 1.26 mmol/mol, SD=0.16, n=88). The BWTs from these data using the equation of Roberts et al. (2016) ranged from 2.6 to 8.2 °C (Figure 4.5c). There were isolated transient warmings (> 6°C) at 20.5, 13.9 – 13.7, 12.8 - 11.8 and 5.6 ka BP. According to our BWT_{Uvig} record (Figure 5c), pre-LGM to HS2 BWTs were on average 4.5°C (SD= 0.4). A cooling of around 1°C was recorded at the beginning of the LGM (SD= 0.2, 23.3 to 22.1 ka BP), followed by a BWT increase to average 6.6°C (SD=0.9) in the middle LGM (21.2 – 20.1 ka BP), that finally dropped to around 4°C at 19.2 ka BP. This rapid ~ 2.3°C cooling led to relatively stable temperatures during the first part of the HS1 (on average 4.7°C, SD=0.4, between 18.9 and 17.1 ka BP), that dropped an additional ~ 0.6°C from 17.1 to 16.4 ka BP (average 4.0°C, SD=0.2) within the HS1. Towards the end of the HS1, BWTs

increased around 1°C when average temperatures of 5°C (SD=0.5) are recorded between 16.4 and 14.4. ka BP. Such warming was followed by an additional 1.2°C increase during the B-A (13.9 – 13.7 ka BP), into a final 1.2°C cooling in the last part of the same period (13.5 – 13 ka BP). The lack of recovery of *U. mediterranea* led to a data gap from 13.1 to 11.8 ka BP that corresponds to the YD, except for a single data point of 8°C at 12.8 ka BP, comparable to the 8.2°C at 11.8 ka BP. The beginning of the Holocene is marked by a cooling to 3.6°C (10.4 to 6.5 ka BP, SD=0.3), interrupted by a ~2°C warming to average 5.6°C from 6.2 to 5.6 ka BP. Our record ends with a Holocene 2.6°C cooling phase between 4.9 and 2.3 ka BP to average 3°C (SD=0.4), ending with a 2°C warming from 1.5 to 0.2 ka BP (~ 5.1°C, SD=0.6).

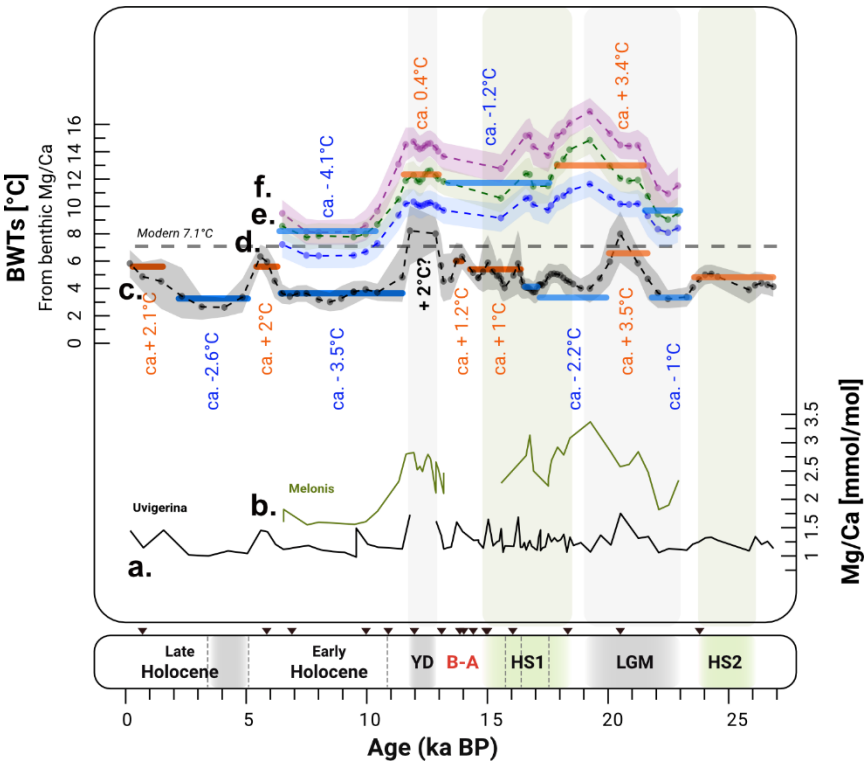

Figure 3.5 *Uvigerina mediterranea* and *Melonis barleeanus* Mg/Ca ratios and Bottom Water Temperatures from site GeoB9512-5 during the last 27 kyrs. Mg/Ca ratios measured in **a.** *U. mediterranea*; and **b.** *M. barleeanus*; Bottom Water Temperature reconstructions (BWT) using **c.** Mg/Ca of *U. mediterranea* in the calibration by Roberts et al. (2016); **d.** BWT (blue) using Mg/Ca of *M. barleeanus* in the calibration of Kristjánsdóttir et al. (2007); **e.** BWT (green) using Mg/Ca of *M. barleeanus* in the calibration of this study (Equation 5, oxygen corrected); **f.** BWT (purple) using Mg/Ca of *M. barleeanus* in the calibration of this study (Equation 4, exponential). All shaded areas correspond to the 95% uncertainty envelope. Blue bars and text represent average cooling periods, and orange bars and text average warming periods calculated from our data. **Key Climate events:** Heinrich Stadial 2 (HS2); Last Glacial Maximum (LGM); Heinrich Stadial 1 (HS1); Younger Dryas (YD). Triangles in the age axis indicate points of radiocarbon ages.

3.3.3 Melonis barleeanus Mg/Ca to fill the YD gap

The BWT_{Uvig} record from site GeoB9512-5 shows the BWT suggest the intermediate tropical eastern Atlantic off the NW African coast show marked temperature shift during the last deglaciation, moreover short-timed intense warming-cooling intervals are characteristic of the last 13 ka BP particularly during the late Holocene. However, missing data from the YD period prevented us from contrasting our results with other BWT reconstructions from the same periods. To fill this gap and improve the resolution of GeoB9512-5 deglacial paleotemperature record, tests of intermediate infaunal *M. barleeanus* were measured for trace element concentrations. *M. barleeanus* Mg/Ca values (Figure 4.5b) in site GeoB9512-5 oscillated between 1.54 and 3.36 mmol/mol (on average 2.46 mmol/mol, SD=0.46, n=36), and the BWT_{Mel} based on the calibration by Kristjánsdóttir et al. (2007) ranged from 6.3°C to 11.9°C (Figure 4.5d), while applying the equation of Hasenfratz et al. (2017) resulted in unrealistically high BWTs between 6.7°C and 22.8°C that were no further considered in the analyses.

With the revised calibrations presented here, BWT_{Mel} ranged from 7.8 to 17.4°C (equation 4, SD=2.5, n=36) and between 7.5 and 15°C (with equation 6 correcting for BWOx, SD=1.9, n=36). The BWT_{Mel} using the calibrations of Kristjánsdóttir et al. (2007, Figure 5d), and equations 4 (Figure 4.5f) and 5 (Figure 4.5e) presented here, show comparable trends during the last deglaciation, and the main difference is that BWTs estimated with our calibration are on average 3.8°C (equation 4) and 1.6°C (equation 5) warmer. To account for BWOx effect on our record, BWT obtained with equation 5 results will be used in the following discussion. Average temperatures of 9.7°C (SD=0.6) were registered during the first part of the LGM (22.9 – 21.6 ka BP), followed by marked ~ 3.4°C warming to average 13°C (SD=1) between 21.2 -17.9 ka BP, when peak temperatures over 14°C are recorded at 19.2 and 18.4 ka BP. The HS1 saw a cooling of around 1.2°C, with average BWTs of 11.8°C (SD=0.5, 17.6 – 12.9 ka BP), followed by an approximate increase of 0.4°C in the YD (average 12.2°C, SD= 0.3, 12.4 – 11.9 ka BP). Toward the end of the BWT_{Mel} record, temperatures rapidly dropped from 11.6 to 10.4 ka BP during the early Holocene, accounting for an overall 4°C cooling (average 8.1°C, SD=0.4, 10.4 – 6.5 ka BP) compared to the previous YD. The changes described here are comparable to the BWT records using

the Kristjánsdóttir et al. (2007) calibration and Equation 4 calibrations (Supplementary Information 4 in Appendix 3.1).

3.3.4 U. mediterranea – M. barleeanus BWTs show no constat offset during the last deglaciation

In general, the paleotemperature record based on *M. barleeanus* Mg/Ca, shows higher temperatures than the observed by the *U. mediterranea* record (Figure 4.5). Although a BWT offset ($\Delta BWT_{offset} = BWT_{Mel} - BWT_{Uvig}$) may be expected as the preferred microhabitat differs for both species, no constant offset could be calculated from our data (Figure 4.6). Furthermore, the ΔBWT_{offset} changes can be grouped in 3 intervals (Figure 4.6). Using the BWT_{Mel} from equation 5, during most part of the LGM (22.5 to 20.1 kyrs), ΔBWT_{offset} was on average 5.8°C (SD=0.9) and increased to average 8°C (SD=1.3°C) in the late LGM and HS1 (19.3 to 13.2 kyrs) in coincidence with the higher *M. barleeanus* Mg/Ca ratios (between 2.29 and 3.36 mmol/mol, on average 2.64 mmol/mol, SD=0.03). The mean ΔBWT_{offset} from the third interval (Figure 4.6), decreased to 4.4°C (SD=0.4) during the YD and early Holocene (12.9 ka BP and, between 10.4 to 6.5 ka BP). These substantial differences prevent a straightforward species composite paleotemperature record including BWT_{Mel} and BWT_{Uvi} for core GeoB9512-5, and furthermore suggests that additional controls influenced *M. barleeanus* Mg/Ca.

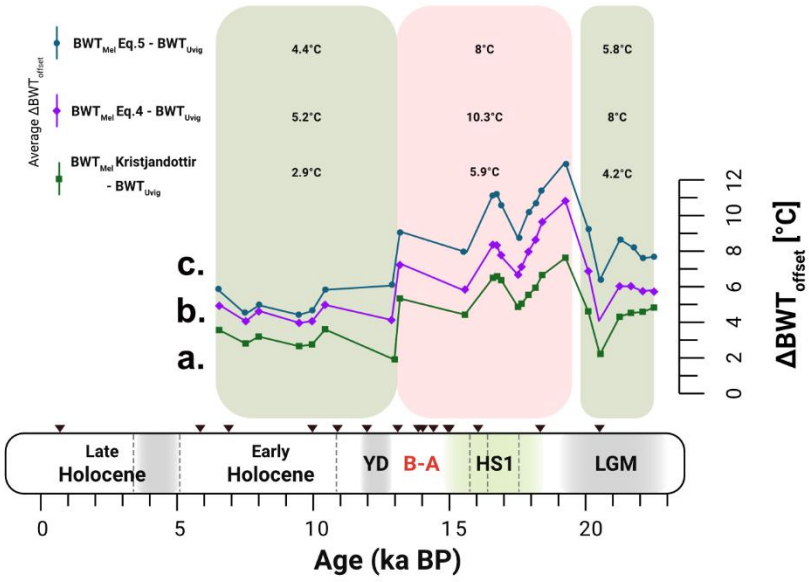

Figure 3.6 Interspecific Bottom Water Temperature offset (ΔBWToffset) in this study. ΔBWT_{offset} between different *Melonis barleeanus* calibrations and *Uvigerina mediterranea* BWTs from site GeoB9512-5 a. (green) using Mg/Ca of *M. barleeanus* in the calibration of Kristjánsdóttir et al. (2007); **b.** (purple) using Mg/Ca of M. barleeanus in the calibration of this study (Equation 4, exponential); **c.** (blue) using Mg/Ca of *M. barleeanus* in the calibration of this study (Equation 5, oxygen corrected). The ΔBWT_{offset} was calculated as the difference BWT_{Mel} - BWT_{Uvig}. **Key Climate events:** Heinrich Stadial 2 (HS2); Last Glacial Maximum (LGM); Heinrich Stadial 1 (HS1); Younger Dryas (YD). Triangles in the age axis indicate points of radiocarbon ages.

However different, BWT_{Mel} follows similar trends to the record from BWT_{Uvig}, which can be seen more clearly when BWT_{Mel} is shifted - 3°C (Figure 3.7). A ~3.4°C warming period is seen in both records in a part of the LGM (22.5 to 21.2 ka BP), and cooling episodes during part of the HS1 (16.6 – 15.6 ka BP), and for the early Holocene (10.4 to 6.5 kyrs) observed in BWT_{Mel} follow similar trends as BWT_{Uvig}. However, LGM warming lasts longer in the BWT_{Mel} (in coincidence with the higher ΔBWT_{offset}) and is followed by 1.2°C cooling in the HS1 (Figure 4.6b), while BWT_{Uvig} shows an earlier 2.2°C cooling event in the HS1. The HS1 to B-A warming observed in the BWT_{Uvig} record, is partially observed in the BWT_{Mel}, however low recovery of *M. barleeanus* in the B-A prevents an accurate comparison. During the YD, the partial warming observed from the *U. mediterranea* record is more or less confirmed by warmer temperatures from the *M. barleeanus* record, since no data was obtained from this species the exact magnitude of said warming is difficult to establish. Finally, during the YD to early Holocene transition, a consistent cooling from more than 3°C is registered in both records.

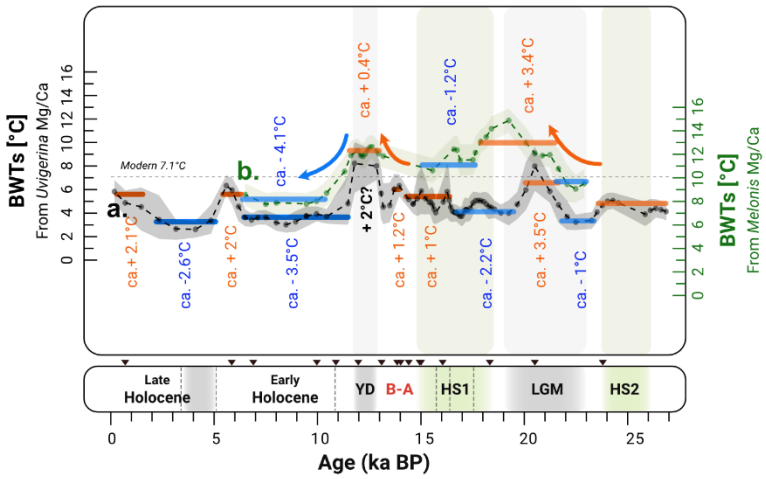

Figure 3.7 Deglacial Bottom Water Temperatures from site GeoB9512-5. Bottom Water Temperatures (BWTs) calculated with a. *Uvigerina mediterranea* Mg/Ca using the calibration of Roberts et al., 2016; and **b.**

Melonis barleeanus Mg/Ca in the calibration of this study (Equation 5, oxygen corrected). Blue arrows indicate cooling, and orange arrows warming. **Key Climate events:** Heinrich Stadial 2 (HS2); Last Glacial Maximum (LGM); Heinrich Stadial 1 (HS1); Younger Dryas (YD). Triangles in the age axis indicate points of radiocarbon ages.

3.4 Microhabitat or paleo-oxygenation changes? Mn/Ca on infaunal foraminifera of the NE Atlantic

The contrast between the BWT records of *U. mediterranea* and *M. barleeanus* (Figures 4.5 and 4.6), suggest that our *M. barleeanus* Mg/Ca is in fact dependant on BWT changes, however it seems to also be influenced by other factors particularly during the LGM and HS1. Mn/Ca of some benthic foraminifera are used to reconstruct bottom water oxygenation changes (e.g., Brinkmann et al., 2023), and in some cases Mn/Ca variability can reflect microhabitat changes (Ní Fhlaithearta et al., 2018). Here, we compared the dissolved oxygen concentrations (ml/l) inferred from the EBFOI (Barragán-Montilla et al., in review) in the same site with both species Mn/Ca and observed no common trends (Supplementary Information 5a-c in Appendix 3.1). Furthermore, a correlation test showed no apparent link (Supplementary information 5 in Appendix 3.1) with *U. mediterranea* (r^2=0.02, p=0.2, n=72) or *M. barleeanus* (r^2=0.0001, p=0.9, n=31) Mn/Ca, suggesting that for at least these two species in the tropical eastern Atlantic deglacial Mn/Ca changes are most likely linked to microhabitat changes as suggested on Section 3.1.1. Potential Mn/Ca as a contamination indicator was also ruled out from the low Mn/Ca ratios (Section 2.3.1) and using SEM images (Supplementary information 6 in Appendix 3.1) before and after applying the cleaning protocol.

If Mn/Ca of the benthic foraminifera species studied here is considered as a proxy for microhabitat changes, the difference in preferred microhabitat between shallow infaunal *U. mediterranea* and intermediate infaunal *M. barleeanus*, implies that the Mn/Ca recorded by *U. mediterranea* would be lower than *M. barleeanus* (e.g. Koho and Piña-Ochoa, 2012; Ní Fhlaithearta et al., 2018). This is true for our data, Mn/Ca of *M. barleanus* (average 0.023 mmol/mol, SD=0.010, n= 35) is higher (Figure 4.7d) to Mn/Ca *U. mediterranea* (average 0.005 mmol/mol, SD=0.002, n= 74) (Figure 4.7c) suggesting a shallower habitat for the latter species.

Mn/Ca of *U. mediterranea* remains relatively stable throughout the studied interval (between 0.002 – 0.012 mmol/mol), while Mn/Ca of *M. barleeanus* increases from average 0.009 mmol/mol (SD=0.002) to average 0.027 mmol/mol (SD=0.011) during the late LGM - HS1 (red shaded area in Figure 4.7c-d). This higher *M. barleeanus* Mn/Ca persists into the YD (average 0.026 mmol/mol, SD=0.003) and decreases during the early Holocene (average 0.014 mmol/mol, SD=0.004, green shaded areas in Figure 4.7c-d). This suggests that *U. mediterranea* in site GeoB9512-5 had a relatively stable microhabitat in the last 27 ka BP, while *M. barleeanus* migrated to deeper microhabitats in the sediment during the late LGM - HS1. However, it is difficult to constrain whether this shift was maintained during the YD due to the limited data between the end of the HS1 and YD, but a potential return to shallower microhabitats could be inferred form the available data (Figure 4.7a-g, green shaded areas).

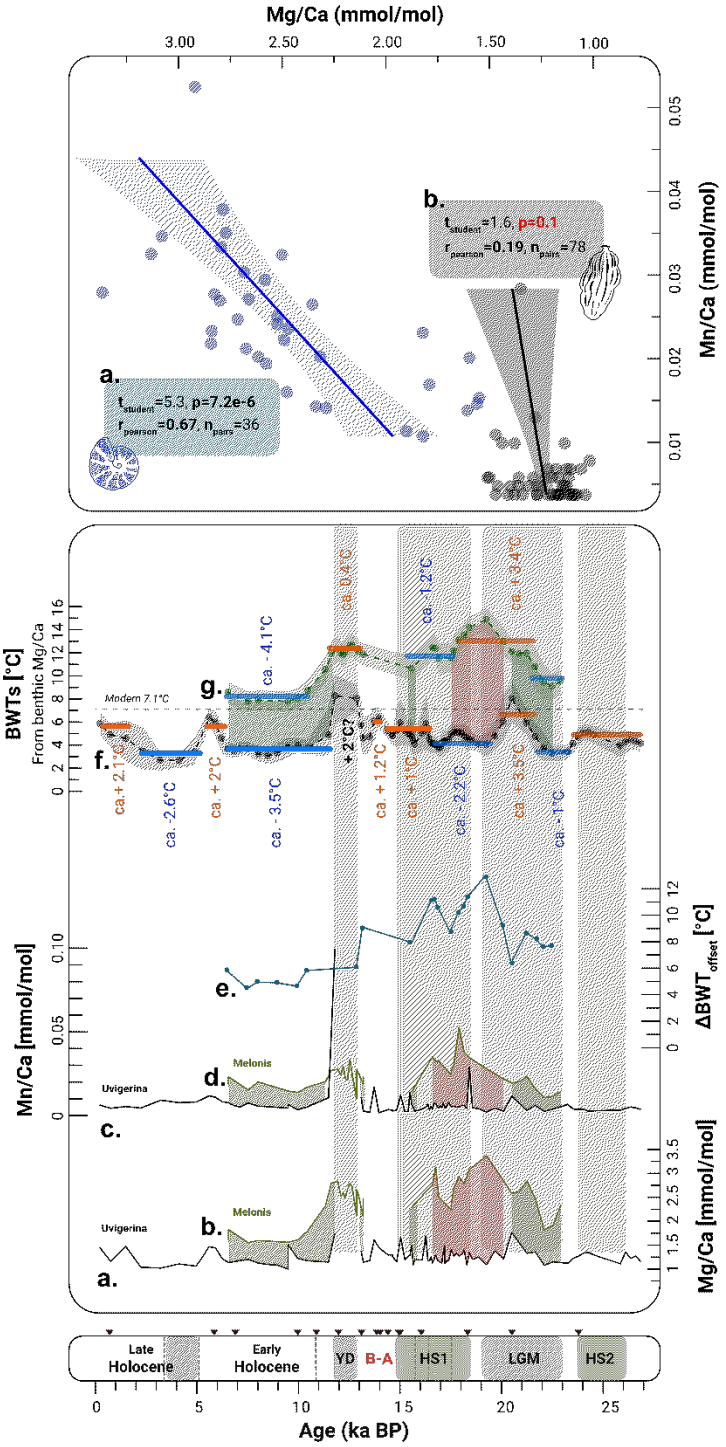

Figure 3.8 *Uvigerina mediterranea* and *Melonis barleeanus* Mg/Ca and Mn/Ca ratios and deglacial Bottom Water Temperatures from site GeoB9512-5. Mg/Ca ratios measured in **a.** *U. mediterranea* and; **b.** *M. barleeanus*; Mn/Ca ratios measured in **c.** *U. mediterranea* and; **d.** *M. barleeanus*; **e.** Offset between *U. mediterranea* BWT and *M. barleeanus* BWT (ΔBWT_{offset}); Bottom Water Temperature reconstructions (BWT) using **f.** Mg/Ca of *U. mediterranea* in the calibration by Roberts et al. (2016) and **g.** BWT using Mg/Ca of *M. barleeanus* in the calibration of this study (Equation 5). Shaded areas in the temperature records correspond to the 95% uncertainty envelope. Blue bars and text represent average cooling periods, and orange bars and text average warming periods calculated from our data. **Key Climate events:** Heinrich Stadial 2 (HS2); Last Glacial Maximum (LGM); Heinrich

Stadial 1 (HS1); Younger Dryas (YD). Triangles in the age axis indicate points of radiocarbon ages. **Top panel:** Correlation test between Mg/Ca and Mn/Ca of **a.** *M. barleeanus* and **b.** *U. mediterranea*.

T The increase in the ΔBWT_{offset} (Figure 4.7e) is visibly linked to higher *M. barleenus* Mg/Ca (Figure 4.7b). Average Mg/Ca ratios from 2.05 mmol/mol in the early LGM (SD=0.23), increase to average 2.67 mmol/mol (SD=0.27) during the late LGM and HS1 when in some cases values up to 3.15 mmol/mol are recorded. During the YD high Mg/Ca are still evidenced by average 2.61 mmol/mol (SD=0.13), which decrease to average 1.76 mmol/mol (SD=0.26) in the early Holocene. The timing of the *M. barleeanus* Mg/Ca increase related to the higher ΔBWT_{offset} described in section 3.3.3 during the late LGM and HS1 in site GeoB9512-5 coincides with the observed increase of this species Mn/Ca (Figure 4.7d). This observation, along with the positive correlation between Mg/Ca and Mn/Ca of *M. barleeanus* in site GeoB9512-5 (r^2=0.44, n=36, Figure 4.7a top panel), suggests microhabitat migration to lower oxygen conditions and not only bottom water warming confirmed by the *U. mediterranea* BWT record, increased Mg/Ca ratios during LGM and HS1 (21 – 17.5 ka BP, red shaded area in figure 4.7c-d). However, is not possible to exactly quantify such an effect with the available data, and further studies should be conducted to better asses this hypothesis.

3.5 Microhabitat changes driven by paleoceanographic changes and its impact on M. barleeanus Mg/Ca

During the last deglaciation, increasing diatom counts and opal content from deep site GeoB7926-2 (20°13'N, 18°27'W, 2,500 m water depth off Mauritania) suggests an upwelling intensification of silica-rich waters during the HS1 and YD due to an increase in NE trade winds leading to enlarged upwelling filaments (Romero et al., 2008). The enhanced upwelling resulted in increased primary productivity that impacted deep-sea benthic ecosystems by increasing organic matter deposition (Filipsson et al., 2011). Our site is located closer to the Senegal coast (around 50 km east of the coastline) under the influence of seasonal upwelling regimes unlike GeoB7926-2 that is within an area of continuous upwelling. However, the peaks of infaunal foraminifera percentages in site GeoB9512-5 (Figure 4.8b, modified from Barragán-Montilla et al.,

in review) during HS1 and B-A, indicate higher organic carbon concentrations at the seafloor (e.g. Jorissen et al., 1995).

Depletion of the *Cibicidoides pachyderma* $\delta^{13}C$ from our site (Figure 8a) suggests increased nutrient content hinting at enhanced upwelling and explaining the increase in organic carbon seen by the infaunal foraminifera peaks (Figure 8b). More importantly, one of these enhanced upwelling – increased primary productivity periods coincide with the largest differences in our *U. mediterranea – M. barleeanus* paleotemperature records (red shaded area in Figure 8e-f), and with the larger offset of Mn/Ca (Figure 7c-d) linked to the higher *M. barleenaus* Mn/Ca (Figure 7d). Increase in organic matter content at the seafloor due to enhanced upwelling off the NW African coast could explain *M. barleeanus* microhabitat migration during the HS1 in coincidence with the larger ΔBWT_{offset}. Intense altered organic matter linked to upwelling has also been seen to impact *M. barleeanus* size, with larger test usually synchronous with enhanced upwelling episodes during the LGM (Caralp et al., 1989), while *M. barleeanus* is regarded as a highly adapting species (Linke and Lutze, 1993). This suggests that the changes in the BWT_{offset} observed between the *U. mediterranea* and *M. barleeanus* paleotemperature records due to the higher *M. barleeanus* Mg/Ca could be linked to microhabitat migration effects due to increased organic matter fluxes related to changes in the upwelling activity in our area.

Influence of total organic carbon on Mg/Ca ratios has been suggested by Hasenfratz et al. (2017), who hypothesized that in environments with elevated organic matter and increased CO_2 as a product of remineralizing bacteria led to a fractionation effect of Mg/Ca in undersaturated pore water. In our site, infaunal foraminifera content suggest moderate to high organic matter concentrations in the last 27,000 years (Figure 4.8b). Interval peaks with average percentages over 77% are registered during the HS1 (between 18.3 and 17.6 ka BP; and between 16.2 and 15.9 ka BP), B-A (between 14.4 and 13.3 ka BP) and in the last part of the Holocene (1.6 – 0.2 ka BP). The main difference between this increase in organic matter, is that during the first interval of the HS1 (18.3 – 17.6 ka BP) the benthic foraminifera assemblage is dominated by *U. mediterranea* (on average > 49.5%), while in the second interval (16.2 -15.9 ka BP) *N.*

turgida/*pulchella* (on average >15%) and *Bolvina subaenariensis* var. *Mexicana* (on average > 33.9%) are the most abundant species. In the B-A interval, *N. turgida*/*pulchella* (on average > 21.1%) and *Oridorsalis umbonatus* (on average > 18.3%) are the most representative benthic foraminifera. These changes in the benthic foraminifera distribution (see Appendix 3.1) suggests that for the HS1 between 18.3 and 17.6 ka BP increased fresh organic matter came from primary productivity potentially linked to upwelling (e.g. Fontanier et al., 2002), while the other two infaunal peak intervals are related to increased altered organic matter from continental sources (e.g. Mojtahid et al. 2010, Bartels-Jónsdóttir et al., 2006). The interval with marked increased in *U. mediterranea* a species that prefers labile organic matter (Fontanier et al., 2002) coincides with the interval of higher ΔBWT_{offset} described here, suggesting that the microhabitat changes of *M. barleeanus* inferred from the measure Mn/Ca were controlled by an increase of fresh organic matter potentially from primary productivity driven by increased upwelling activity.

The exact quantification of microhabitat migration on Mg/Ca uptake is more elusive, however an approximation can be made if we assume the Mn/Ca ratios are a quantitative measure of microhabitat migration. If the *U. mediterranea* paleotemperature record is used as a reference of the theoretical real deglacial bottom water temperatures, an approximation can be made of the amount of *M. barleeanus* Mg/Ca necessary to obtain such theoretical temperature, therefore allowing to estimate the excess Mg/Ca from the measured here (form now on referred as Mg/Ca residuals). By obtaining the BWT accounted by the Mg/Ca residuals from *M. barleeanus* and contrasting through a linear regression with the measured Mn/Ca ratios (understood as a microhabitat proxy e.g. Koho et al., 2015), we observe that a 0.002 mmol/mol of Mn/Ca corresponds to a + 0.49 mmol/mol Mg/Ca, or in other words accounts for a 1°C increase. The average Mn/Ca change in *M. barleanus* is ~ 0.010, accounting for approximately 5.5°C, meaning that even small changes in microhabitat induce large uncertainties in paleotemperature reconstructions. However, only with precise core top calibrations accounting for microhabitat changes, it will be possible to establish a more precise BWT estimation.

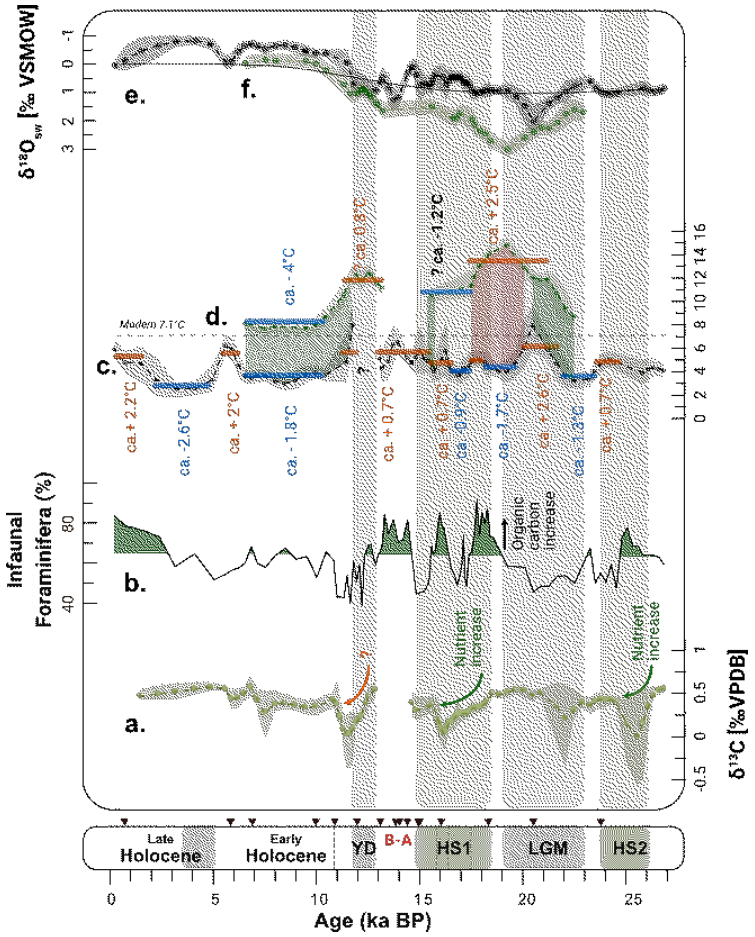

Figure 3.9 GeoB9512-5 benthic foraminifera infaunal content (from Barragán-Montilla et al., in review), and $\delta^{13}C$, $\delta^{18}O$, Mg/Ca, Mn/Ca and bottom water temperatures (this study). a. *Cibicidoides pachyderma* $\delta^{13}C$ record; b. Benthic Infaunal percentages (modified from Barragán-Montilla et al., in review); Bottom Water Temperature reconstructions (BWT) using **c.** Mg/Ca of *U. mediterranea* in the calibration by Roberts et al. (2016); **d**. Mg/Ca of *M. barleeanus* in the calibration of this study (Equation 5); Seawater δ18O calculated using *Cibicidoides pachyderma* $\delta^{18}O$ e. corrected by a *Uvigerina* offset of +0.64 ‰ and *Uvigerina* Bottom Water Temperatures (BWTs) in the formula from Shackleton (1974); and **f**. with no offset and *Melonis* BWTs in the formula from Shackleton (1974); global seawater $\delta^{18}O$ (Waelbroeck et al., 2001) included for reference. Shaded areas in the temperature and stable isotope records correspond to the 95% uncertainty envelope. In the temperature record blue bars and text represent average cooling periods, and orange bars and text average warming periods. **Key Climate events:** Heinrich Stadial 2 (HS2); Last Glacial Maximum (LGM); Heinrich Stadial 1 (HS1); Younger Dryas (YD). Triangles in the age axis indicate points of radiocarbon ages.

3.6 Paleoceanographic implications

Contrasting results from our Mg/Ca-based BWTs reconstructions raise relevant issues in benthic foraminifera pelothermometry. On the one hand, BWT records are important to understand changes in ocean heat distribution in the past, that could hint on its relationship to oceanographic changes. On the other hand, reliable BWT reconstructions are also important to study ocean salinity variations based on $\delta^{18}O$,

meaning that BWTs uncertainties are transferred to other paleoceanographic proxies that depend on temperature corrections. For GeoB9512-5, we see that *Cibicidoides pachyderma* $\delta^{18}O$ (Figure 8e-f) corrected by a temperature effect using the *U. mediterranea* records (Figure 8e) show good agreement with the global $\delta^{18}O$. When applying the same correction to $\delta^{18}O$ using the *M. barleeanus* (Figure 8f) paleotemperature records, the $\delta^{18}Osw$ trend follows the global signal, but has an approximate 0.75 ‰ increase from the LGM until the HS1 suggesting the presence of a more saline water mass like the Mediterranean Outflow Water or the North Atlantic Central Water during the LGM – HS1 transition in our site, that could also explain the high temperatures observed in the *M. barleeanus* paleotemperature record.

From our observations, an intense warming during the LGM like the one seen by the *M. barleeanus* BWT records seems unlikely. Other temperature records in the tropical western Atlantic show intermediate water warming starting in the HS1 (Oppo et al., 2023), via enhanced downward heat transport in Atlantic Meridional Overturning Circulation as predicted by climate models (Zhang et al. 2017). Similar observations in the eastern tropical North Atlantic have been also registered by benthic foraminifera Mg/Ca, with warming periods between 17.5 and 14.5 ka BP in the HS1 and 12.9 and 11.6 ka BP in the YD (Weldeab et al., 2016). Although the intense warming seen in the LGM - HS1 by the *M. barleeanus* record is most likely related to microhabitat changes linked to enhanced organic matter content, the ~1°C during the YD followed by a ~4°C cooling in the Holocene seemingly corresponds to real temperature signals, and not microhabitat effects as seen by the *Uvigerina* BWT record. Warming in the HS1 is difficult to constrain due to the bias in the *M. barleeanus* paleotemperature record, but a 0.8°C warming is shown by the *U. mediterranea* record between 15.6 and 14.9 ka BP that persisted into the B-A.

From our data, we find that the BWT from *U. mediterranea* Mg/Ca records changes of intermediate water temperatures during the last deglaciation. The warming periods observed at the end of the HS1 and potentially during the YD (which is partially confirmed by the BWT_{Mel} record), agree with other records from the eastern tropical North Atlantic (Weldeab et al., 2016). Furthermore, our record is consistent with a

decreased heat transport to higher latitudes, that would have resulted in increased accumulation of heat at intermediate depths (e.g. Oppo et al., 2023) in the tropics.

4 Conclusions

This new multiproxy approach brings new evidence on the complexity of benthic foraminifera calcification in the tropical eastern Atlantic. The strong correlation between Mg/Ca of intermediate infaunal *Melonis barleeanus* allowed to estimate bottom water temperatures using the equation 4 (Mg/Ca [mmol/mol] = 0.817 * exp (0.0815*BWT[°C]), r^2=0.8, n=140), and 5 (Mg/Ca [mmol/mol] = 0.22*BWT[°C] + 0.13*BWOx[ml/l] - 0.44 , r^2=0.9, n=22), that latter decreasing temperature uncertainties by ~ 50% compared to previous calibrations. The marked sensitivity of *M. barleeanus* Mg/Ca to temperature changes, makes this species a reliable paleothermometer in the NE Atlantic, however, we found that other bottom water conditions like BWOx, and microhabitat changes due to paleoenvironmental modifications can affect *M. barleeanus* Mg/Ca, particularly in the eastern tropical North Atlantic. Such parameters are not static in the geologic record, making it necessary to calibrate our proxies to account for other effects, or look for more static species, since microhabitat changes are more difficult to assess.

Using this new approach in the intermediate depth core GeoB9512-5 of the eastern tropical North Atlantic, we found that the BWT records based on *U. mediterranea* Mg/Ca shows less abrupt changes in the last 27kyrs compared to the BWT record from *M. barleeanus* Mg/Ca. Furthermore, the latter shows higher temperatures, and registers intense warming periods at the end of the LGM through HS1 and during the YD. We show that the intense LGM – HS1 warming in the *M. barleeanus* record seems to be overestimated due to microhabitat changes induced by modifications in the organic matter fluxes related to enhanced primary productivity in times of more intense upwelling off NW Africa. However, the YD warming is in line with other BWTs reconstructions during the last deglaciation in the western and eastern intermediate tropical Atlantic, as well as the subsequent strong cooling at the beginning of the Holocene seen in both records. These results underline the relevance of using multi species Mg/Ca records to reconstruct bottom water paleotemperatures. Moreover,

local calibrations are strongly suggested as they can improve paleoceanographic reconstructions and interpretations by significatively decreasing uncertainties.

Acknowledgements

This research was carried out within the Cluster of Excellence EXC 2077 “The Ocean Floor – Earth’s Uncharted Interface” at MARUM institute – University of Bremen, funded by “Deutsche Forschungsgemeinschaft” (DFG). This research is also supported by GLOMAR – Bremen International Graduate School for Marine Sciences, University of Bremen. Core materials were provided by the GeoB Core Repository of Bremen, and we would like to thank Dr. Jürgen Titschack who kindly located most of the core top samples used here. SEM images in the supplementary information were kindly provided by Jim Buckman from the Scanning Electron Microscopy Facility at Heriot-Watt University. Core top samples from the tropical South Atlantic were provided by Dr. Enno Shefuss from MARUM.

Data availability

Barragán-Montilla, Sofía; Mulitza, Stefan (in review): Radiocarbon ages of sediment core GeoB9512-5. PANGAEA, https://doi.org/10.1594/PANGAEA.962899

Barragán-Montilla, Sofía (in review): Benthic foraminifera stable isotopes (d18O and d13C) of sediment core GeoB9512-5. PANGAEA, https://doi.org/10.1594/PANGAEA.962968

Barragán-Montilla, Sofía; Johnstone, Heather J H (in review a): Benthic foraminifera minor element to calcium ratios for core-tops from the eastern Tropical Atlantic. PANGAEA, https://doi.pangaea.de/10.1594/PANGAEA.964299

Barragán-Montilla, Sofía; Johnstone, Heather J H (in review b): Benthic Foraminifera trace elements to calcium ratios and bottom water temperatures from the last 27,000 years of sediment core GeoB9512-5. PANGAEA, https://doi.pangaea.de/10.1594/PANGAEA.964318

Chapter 4: Stagnant North Atlantic Deep Water heat uptake with reduced Atlantic Meridional Overturning Circulation during the last deglaciation

Published in *Paleoceanography and Paleoclimatology*. Adjusted to fit the format style
https://doi.org/10.1029/2022PA004575

S. Barragán-Montilla[1], S. Mulitza[1], H.J.H. Johnstone[1] and H. Pälike[1]

[1] MARUM – Center for Marine Environmental Sciences and Department of Geosciences, University of Bremen, Bremen, Germany

Corresponding author: Sofía Barragán Montilla (sbarraganmontilla@marum.de)

Key Points

- Intense North Atlantic Deep-Water warming at the beginning of Heinrich Stadial 1 and the Younger Dryas
- With a weak AMOC during HS1 and the YD deep water temperature remained stable in poorly ventilated bottom waters
- Weaker HS1 and YD NADW formation, may reduce heat dissipation into the deep Atlantic

Key words

AMOC slowdown, Deep-Water Warming, Benthic Foraminifera Mg/Ca, Deglaciation, Paleotemperature

Abstract

Atlantic Meridional Overturning Circulation (AMOC) plays a major role in the climate system by modulating the depth and rate of oceanic heat storage. Some climate simulations suggest that reduced AMOC decreases bottom water ventilation and that the heat absorbed by the ocean starts to mix downwards, warming Atlantic intermediate waters. This has been corroborated for the western North Atlantic by benthic foraminifera geochemical records from periods of reduced AMOC during the

last deglaciation. However, the deep-water response remains poorly constrained, and the lack of direct paleotemperature reconstructions limits our understanding about the effects of reduced circulation on ocean heat uptake. We present a new reconstruction of bottom water temperatures from core GeoB9508-5 (2,384 m water depth, 15°29.90N/17°56.88W) off the northwestern African Margin. Our paleotemperature record, based on Uvigerina spp. Mg/Ca, shows two episodes of intense transient deep water warming in times of decreasing overturning circulation, followed by long periods of heat uptake stagnation. First, during AMOC slowdown in the Heinrich stadial 1, when paleotemperatures of ~2°C persisted for ~5.4 kyrs coincident with the weakest stage of AMOC; and second in the Younger Dryas, when bottom water temperatures >4°C lasted ~2.5 kyrs during a less intense AMOC decline. This suggests a stagnation of deep-water heat uptake in the deep NE Atlantic possibly linked to a reduced downward advection of heat during times of a reduced AMOC, supporting the hypothesis that AMOC strength sets the depth of oceanic heat storage in the North Atlantic.

Plain Language Summary

Anthropogenic activity affects earth-atmosphere energy balance enhancing climate change in the last decades. The ocean plays a key role in this balance, by taking up to 90% of the excess heat from the atmosphere and redistributing it globally though the Atlantic Meridional Overturning Circulation (AMOC). For the 21st century, a possible 34 – 45 % AMOC reduction has been hypothesized, raising concern on its effects on ocean heat uptake and climate change. To contribute to the understanding of these possible effects, we reconstructed bottom water temperatures changes for eastern North Atlantic deep waters over the last 46.000 years, including two periods with a significantly reduced AMOC: (1) Heinrich Stadial 1 (18.200 to 14.900 years ago) and (2) the Younger Dryas (12.800 to 11.700 years ago). Our results suggest that with a weak AMOC, Atlantic intermediate waters warm as ventilation decreases, at the same time this heat stops being transferred to the deep eastern North Atlantic for thousands of years. The implications of these processes for global warming still need to be investigated.

1 Introduction

Increasing anthropogenic greenhouse gases have made radiative forcing and ocean heat uptake the main controls of global climate and global sea-level rise (Marshall and Zanna, 2014). Since 1950, 80 to 90% of the excess heat that accumulated in the Earth System was absorbed by the ocean through heat uptake (Cummins et al., 2016; Levitus et al., 2000; Levitus et al., 2005; Marshall and Zanna, 2014) and almost half of this heat uptake took place in the North Atlantic between 35° and 70°N (Kostov et al. 2014) where the North Atlantic Deep Water (NADW) is formed. NADW formation is a main component of the overturning cell in the Atlantic and potentially influences the rate of global warming (e.g., Muschitiello et al., 2019; Talley 2003, 2013; Zhang et al., 2019) as it transports energy away from the sea surface and distributes heat to the south in the ocean interior as part of the lower limb of the AMOC.

It has been speculated that future AMOC slowdown may accelerate global warming (Liu et al., 2020; IPCC, 2013; IPCC, 2022; Zhang et al., 2019), as it reduces the heat capacity of the ocean. This is of concern as recent studies suggest an ongoing AMOC slowdown during the 19th and 20th century as a response to increasing atmospheric CO_2 and greenhouse gases (GHGs) concentrations (Caesar et al., 2021; Dima et al., 2021; IPCC, 2022; Rahmstorf et al., 2015). These results are however controversial due to large uncertainties introduced by limited data availability and coverage (Caesar et al., 2022; Kilbourne et al., 2021; Latif et al., 2022), and additionally other datasets suggest such an AMOC slowdown will not likely occur in the next century e.g. Lobelle et al., 2020; Jackson et al., 2022). However, a 34 – 45% AMOC decline during the 21st century is consistently projected in all models from the phase 6 of the Coupled Model Intercomparison Project (CMIP6) (Weijer et al., 2020), supported by numerical analysis, multi-parameter studies, and process-based probabilistic assessments (Dima et al., 2021; Robson et al., 2018; Schleussner et al., 2014). Even though the possibility of AMOC slowdown remains under debate, concern about the future of AMOC slowdown is thoroughly discussed in IPCC reports (e.g. IPCC, 2022), citing an already observed (medium confidence) slowdown between 1850 – 2015, and a very likely AMOC slow down over the 21st century (high confidence) (Dodman et al., 2022 in IPCC, 2022).

The available instrumental record of AMOC strength variability is still too short for its effect on the deep ocean heat reservoir to be understood. The sedimentary record of the last deglaciation in the North Atlantic, however, provides the opportunity to study the effects of AMOC variations in deep water heat uptake from the last millennia. Since the end of the Last Glacial Maximum (19 kyrs BP), AMOC variability has been recorded by the kinematic proxy 231Pa/230Th in sediment cores of the Atlantic Ocean (Gherardi et al., 2005; McManus et al., 2004; Böhm et al., 2015; Ng et al., 2018). Additional evidence of AMOC changes is also provided by the bipolar seesaw pattern observed in the northern and southern hemispheres (Marino et al., 2015), South Atlantic (Barker et al., 2009), and ice cores (EPICA, 2006), and in part by the Intertropical Convergence Zone (ITCZ) shift towards the south predicted by climate models and proxy data (e.g. Broccoli et al., 2006; Dupont et al., 2010, Mulitza et al. 2017). However, it is important to note that the ITCZ shift during the HS1 and YD can also be driven (along with other climate feedback and processes) by changes in top-of-atmosphere (TOA) radiation related to meltwater discharge (Li and Liu, 2022). According to this research, a significant AMOC decline occurred during the Heinrich Stadial 1 (18.3 -15.4 kyrs BP) followed by a time of temporary AMOC reinvigoration during the Bølling–Allerød (B-A). A shorter and less pronounced slowdown of the overturning circulation occurred during the Younger Dryas (12.9- 11.7 kyrs BP), which was followed by a fully restored AMOC during the Holocene. Additional to 231Pa/230Th, evidence of reduced ventilation as a response of AMOC slowdown has also been observed from benthic foraminifera δ13C. Drops in the carbon isotopic values of epifaunal foraminifera in the western North Atlantic show that during the Heinrich Stadial 1 (HS1) and Younger Dryas (YD) ventilation decrease is consistent with a weaker AMOC (e.g., Oppo et al., 2015).

To investigate temperature changes in the deep ocean associated with AMOC changes, we present a new deglacial record of bottom water temperatures from the continental slope off Senegal in 2384 m water depth, in the NADW, based on Mg/Ca ratios of Uvigerina spp. Our data shows an intense deep water warming at the onset of HS1 and the YD, and deep waters remained warm during subsequent periods of reduced deep-water ventilation and accelerated global warming. These results

suggest that the state of the AMOC can indeed affect the heat uptake of the deep Atlantic.

2 Materials and Methods

2.1 Core Location and Chronology

The sediments of gravity core GeoB9508-5 were retrieved from 2384 m water depth at 15°29.90'N/17°56.88'W (Figure 4.1) from the continental slope off Northwest Africa (Mulitza et al., 2006). The ambient water mass at the core location is North Atlantic Deep Water (NADW) with a bottom water temperature of about 2.7°C (Locarnini et al., 2010) and a $\delta^{18}O$ of 0.26 ‰ SMOW (LeGrande and Schmidt, 2006).

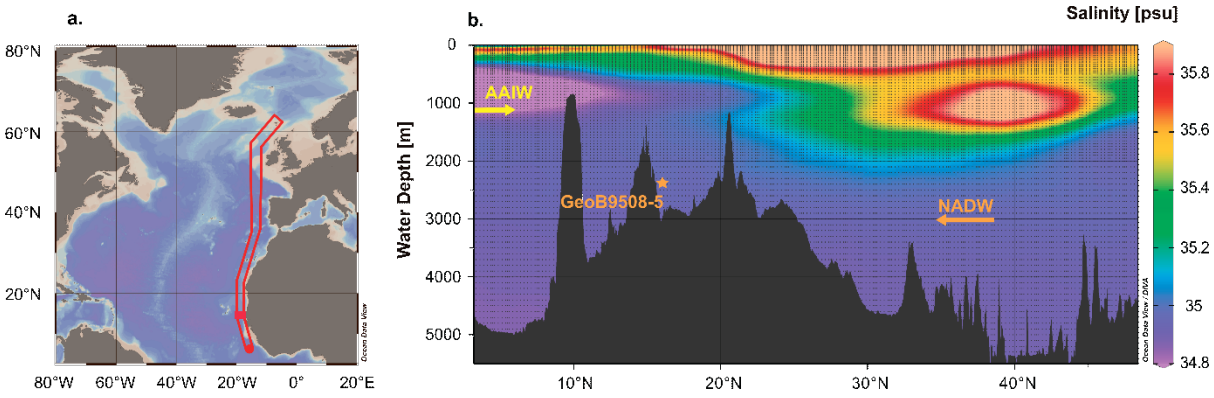

Figure 4.1 ***GeoB9508-5 Location*** **a.** Geographical location overview of GeoB9508-5 (15°29.90N, 17°56.88W, 2384 m water depth) in the eastern North Atlantic off the coast of Senegal (Northwestern Africa); **b.** GeoB9508-5 water depth in a modern salinity section. Schlitzer, R., Ocean Data View, https://odv.awi.de, 2018

The chronology of the core is based on 11 radiocarbon ages (Mulitza et al. 2008). The downcore age-depth relation and age uncertainty was modelled using the R script BACON (Blaauw and Christen, 2011) version 2.5.5 using the Marine20 calibration (Heaton et al., 2020). The core contains an undisturbed deglacial sequence with no reversals over the last 47.6 kyrs (Figure 4.2). Sediments from the Last Glacial Maximum (LGM, ~ 23 – 19 kyrs BP) are present from ~ 348 to 203 cm depth and from the Younger Dryas (YD, ~ 12.8 - 11.7 kyrs BP) between ~ 160.5 – 125.5 cm. The core also covers the last 5 Heinrich Stadials (HS) associated with decreased Fe/K and Al/Si ratios (Zabel, 2010) due to increased continental aridity and dust input providing age-independent evidence of these events (e.g., Mulitza et al., 2008). Heinrich Stadial 1 (HS1 ~ 18.2 - 14.9 kyrs BP) is recorded from ~ 283 to 208 cm depth, the HS2 (~26 – 22.7 kyrs BP) appears from 344 to 400 cm, the HS3 (~29.5 – 28.5 kyrs BP) from 448

to 468 cm, the HS4 (~39.6 – 36.7 kyrs BP) from 600 to 648 cm and the HS5 (~46.1 – 44.5 kyrs BP) from 748 to 780 cm. Additionally to these key intervals, the Bølling–Allerød warming (B-A, ~ 14.7 – 12.9) is recorded within 205.5 – 163 cm depth.

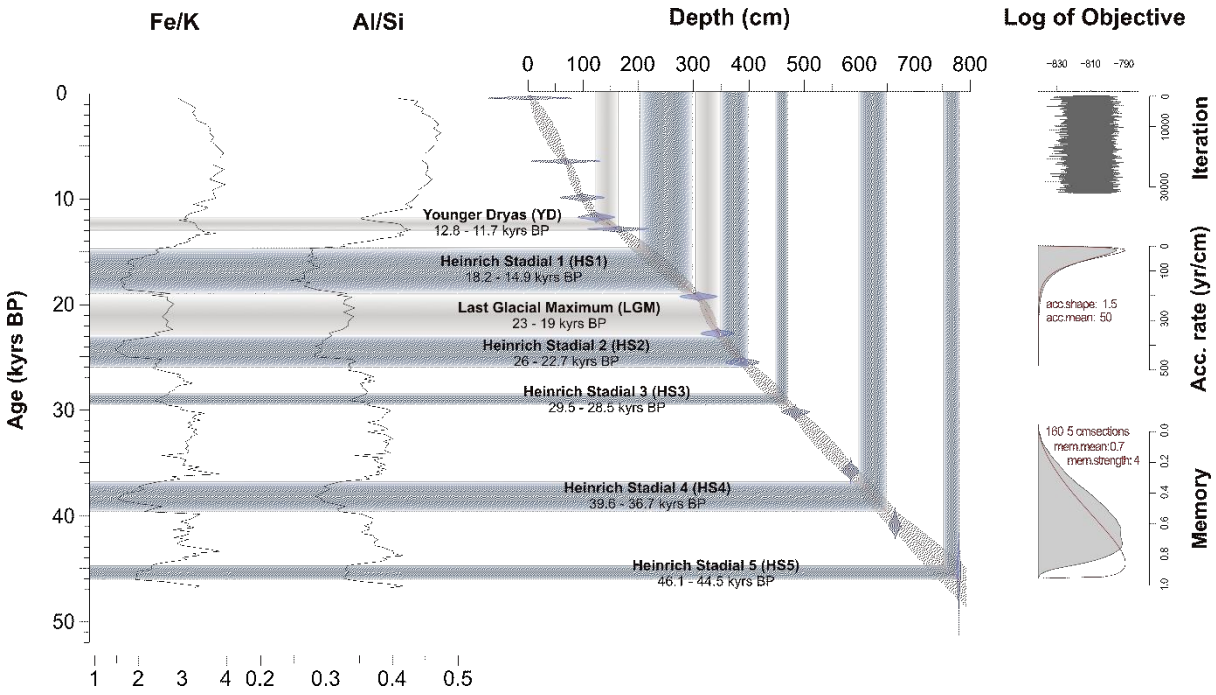

Figure 4.2 ***GeoB9508-5 Age Model showing key climatic events of the last 50 kyrs*****.** The downcore age-depth relation was modelled using the Bacon package (Blaauw and Christen, 2011) and the Marine20 calibration curve (Heaton et al., 2020) on R studio. Fe/K and Al/Si (Zabel, 2010) are included to calibrate Heinrich events.

2.2 Mg/Ca determinations in benthic foraminifera of genus *Uvigerina*

Tests of the benthic foraminiferal genus *Uvigerina* spp. were picked from washed sediment previously used for stable isotopic measurements (Mulitza et al. 2008, Niedermeyer et al. 2009) and measurements of planktonic Mg/Ca ratios (Zarriess et al. 2011). *Uvigerina* samples consisted of 2 to 6 tests (85 of 93 samples contained 5 tests), most specimens were U. peregrina, but they were combined with other Uvigerina species where necessary. Foraminifera were crushed and then cleaned with water, methanol and hot hydrogen peroxide solution (no reductive cleaning step) using a pipette robot programmed to follow the protocol of Barker et al. (2003). The method differed from Johnstone et al. (2016) in that a Framestar 200 96 well-tray with conical wells and maximum volume of 200 µL was used to hold the samples.

Trace element concentrations were measured using an Inductively Coupled Plasma Optical Emission Spectrometer (ICP-OES)—Agilent Technologies 700 Series with Cetac ASX-520 autosampler. Elements were measured at the following spectral lines: Mg (279.6 nm), Ca (315.9 nm), Sr (421.6), Al (167.0 nm), Fe (238.2 nm), and Mn (257.6 nm). Calibrations for all elements were based on linear regressions. Instrumental precision was monitored using an in-house standard solution, run after every 8 samples, for which long term (5 years) standard deviation for Mg/Ca is < 2%, and commercial limestone standard, ECRM 752-1, run after every 32 samples. Mean Mg/Ca of ECRM 752-1 run during the analyses presented here was 3.73 (relative standard deviation (RSD) 0.13%, standard error (SE) 0.0016) which is within 1% of the value reported by Greaves et al., [2005] for centrifuged samples, of 3.75 (RSD 0.31 %, SE 0.0011).

2.3 Calculation of bottom water temperature, $\delta^{18}O$ and $\delta^{13}C$ and uncertainty assessment

Bottom water temperature (BWT) was calculated with the equation (2.1):

$$\text{Mg/Ca [mmol/mol]} = 0.0915 * \text{BWT[°C]} + 0.843 \qquad (2.1)$$

following the calibration by Roberts et al. (2016), which was proposed specifically for the South Atlantic Ocean. $\delta^{18}O$ of seawater was estimated from BWT and the $\delta^{18}O$ of *Cibicides wuellerstorfi* (corrected by a species-specific offset of +0.64 ‰) using the equation by Shackleton (1974). No further correction was applied to the $\delta^{13}C$ of C. wuellerstorfi. The uncertainty of the resulting time series was assessed by producing ensembles with 10000 possible time series for each proxy. To this end, the 10000 downcore age-depth relations produced with Bacon (Blaauw and Christen, 2011) were combined with 10000 downcore proxy series by randomly generating 10000 normal distributed proxy values for each depth with a standard deviation of 0.7 °C for BWT (Roberts et al. 2016) and 0.07/0.05 for δ18O and δ13C (Mulitza et al. 2008). The resulting 10000 time series were linearly interpolated to the Median ages of the depths of the BWT values. δ18O of seawater was calculated from δ18O of C. wuellerstorfi and BWT for all individual ensemble time series. Finally, the mean and 95%

uncertainty envelope were calculated for BWT, δ18O and δ13C of sea water for all ensemble values at the median ages.

3 Results

3.1 *Cibicidoides wuellerstorfi* $\delta^{18}O$ and $\delta^{13}C$ Stable Isotopes

The observed changes in seawater δ18O (δ18Osw) are consistent with the global change in δ18O associated with ice effect (Waelbrock et al. 2001) and register relatively stable glacial and LGM average values around 1.2 ‰ (Figure 2.3b). All values used for interpretation come from analyses made on the ensemble medians. The start of the deglaciation is associated with an increase in δ18Osw to ~1.4‰ during HS1, followed by a decrease from the B-A (on average ~0.9 ‰) that persists into the Holocene (on average ~0.4 ‰). This decrease in sea water δ18O was only interrupted by a step of ~0.4 ‰ after the end of the YD (10.9 - 11.8 kyrs) and stable values of ~0.2 ‰ (close to modern values at the core location of 0.26‰) persisted in the last 8.6 kyrs.

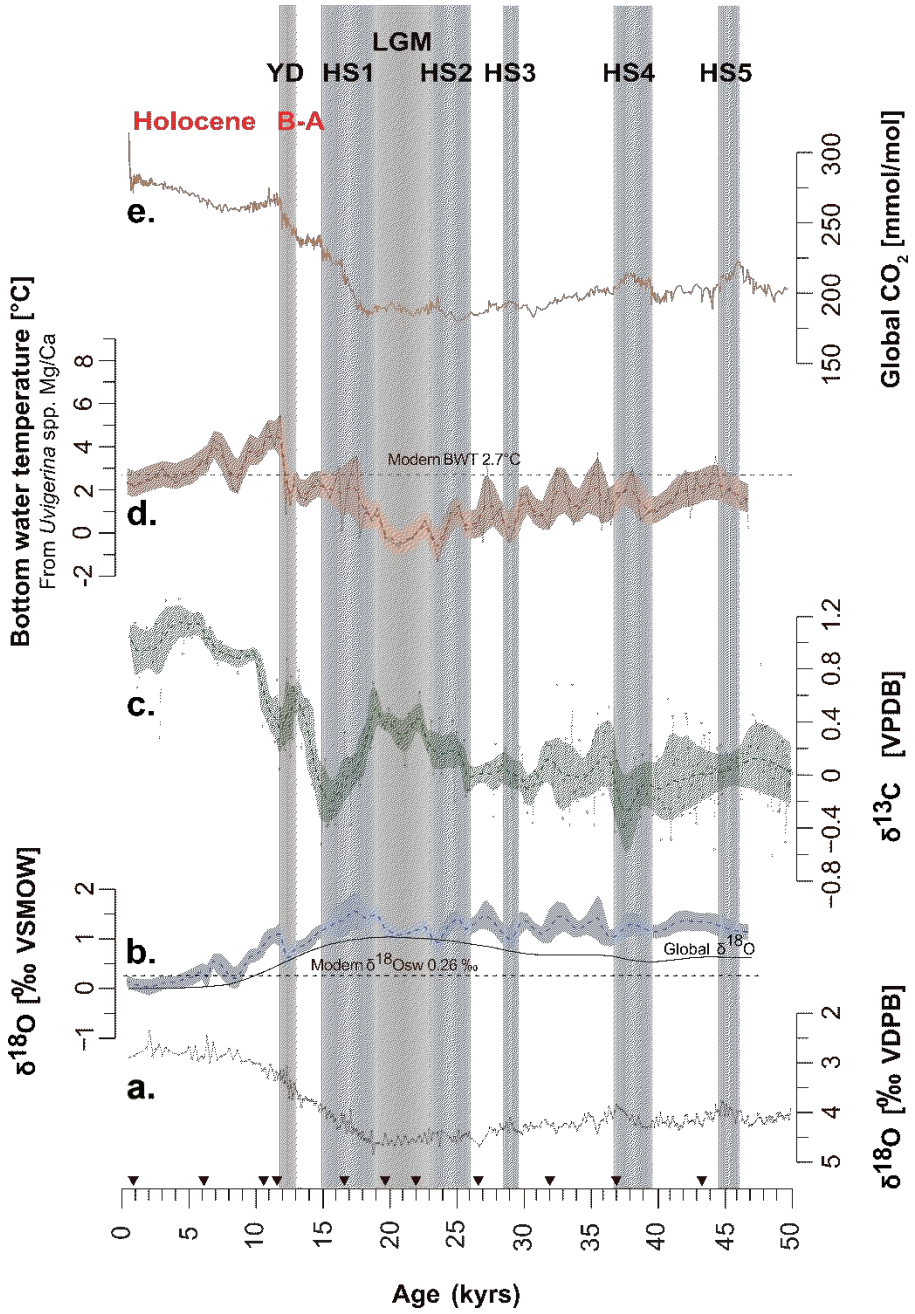

Figure 4.3 Benthic foraminifera proxies from core GeoB9508-5 showing the deglacial evolution of the eastern North Atlantic in the last 45 kyrs. Ages were modeled from radiocarbon datings (triangles) and shaded areas represent the 95% confidence intervals **a.** $\delta^{18}O$ of Cibicidoides wuellerstorfi; **b.** $\delta^{18}O$ of seawater estimated from $\delta^{18}O$ measurements on C. wuellerstorfi corrected by a species-specific offset of +0.64 ‰ and Bottom Water Temperatures (BWT) using the formula from Shackleton (1974); Global $\delta^{18}O$ of seawater is included for reference (Waelbroeck et al. 2001); **c.** $\delta^{13}C$ measured on C. wuellerstorfi (gray curve is raw data); **d.** Bottom water temperatures (BWT) calculated from Uvigerina spp. Mg/Ca ratios (gray curve is raw data), following the equation of Roberts et al. (2016); **e.** Global CO_2 included for reference (Köhler et al., 2017). Key Climate events: Last Glacial Maximum (LGM); Heinrich Stadial 1 (HS1); Younger Dryas (YD). Triangles in the age axis indicate points of radiocarbon ages.

The *C. wuellerstorfi* δ13C record follow an overall increasing trend from the LGM to Holocene times (Figure 3c). The data starts in pre-HS5 times (53.3 to 46.3 kyrs), when

average carbon isotope of 0.04‰ are recorded. During HS5 to HS4 times (from 53 to 36.6 Kyrs), carbon isotope ratio decreased (between -0.23 to 0.1 ‰), with minimum (-0.29 ‰) occurring during the HS4. Rapid increase on benthic foraminifera δ13C is observed from the end of HS4 into the HS3, with relatively stable values (on average 0.002 ‰) from 34.8 to 26.7 kyrs. The onset of HS2, is recognized by higher δ13C with average of 0.1 ‰, followed by an overall average increase of 0.18 ‰ during the LGM (average 0.3 ‰). However, two important decreases in δ13C were registered during the HS1 and YD cold periods. During the HS1, δ13C had an average low signal of -0.07 ‰, that increased above 0.4 ‰ during the warmer B-A and dropped again below 0.35 ‰ during the YD and the beginning of the Holocene. During the first part of the Holocene, δ13C increased from 0.3 ‰ at 11.4 kyrs to 0.7 ‰ at 10.3 kyrs. This increase was followed by a stable period of 2.9 kyrs with average δ13C of ~ 0.75 ‰. Higher δ13C (average ~ 0.9 ‰) was observed again from 6.8 to 3.6 kyrs, followed by a final decrease of around 0.1 ‰ during the last 2.8 kyrs of the core (3.6 to 0.6 kyrs BP).

3.2 Bottom water temperature reconstructions based on Uvigerina Mg/Ca

Recent research has shown that other parameters other than BWT of pore waters potentially influence benthic foraminifera Mg/Ca ratios (Elderfield et al., 2010; Weldeab et al., 2016). This has led to a reevaluation of some paleotemperature records on epibenthic foraminifera (e.g. Yu and Elderfield, 2008). However, the effects on infaunal foraminifera are still poorly constrained. Some of these factors include, among others, carbonate ion saturation (Δ [CO_3^(2-)]). Although not definitive, Hasenfratz et al. (2017) provided sufficient evidence showing that there is no correlation between Δ [CO_3^(2-)] and Mg/Ca of *Melonis*, suggesting that infaunal species of *Melonis* and *Uvigerina* are less affected by Δ [CO_3^(2-)] of pore waters as previously proposed by Elderfield et al. (2010). In contrast, Weldeab et al. (2007) found a Δ [CO_3^(2-)] effect on Globobulimina Mg/Ca and hypothesized a similar effect must exist on Uvigerina Mg/Ca. Such straightforward assessments have not yet been made for Uvigerina. Stirpe et al. (2021) found that anomalous high Uvigerina Mg/Ca from the deep Southwest Pacific (Mg/Ca on average 1.4 mmol/mol, 0.6 to 2.1 mmol/mol, standard deviation 0.36) cannot be explained solely by temperature gradients, but the available data could not help discriminating which other factors potentially affect the Uvigerina Mg/Ca signal in that study.

From our available data, we cannot definitely rule out a Δ [CO_3^(2-)] effect on our Mg/Ca estimates, however low correlation (r^2=0.10, p=〖1.77x10〗^(-3), n=93) of our *Uvigerina* Mg/Ca with Sr/Ca, a geochemical proxy related to carbonate ion saturation according to Yu et al., 2014, suggests no major control of Δ [CO_3^(2-)] in Uvigerina Mg/Ca (Figure 4). Our Uvigerina Mg/Ca ratios (between 0.72 and 1.34 mmol/mol, on average 1.01 mmol/mol, standard deviation 0.13) are within the previously reported values for the North Atlantic (e.g. Elderfield et al., 2010; Roberts et al., 2016), and show no apparent anomalies. In addition, confidence that our Mg/Ca records are not reflecting high and erratic values as those observed by Stirpe et al. (2021) is given by the running standard deviation which shows no increase in periods of our record recording high Mg/Ca (Figure 4.4), i.e. these high values are not more variable than in other parts of the record. This along with the consistent δ^{18}Osw and the Global δ^{18}O of Waelbroeck et al. (2001) in Figure 4.3b, suggests our Mg/Ca based BWTs reconstructions are reflecting real temperature changes in the deglacial record of GeoB9508-5, rather than other geochemical anomalies.

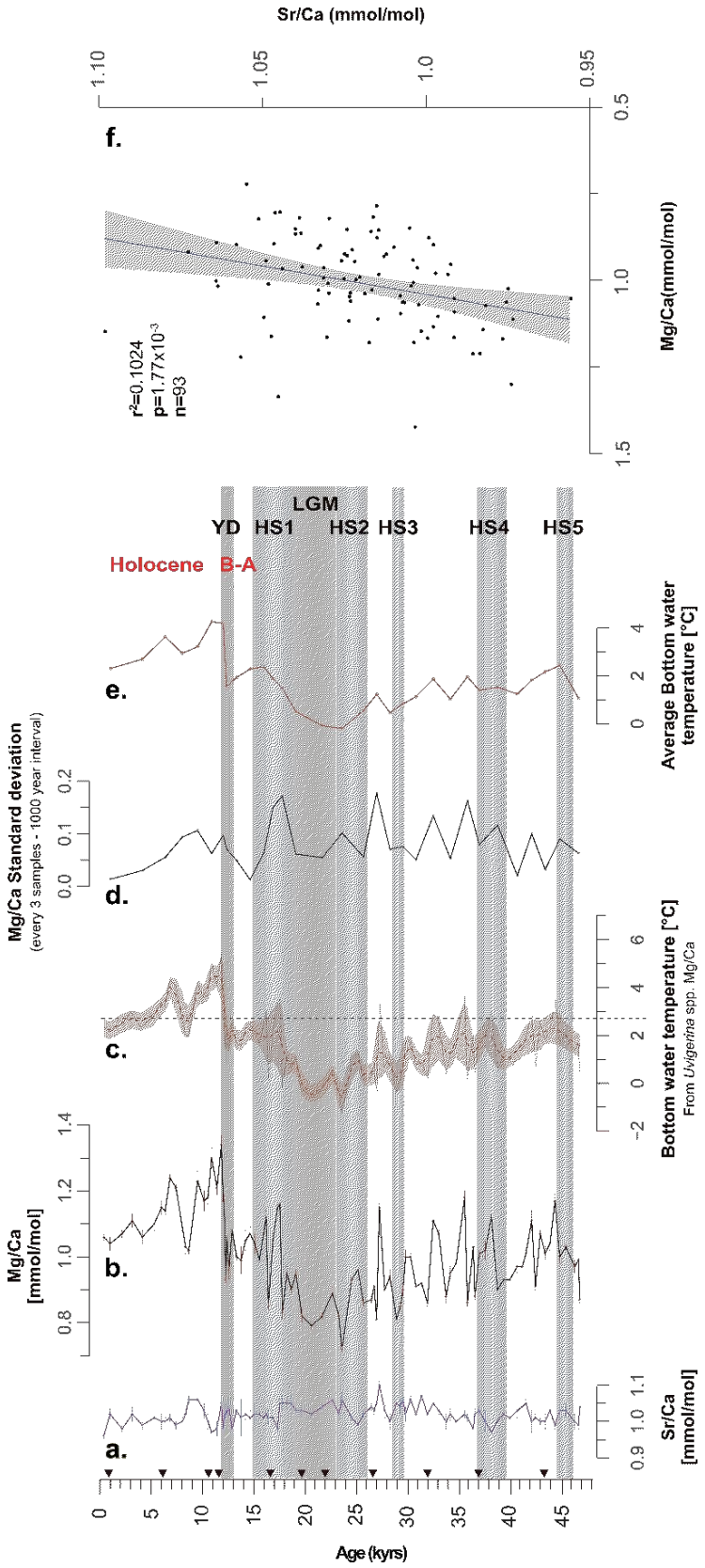

Figure 4.4 ***Bottom water temperatures and trace element concentrations measured in Uvigerina spp. from Core GeoB9508-5*** **a.** Sr/Ca; **b.** Sr/Ca; **c.** Bottom Water Temperature (BWT) using the calibration of Roberts et al. (2016) for the Atlantic Ocean; **d.** Mg/Ca standard deviation for a 3-sample window (approximately every 1.000 years); **e.** average BWT for a 3-sample window (approximately every 1.000 years); f. Relationship between Uvigerina Mg/Ca and Sr/Ca.

3.3 Deglacial bottom water temperatures in the deep Eastern North Atlantic

BWT estimates show an overall trend towards warmer bottom waters from the LGM to Holocene times (Figure 4.3). During the glacial, temperatures remained stable at ~1.5°C, and dropped by approximately 1.3°C on average during the LGM when minimum temperatures down to -0.6°C were registered. The end of the LGM is marked by a ~2°C bottom water warming, followed by a ~5.4 kyrs stable period during the HS1 and B-A when BWT was ~2°C. This was followed by very rapid warming into the late YD. Maximum temperatures, of above 4°C, occurred at the end of the YD and beginning of the Holocene epoch. This intense warmth lasted for approximately 2.5 kyrs and was followed by a cooling of ~1.2°C that concluded in BWT of 2.2°C, which is similar to that of modern times.

4 Discussion

4.1 Ventilation during times of reduced AMOC

AMOC variability in GeoB9508-5 can be observed from bottom water ventilation changes shown by our δ13C record (Figure 5), where low δ13C suggests weaker bottom water ventilation (e.g. Oppo et al., 2015; Eide et al., 2017). On the broad scale, the carbon isotope signal shows strong similarity with the 231Pa/230Th record (Figure 5) from the west North Atlantic (McManus et al., 2004, Mulitza et al. 2017), one of the main proxies used to trace the strength of AMOC during the last deglaciation. During the HS1, the carbon isotope signal declines (from an average of 0.2 ‰ during the LGM to -0.03 ‰ in the HS1) consistent with a reduced deep-water ventilation related to AMOC slowdown (Niedermeyer et al., 2009). A similar but less intense response occurs during the YD (from 0.4 ‰ during the B-A to 0.3 ‰), which coincides with a less pronounced decrease of AMOC circulation according to the data from McManus et al. (2004). In contrast, AMOC reinvigoration is inferred for the B-A warming from the 231Pa/230Th records of the west Atlantic (McManus et al., 2004). This temporal activation coincides with the stronger ventilation observed from our δ13C records during this time.

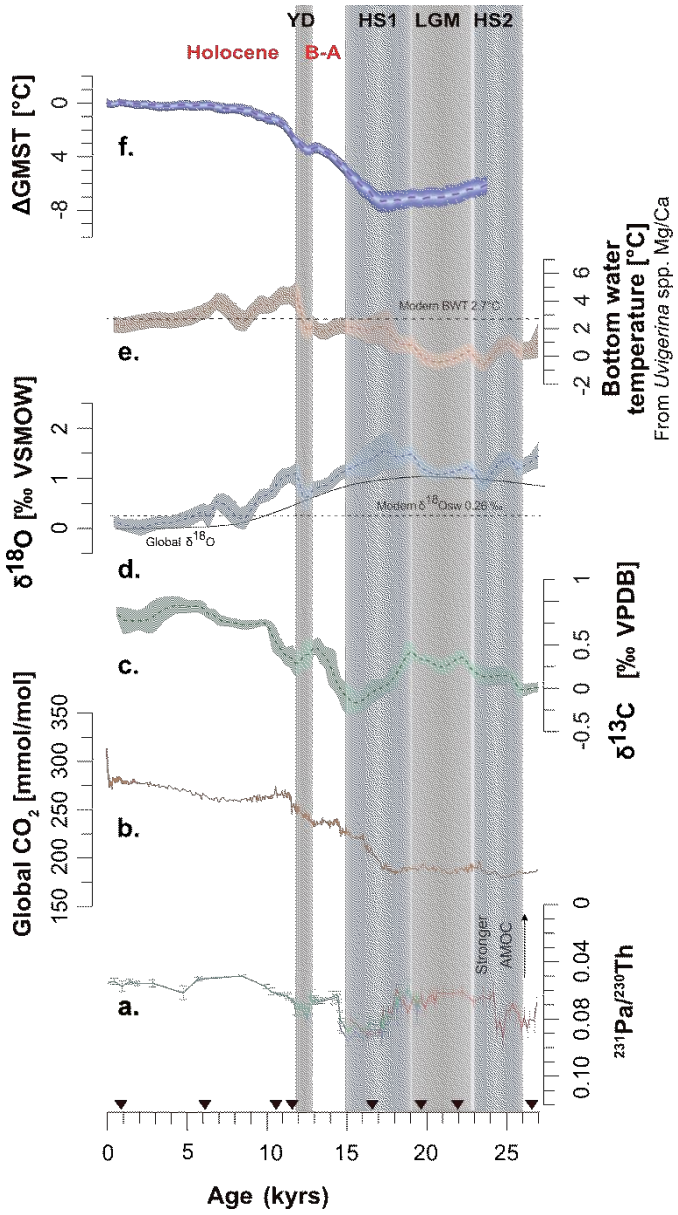

Figure 4.5 $^{231}Pa/^{230}Th$ records from the North Atlantic, Global CO_2 fluctuations, Global Mean Surface Temperature (GMST) and benthic foraminifera proxies from core GeoB9508-5 (this study) spanning the last 25 kyrs. a. $^{231}Pa/^{230}Th$ from the Bermuda Rise (blue and green from McManus et al., 2004); and from the deep NW Atlantic (red from Böhm et al., 2015); **b.** Global CO2 concentration (Köhler et al., 2017); **c**. $\delta^{13}C$ measured on *C. wuellerstorfi* (this study); **d.** $\delta^{18}O$ of seawater and global $\delta^{18}O$ of seawater anomaly (Waelbroeck et al. 2001); **e.** Bottom water temperatures (BWT) calculated from Uvigerina spp. Mg/Ca ratios (this study), following the equation of Roberts et al. (2016); **f.** Global mean surface temperature computed relative to the preindustrial average of the last millennium (Osman et al., 2021). Key Climate events: Last Glacial Maximum (LGM); Heinrich Stadial 1 (HS1); B-A: Bølling–Allerød; Younger Dryas (YD). Triangles in the age axis indicate radiocarbon ages.

4.2 Deglacial Bottom Water Temperatures response

The changes in bottom water ventilation registered in our core are directly associated with AMOC fluctuations, and these are reflected in variations in the BWT, albeit with different timing. The relatively more ventilated deep waters during the LGM inferred from the carbon isotope records, coincide with a ~1.2°C drop in BWT compared to

pre-LGM paleotemperatures (Figure 5). Moreover, minimum temperatures of around -0.5°C occur in times of increasing ventilation (~0.3‰ $\delta^{13}C$ at 20.6 kyrs).

At the onset of HS1, (~18.2 kyrs BP), BWTs in the deep NE Atlantic increased by ~1.6°C and subsequently remained at ~2°C for approximately 5.3 kyrs. The warming during this early stage of the Heinrich Stadial is associated with direct meltwater input from the European Ice Sheets via Channel River into the Bay of Biscay (Ménot et al. 2006, Toucanne et al. 2015), far away from the regions of deep-water formation and hence with little impact on the AMOC. The heat uptake during warm summers (Denton et al. 2022) together with a still active overturning circulation may have contributed to the warming of North Atlantic Deep Water observed in our Mg/Ca record. Stable BWTs persisted into the B-A warming, suggesting that AMOC slowdown effects were so strong that even when circulation resumed with improved ventilation, the deep-water masses did not distribute this heat and heat uptake remained stalled at the same time global mean surface temperature was increasing (Osman et al., 2021, shown in Figure 5). However, the precise mechanisms explaining BWTs stability in the NE Atlantic during AMOC resumption times in the B-A should be further explored.

Although AMOC slowdown during the YD was much less abrupt, and ventilation was higher, compared to HS1 conditions, our Mg/Ca records registered maximum BWTs above 3.7°C that persisted for 2.5 kyrs (from 9.5 to 12.1 kyrs) into the beginning of the Holocene. We suggest that although AMOC circulation decline was less abrupt compared to HS1 times, and was already partially recovered during the B-A, heat redistribution was still not fully restored during the YD.

High $\delta^{18}O_{sw}$ values at the beginning of HS1 and the YD (Figure 4.5d) suggest the presence of a bottom water mass with relatively high salinity. The higher salt content may provide the necessary density to allow the formation of relatively deep warm bottom waters. This interpretation is consistent with high subsurface salinities and temperatures reconstructed for the beginning of HS1 and the YD near the NADW source regions in the North Atlantic (Max et al., 2022).

Our Mg/Ca BWT reconstruction shows notable differences to the mean ocean temperature (MOT) reconstruction by Bereiter et al. (2018). MOT shows warmings during the height of HS1 and the YD when BWTs off NW Africa remain rather constant. This difference in timing indicates that other depth levels or basins of the global ocean must provide a stronger contribution to MOT increases during HS1 and the YD. Indeed, strong intermediate water warmings have been observed for HS1 and the YD in the South Atlantic (Roberts et al. 2016), the northern North Atlantic (Ezat et al. 2014) and the tropical Pacific (Lo Giudice Cappelli et al. 2016). In the Atlantic, this subsurface/intermediate warming occurs as a direct consequence of the suppression of vertical convection (Brady and Otto-Bliesner, 2011, He et al. 2020) and are thus consistent with our interpretation that less heat is flushed to the deep Atlantic during HS1 and the YD.

The Atlantic overturning circulation recovered during the Holocene, in coincidence with decreasing BWTs during the last 9 ka as shown by our records. In this time period, GeoB9508-5 carbon isotope records indicate an improvement in bottom water ventilation, adding to evidence of a more active AMOC. This stabilization in deep water circulation appears associated with BWT decrease of ~1°C and reduced salinity of bottom waters, pointing to restored heat redistribution in this part of the Atlantic during the Holocene (Figure 4.5e).

4.3 Bottom Water Temperature changes during pre-LGM times

HS5 (average BWT of 2.04°C) sees an average increase of around 0.4°C (Figure 4.3d) compared to pre-HS5 times (average BWT of 1.6°C), while a gradual cooling trend is observed from 42 kyrs BP into the LGM, when average BWT were ~ 0.1°C as they decrease approximately by 1.2°C when compared to pre-LGM data. Maximum temperatures of around 2°C during HS4 (from 38.1 to 37.5 kyrs) coincide with minimum $\delta^{13}C$ further corroborating that a transient and strong decrease in ventilation is associated with deep water warming at our site. Again, this is associated with a weakening AMOC as seen by the $^{231}Pa/^{230}Th$ records of Böhm et al. (2015) and Henry et al. (2016). A similar trend is observed at the end of the HS5 (38.1 – 37.5 kyrs), when BWTs around 2°C also coincide with decreased ventilation in times of weaker AMOC.

In subsequent Heinrich Stadials (HS3 and HS2), bottom water warming is less pronounced.

Although warming during HS5 and HS4 is associated with decreased ventilation, as shown by our $\delta^{13}C$ records, temperature increase is small (usually < 1°C). The subdued response may be linked to weaker radiative forcing from CO_2.

5 Conclusions

Our reconstruction of the North Atlantic Deep Water deglacial history for the last 45 kyrs, shows clear evidence of intense deep-water warming at the onsets of HS1 and the late YD in times of global warming and still active, albeit reduced, NADW formation.

During HS1, relatively stable temperatures around 2°C persisted for ~ 5.4 kyrs at our site, pointing to a reduced deep-ocean heat uptake as a response to the extremely reduced AMOC. For the late YD, with a less extreme AMOC slowdown, our Mg/Ca records show maximum paleotemperatures above 4°C at the same time bottom water ventilation declined and salinity increased. This warming can be explained by a temporal heat uptake restoration at intermediate depths, related to a transient reinvigoration of overturning circulation in the Atlantic as seen by improved ventilation during the B-A. However, AMOC slowdown during the YD led to pause in heat uptake lasting 2.5 kyrs, evidenced by BWTs above 4°C at the end of the YD and into the beginning of the Holocene.

Our results show that the predicted AMOC slowdown during the 21st century has the potential to significantly affect BWT in the deep east NE Atlantic. We suggest that AMOC not only sets the depth of oceanic heat storage but can temporarily reduce heat uptake capacity of the deep Atlantic Ocean during slowdowns. Further research investigating the link between the state of the AMOC, and oceanic heat storage is needed to assess the potential consequences of a future AMOC slowdown for global warming.

Acknowledgments

This research was funded by the “Deutsche Forschungsgemeinschaft” (DFG) through the Cluster of Excellence “The Ocean Floor – Earth’s Uncharted Interface” from MARUM – Center for Marine Environmental Sciences, University of Bremen, Germany. Sample material was provided by the GeoB Core Repository at the MARUM – Center for Marine Environmental Sciences, University of Bremen, Germany. This research is also supported by GLOMAR – Bremen International Graduate School for Marine Sciences, University of Bremen. The authors deeply appreciate the comments and suggestions of the reviewers, that sparked interesting scientific discussion and improved significatively the final manuscript. The first author would like to thank the GeoLatinas organization for their support and constant feedback throughout this research.

Open Research

The benthic foraminifera stable isotope and Bottom Water Temperature reconstructions data used for this research is available with open access at PANGAEA® - Data Publisher for Earth & Environmental Science via Barragán-Montilla et al., 2023a and Barragán-Montilla et al., 2023b with license Creative Commons Attribution 4.0 International.

Supplementary Information for Chapter 4

Published by Paleoceanography and Paleoclimatology modified to fit format

Supporting Information for

Stagnant North Atlantic Deep Water heat uptake with reduced Atlantic Meridional Overturning Circulation during the last deglaciation

S. Barragán-Montilla[1], S. Mulitza[1], H.J.H. Johnstone[1] and H. Pälike[1]

[1]MARUM – Center for Marine Environmental Sciences and Department of Geosciences, University of Bremen, Bremen, Germany
Corresponding author: Sofía Barragán Montilla (sbarraganmontilla@marum.de)

Contents of this file

Text S1 and S2

Figure S1

Figure S2

Table S1

Introduction

This information was provided during the peer review process and aims to clarify some of the points raised during the discussion. Text S1 gives information about additional calibrations considered when calculating the bottom water temperatures (BWT) reported in this study. In addition, another correction to the $\delta^{18}O$ of *Cibicidoides wuellerstorfi* was considered. Figure S1 shows the results of these analyses to justify the final methodology cited in the paper.

Text S1 and S2.

During the data analysis, the bottom water temperature (BWT) calibrations by Elderfield et al. (2010) and Roberts et al. (2016) were also considered using a correction of 0.47 ‰ (Marchitto et al., 2014) to the $\delta^{18}O$ of *Cibicidoides wuellerstorfi,* as an alternative to 0.64 ‰ (Shackleton, 1974). For interpretation, the calibration by Roberts et al. (2016) was considered more suitable, as the BWT (2.3°C) from the most

recent sample of the core (400 years old) is closer to the modern BWT (2.7°C) than the temperature calculated using Elderfield et al. (2010) calibration (3.3°C). Additionally, the correction of +0.64 ‰ to the $\delta^{18}O$ of *Cibicidoides wuellerstorfi* following Shackleton (1974) agrees with the measured uncertainty of the unpublished average deglacial offset of *Uvigerina peregrina* – *Cibicidoides wuellerstorfi* $\delta^{18}O$ from the nearby core GeoB9506-1 retrieved at 2.9 km water depth (Figure S2) and other published records off NW-Africa (Zahn et al. 1986).

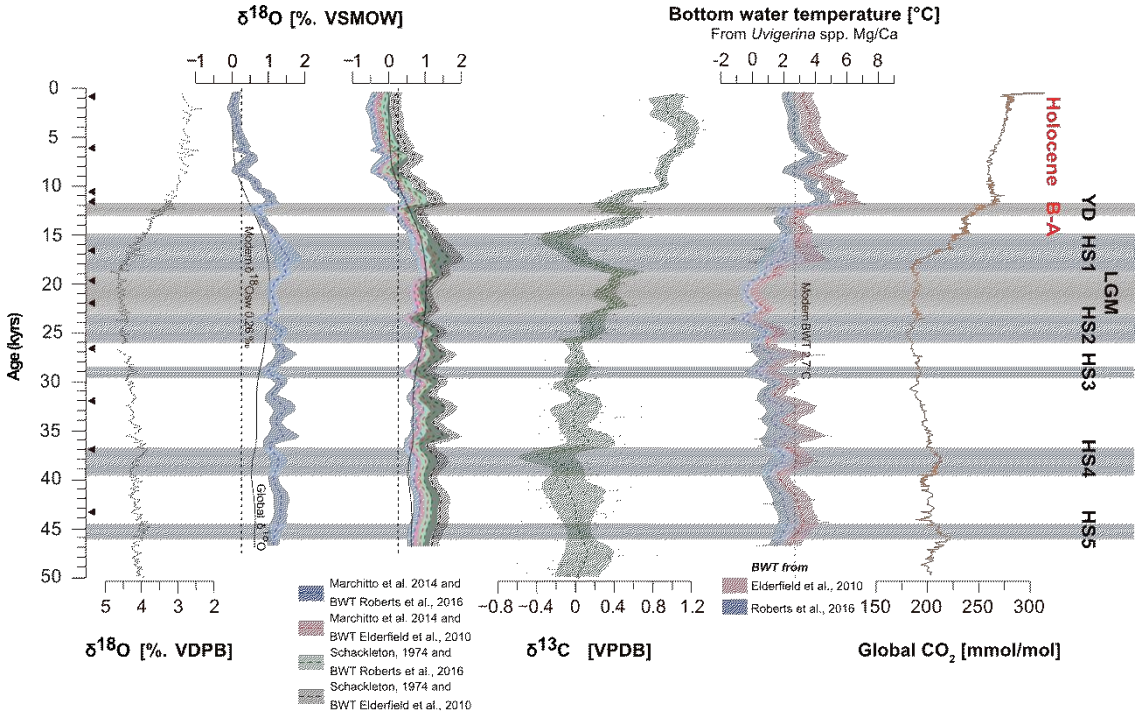

Figure S1. Benthic foraminifera proxies from core GeoB9508-5 showing the deglacial evolution of BWT the eastern North Atlantic in the last 45 kyrs. Ages were modeled from radiocarbon dating (triangles) and shaded areas represent the 95% confidence intervals a. $\delta^{18}O$ of Cibicidoides wuellerstorfi; b. (blue) $\delta^{18}O$ of seawater estimated using equation (14) from Marchitto et al. (2014) from $\delta^{18}O$ measurements on C. wuellerstorfi corrected by a species-specific offset of +0.47 ‰ and Bottom Water Temperatures (BWT) estimated using Roberts et al. (2016); (red) a species-specific offset of +0.47 ‰ and Bottom Water Temperatures (BWT) estimated using Elderfield et al. (2010), using equation (14) from Marchitto et al. (2014); (green) a species-specific offset of +0.64 ‰ and Bottom Water Temperatures (BWT) estimated using Roberts et al. (2016), using the formula from Shackleton (1974); (black) a species-specific offset of +0.64 ‰ and Bottom Water Temperatures (BWT) estimated with Elderfield et al. (2010), using the formula from Shackleton (1974); Global $\delta^{18}O$ of seawater is included for reference (Waelbroeck et al. 2001); c. $\delta^{13}C$ measured on C. wuellerstorfi (gray curve is raw data); d. Bottom water temperatures (BWT) calculated from Uvigerina spp. Mg/Ca ratios (gray curve is raw data), following the equation of Roberts et al. (2016); e. Global CO_2 included for reference (Köhler et al., 2017). **Key Climate events:** Last Glacial Maximum (LGM); Heinrich Stadial 1 (HS1); Heinrich Stadial 2 (HS2); Heinrich Stadial 3 (HS3); Heinrich Stadial 4 (HS4); Heinrich Stadial 5 (HS5); Younger Dryas (YD); Bølling–Allerød warming (B-A). Triangles in the age axis indicate points of radiocarbon ages.

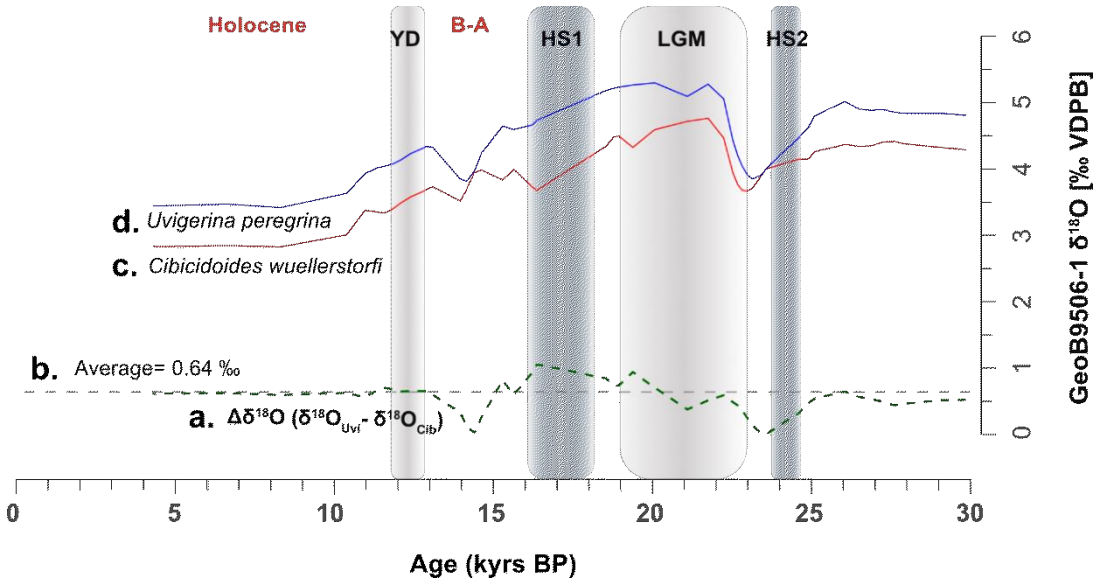

Figure S2. Benthic foraminifera δ18O from nearby core GeoB9506-1 (15°36'36.00''/18°21'0.60''W, 2956 m water depth) showing average δ18O offset between Uvigerina peregrina and Cibicidoides wuellerstorfi in the NE Atlantic during the last deglaciation a. Δδ18O calculated extracting the δ18O of Cibicidoides wuellerstorfi (δ18OCib) to the δ18O of Uvigerina peregrina (δ18OUvi) ; b. Average value of Δδ18O; c. δ18O from Cibicidoides wuellerstorfi in core GeoB9506-1; d. δ18O from Uvigerina peregrina in core GeoB9506-1. Key Climate events: Last Glacial Maximum (LGM); Heinrich Stadial 1 (HS1); Heinrich Stadial 2 (HS2); Heinrich Stadial 3 (HS3); Heinrich Stadial 4 (HS4); Heinrich Stadial 5 (HS5); Younger Dryas (YD); Bølling–Allerød warming (B-A). Triangles in the age axis indicate points of radiocarbon ages.

Table S1.

GeoB9508-5 *Uvigerina* trace element concentration (Mg/Ca and Sr/Ca and instrument) and bottom water temperature estimations (BWT) using the equation by Elderfield et al., (2010) and Roberts et al. (2016).

Depth (cm)	Age (kyrs)	Mg/ Ca	stdv Mg/Ca	Sr/Ca (mmol/mol)	stdv Sr/Ca	BWT (°C) - Elderfield	BWT (°C) - Roberts
3	0.39	1.06	0.03	0.96	0.02	3.33	2.33
10.5	0.99	1.04	0.00	1.02	0.00	3.10	2.15
23	2.17	1.07	0.01	0.98	0.01	3.46	2.44
33	3.16	1.11	0.02	1.02	0.02	4.11	2.97
43	4.13	1.06	0.02	0.99	0.01	3.33	2.33
55.5	5.29	1.10	0.02	1.01	0.02	3.91	2.80
63	6	1.15	0.02	1.00	0.02	4.59	3.35
68	6.36	1.14	0.01	1.00	0.01	4.42	3.21
73	6.82	1.24	0.01	1.01	0.01	5.79	4.32
78	7.4	1.21	0.01	0.99	0.01	5.47	4.06

83	8.03	1.09	0.01	1.00	0.01	3.82	2.73
85.5	8.34	1.03	0.02	1.02	0.02	2.98	2.05
88	8.65	1.02	0.01	1.06	0.01	2.83	1.93
95.5	9.51	1.23	0.03	1.06	0.03	5.61	4.18
103	10.14	1.17	0.03	1.03	0.02	4.83	3.54
108	10.51	1.18	0.02	1.00	0.02	5.04	3.71
113	10.88	1.30	0.03	0.97	0.02	6.66	5.03
120.5	11.4	1.21	0.02	0.98	0.02	5.47	4.06
130.5	11.83	1.34	0.03	1.05	0.02	7.15	5.42
135.5	12	1.17	0.00	0.98	0.00	4.89	3.60
138	12.08	1.17	0.02	1.00	0.02	4.87	3.58
143	12.25	0.93	0.01	1.03	0.02	1.57	0.91
145.5	12.33	1.06	0.00	1.02	0.00	3.43	2.41
153	12.58	0.96	0.03	1.04	0.03	2.09	1.33
163	12.88	1.08	0.03	0.98	0.03	3.59	2.55
173	13.3	1.00	0.01	1.03	0.01	2.52	1.68
183	13.74	0.99	0.04	1.01	0.05	2.38	1.56
193	14.18	1.05	0.03	1.02	0.03	3.24	2.26
203	14.62	1.07	0.02	1.01	0.02	3.47	2.45
213	15.08	1.04	0.03	1.02	0.03	3.13	2.17
223	15.53	0.99	0.01	1.02	0.01	2.49	1.65
233	15.97	1.07	0.00	1.01	0.00	3.46	2.44
238	16.19	1.12	0.02	1.02	0.02	4.19	3.03
243	16.4	0.85	0.01	1.01	0.02	0.57	0.10
253	16.86	1.05	0.02	1.01	0.02	3.21	2.24
263	17.31	1.15	0.01	0.98	0.01	4.53	3.31
268	17.53	1.16	0.01	1.05	0.01	4.79	3.52
273	17.76	0.83	0.02	1.05	0.02	0.21	-0.19
283	18.22	0.95	0.02	1.05	0.02	1.85	1.14
293	18.65	0.90	0.01	1.05	0.02	1.18	0.60
303	19.08	0.95	0.01	1.03	0.01	1.84	1.12
313	19.66	0.82	0.02	1.03	0.02	0.19	-0.21
323	20.61	0.79	0.01	1.02	0.02	-0.30	-0.61
333	21.66	0.82	0.01	1.04	0.01	0.17	-0.22
343	22.64	0.89	0.02	1.06	0.02	1.14	0.56
353	23.27	0.82	0.01	1.02	0.01	0.14	-0.25

358	23.58	0.72	0.01	1.06	0.02	-1.15	-1.29
373	24.52	0.93	0.01	1.01	0.01	1.58	0.92
383	25.13	0.96	0.00	0.99	0.00	1.99	1.25
393	25.67	0.86	0.01	1.02	0.01	0.62	0.14
408	26.44	0.87	0.01	1.04	0.01	0.77	0.26
413	26.7	0.91	0.01	1.03	0.01	1.35	0.73
418	26.94	0.81	0.00	1.05	0.00	-0.06	-0.41
423	27.2	1.15	0.02	1.10	0.01	4.61	3.37
433	27.73	0.90	0.02	1.03	0.02	1.25	0.65
443	28.24	0.94	0.02	1.00	0.02	1.82	1.11
455.5	28.88	0.81	0.01	1.05	0.02	-0.04	-0.39
463	29.26	0.85	0.01	1.04	0.02	0.60	0.12
468	29.51	0.90	0.02	1.06	0.02	1.21	0.62
473	29.76	1.00	0.02	1.02	0.02	2.59	1.73
483	30.24	1.00	0.01	1.06	0.01	2.63	1.77
493	30.77	0.91	0.00	1.02	0.00	1.41	0.78
503	31.32	0.92	0.01	1.07	0.01	1.50	0.85
513	31.88	0.86	0.01	1.02	0.01	0.69	0.20
523	32.45	1.11	0.00	1.05	0.00	4.05	2.92
533	32.99	1.07	0.01	1.03	0.01	3.53	2.50
545.5	33.7	0.88	0.02	1.00	0.02	0.94	0.40
553	34.12	0.95	0.02	1.02	0.02	1.87	1.16
563	34.68	0.98	0.00	1.00	0.00	2.33	1.52
578	35.51	1.18	0.02	1.02	0.01	5.04	3.71
583	35.78	0.86	0.01	1.01	0.01	0.64	0.16
593	36.35	1.03	0.00	0.98	0.00	2.93	2.01
595.5	36.5	0.88	0.01	1.02	0.02	0.94	0.40
603	36.94	1.01	0.01	1.03	0.01	2.72	1.84
613	37.53	1.02	0.03	1.00	0.03	2.82	1.92
623	38.12	1.12	0.01	0.97	0.00	4.13	2.98
633	38.72	0.90	0.02	1.00	0.03	1.21	0.62
643	39.31	0.93	0.01	1.02	0.01	1.64	0.97
653	39.9	0.93	0.00	1.01	0.00	1.66	0.99
665.5	40.63	0.97	0.02	1.03	0.02	2.12	1.35
675.5	41.11	0.97	0.00	1.04	0.00	2.16	1.39
683	41.47	1.01	0.01	1.05	0.01	2.75	1.86

695.5	42.04	1.11	0.03	1.00	0.03	4.01	2.88
703	42.39	0.91	0.01	1.01	0.01	1.32	0.71
713	42.87	1.07	0.01	1.00	0.01	3.56	2.52
723	43.34	1.01	0.02	1.00	0.02	2.70	1.82
733	43.81	1.04	0.02	1.03	0.02	3.11	2.16
743	44.3	1.17	0.02	0.99	0.01	4.84	3.55
753	44.78	1.00	0.02	1.03	0.02	2.55	1.70
765.5	45.37	1.03	0.01	1.03	0.02	3.00	2.06
783	46.21	0.97	0.02	1.00	0.02	2.12	1.35
790.5	46.59	0.99	0.01	0.99	0.01	2.37	1.56
793	46.72	0.87	0.01	1.04	0.01	0.79	0.28

References

Marchitto, T.M., Curry, W.B., Lynch-Stieglitz, J., Bryan, S.P., Cobb, K.M., Lund, D.C. (2014). Improved oxygen isotope temperature calibrations for cosmopolitan benthic foraminifera. Geochimica et Cosmochimica Acta, 130, 1-11. https://doi.org/10.1016/j.gca.2013.12.034

Shackleton, N. J. (1974). Attainment of isotopic equilibrium between ocean water and the benthonic foraminiferal genus Uvigerina: Isotopic changes in the ocean during the last glacial. Centre National de la Recherche Scientifique Colloques Internationaux, 219, 203–209.

Zahn, R., Winn, K., and Sarnthein, M. (1986). Benthic foraminiferal d13C and accumulation rates of organic carbon: Uvigerina peregrina group and Cibicidoides wuellerstorfi, Paleoceanography, 1, 27–42, https://doi.org/10.1029/PA001i001p00027

Chapter 5: Eastern Tropical North Atlantic shallow mode heat storage in the Last Glacial Maximum shifted to deep mode in the Holocene

In preparation for submission

Sofía Barragán-Montilla[1,2], Stefan Mulitza[1], Heather J. H. Johnstone[1], Heiko Pälike[1]

[1] MARUM – Center for Marine Environmental Sciences and Department of Geosciences, University of Bremen, Bremen, 28359, Germany
[2] Faculty of Geosciences, University of Bremen, Bremen, Germany

Abstract

The Atlantic Ocean stores a large amount of excess heat from the atmosphere and distributes it globally through the Atlantic Meridional Overturning Circulation (AMOC) influencing global climate. During the last deglaciation, significant decline of AMOC strength was registered during the Heinrich Stadial 1 (HS1) and Younger Dryas (YD), when deep water paleotemperature records suggest a stagnation of heat uptake in the eastern tropical North Atlantic. The response of intermediate water temperatures in this part of the Atlantic remains poorly constrained, furthermore the relationship between deep and intermediate bottom water temperatures (BWT) is yet to be explored. During this study, we used benthic foraminifera *Uvigerina* spp. Mg/Ca to reconstruct the paleotemperature changes of intermediate depth site GeoB9512-5 (793 m water depth) and deep-water site GeoB9506-1 (2,956 m water depth) during the last 27,000 years. Our intermediate water paleotemperature record shows intense warming during the HS1 and YD for the eastern tropical Atlantic and is compatible with other records from intermediate waters in the tropical Atlantic. At the same time, our results show stagnation of heat uptake in the deep ocean as previously observed in a nearby site. These results suggest that in times of reduced AMOC, heat storage was mainly concentrated in the upper Atlantic, while in the Holocene with a stronger AMOC heat storage depth shifted and occured primarily in the deep Atlantic.

1 Introduction

The North Atlantic has been taking up around 45% of the excess heat from the atmosphere over the last 70 years (Kostov et al., 2014, Cummins et al., 2016; Levitus et al., 2000, 2005; Marshall & Zanna, 2014; von Schuckmann et al., 2023), transporting it south through the Atlantic Meridional Overturning Circulation (AMOC). Global warming is very likely to be enhanced by anthropogenic forcing on ocean heat uptake (Liu et al., 2020; IPCC, 2023). Since ocean heatuptake is closely linked to AMOC strength changes (Liu et al., 2020; IPCC, 2023), a comprehensive understanding of this processes and its potential impacts, can be accomplished by using paleotemperature reconstructions in deglacial marine sediments at different depths, particularly since the instrumental record of AMOC is still too limited to investigate its effects in heatuptake. One of the best-established proxies used to study temperature changes in the geological record is foraminifera Mg/Ca ratios (Elderfield et al., 2010; Elderfield and Ganssen, 2000; Yu and Elderfield, 2008). Planktic foraminifera provide valuable information about surface and subsurface paleotemperature changes (e.g. Max et al., 2022; Schmidt et al., 2012) while benthic foraminifera are key to understand the paleoceanographic changes (e.g. Oppo et al., 2023). Numerous paleotemperature records from the deep Atlantic are well constrained and available at different latitudes (Came et al., 2007; He et al., 2020; Martin et al., 2002; Oppo et al., 2023; Poggeman et al., 2018; Roberts et al. 2016; Schmidt et al., 2012; Skinner et al., 2003), however paleotemperature information from shallower depths remain scarce and are mainly focused on higher latitudes (Kristjánsdóttir, et al., 2007; Ezat et al., 2014; El bani Altuna et al., 2021a and 2021b), whereas at lower latitudes in the eastern North Atlantic mid-depth paleotemperature reconstructions remain sparse (Weldeab et al., 2016).

The last deglaciation provides a high-resolution frame to understand changes in heat uptake and heat storage in times of major ocean circulation reorganization like changes in AMOC strength. After the end of the Last Glacial Maximum (LGM), AMOC slowdown was recorded by $^{231}Pa/^{230}Th$ records during the Heinrich Stadial 1 (HS1) and Younger Dryas (YD) (Böhm et al., 2015; Gherardi et al., 2005; McManus et al., 2004; Ng et al., 2018; Valley et al., 2017), decreasing bottom water ventilation in the deep Atlantic (Barragán-Montilla et al., 2023; Oppo et al., 2015) as subtropical gyre

circulation was enhanced and brought more ventilated waters into the shallower Atlantic (Barragán-Montilla et al., in review). In addition, models suggest that with a weaker AMOC heat accumulates at ocean depths over 2,000 m (e.g. Liu et al., 2009; Zhang et al., 2017). Since the instrumental record of AMOC is still too short to understand the impact of major changes in deep overturning on ocean heat uptake and storage, the deglacial record of the last ~ 25.000 years becomes the best alternative to shed light on this matter.

The records from the deep Atlantic show that at North Atlantic Deep Water (NADW) depths, AMOC slowdown leads to heat uptake stagnation in the eastern North Atlantic (Barragán-Montilla et al., 2023). This is registered as a transient warming of ~2°C during HS1 that preceded stable Bottom Water Temperatures (BWTs) for ~5.4 kyrs, while during the YD temperatures of >4°C persisted for ~2.5 kyrs. The response of subsurface waters to weakened AMOC in the equatorial Atlantic is limited, however intense mid-depth warming of 3.9 and 5.2°C has been consistently observed un benthic foraminifera Mg/Ca records during the HS1 and YD respectively (Weldeab et al., 2016), and in the western tropical Atlantic, where BWTs reconstructions from benthic foraminifera Mg/Ca show a regional subsurface water warming during the HS1 (Oppo et al., 2023), compatible with subsurface warming in other parts of the Atlantic above 1500 m water depth, and with an additional YD warming in the tropical western Atlantic (Came et al., 2007; Poggemann et al., 2018; Rühlemann et al., 2004) and subpolar Atlantic (Marcott et al., 2011).

Here we used Uvigerina spp. Mg/Ca records to reconstruct paleotemperature changes in the tropical eastern Atlantic at intermediate (GeoB9512-5, 15°20'13.20''N, 17°22'1.20''W, 793 m water depth) and deep (GeoB9506-1, 15°20'13.20''N, 17°22'1.20''W, 793 m) depths. Our records suggest, that during the LGM and in times of AMOC slowdown heat storage was mainly concentrated at intermediate depths, at the same time the deep ocean shows little variation in BWTs in accordance with the heat uptake stagnation from nearby site GeoB9508-5 (Barragán-Montilla et al., 2023). During the Holocene, with a reinvigorated AMOC, deep BWTs increased (~3°C) as intense intermediate cooling (~3.5°C) took place in the eastern tropical Atlantic,

showing that heat storage shifted towards the deep ocean in a modern-like ocean circulation state.

2 Methods

2.1 Location and materials

Downcore reconstructions were made from marine sediment core GeoB9512-5 (793 m water depth) off the coast of Senegal, North-western Africa (Figure 1b) (Multiza et al., 2005). The core is in the mixing zone of the Eastern North Atlantic Central Water (ENACW) and the Eastern South Atlantic Central Water (ESACW), with an approximate modern BWT of 6.9°C and salinity of ~34.89 (Figure 5.1a-b, Lauvset et al., 2022). The studied interval corresponds to the top 548.5 cm of the core sampled every 5 cm with an average age resolution of 0.2 kyrs (Barragán-Montilla et al., in review). The interval consisted mainly of unconsolidated dark grey to brownish mud with abundant microfossil content, color and textures were homogeneous throughout the studied interval (Mulitza et al., 2005). Sediment samples were (1) washed through a 63 µm sieve with deionized water; (2) dried in an oven at temperatures ~ 45°C for no more than 24 hours; and (3) dry sieved through 63, 125, 150 and 250 µm stored and labelled in glass vials. Benthic foraminifera (for geochemical analyses) and planktic foraminifera (for radiocarbon dating) were picked from the >150 um fraction.

A total of 155 samples from core GeoB9506-1 (2.956 m water depth) were analyzed between 0 and 260 cm core depth. From these, 104 samples were extracted from the core every 5 cm with an average age resolution of 0.4 kyrs. These sediments were washed as described above, and the foraminiferal tests for geochemical measurements (foraminifera accelerator mass spectrometry dating in planktic and stable isotopes and minor elements to calcium ratios in benthic) were also collected from the >150 um fraction. The remaining 49 samples used in this study were provided by the GeoB Core repository at MARUM and have been previously washed. The GeoB9506-1 sediments were deposited in the lower bathyal zone, and consist of brown to green muds, with a turbiditic event (202.5 to 217.5 cm) seen as a more porous, coarser grained interval (Mulitza et al., 2005). This event is inferred as a contourite deposition interval, based on the glauconite content observed during the micropaleontological analyses in this study (including foraminifera filled with dark to

light green glauconite) suggesting active bottom current activity (Tallobre et al., 2019). Site GeoB9506-1, and GeoB95108-5 (Barragán-Montilla et al., 2023) were recovered from the North Atlantic Deep Water (NADW, Figure 5.1b), with a temperature of ~ 3.1°C and salinity of 34.95 (Lauvset et al., 2022) and a $\delta^{18}O$ of 0.26 ‰ SMOW (LeGrande & Schmidt, 2006) at GeoB9508-5 water depth. For site GeoB9506-1 water depth. temperature is ~ 2.7°C and salinity 34.98 (Lauvset et al., 2022).

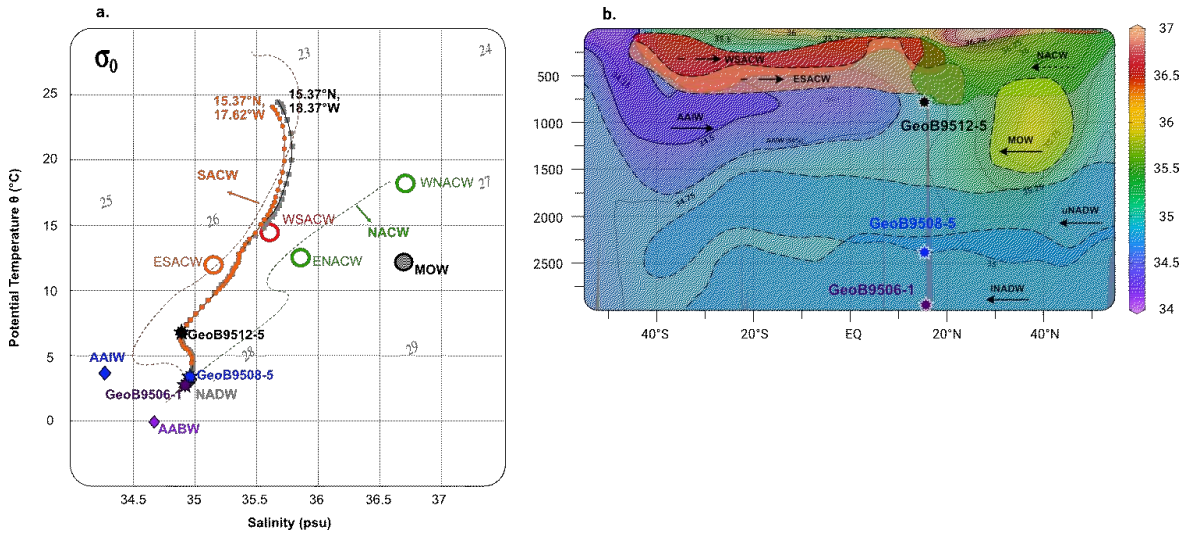

Figure 5.1 Oceanographic and geographical situation of sites GeoB9512-5, GeoB9506-1 and GeoB9508-5. a. Temperature – Salinity diagram showing the water masses sources in the studied area, and the situation of the studied sites; **b.** Hydrographic salinity section showing the modern water masses in the studied area and the location of the sites used in this study. Plotted with Ocean Data View (Schlitzer, 2023), and data from WOA 2018 (Boyer et al., 2018; García et al., 2019).

2.2 Chronology and Age model

The GeoB9512-5 ages used here correspond to those calculated by Barragán-Montilla et al. (in review), while the age model from site GeoB9506-1 (Figure 5.2) was calculated using the same methodology. Planktic foraminifera accelerator mass spectrometry dating was obtained for 16 samples of GeoB9512-5 (Barragán-Montilla and Mulitza, in review a) and 12 from GeoB9506-1 (Barragán-Montilla and Mulitza, in review b). These were measured at the MICADAS laboratory at the Alfred Wegener Institute (AWI)-Bremerhaven (Mollenhauer et al., 2021). Median ages and corresponding uncertainties were estimated using the BACON script of Blaauw and Christen (2011) version 2.5.5, along with the Marine20 calibration curve of Heaton et al. (2020) with no reservoir corrections. In addition, Heinrich Stadials were correlated visually using uncalibrated XRF Fe/Ca ratios (Völpel et al., 2019). The age models

show no reversals, resulting in continuous deglacial sedimentary sequences deposited in the last 28.000.

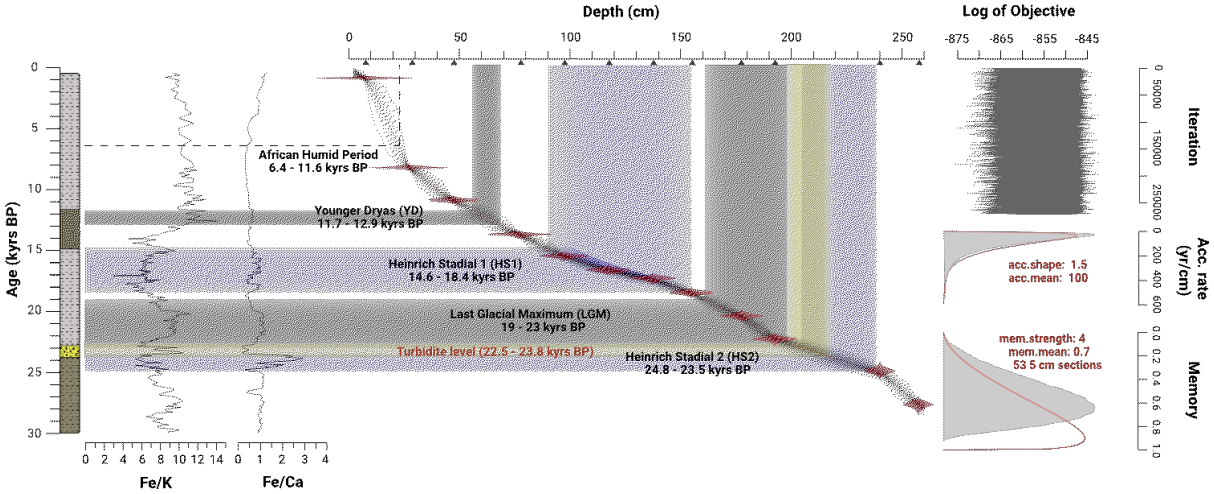

Figure 5.2 Age model from site GeoB9506-1 a. GeoB9506-1 downcore ages modelled using 12 radiocarbon ages (triangles) in the BACON script (Blaaw and Christen, 2011) and the Marine20 calibration (Heaton et al., 2020). Uncalibrated Fe/Ca and Fe/K (Völpel et al., 2019) are included to visually align Heinrich Stadial events. Key Climate events: Heinrich Stadial 2 (HS2); Last Glacial Maximum (LGM); Heinrich Stadial 1 (HS1); Bølling–Allerød (B-A); Younger Dryas (YD).

For site GeoB9512-5, the section includes the key climatic periods Heinrich Stadial 2 (HS2, 25.9 - 24.2 ka BP; 524 – 490 cm core depth), Last Glacial Maximum interval (LGM, 23 - 19 ka BP; 420-468 cm core depth), Heinrich Stadial 1 (HS1, 18.3 - 15.4 ka BP; 404 - 248 cm core depth), the Bølling–Allerød warming (B-A, 15.4 - 13 ka BP; 44 - 182 cm core depth) and the Younger Dryas (YD, 12.9-11.7 ka BP; 180 – 130 cm core depth). The Holocene Fe/Ca minima was found at 6.6 kyrs (53 cm core depth), which position the African Humid Period between 11.7 and 6.6 ka BP.

For site GeoB9506-1(Figure 4.2) the timing of the LGM (205 – 160 cm core depth) and YD (68 – 57.5 cm core depth) was identified at the same ages, while the HS2 was observed between 24.8 – 23.5 ka BP (235 – 213 cm core depth), HS1 between 18.4 – 14.6 ka BP (153 – 87.5 cm core depth), and the B-A between 14.4 – 13.1 ka BP (85 - 70 cm core depth). Finally, the Holocene Fe/Ca minima was observed at 6.4 ka BP, therefore the African Humid Period is found between 11.4 and 6.6 ka BP (53 – 22.5 cm core depth).

2.3 Benthic foraminifera geochemistry and Paleoceanography

For core GeoB9512-5, 110 samples were used for BF stable isotopes and trace element measurements. Paleoceanographic inferences are based on epifaunal foraminifera *Cibicidoides pachyderma,* and *Lobatula lobatula* stable isotopes, including $\delta^{13}C$ and $\delta^{18}O$ measurements (Barragán-Montilla, in review a). These analyses were made using a ThermoFisher Scientific 253 plus gas isotope ratio mass spectrometer, with a Kiel IV automated carbonate preparation device, at MARUM - Center for Marine Environmental Sciences of the University of Bremen. The data is reported in the delta-notations versus V-PDB. Instruments were calibrated against the house standard (ground Solnhofen limestone), and against the NBS-19 calcite. The house standard deviation was 0.03 ‰ for $\delta^{13}C$ and 0.06 ‰ for $\delta^{18}O$ over the measurement period. Stable isotopes from site GeoB9506-1 were made using the same methodology, in 77 samples using *Cibicidoides wuellerstorfi*. For these set of measurements, house standard deviation was 0.04 ‰ for $\delta^{13}C$ and 0.06 ‰ for $\delta^{18}O$. This data was compiled with previously published isotope data made on the same species (Barragán-Montilla, in review b).

Element concentrations in GeoB9512-5 were measured on shallow infaunal foraminifera *Uvigerina mediterranea* (Barragán-Montilla and Johnstone, in review a), and for site GeoB9506-1 on *Uvigerina peregrina* (Barragán-Montilla and Johnstone, 2024b). Foraminifera were crushed and cleaned with MiliQ water, methanol, and hot hydrogen peroxide solution (no reductive cleaning step) using a pipette robot programmed to follow the protocol of Barker et al. (2003) (Johnstone et al., 2016).

Minor element concentrations were measured with an Inductively Coupled Plasma Optical Emission Spectrometer (ICP-OES)—Agilent Technologies 700 Series with Cetac ASX-520 autosampler (Barragán-Montilla and Johnstone, in review a, b). Measurements follow the spectral lines: Mg (279.6 nm), Ca (315.9 nm), Sr (421.6), Al (167.0 nm), Fe (238.2 nm), and Mn (257.6 nm), and were calibrated with linear regressions. Standards of calibration consisted of a blank and five multi-element standards (Mg, Sr, Al, Fe, Mn) between 20 and 100 ppm Ca. We monitored the instrumental precision using a commercial multi-element standard solution (SCP, France), and commercial powder sample ECRM752-1. Theoretical value (measured

value, σ standard deviation, standard error) in mmol/mol for the SCP standard during these runs were: Mg/Ca, 2.955 (2.959, σ 0.030, 0.0029), Sr/Ca, 1.402 (1.402, σ 0.016, 0.0015), Mn/Ca 0.3234 (0.3291, σ 0.0019, 0.00019), Fe/Ca, 0.3312 (0.3228, σ 0.0034, 0.00033), Ba/Ca, 0.00832 (0.00840, σ 0.00034, 0.000033) and Al/Ca 0.678 (0.695, σ 0.018, 0.0018), n=108. Mg/Ca of dissolved, centrifuged, ECRM 752-1 (measured at 3.750 σ 0.015, 0.0014 by Greaves et al. (2005) was 3.735 σ 0.031, 0.0057. Long term standard deviation is better than 2%. During the measurement runs reported here. The Al/Ca ratios were used to monitor contamination (Barker et al., 2003; Johnstone et al., 2016).

2.3.1 Mg/Ca ratios quality control

Clay contamination and Mn-rich coatings visibly affect Mg/Ca measurements (Barker et al., 2003). These coatings can still be present even after following careful cleaning protocols and can influence Mg/Ca ratios. To remove samples with potential contamination, samples with Al/Ca > 0.5 mmol/mol and/or Mn/Ca > 0.25 mmol/mol (Hasenfratz et al., 2017) were not furthered considered for analyses and interpretation (see chapter 3 - methods).

U. mediterranea measurements from site GeoB9512-5, show average Al/Ca of 0.06 mmol/mol, and 4 samples with Al/Ca > 0.5 mmol/mol were not retained. Low correlation between remaining Al/Ca and Mg/Ca of the remaining samples (r^2 = 0.8, n=81) suggest no clay contamination. Duplicates of 2 samples were measured showing good accordance between element concentrations (average standard deviations in Mg/Ca was 0.13 mmol/mol).

2.3.2 Bottom Water Temperatures (BWTs), sea water $\delta^{18}O$, and salinity calculations

Downcore BWTs of sites GeoB9512-5 and GeoB9506-1, were estimated using the *Uvigerina* spp. Mg/Ca in the calibration of Roberts et al. (2016).

$$\frac{Mg}{Ca}\left[\frac{mmol}{mol}\right] = 0.0915 * BWT_{Uvig}[°C] + 0.843,\ r^2 = 0.92 \qquad \textbf{(1)}$$

The seawater $\delta^{18}O$ ($\delta^{18}O_{sw}$) was obtained by extracting the temperature effect to the $\delta^{18}O_c$ of *Cibicidoides* spp. (also corrected by a species-specific offset of +0.64 ‰) in the Shackleton (1974) equation. To estimate a more accurate $\delta^{18}O_{sw}$ we subtracted the ice effect global signal ($\delta^{18}O_{sw\text{-}ice}$) using the data of Waelbroeck et al. (2001) interpolated to our data ages. This $\delta^{18}O_{sw\text{-}ice}$ was then used to estimate salinities using the formula of LeGrande and Schmidt (2006) for the North Atlantic Ocean (equation 2).

$$\delta^{18}O = 0.55 * S - 18.98,\ r^2 = 0.95, n = 743 \qquad \textbf{(2)}$$

Age model uncertainties are used as described by Barragán-Montilla et al. (in review), obtained with the Bacon R-package (Blaauw and Christen, 2011), calculating groups of 10,000 potential time series for each proxy (BWT and stable isotopes). The 10,000 downcore age-depth relations were used to randomly produce 10,000 normal-distributed values for the sampled depths, that were integrated with the 10000 downcore proxy records. The uncertainty of the paleotemperature records were estimated using the standard deviation of duplicate samples calculated as 0.4 °C for GeoB9512-5 and 1.1°C for GeoB9506-1. These standard deviations, including the SDs of the stable isotope measurements ($\delta^{18}O$ SD=0.06 ‰, and $\delta^{13}C$ SD=0.03 ‰ for GeoB9512-5; $\delta^{18}O$ SD=0.06 ‰ and $\delta^{13}C$ SD=0.04 ‰ for GeoB9506-1), were used in the cited script to calculate the 95% ensemble for each proxy. The final proxy records presented here (Supplementary Information 5.1, 5.2, 5.3, 5.4 and 5.5) include the calculated median ages for each observation, the mean values of each proxy for all ensemble values at each median age, and the 95 % uncertainty envelope.

3 Results

3.1 Stable Isotopes

3.1.1 Intermediate depths (GeoB9512-5)

Cibicidoides pachyderma $\delta^{18}O$ was previously described in Chapter 3. The values were recorded between 1.9 and 3.6 ‰ and follow a compatible trend consistent with the ice effect related to global changes of $\delta^{18}O$ (Waelbrock et al., 2001, Figure 5.3a in black). The resulting $\delta^{18}O_{sw}$ record shows average 1.02 ‰ from ca. 27 ka BP

throughout the LGM until 17.5 ka BP (SD=0.3, n= 30). During the deglaciation, average values dropped to 0.58 ‰ during the HS1 (17.4 – 14.8 ka BP, SD=0.01, n=26), and persisted during the B-A (average 0.61 ‰ between 14.6 and 13.1 ka BP, SD=0.4, n= 39). In the YD data is limited, and available $\delta^{18}O_{sw}$ shows an increase to 0.94 ‰ at 12.9 ka BP and 0.71 ‰ at 11.5 ka BP, followed by a rapid drop to average -0.46 ‰ in the Holocene (11.5 – 0.2 ka BP, SD=0.26, n= 21).

The carbon isotope record ranged between 0.0 and 0.6 ‰ and starts with average $\delta^{13}C$ of 0.5 ‰ in pre-LGM times (27.1 – 26.6 ka BP, SD=002, n=7), that drop to ~ 0.3 (SD=0.2, n=12) in the HS2 where minimum values between 0 and 0.2 ‰ were recorded from 25.9 to 25.1 ka BP (Figure 5.4e). Benthic foraminifera $\delta^{13}C$ increased to average 0.4 in the LGM (SD=0.1, n=21), and values over 0.5 ‰ occurred at the end of this climate period (10.9 – 19.3 ka BP). The onset of the deglaciation, is represented by $\delta^{13}C$ lower than 0.4 ‰ from 18.2 to 17.5 ka BP in the first part of the HS1, and consistently dropped during this period in three steps: to average 0.3 ‰ from 17.4 to 16.7 ka BP (SD=0.0, n=20), 0.2 ‰ from 16.7 to 16.4 ka BP (SD=0.0, n=7), and to average 0.1 ‰ from 16.3 to 15.9 ka BP (SD=0.0, n=5), with a minima of 0.03 ‰ at 16.2 ka BP. The end of the HS1 (15.6 – 14.6 ka BP) is seen as an increase to average 0.3 ‰ (SD=0.0, n=5), that persisted into the beginning of the YD (12.9 – 12.4 ka BP) with average $\delta^{13}C$ of 0.5 ‰ (SD=0.1, n=4). A transient drop to values lower than 0.25 ‰ was also observed during the YD at 12.2 ka BP leading into minima of 0.1 ‰ at 11.8 ka BP. These low carbon isotope radios persisted into the first part of the Holocene (11.6 – 11.2 ka BP) with average 0.1 ‰ (SD=0.09, n=10), followed by increasing average $\delta^{13}C$ of 0.4 ‰ (SD=0.0, n= 15). Carbon isotope ratios dropped to average 0.3 ‰ (SD=0.0, n= 3) at 7.5 ka BP, however the increasing trend continued into the late Holocene (7.2 – 1.5 ka BP) with average 0.5 ‰ (SD=0.0, n=23) and maximum values of 0.6 ‰ recorded between 5.6 and 4 ka BP.

3.1.2 Deep water sites (GeoB9506-1)

At site GeoB9506-1, $\delta^{18}O$ was measured between 2.81 and 4.77 ‰ also showing trends comparable to the global ice effect-related global $\delta^{18}O$ (Waelbrock et al., 2001,), and compatible with the GeoB9508-5 results (Barragán-Montilla et al., 2023, Figure 3a in blue). The $\delta^{18}O_{sw}$ record (Figure 5.3a in purple), showed average values of 1.05

‰ from 27.7 to 14.9 ka BP (SD=0.15, n=36), that dropped to average 0.74 ‰ during the B-A (14. 2 to 13.1 ka BP, SD=0.1, n=7). A decline continued into the YD (average 0.6 ‰, SD=0.1, n=7), leading into lower values on average 0.34 ‰ (SD=0.21, n=20) in the early Holocene (11.6 to 6.6 ka BP), while in the late Holocene between 5.4 and 0.6 ka BP average values were closer to 0 (0.06 ‰, SD=0.14, n=8).

The carbon isotope values, ranged between -0.07 and 0.98 ‰ with an overall trend to higher $\delta^{13}C$ towards the Holocene. During the HS2 and the LGM (24.7 to 19.8 ka BP) $\delta^{13}C$ was on average 0.24 ‰ (SD=0.03, n=16), and dropped to average 0.06 ‰ at the beginning of the HS1 (18.9 – 18.6 ka BP, SD=0.07, n=4). The remaining of the HS1 was seen as a 0.25 ‰ average (between 18.1 and 14.9 ka BP, SD=0.08, n=18), that increased to ~ 0.48 ‰ (SD=0.07, n=8) in the B-A (14.2 – 13.1 ka BP). These values persisted in the YD (12.9 – 11.6 ka BP, average 0.45 ‰, SD=0.03, n=7) and increased to ~ 0.77 ‰ in the Holocene (11.4 – 0.4 ka BP, SD=0.15, n=25).

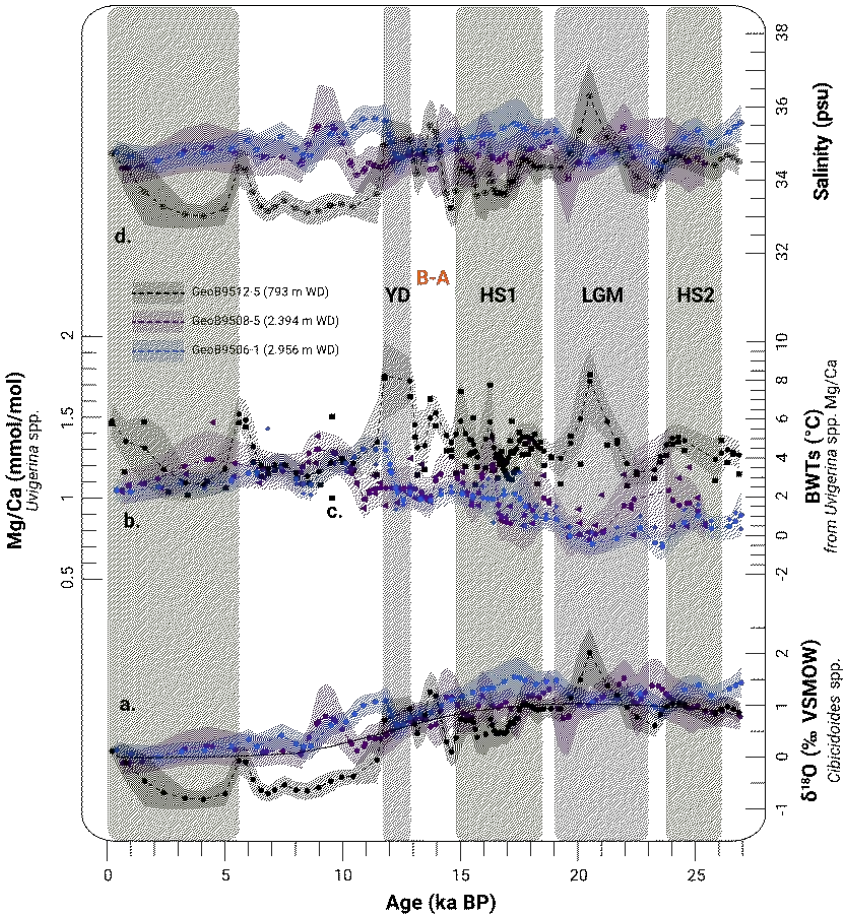

Figure 5.3 Downcore $\delta^{18}O_{sw}$, Mg/Ca, and paleotemperature and salinity calculations for sites GeoB9512-5, GeoB9506-1 and GeoB9508-5 **a**. Seawater $\delta^{18}O$; b. *Uvigerina* spp. Mg/Ca and c. Bottom Water Temperature

record estimated from b; d. Salinity estimated using the equation of LeGrande and Schmidt (2006) and the BWT calculated from Benthic Foraminifera Mg/Ca. GeoB9506-1 in purple; GeoB9508-5 in blue and GeoB9512-5 in black. Shaded areas correspond to the 95% confidence envelope. Key Climatic Periods: Heinrich Stadial 2 (HS2); Last Glacial Maximum (LGM); Heinrich Stadial 1 (HS1); Bølling–Allerød (B-A); Younger Dryas (YD).

3.3 LGM to Holocene intermediate cooling in the tropical eastern Atlantic

Mg/Ca of *U. mediterranea* in core GeoB9512-5 (Figure 5.3c, black squares) was between 1 to 1.76 mmol/mol (average 1.26 mmol/mol, SD=0.16, n=88). The BWTs from these data ranged from 2.6 to 8.2 °C (Figure 5.3b and 5.4a, black curve) with isolated transient warmings (> 6°C) at 20.5 – 20.1, 13.9 – 13.7, 12.9 - 11.8 and 5.6 ka BP. According to our BWT record (Figure 5.3c, black curve), pre-LGM to HS2 (27.1 – 23.8 ka BP) BWTs were on average 4.5°C (SD= 0.4, n=10), followed by a cooling to average 3.8°C (SD=0.6, n=4) and an intense warming to average 6.6°C between 20.5 and 20.1 ka BP (SD=0.9, n=3). A cooling of around 1.9°C was recorded at the end of the LGM and HS1 (average BWTs of 4.7°C SD= 0.4, n= 11, 19.7 to 17.6 ka BP), into average temperatures of 4.2°C from 17.5 to 16.4 ka BP (SD=0.3, n=16). During the end of the HS1 (16.4 – 14.8 ka BP), BWTs continued to increase reaching an average of 5°C (SD=0.2, n=11). This warming persisted into the B-A period, when average temperatures of 5.3°C (SD=0.4, n=7) between 14.6 and 13.1 ka BP are recorded and a 6.2°C peak (SD=0.1, n=2) occurs from 13.9 to 13.7 ka BP. For the YD, only two data points were measured showing a ~3°C, seen by BWTs > 8°C at 12.9 and at 11.8 ka BP. In the Holocene, a ~3°C transient cooling was registered to average 3.7°C from 11.5 to 6.2 ka BP. Between 5.9 and 5.6 ka BP a final peak to BWTs > 6 °C, followed by a rapid 3°C cooling to average 3°C (SD=0.4, n=4). The end of the Holocene consisted of a strong warming to average 5.1°C (SD=0.6, n=3) in the last part of the record (1.6 – 0.2 ka BP).

3.4 Deep water Holocene warming

Uvigerina peregrina from site GeoB9506-1 showed Mg/Ca ratios between 0.74 and 1.47 mmol/mol (average 1.03 mmol/mol, SD=0.16, n=93). The resulting BWTs ranged from -0.2 to 4.9°C (average 2.2°C, SD=1.3, n=102). One particularity of this site is the occurrence of a turbiditic level between 200 and 230 cm core depth (Mulitza et al., 2005). This level was also seen in the micropaleontological analyses of the present study between 198 and 218 cm core depth. It is characterized by abundant coarser

sediment, glauconite grains, foraminifera filled with glauconite, glauconite foraminiferal fillings, and abundant fragments of microbivalves, microgastropods, briozoa and sponge spicules, in occasions even well preserved (Supplementary information 5.1). Some of these features were also recognized in individual samples at core depths 260, 252.2 – 245, 238, 230, 187.5, 170, 165, 162.5, 153, 138, 112.5, 58 and 34, suggesting that part of these sediments also contain reworked material from shallower depths. The very well defined contourite level and the individual samples identified with potential reworking were not furthered considered in these analyses. In fact, record temperatures of over 3.5°C between 23.6 and 22.5 ka BP (215 – 197.5 cm core depth) indicate the measured specimens correspond to reworked benthic foraminifera from shallower – warmer depths. The remaining samples yielded BWTs between -0.2 and 4.5°C (average 2.2°C, SD=1.2, n=75).

The temperature time series of site GeoB9506-1 (Figure 5.3c, purple curve) starts with average BWTs of 0.6°C (SD=0.3, n=3) between 27.7 and 25.4 ka BP, that rapidly warm through the HS2 into the LGM to average 1.7°C (between 25.1 and 21.9 ka BP, SD=0.3, n=9). The remaining part of the LGM (21.1 – 19.6 ka BP) was observed as an intense cooling to average 0°C (SD=0.1, n=7) when the coldest temperatures of the record are seen (-0.2 at 20.5 ka BP and -0.1°C at 19.6 ka BP). A rapid increase to BWTs over 1.5°C marked the beginning of the HS1 (18.8 – 17.9 ka BP), shortly interrupted by a cooling period to average 0.8°C (SD=0.2, n=4) between 17.7 and 16.7 ka BP. In the following 6 kyrs (16.6 – 10.6 ka BP), BWTs became relatively stable and were on average 2.3°C (SD=0.3, n=27) accounting for an overall 1.5°C warming compared to the previous interval. Into the Holocene, BWTs increased to over 3°C, and were on average 3.8°C (SD=0.4, n=17) between 10.4 and 3.3 ka BP, when the highest temperatures over 4°C were recorded between 9.7 and 8.6 ka BP. This record culminated with an average 1.2°C cooling between 2.2 and 0.6 ka BP, with average BWTs of 2.3 (SD=0.2, n=4).

Overall, the BWTs from site GeoB9506-1 (2,956 m) show similar trends to the observed on the shallower site GeoB9508-5 (2,384 m, Barragán-Montilla et al., 2023). Major differences were observed during the HS2, when BWTs increased around 0.2°C (24.3 – 21.9 ka BP) in site GeoB9506-1 (Figure 5.3c, purple curve) compared to an

approximate 1°C cooling at site GeoB9508-5 between 24.5 and 22.6 ka BP (Figure 5.3c, blue curve), furthermore the warming and heat uptake stagnation periods observed in the latter record (Barragán-Montilla et al., 2023) were also registered in GeoB9506-1 although with an approximate delay of 1.6 kyrs.

3.5 Salinity changes at intermediate and deep water in the eastern tropical North Atlantic

Salinity calculations show values between 33.0 and 36.3 in site GeoB9512-5 (Figure 5.3d in black), between 34.0 and 35.5 in site GeoB9506-1 (Figure 5.3d in purple), and between 34.4 and 35.7 in site GeoB9508-5 (Figure 5.3d in blue).

At intermediate depths (GeoB9512-5) salinity was higher during the HS2 (average 34.57), LGM (average 37.87) and in the first part of the HS1 (18.6 – 17.6 ka BP, average 34.44). In the deep eastern North Atlantic salinities were between 34.87 and 35.31 at site GeoB9508-5, and between 34.66 and 34.87 at GeoB9506-1 from HS2 to HS1. The rest of the HS1 at site GeoB9512-5 was characterized by consistently lower salinities between 33.81 and 34.09. During the B-A, salinity increased to an average of 34.29 as in the deeper sites (averages of 34.90 and 34.58 at GeoB9508-5 and GeoB9506-1 respectively). Maximum salinities were recorded during the YD at intermediate depths with salinities ~ 35.02 coincide with average 35.18 values at site GeoB9508-5, and 34.55 at site GeoB9506-1. In the Holocene salinities at intermediate depths dropped to 33.39 in the first part of the Holocene (11.5 – 5.9 ka BP) and to 33.70 in the second part (5.6 – 0.2 ka BP). In the deeper sites, average salinities of 35.18 and 34.71 were recorded in the first part of the Holocene in sites GeoB9508-5 and GeoB9506-1 respectively, into the late Holocene when average values of 34.77 (GeoB9508-5) and 34.61 (GeoB9506-1) were recorded.

4 Discussion

4.1 Glacial to deglacial temperature stratification decline

The calculated salinity records show similar trends between deep sites GeoB9506-1 (Figure 5.3d, purple curve) and GeoB9508-5 (Figure 5.33d, blue curve). Overall, salinities at the intermediate site were consistently lower than at the deeper sites, except for the YD and the HS2-LGM when salinities have similar values (Figure 5.3d).

Temperatures were consistently higher at intermediate depths; however larger differences were recorded from the HS2 until the HS1 (Figure 5.3c). The rapid warming registered in the deeper sites coincides with relatively stable BWTs at GeoB9512-5 making the temperature difference decrease into the B-A. The largest temperature stratification was registered during the YD during the intense ~ 3°C intermediate water warming synchronous with the heat uptake stagnation period observed at deeper sites (Barragán-Montilla et al., 2023). Into the early Holocene the transient ~ 3°C cooling observed at site GeoB9512-5 coincides with the ~ 0.8°C deep-water warming observed at site GeoB9508 (Barragán-Montilla et al., 2023) and in site GeoB9506-1, that has already warm ~ 0.8°C in the YD. The end of our records show a ~ 0.3°C intermediate water warming synchronous BWTs decreased ~ 0.9°C in site GoB9508-5.

4.1 Paleoceanographic implications: deglacial shallow to Holocene deep heat storage in the tropical Eastern Atlantic

During slowdown of AMOC in the HS1 and YD (Figure 5.4d, e.g. McManus et al., 2004; Böhm et al., 2015) limited heat transport form the tropical Atlantic to northern latitudes is evidenced by an intense warming of intermediate waters in the tropical Atlantic (Oppo et al., 2023; Poggeman et al., 2018; Rühlemann et al., 2004; Weldeab et al., 2016), and subpolar Atlantic (Max et al., 2022). In our area of study, from HS1 until the end of YD, higher intermediate BWTs (GeoB9512-5) are coeval with colder deep-water temperatures in the NE Atlantic (GeoB9506-1 and GeoB9508-5) and are followed by an intense cooling of intermediate waters during the Holocene synchronous with a rapid warming in deeper sites (Figure 5.5a). This suggests that in times of reduced deep overturning, heat storage shifted to shallower depths, in agreement with the limited deep heat uptake observed in the NE Atlantic (Barragán-Montilla et al., 2023), related to a decrease in heat transport to higher latitudes as suggested by some models and proxy data (e.g. Liu et al., 2009; Lynch-Stieglitz et al., 2014; Mecking and Drijfhout, 2023).

The situation of GeoB9512-5 in the mixing area of the North Atlantic and South Atlantic Central waters (Figure 5.1b, NACW and SACW), also suggests that a warmer signal in our records could be interpreted as a stronger contribution of warmer central waters,

while lower temperatures suggest a stronger influence of the Antarctic Intermediate Water (AAIW, Figure 5.1b). The NACW is known to have penetrated further south when the North Atlantic Subtropical gyre was stronger (Huang et al., 2012; Reißig et al., 2019), during HS1 and YD (Huang et al., 2012) compatible with the warmer BWTs observed in GeoB9512-5 record in the same periods. Furthermore, higher salinity of the thermocline during the LGM (200 – 550 m water depth) and HS1 (200 – 400 m water depth) suggests that the eastern North Atlantic was ventilated northern-sourced surface waters indicating the frontal mixing zone between the NACW and SACW moved south during this time (Huang et al., 2012).

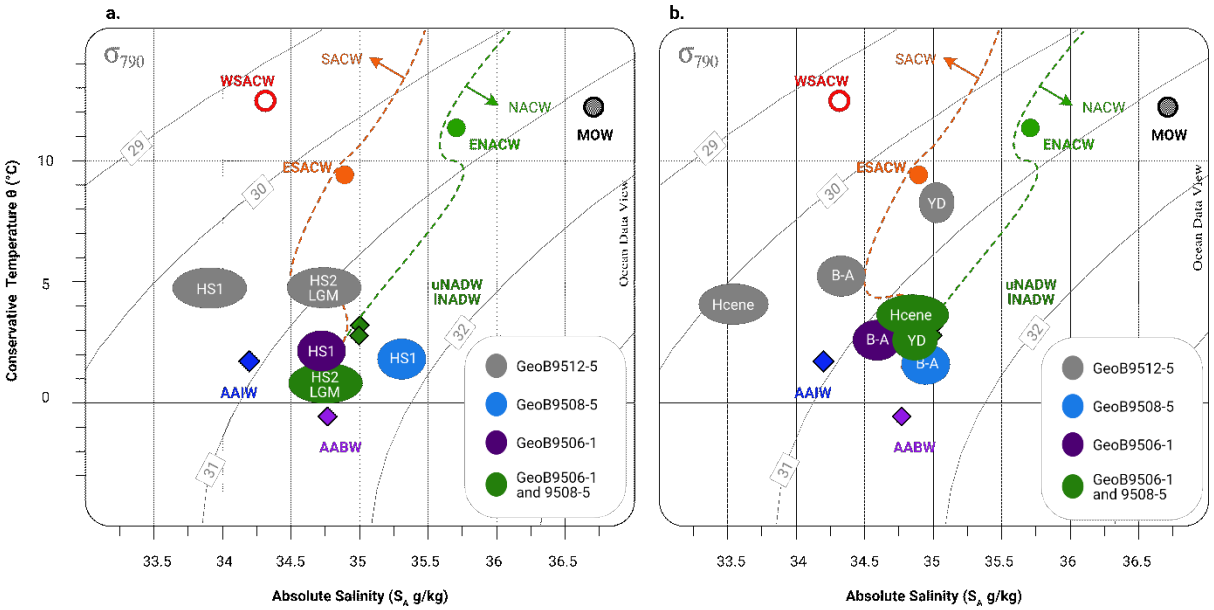

Figure 5.4 T-S diagram showing the average BWTs and salinities for each climatic period in the studied cores. a. Heinrich Stadial 2 (HS2) to Last Glacial Maximum (LGM); **b.** Bølling–Allerød (B-A) to Holocene (Hcene). Key Climatic Periods: Heinrich Stadial 2 (HS2); Last Glacial Maximum (LGM); Heinrich Stadial 1 (HS1); Bølling–Allerød (B-A); Younger Dryas (YD).

To better understand the potential influence of water masses in our sites we plotted the average BWTs and salinities for each climatic period in the studied cores in a T-S diagram (Figure 5.4). We find that during the HS1, intermediate waters were influenced by the warmer Eastern South Atlantic Central Water (ESACW, Figure 5.4a) and to some extent by the Antarctic Intermediate Water (AAIW), while in the YD warm and saline waters in site GeoB9512-5 show a strong influence of the ESACW and the Eastern North Atlantic Central Water (ENACW in Figure 5.4b). During the Holocene, BWTs and salinity decrease is compatible with a water mass more influenced by the

AAIW (Figure 5.4b). In fact, this agrees with studies that show that AAIW northward penetration is positively correlated with AMOC strength, and in times of AMOC slowdown AAIW retreats southwards, at the same time it thicknesses and depth increases (Gu et al., 2017; Huang et al., 2014; Xie et al., 2012). For the deep sites, a clear North Atlantic Deep Water (NADW) was seen during the last deglaciation and the Holocene (Figure 5.4a, b), while during the HS2 to HS1 seems to be influenced to some extent by the AAIW (except for the HS1 in site GeoB9508-5, Figure 5.4a). However, uncertainties of approximately ±1 introduce important margins of error to the salinity calculations at site GeoB9512-5 (Supplementary Information 3) and could underestimate the influence of a water mass more compatible with the NACW for site GeoB9512-5 during from the LGM until and HS1.

Carbon isotopes from the deep sites GeoB9508-5 and GeoB9506-1 show a consistent decrease in deep water ventilation (Figure 5.5c) in times of AMOC slowdown (Figure 5.5b) (Barragán-Montilla et al., 2023). For site GeoB9512-5 the $\delta^{13}C$ record is less clear and depletion during the YD and HS1 seems to respond to increasing nutrient contents, synchronous with the enhanced upwelling activity observed by Romero et al. (2008) near our area of study. Since the nutrient imprint is difficult to remove from this record, ventilation inferences for this site rely on the bottom water oxygen reconstruction (Barragán-Montilla et al., in review – Chapter 2).

As AMOC slowed down during the HS1 and YD (Figure 5.5b), deep water ventilation decreased in the NADW in the eastern tropical North Atlantic indicated by the decrease in carbon isotopes (Barragán-Montilla et al., 2023). In contrast, oxygen increase at intermediate depths suggests that intermediate waters in the eastern tropical North Atlantic Oxygen Minimum Zone were more ventilated. This is explained by acceleration in the North Atlantic Subtropical Gyre driven by stronger winds as the temperature gradient increased when heat was no longer being transported to higher latitudes by deep overturning (Barragán-Montilla et al., in review – Chapter 2).

Since subsurface circulation was enhanced in times of AMOC decline, the heat accumulating in the western North Atlantic and transported by the subtropical cell led to the intense warming episodes observed in the HS1 and YD within the Atlantic

subsurface (Oppo et al., 2023; Came et al., 2007; Poggemann et al., 2018; Rühlemann et al., 2004). This could explain the temperature increase observed in parts of the HS1 and in the YD, while the rapid cooling in the Holocene seen in site GeoB9512-5 and in the other parts of the upper Atlantic (Oppo et al., 2023; Weldeab et al., 2016), is mostly synchronous with deep water temperature increase from sites GeoB9508-5 and GeoB9506-1 consistent with a resumption of AMOC circulation (Figure 5.5b). This resumption allowed for heat transport to higher latitudes to resume cooling intermediate waters.

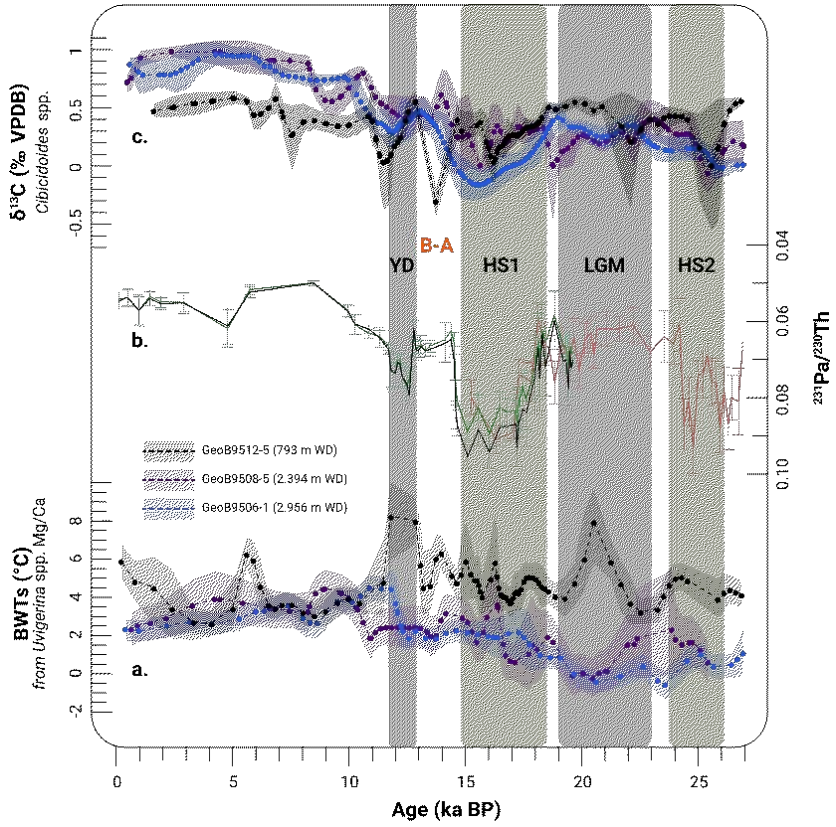

Figure 5.5 Western Atlantic $^{231}Pa/^{230}Th$ and benthic Foraminifer paleotemperature and $\delta^{13}C$ from sites GeoB9512-5, GeoB9506-1 and GeoB9508-5 a. Bottom Water Temperature records estimated from *Uvigerina* spp. Mg/Ca; **b.** Atlantic $^{231}Pa/^{230}Th$ from Bermuda Rise sites (blue and green curves, McManus et al., 2004); and deep NW Atlantic (red curve, Böhm et al., 2015); **c.** *Cibicidoides* spp. carbon isotopes ($\delta^{13}C$) from the studied sites. GeoB9506-1 in purple; GeoB9508-5 in blue and GeoB9512-5 in black. Shaded areas correspond to the 95% confidence envelope. Key Climatic Periods: Heinrich Stadial 2 (HS2); Last Glacial Maximum (LGM); Heinrich Stadial 1 (HS1); Bølling–Allerød (B-A); Younger Dryas (YD).

Warmer temperatures on site GeoB9512-5 during the LGM can also be the result of the ~ 100 m sea level drop (e.g. Völpel et al., 2019), however the variations registered here are too large to be explained only by this. An alternative explanation is that with

a strong AMOC, intermediate water temperature increase could be related to a shallower NADW cell (e.g. Howe et al., 2016) bringing warmer waters to intermediate depths.

5 Conclusions

Our data provide evidence of the heat storage changes related to AMOC strength variability during the last deglaciation. We find intense subsurface warming during HS1 and YD, also identified in other parts of the tropical Atlantic and related to reduced AMOC and increasing atmospheric CO_2 (Köhler et al., 2017). As this subsurface warming took place, heat uptake was paused at deeper waters, suggesting that ocean heat was mainly stored at intermediate depths in the eastern tropical North Atlantic. In the B-A with a resumption of the AMOC, temperature stratification decreased between intermediate and deep waters. However, warmer intermediate waters persisted, indicating that even though AMOC strength increased, heat distribution was not fully restored, and deep Atlantic heat uptake stagnation persisted as global mean surface temperatures increased (Osman et al., 2021). In the Holocene with a stronger AMOC, heat transport from the tropical Atlantic to higher latitudes resumed allowing intermediate waters to cool, as heat storage started to take place in the deep Atlantic again. This study provides further evidence that AMOC sets the depth of ocean heat storage and shows that a potential AMOC slowdown in the 21st century can significatively modify the ocean heat uptake and storage mechanisms.

Acknowledgements

This research was carried out within the Cluster of Excellence EXC 2077 at MARUM institute – University of Bremen, funded by “Deutsche Forschungsgemeinschaft” (DFG). This research is also supported by GLOMAR – Bremen International Graduate School for Marine Sciences, University of Bremen. We thank the GeoB Core repository at MARUM who provided the samples used in this study.

Data availability

Barragán-Montilla, Sofía; Mulitza, Stefan (in review a): Radiocarbon ages of sediment core GeoB9512-5. PANGAEA, https://doi.org/10.1594/PANGAEA.962899

Barragán-Montilla, Sofía; Mulitza, Stefan (in review b): Radiocarbon ages of sediment core GeoB9506-1. PANGAEA, https://doi.org/10.1594/PANGAEA.962888

Barragán-Montilla, Sofía (in review a): Benthic foraminifera stable isotopes (d18O and d13C) of sediment core GeoB9512-5. PANGAEA, https://doi.org/10.1594/PANGAEA.962968

Barragán-Montilla, Sofía (in review b): δ18O and δ13C stable isotopes of benthic foraminifera Cibicidoides wuellerstorfi from sediment core GeoB9506-1. PANGAEA, https://doi.org/10.1594/PANGAEA.962981

Barragán-Montilla, Sofía; Johnstone, Heather J H (in review a): Benthic Foraminifera trace elements to calcium ratios and bottom water temperatures from the last 27,000 years of sediment core GeoB9512-5. PANGAEA, https://doi.pangaea.de/10.1594/PANGAEA.964318

Barragán-Montilla, Sofía; Johnstone, Heather J H (in review b): Benthic foraminifera element to calcium ratios and bottom water temperatures of sediment core GeoB9506-1. PANGAEA, https://doi.pangaea.de/10.1594/PANGAEA.964374

Barragán-Montilla, Sofía; Johnstone, Heather J H; Mulitza, Stefan; Pälike, Heiko (2023a): Bottom water temperatures (raw and processed including confidence intervals) calculated using Mg/Ca ratios of endobenthic Uvigerina spp. from the last 50.000 years from site GeoB9508-5 off NW Africa. PANGAEA, https://doi.org/10.1594/PANGAEA.950494

Barragán-Montilla, Sofía; Johnstone, Heather J H; Mulitza, Stefan; Pälike, Heiko (2023b): Processed stable isotope (carbon and oxygen) data from epibenthic Cibicidoides spp., including confidence intervals from the last 50.000 years from site GeoB9508-5 off NW Africa. PANGAEA, https://doi.org/10.1594/PANGAEA.950502

Final conclusions and Outlook

This project shows the power of using benthic foraminifera for paleoceanographic reconstruction. During this research, a benthic foraminifera multiproxy approach was used to investigate the effects of Atlantic Meridional Overturning Circulation (AMOC) on ocean heat uptake and storage and oxygen concentrations in benthic ecosystems in the eastern tropical North Atlantic. In addition, using benthic foraminifera taxonomical and quantitative analyses, we contribute to the understanding of potential vital effects on Mg/Ca paleothermometry, and propose alternatives to reduce uncertainties and improve paleotemperature reconstruction on areas influenced by upwelling activity which modify paleoenvironmental conditions at the seafloor and therefore induce adaptations strategies that can affect biomineralization of certain benthic foraminifera species used in paleoceanography.

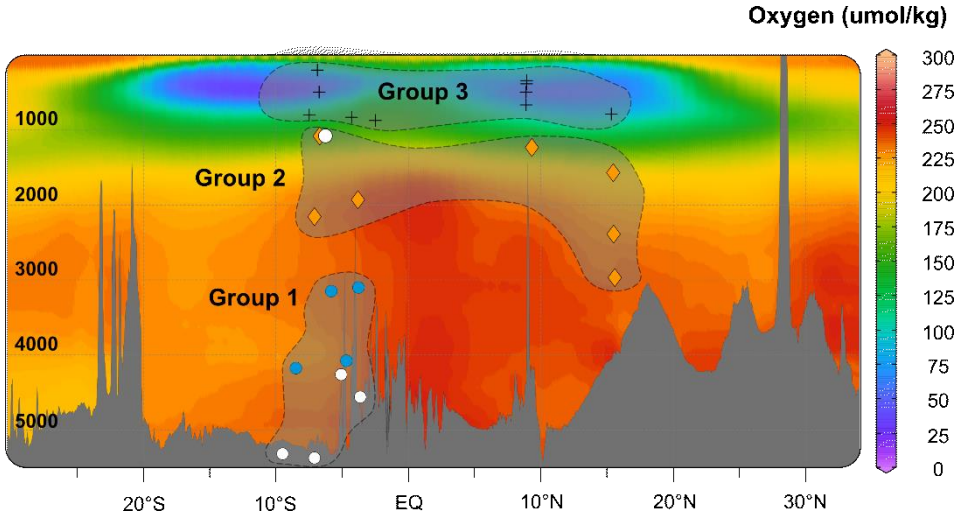

Figure C.1 Distribution of core top samples in relation to water depth in the eastern tropical Atlantic. Modified from Chapter 1. Groups correspond to samples with similar benthic foraminifera assemblages as described in Chapter 1 – Section 3.

Research question 1 (Chapter 1) *how benthic foraminifera are distributed in the NE Atlantic and what are the main environmental parameters influencing their diversity* was tackled using surface samples from the eastern tropical Atlantic. We find that benthic foraminifera distribution is controlled by oxygen and organic matter content. The first parameter is controlled by the presence of the Oxygen Minimum Zones off NW Africa, while organic matter is linked to primary productivity related to upwelling conditions. An important outcome is the grouping of samples in different

paleoenvironmental regimes, with a clear differentiation of subsurface (< 1,200 m water depth) and deep-water assemblages (Figure 1). This is seen as a shift from low oxic to suboxic – high organic matter bottom water conditions (< 1,200 WD) to high oxic – moderate organic matter concentrations at deeper settings (>1,200 m WD). Such differentiation has also been found in data form Lutze and Coulbourn (1980) and Haake (1980) and agrees with Jorissen et al. (1998) observations that benthic foraminifera from water depths above 1,200 m in this area are more influenced by organic matter from upwelling activity.

Using a detailed taxonomy and quantitative analyses of benthic foraminifera, we were able to reconstruct oxygen changes in site GeoB9512-5 (793 m water depth) which suggest changes in the Eastern Tropical North Atlantic Oxygen Minimum Zone (ETNA – OMZ) during times of AMOC strength changes. This tackles research question 3 and allowed us to provide new insights into the response of subsurface circulation to AMOC slowdown (Chapter 2). Our records show periods of increased oxygenation that are synchronous with AMOC decline during the last deglaciation. This suggests that in times of AMOC slowdown, subsurface circulation was enhanced due to an intensification of wind strength as a result of steeper temperature gradients, as heat is no longer being transported to northern latitudes with an inactive AMOC.

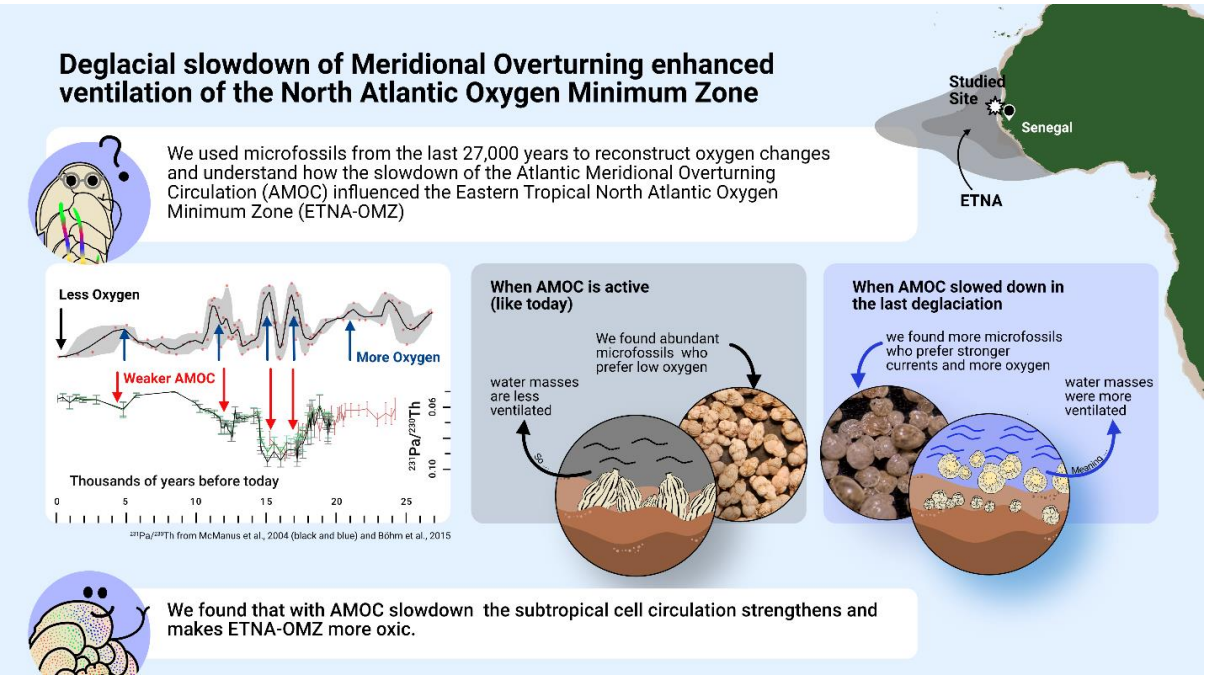

Figure C.2 Graphic Abstract summarizing the findings of Chapter 2.

These oxygen changes in the upper Atlantic are also met with changing upwelling activity during the last deglaciation leading to an increase in organic matter from primary productivity. This has also been seen to affect individual species of benthic foraminifera such as *M. barleeanus* (Caralp et al., 1989), who are known to migrate vertically in the sediment with changes in oxygen and organic matter (Linke and Lutze, 1993). In Chapter 3 (Research question 3) we explore the potential effects of this adaptation strategies in a paleotemperature record from site GeoB9512-5, which shows an early LGM warming incompatible with a paleotemperature record from *Uvigerina mediterranea* Mg/Ca in the same site. Two new calibrations are proposed, one of them attempting to remove a potential oxygen effect on *M. barleeanus* Mg/Ca observed in our coretops measurements. Even with this new calibration, such warming is still seen in the *M- barleeanus* record, and our Mn/Ca observation suggests that this species migrated in the sediment during this time, potentially hinting to additional microhabitat effect on Mg/Ca ratios in our site (Figure 2, Graphic Abstract - Chapter 3).

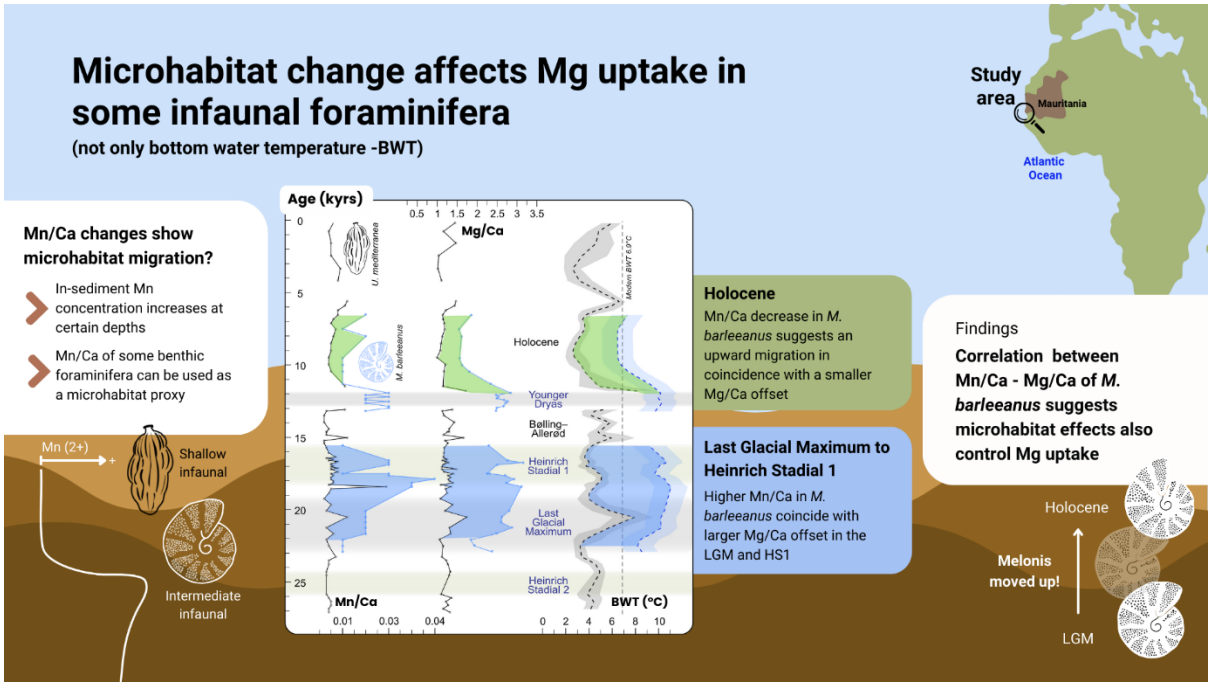

Figure C.3 Graphic Abstract summarizing the findings of Chapter 3.

After these considerations, we can conclude that *Uvigerina* Mg/Ca remains one of the best paleothermometry tool in paleoceanographic studies. With this in mind, we dive

into research question 4 **how the Atlantic Meridional Overturning Circulation (AMOC) changes in the last 30,000 years influenced deep ocean heat uptake in the eastern North Atlantic?** Using *Uvigerina* Mg/Ca records in site GeoB9508-5 (2,384 m water depth, Chapter 4) we find that in times of AMOC slowdown (Figure 4a) seen in this site as a decreased ventilation periods ($\delta^{13}C$ Figure 4b, Chapter 4), the deep Atlantic rapidly warmed and stopped taking up heat (Figure 4c) until AMOC became active again (Figure 4a). This was confirmed observed in the paleotemperature record of site GeoB9506-1 (Figure 4c, 2,956 water depth, Chapter 5). At intermediate depths warming continued during these deep-water heat uptake stagnation periods (red arrow, Figure 4d). Furthermore, intermediate waters remained warmer during the LGM and subsequent deglaciation (Figure 4d). As described in Chapter 5, we infer that during the LGM until the YD most heat was stored at shallower depths, particularly in times of AMOC slowdown including the HS1 and YD warming seen in our records. During the Holocene, intermediate waters rapidly cooled around 3°C as deep water (blue arrow in Figure 4d) started to warm approximately 1.8°C, indicating heat was now being stored at deeper waters as AMOC circulation increased again (e.g. McManus et al., 2004).

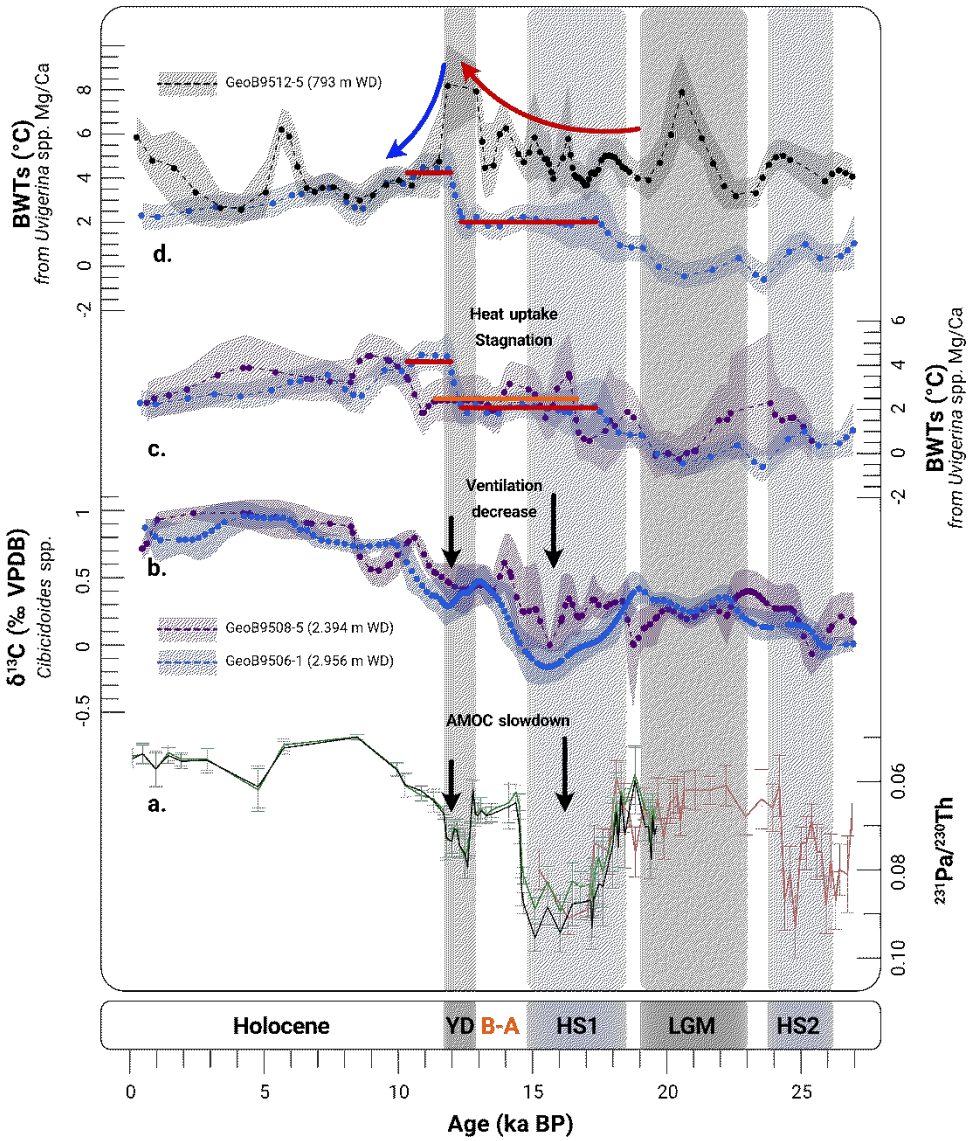

Figure C.4 Global AMOC proxy and benthic foraminifera paleotemperature and $\delta^{13}C$ from sites GeoB9512-5, GeoB9506-1 and GeoB9508-5 modified from Chapter 5 a. $^{231}Pa/^{230}Th$ kinematic proxy of AMOC from the Bermuda Rise (McManus et al., 2004 in blue and green); and deep NW Atlantic (Böhm et al., 2015 in red); **b.** *Cibicidoides* spp. carbon isotopes ($\delta^{13}C$) from the GeoB9506-1 in purple and GeoB9508-5 in blue; **c-d.** Bottom Water Temperature records estimated from *Uvigerina* spp. Mg/Ca, GeoB9508-5 in blue, and GeoB9512-5 in black. Shaded areas correspond to the 95% confidence envelope. Key Climatic Periods: Heinrich Stadial 2 (HS2); Last Glacial Maximum (LGM); Heinrich Stadial 1 (HS1); Bølling–Allerød (B-A); Younger Dryas (YD).

Our results show that AMOC has the potential to set the depth of heat storage and a slowdown in times of global warming limits heat uptake in the deep ocean as the upper Atlantic warmed. These results are comparable to intermediate water warming seen in other parts of the Atlantic (Oppo et al., 2023; Came et al., 2007; Poggemann et al., 2018; Rühlemann et al., 2004, Weldeab et al., 2016). The consequences for the global warming rate are unclear, and studies integrating paleotemperature records of different parts of the Atlantic Ocean and at different ocean depths are necessary to

better constrain the consequences of AMOC slowdown in global warming via ocean heat uptake modifications.

In addition, more comprehensive analyses on benthic foraminifera biomineralization are important, to constrain the effects of vital effects changes in response to paleoenvironmental conditions, which occur in times of global paleoceanographic organization as shown in Chapter 3. This information is crucial to evaluate the accuracy of paleoceanographic reconstructions of the deep ocean, that we rely on to understand climate change over longer time scales.

Finally, from Chapter 2, we outline the importance of benthic foraminifera in paleo-oxygenation reconstructions, as they not only give information about the dynamics of Oxygen Minimum Zones in a climate change scenario, but also can give valuable information about the carbon pump and other oceanographic processes that influence global climate. Furthermore, future studies to constrain the effects of AMOC slowdown on the South Atlantic Oxygen Minimum Zone are important to fill crucial gaps in our understanding of the paleoceanographic processes of this ocean basin that plays a key role in global climate.

Acknowledgements

Firstly, I want to thank God and my family, especially my mother Lyda, for their never-ending support, understanding and patience throughout my career so far away from home. To my incredible community GeoLatinas, particularly to Rocío, Rehemat, Moka, Angelique, Dariana, Giulia and Danita for their encouragement and feedback before and during this journey, as well as Natasha, Gabriela and Angely who welcomed me in Bremen in a difficult time and made my transition into this new culture much easier. Thank you for being a little piece of my home country during this time, I hold this close to my heart.

I am also deeply grateful to Dr. Stefan Mulitza, Prof. Dr. Heiko Pälike and Dr. Heather Johnstone for this opportunity and their support and guidance during the development. of this research. To my advisors Prof. Dr. Carlos Alberto Sanchez Quiñonez from Colombia and Prof. Dr. Laia Alegret in Spain, I always thank for supporting and encouraging my passion for benthic foraminifera and earth sciences, I would not be here without their constant mentorship after so many years. I also thank Prof. Dr. Babette Hoogakker, and her wonderful team Dharma, Sebastian and Tommaso who welcomed me at The Lyell Centre in Edinburgh during my research stay, it was an incredible learning experience, and an amazing motivation at the end of my doctorate. Thank you, Dharma, for your support and for being an active part of my research.

I want to specially thank my life partner Alex, your support, patience, encouragement, and love towards my research, outreach and in our life together was essential in this. process. Thank you for reading my abstracts, papers, practicing my presentations and of course, for your support with my coding problems. I am also grateful to Ute, Klaus, Chris and Clarissa for their interest in my research, but most importantly your support so far away from home, you always make me feel welcome and warm. I also thank Marie and Leia who set uncountable hours as I analyzed and interpreted my data. Finally, I thank my friends, Dani, Mafe, Javier, Erik, Liz, Edu and Nesti, for their unconditional support in the distance, as well as their beautiful energy and encouragement in this path. A special thanks to my colleagues at MARUM, especially Jing and Karla with whom I walked this path together, your words of support and the

time spent chatting and laughing was always a breath of fresh air. Lastly, I want to express my gratitude to Germany, the University of Bremen, MARUM and GLOMAR fore for this unique opportunity, for allowing me be part of the research team, and for the countless training and learning opportunities you made possible in the last three years. I am sure that your visible efforts to increase diversity, equity and inclusion in science will continue to evolve and strengthen. I sincerely hope that my research, along with the multiple collaborations and outreach that stemmed from my work at MARUM, contributes to advance the institute's research and encourages the inclusion of more research involving benthic foraminifera applications in paleoceanographic and climate change studies. There is still a lot of work to do in this field.

I dedicate this thesis and research to our little bean, who has already brought so much joy and excitement to Alex's and my own life. You have been a wonderful companion in the last phase of this process.

Gracias totales.

References

Abstract

Böhm, E., Lippold, J., Gutjahr, M., Frank, M., Blaser, P., Antz, B., Fohlmeister, J., Frank, N., Andersen, M.B., Deininger, M., 2015. Strong and deep Atlantic meridional overturning circulation during the last glacial cycle. Nature 517, 73–76. https://doi.org/10.1038/nature14059

Caesar, L., McCarthy, G.D., Thornalley, D.J.R., Cahill, N., Rahmstorf, S., 2021. Current Atlantic Meridional Overturning Circulation weakest in last millennium. Nat. Geosci. 14, 118–120. https://doi.org/10.1038/s41561-021-00699-z

Calvin, K., Dasgupta, D., Krinner, G., Mukherji, A., Thorne, P.W., Trisos, C., Romero, J., Aldunce, P., Barrett, K., Blanco, G., Cheung, W.W.L., Connors, S., Denton, F., Diongue-Niang, A., Dodman, D., Garschagen, M., Geden, O., Hayward, B., Jones, C., Jotzo, F., Krug, T., Lasco, R., Lee, Y.-Y., Masson-Delmotte, V., Meinshausen, M., Mintenbeck, K., Mokssit, A., Otto, F.E.L., Pathak, M., Pirani, A., Poloczanska, E., Pörtner, H.-O., Revi, A., Roberts, D.C., Roy, J., Ruane, A.C., Skea, J., Shukla, P.R., Slade, R., Slangen, A., Sokona, Y., Sörensson, A.A., Tignor, M., Van Vuuren, D., Wei, Y.-M., Winkler, H., Zhai, P., Zommers, Z., Hourcade, J.-C., Johnson, F.X., Pachauri, S., Simpson, N.P., Singh, C., Thomas, A., Totin, E., Arias, P., Bustamante, M., Elgizouli, I., Flato, G., Howden, M., Méndez-Vallejo, C., Pereira, J.J., Pichs-Madruga, R., Rose, S.K., Saheb, Y., Sánchez Rodríguez, R., Ürge-Vorsatz, D., Xiao, C., Yassaa, N., Alegría, A., Armour, K., Bednar-Friedl, B., Blok, K., Cissé, G., Dentener, F., Eriksen, S., Fischer, E., Garner, G., Guivarch, C., Haasnoot, M., Hansen, G., Hauser, M., Hawkins, E., Hermans, T., Kopp, R., Leprince-Ringuet, N., Lewis, J., Ley, D., Ludden, C., Niamir, L., Nicholls, Z., Some, S., Szopa, S., Trewin, B., Van Der Wijst, K.-I., Winter, G., Witting, M., Birt, A., Ha, M., Romero, J., Kim, J., Haites, E.F., Jung, Y., Stavins, R., Birt, A., Ha, M., Orendain, D.J.A., Ignon, L., Park, S., Park, Y., Reisinger, A., Cammaramo, D., Fischlin, A., Fuglestvedt, J.S., Hansen, G., Ludden, C., Masson-Delmotte, V., Matthews, J.B.R., Mintenbeck, K., Pirani, A., Poloczanska, E., Leprince-Ringuet, N., Péan, C., 2023. IPCC, 2023: Climate Change 2023: Synthesis Report. Contribution of Working Groups I, II and III to the Sixth Assessment Report of the Intergovernmental Panel on Climate Change [Core Writing Team, H. Lee and J. Romero (eds.)]. IPCC, Geneva, Switzerland. Intergovernmental

Panel on Climate Change (IPCC). https://doi.org/10.59327/IPCC/AR6-9789291691647

Cummins, P.F., Masson, D., Saenko, O.A., 2016. Vertical heat flux in the ocean: Estimates from observations and from a coupled general circulation model. JGR Oceans 121, 3790–3802. https://doi.org/10.1002/2016JC011647

Dima, M., Nichita, D.R., Lohmann, G., Ionita, M., Voiculescu, M., 2021. Early-onset of Atlantic Meridional Overturning Circulation weakening in response to atmospheric CO2 concentration. npj Clim Atmos Sci 4, 27. https://doi.org/10.1038/s41612-021-00182-x

Du, J., Haley, B.A., Mix, A.C., 2020. Evolution of the Global Overturning Circulation since the Last Glacial Maximum based on marine authigenic neodymium isotopes. Quaternary Science Reviews 241, 106396. https://doi.org/10.1016/j.quascirev.2020.106396

Gherardi, J., Labeyrie, L., Mcmanus, J., Francois, R., Skinner, L., Cortijo, E., 2005. Evidence from the Northeastern Atlantic basin for variability in the rate of the meridional overturning circulation through the last deglaciation. Earth and Planetary Science Letters 240, 710–723. https://doi.org/10.1016/j.epsl.2005.09.061

Intergovernmental Panel On Climate Change (Ipcc), 2022. The Ocean and Cryosphere in a Changing Climate: Special Report of the Intergovernmental Panel on Climate Change, 1st ed. Cambridge University Press. https://doi.org/10.1017/9781009157964

Levitus, S., Antonov, J.I., Boyer, T.P., Stephens, C., 2000. Warming of the World Ocean. Science 287, 2225–2229. https://doi.org/10.1126/science.287.5461.2225

Liu, Z., 2023. Evolution of Atlantic Meridional Overturning Circulation since the last glaciation: model simulations and relevance to present and future. Phil. Trans. R. Soc. A. 381, 20220190. https://doi.org/10.1098/rsta.2022.0190

McManus, J.F., Francois, R., Gherardi, J.-M., Keigwin, L.D., Brown-Leger, S., 2004. Collapse and rapid resumption of Atlantic meridional circulation linked to deglacial climate changes. Nature 428, 834–837. https://doi.org/10.1038/nature02494

Oppo, D.W., Curry, W.B., McManus, J.F., 2015. What do benthic δ 13 C and δ 18 O data tell us about Atlantic circulation during Heinrich Stadial 1? Paleoceanography 30, 353–368. https://doi.org/10.1002/2014PA002667

Rahmstorf, S., Box, J.E., Feulner, G., Mann, M.E., Robinson, A., Rutherford, S., Schaffernicht, E.J., 2015. Exceptional twentieth-century slowdown in Atlantic Ocean overturning circulation. Nature Clim Change 5, 475–480. https://doi.org/10.1038/nclimate2554

Roberts, N.L., Piotrowski, A.M., McManus, J.F., Keigwin, L.D., 2010. Synchronous Deglacial Overturning and Water Mass Source Changes. Science 327, 75–78. https://doi.org/10.1126/science.1178068

Introduction and Methods

Alegret, L., Arreguín-Rodríguez, G.J., Trasviña-Moreno, C.A., Thomas, E., 2021. Turnover and stability in the deep sea: Benthic foraminifera as tracers of Paleogene global change. Global and Planetary Change 196, 103372. https://doi.org/10.1016/j.gloplacha.2020.103372

Assis, J., Failler, P., Fragkopoulou, E., Abecasis, D., Touron-Gardic, G., Regalla, A., Sidina, E., Dinis, H., Serrao, E.A., 2021. Potential Biodiversity Connectivity in the Network of Marine Protected Areas in Western Africa. Front. Mar. Sci. 8, 765053. https://doi.org/10.3389/fmars.2021.765053

Blaauw, M., Christen, J.A., 2011. Flexible paleoclimate age-depth models using an autoregressive gamma process. Bayesian Anal. 6, 457–474. https://doi.org/10.1214/ba/1339616472

Böhm, E., Lippold, J., Gutjahr, M., Frank, M., Blaser, P., Antz, B., Fohlmeister, J., Frank, N., Andersen, M.B., Deininger, M., 2015. Strong and deep Atlantic

meridional overturning circulation during the last glacial cycle. Nature 517, 73–76. https://doi.org/10.1038/nature14059

Boyer, T.P., García, H.E., Locarnini, R.A., Zweng, M.M., Alexey, V., Reagan, J.R., Weathers, K.A., Baranova, O.K., Paver, C.R., Seidov, Dan, Smolyar, I.V., 2018. World Ocean Atlas 2018. [Annual Data, 1.00 Degree all years].

Brandt, P., Bange, H.W., Banyte, D., Dengler, M., Didwischus, S.-H., Fischer, T., Greatbatch, R.J., Hahn, J., Kanzow, T., Karstensen, J., Körtzinger, A., Krahmann, G., Schmidtko, S., Stramma, L., Tanhua, T., Visbeck, M., 2015. On the role of circulation and mixing in the ventilation of oxygen minimum zones with a focus on the eastern tropical North Atlantic. Biogeosciences 12, 489–512. https://doi.org/10.5194/bg-12-489-2015

Broccoli, A.J., Dahl, K.A., Stouffer, R.J., 2006. Response of the ITCZ to Northern Hemisphere cooling. Geophysical Research Letters 33. https://doi.org/10.1029/2005GL024546

Bruno, J.F., Bates, A.E., Cacciapaglia, C., Pike, E.P., Amstrup, S.C., Van Hooidonk, R., Henson, S.A., Aronson, R.B., 2018. Climate change threatens the world's marine protected areas. Nature Clim Change 8, 499–503. https://doi.org/10.1038/s41558-018-0149-2

Cropper, T.E., Hanna, E., Bigg, G.R., 2014. Spatial and temporal seasonal trends in coastal upwelling off Northwest Africa, 1981–2012. Deep Sea Research Part I: Oceanographic Research Papers 86, 94–111. https://doi.org/10.1016/j.dsr.2014.01.007

Dupont, L.M., Schlütz, F., Ewah, C.T., Jennerjahn, T.C., Paul, A., Behling, H., 2010. Two-step vegetation response to enhanced precipitation in Northeast Brazil during Heinrich event 1. Global Change Biology 16, 1647–1660. https://doi.org/10.1111/j.1365-2486.2009.02023.x

García, H.E., Weathers, K.A., Paver, C.R., Smolyar, I.V., Boyer, T.P., Locarnini, R.A., Zweng, M.M., Mishonov, A.V., Baranova, O.K., Seidov, Dan, Reagan, J.R.,

2019. World Ocean Atlas 2018, Volume 3: Dissolved Oxygen, Apparent Oxygen Utilization, and Oxygen Saturation. A. Mishonov Technical Ed.

Gilly, W.F., Beman, J.M., Litvin, S.Y., Robison, B.H., 2013. Oceanographic and Biological Effects of Shoaling of the Oxygen Minimum Zone. Annu. Rev. Mar. Sci. 5, 393–420. https://doi.org/10.1146/annurev-marine-120710-100849

Heaton, T.J., Köhler, P., Butzin, M., Bard, E., Reimer, R.W., Austin, W.E.N., Bronk Ramsey, C., Grootes, P.M., Hughen, K.A., Kromer, B., Reimer, P.J., Adkins, J., Burke, A., Cook, M.S., Olsen, J., Skinner, L.C., 2020. Marine20—The Marine Radiocarbon Age Calibration Curve (0–55,000 cal BP). Radiocarbon 62, 779–820. https://doi.org/10.1017/RDC.2020.68

Intergovernmental Panel On Climate Change (Ipcc), 2023. Climate Change 2022 – Impacts, Adaptation and Vulnerability: Working Group II Contribution to the Sixth Assessment Report of the Intergovernmental Panel on Climate Change, 1st ed. Cambridge University Press. https://doi.org/10.1017/9781009325844

Intergovernmental Panel On Climate Change (Ipcc), 2022. The Ocean and Cryosphere in a Changing Climate: Special Report of the Intergovernmental Panel on Climate Change, 1st ed. Cambridge University Press. https://doi.org/10.1017/9781009157964

Itambi, A.C., 2010. X-ray fluorescence measurements (Ti, Ca and Fe) of sediment core GeoB9506-1. https://doi.org/10.1594/PANGAEA.734380

Lauvset, S.K., Lange, N., Tanhua, T., Bittig, H.C., Olsen, A., Kozyr, A., Alin, S., Álvarez, M., Azetsu-Scott, K., Barbero, L., Becker, S., Brown, P.J., Carter, B.R., Da Cunha, L.C., Feely, R.A., Hoppema, M., Humphreys, M.P., Ishii, M., Jeansson, E., Jiang, L.-Q., Jones, S.D., Lo Monaco, C., Murata, A., Müller, J.D., Pérez, F.F., Pfeil, B., Schirnick, C., Steinfeldt, R., Suzuki, T., Tilbrook, B., Ulfsbo, A., Velo, A., Woosley, R.J., Key, R.M., 2022. GLODAPv2.2022: the latest version of the global interior ocean biogeochemical data product. Earth Syst. Sci. Data 14, 5543–5572. https://doi.org/10.5194/essd-14-5543-2022

Lefèvre, N., Veleda, D., Hartman, S.E., 2023. Outgassing of CO2 dominates in the coastal upwelling off the northwest African coast. Deep Sea Research Part I: Oceanographic Research Papers 200, 104130. https://doi.org/10.1016/j.dsr.2023.104130

Liu, M., Tanhua, T., 2021. Water masses in the Atlantic Ocean: characteristics and distributions. Ocean Sci. 17, 463–486. https://doi.org/10.5194/os-17-463-2021

Liu, W., Fedorov, A.V., Xie, S.-P., Hu, S., 2020. Climate impacts of a weakened Atlantic Meridional Overturning Circulation in a warming climate. Sci. Adv. 6, eaaz4876. https://doi.org/10.1126/sciadv.aaz4876

Marino, G., Rohling, E.J., Rodríguez-Sanz, L., Grant, K.M., Heslop, D., Roberts, A.P., Stanford, J.D., Yu, J., 2015. Bipolar seesaw control on last interglacial sea level. Nature 522, 197–201. https://doi.org/10.1038/nature14499

McManus, J.F., Francois, R., Gherardi, J.-M., Keigwin, L.D., Brown-Leger, S., 2004. Collapse and rapid resumption of Atlantic meridional circulation linked to deglacial climate changes. Nature 428, 834–837. https://doi.org/10.1038/nature02494

Mollenhauer, G., Grotheer, H., Gentz, T., Bonk, E., Hefter, J., 2021. Standard operation procedures and performance of the MICADAS radiocarbon laboratory at Alfred Wegener Institute (AWI), Germany. Nuclear Instruments and Methods in Physics Research Section B: Beam Interactions with Materials and Atoms 496, 45–51. https://doi.org/10.1016/j.nimb.2021.03.016

Mulitza, S., Prange, M., Stuut, J.-B., Zabel, M., von Dobeneck, T., Itambi, A.C., Nizou, J., Schulz, M., Wefer, G., 2008. Sahel megadroughts triggered by glacial slowdowns of Atlantic meridional overturning. Paleoceanography 23. https://doi.org/10.1029/2008PA001637

Mulitza, S., Bickert, T., Bostock, H.C., Chiessi, C.M., Donner, B., Govin, A., Harada, N., Huang, E., Johnstone, H., Kuhnert, H., Langner, M., Lamy, F., Lembke-Jene, L., Lisiecki, L., Lynch-Stieglitz, J., Max, L., Mohtadi, M., Mollenhauer, G., Muglia, J., Nürnberg, D., Paul, A., Rühlemann, C., Repschläger, J., Saraswat, R., Schmittner, A., Sikes, E.L., Spielhagen, R.F., Tiedemann, R., 2022. World Atlas of late Quaternary

Foraminiferal Oxygen and Carbon Isotope Ratios. Earth Syst. Sci. Data 14, 2553–2611. https://doi.org/10.5194/essd-14-2553-2022

Mulitza, S., Chiessi, C.M., Schefuß, E., Lippold, J., Wichmann, D., Antz, B., Mackensen, A., Paul, A., Prange, M., Rehfeld, K., Werner, M., Bickert, T., Frank, N., Kuhnert, H., Lynch-Stieglitz, J., Portilho-Ramos, R.C., Sawakuchi, A.O., Schulz, M., Schwenk, T., Tiedemann, R., Vahlenkamp, M., Zhang, Y., 2017. Synchronous and proportional deglacial changes in Atlantic meridional overturning and northeast Brazilian precipitation. Paleoceanography 32, 622–633. https://doi.org/10.1002/2017PA003084

Mulitza, S., Zabel, M., 2009. Elemental ratios of sediment core GeoB9508-5. https://doi.org/10.1594/PANGAEA.726769

Murray, J.W., 2006. Ecology and Applications of Benthic Foraminifera, 1st ed. Cambridge University Press. https://doi.org/10.1017/CBO9780511535529

Murray, J.W., 1991. Ecology and palaeoecology of benthic foraminifera. Longman scientific and technical copublished in the United States with John Wiley and sons, Essex New York.

Muschitiello, F., D'Andrea, W.J., Schmittner, A., Heaton, T.J., Balascio, N.L., deRoberts, N., Caffee, M.W., Woodruff, T.E., Welten, K.C., Skinner, L.C., Simon, M.H., Dokken, T.M., 2019. Deep-water circulation changes lead North Atlantic climate during deglaciation. Nat Commun 10, 1272. https://doi.org/10.1038/s41467-019-09237-3

Nürnberg, D., Riff, T., Bahr, A., Karas, C., Meier, K., Lippold, J., 2021. Western boundary current in relation to Atlantic Subtropical Gyre dynamics during abrupt glacial climate fluctuations. Global and Planetary Change 201, 103497. https://doi.org/10.1016/j.gloplacha.2021.103497

Oppo, D.W., Curry, W.B., McManus, J.F., 2015. What do benthic δ13C and δ18O data tell us about Atlantic circulation during Heinrich Stadial 1? Paleoceanography 30, 353–368. https://doi.org/10.1002/2014PA002667

Pelegrí, J.L., Peña-Izquierdo, J., 2015. Eastern boundary currents off North-West Africa, in: Oceanographic and Biological Features in the Canary Current Large Marine Ecosystem, IOC Technical Serie. pp. 81–92.

Poole, R., Tomczak, M., 1999. Optimum multiparameter analysis of the water mass structure in the Atlantic Ocean thermocline. Deep Sea Research Part I: Oceanographic Research Papers 46, 1895–1921. https://doi.org/10.1016/S0967-0637(99)00025-4

Schlitzer, R., 2023. Ocean Data View, odv.awi.de.

Schmidtko, S., Stramma, L., Visbeck, M., 2017. Decline in global oceanic oxygen content during the past five decades. Nature 542, 335–339. https://doi.org/10.1038/nature21399

Stramma, L., Johnson, G.C., Sprintall, J., Mohrholz, V., 2008. Expanding Oxygen-Minimum Zones in the Tropical Oceans 320, 655–658. https://doi.org/10.1126/science.1153847

Stramma, L., Prince, E.D., Schmidtko, S., Luo, J., Hoolihan, J.P., Visbeck, M., Wallace, D.W.R., Brandt, P., Körtzinger, A., 2012. Expansion of oxygen minimum zones may reduce available habitat for tropical pelagic fishes. Nature Clim Change 2, 33–37. https://doi.org/10.1038/nclimate1304

Stramma, L., Schmidtko, S., 2021. Tropical deoxygenation sites revisited to investigate oxygen and nutrient trends. Ocean Sci. 17, 833–847. https://doi.org/10.5194/os-17-833-2021

Talley, L., 2013. Closure of the Global Overturning Circulation Through the Indian, Pacific, and Southern Oceans: Schematics and Transports. oceanog 26, 80–97. https://doi.org/10.5670/oceanog.2013.07

Talley, L.D., 2003. Shallow, Intermediate, and Deep Overturning Components of the Global Heat Budget. J. Phys. Oceanogr. 33, 530–560. https://doi.org/10.1175/1520-0485(2003)033<0530:SIADOC>2.0.CO;2

Völpel, R., Mulitza, S., Paul, A., Lynch-Stieglitz, J., Schulz, M., 2019. Water Mass Versus Sea Level Effects on Benthic Foraminiferal Oxygen Isotope Ratios in the Atlantic Ocean During the LGM. Paleoceanog and Paleoclimatol 34, 98–121. https://doi.org/10.1029/2018PA003359

Weijer, W., Cheng, W., Garuba, O.A., Hu, A., Nadiga, B.T., 2020. CMIP6 Models Predict Significant 21st Century Decline of the Atlantic Meridional Overturning Circulation. Geophysical Research Letters 47, e2019GL086075. https://doi.org/10.1029/2019GL086075

Zhang, R., Sutton, R., Danabasoglu, G., Kwon, Y., Marsh, R., Yeager, S.G., Amrhein, D.E., Little, C.M., 2019. A Review of the Role of the Atlantic Meridional Overturning Circulation in Atlantic Multidecadal Variability and Associated Climate Impacts. Reviews of Geophysics 57, 316–375. https://doi.org/10.1029/2019RG000644

Chapter 1

Altenbach, A.V., Bernhard, J.M., Seckbach, J. (Eds.), 2012. Anoxia: Evidence for Eukaryote Survival and Paleontological Strategies, Cellular Origin, Life in Extreme Habitats and Astrobiology. Springer Netherlands, Dordrecht. https://doi.org/10.1007/978-94-007-1896-8

Bartels-Jónsdóttir, H.B., Knudsen, K.L., Abrantes, F., Lebreiro, S., Eiríksson, J., 2006. Climate variability during the last 2000 years in the Tagus Prodelta, western Iberian Margin: Benthic foraminifera and stable isotopes. Marine Micropaleontology 59, 83–103. https://doi.org/10.1016/j.marmicro.2006.01.002

Corliss, B.H., 1985. foraminifera within deep-sea sediments 314.

Corliss, B.H., Emerson, S., 1990. Distribution of rose bengal stained deep-sea benthic foraminifera from the Nova Scotian continental margin and Gulf of Maine. Deep Sea Research Part A. Oceanographic Research Papers 37, 381–400. https://doi.org/10.1016/0198-0149(90)90015-N

Cushman, J.A., 1931. The Foraminifera of the Atlantic Ocean pt. 8: Rotaliidae, Amphisteginidae, Calcarinidae, Cymbaloporettidae, Globorotaliidae, Anomalinidae, Planorbulinidae, Rupertiidae, and Homotremidae. Bulletin of the United States National Museum i–179. https://doi.org/10.5479/si.03629236.104.7

Cushman, J.A., 1923. The Foraminifera of the Atlantic Ocean pt. 4: Lagenidae. Bulletin of the United States National Museum i–228. https://doi.org/10.5479/si.03629236.104.3

Fontanier, C., 2006. SEASONAL VARIABILITY OF BENTHIC FORAMINIFERAL FAUNAS AT 1000 M DEPTH IN THE BAY OF BISCAY. The Journal of Foraminiferal Research 36, 61–76. https://doi.org/10.2113/36.1.61

Fontanier, C., Jorissen, F.J., Chaillou, G., Anschutz, P., Grémare, A., Griveaud, C., 2005. Live foraminiferal faunas from a 2800m deep lower canyon station from the Bay of Biscay: Faunal response to focusing of refractory organic matter. Deep Sea Research Part I: Oceanographic Research Papers 52, 1189–1227. https://doi.org/10.1016/j.dsr.2005.01.006

Fontanier, C., Jorissen, F.J., Licari, L., Alexandre, A., Anschutz, P., Carbonel, P., 2002. Live benthic foraminiferal faunas from the Bay of Biscay: faunal density, composition, and microhabitats. Deep Sea Research Part I: Oceanographic Research Papers 49, 751–785. https://doi.org/10.1016/S0967-0637(01)00078-4

Geslin, E., Heinz, P., Jorissen, F., Hemleben, Ch., 2004. Migratory responses of deep-sea benthic foraminifera to variable oxygen conditions: laboratory investigations. Marine Micropaleontology 53, 227–243. https://doi.org/10.1016/j.marmicro.2004.05.010

Gooday, A.J., 2001. Benthic Foraminifera, in: Encyclopedia of Ocean Sciences. Elsevier, pp. 274–286. https://doi.org/10.1006/rwos.2001.0217

Gooday, A.J., Levin, L.A., Linke, P., Heeger, T., 1992. The Role of Benthic Foraminifera in Deep-Sea Food Webs and Carbon Cycling, in: Rowe, G.T., Pariente, V. (Eds.), Deep-Sea Food Chains and the Global Carbon Cycle. Springer Netherlands, Dordrecht, pp. 63–91. https://doi.org/10.1007/978-94-011-2452-2_5

Griveaud, C., Jorissen, F., Anschutz, P., n.d. Spatial variability of live benthic foraminiferal faunas on the Portuguese margin.

Haake, F.W., 1980. Benthische Foraminiferen in Oberflächen-Sedimenten und Kernen des Ostatlantiks vor Senegal/Gambia (Westafrika).

Holbourn, A.E.L., Henderson, A.S., 2013. Atlas of benthic foraminifera. Natural History Museum, Chichester, West Sussex ; Hoboken, NJ.

Jansen, J.H.F., De Lange, G.J., van Bennekom, A.J., 1990. (Pale)oceanography and geochemistry of the Angola Basin (South Atlantic Ocean) : cruise report R.V. Tyro 30 September-19 November 11–65.

Jones, R.W., Brady, H.B., 1994. The Challenger foraminifera. Oxford University Press, Oxford ; New York.

Jorissen, F.J., 1999. Benthic foraminiferal microhabitats below the sediment-water interface, in: Modern Foraminifera. Springer Netherlands, Dordrecht, pp. 161–179. https://doi.org/10.1007/0-306-48104-9_10

Jorissen, F.J., De Stigter, H.C., Widmark, J.G.V., 1995. A conceptual model explaining benthic foraminiferal microhabitats. Marine Micropaleontology 26, 3–15. https://doi.org/10.1016/0377-8398(95)00047-X

Jorissen, F.J., Wittling, I., Peypouquet, J.P., Rabouille, C., Relexans, J.C., 1998. Live benthic foraminiferal faunas off Cape Blanc, NW-Africa: Community structure and microhabitats. Deep Sea Research Part I: Oceanographic Research Papers 45, 2157–2188. https://doi.org/10.1016/S0967-0637(98)00056-9

Kaiho, K., 1994. Benthic foraminiferal dissolved-oxygen index and dissolved-oxygen levels in the modern ocean. Geol 22, 719. https://doi.org/10.1130/0091-7613(1994)022<0719:BFDOIA>2.3.CO;2

Koho, K.A., Piña-Ochoa, E., Geslin, E., Risgaard-Petersen, N., 2011. Vertical migration, nitrate uptake and denitrification: survival mechanisms of foraminifers (Globobulimina turgida) under low oxygen conditions: Survival mechanisms of

foraminifers. FEMS Microbiology Ecology 75, 273–283. https://doi.org/10.1111/j.1574-6941.2010.01010.x

Kranner, M., Harzhauser, M., Beer, C., Auer, G., Piller, W.E., 2022. OPEN Calculating dissolved. Scientific Reports.

Lauvset, S.K., Lange, N., Tanhua, T., Bittig, H.C., Olsen, A., Kozyr, A., Alin, S., Álvarez, M., Azetsu-Scott, K., Barbero, L., Becker, S., Brown, P.J., Carter, B.R., Da Cunha, L.C., Feely, R.A., Hoppema, M., Humphreys, M.P., Ishii, M., Jeansson, E., Jiang, L.-Q., Jones, S.D., Lo Monaco, C., Murata, A., Müller, J.D., Pérez, F.F., Pfeil, B., Schirnick, C., Steinfeldt, R., Suzuki, T., Tilbrook, B., Ulfsbo, A., Velo, A., Woosley, R.J., Key, R.M., 2022. GLODAPv2.2022: the latest version of the global interior ocean biogeochemical data product. Earth Syst. Sci. Data 14, 5543–5572. https://doi.org/10.5194/essd-14-5543-2022

Licari, L.N., 2003. COMMUNITIES AND MICROHABITATS OF LIVING BENTHIC FORAMINIFERA FROM THE TROPICAL EAST ATLANTIC: IMPACT OF DIFFERENT PRODUCTIVITY REGIMES. The Journal of Foraminiferal Research 33, 10–31. https://doi.org/10.2113/0330010

Linke, P., Lutze, G.F., 1993. Microhabitat preferences of benthic foraminifera—a static concept or a dynamic adaptation to optimize food acquisition? Marine Micropaleontology 20, 215–234. https://doi.org/10.1016/0377-8398(93)90034-U

Loeblich Jr, A.R., Tappan, H., 2015. Foraminiferal Genera and Their Classification. Springer, New York, NY.

Lutze, G.F., Coulbourn, W.T., n.d. RECENT BENTHIC FORAMINIFERA FROM THE CONTINENTAL MARGIN OF NORTHWEST AFRICA: COMMUNITY STRUCTURE AND DISTRIBUTION.

Mackensen, A., Schmiedl, G., Harloff, J., Giese, M., 1995. Deep-Sea Foraminifera in the South Atlantic Ocean: Ecology and Assemblage Generation. Micropaleontology 41, 342. https://doi.org/10.2307/1485808

Morkhoven, F.P.C.M. van, Berggren, W.A., Edwards, A.S., 1986. Cenozoic cosmopolitan deep-water benthic foraminifera, Bulletin des Centres de Recherches Exploration - Production Elf-Aquitaine Mémoires. Elf Aquitaine, Pau.

Mulitza, S., Bouimetarhan, I., Bruening, M., Freesemann, A., Gussone, N., Filipsson, H.L., Heil, G., Hessler, S., Jaeschke, A., Johnstone, H.J.H., Klann, M., Klein, F., Kuester, K., Maerz, C., McGregor, H., Minning, M., Mueller, H., Ochsenhirt, W.-T., Paul, A., Pokorna, M., Schewe, F., Schulz, M., Steinloechner, J., Stuut, J.-B., Tjallingii, R., von Dobeneck, T., Wiesmaier, S., Zabel, M., Zonneveld, C., 2005. Report and preliminary results of METEOR Cruise M65/1, Dakar - Dakar, 11.06. - 1.07.2005.

Murray, J.W., 2006. Ecology and Applications of Benthic Foraminifera, 1st ed. Cambridge University Press. https://doi.org/10.1017/CBO9780511535529

Murray, J.W., 1991. Ecology and palaeoecology of benthic foraminifera. Longman scientific and technical copublished in the United States with John Wiley and sons, Essex New York.

Schefuß, E., Versteegh, G.J.M., Jansen, J.H.F., Sinninghe Damsté, J.S., 2004. Lipid biomarkers as major source and preservation indicators in SE Atlantic surface sediments. Deep Sea Research Part I: Oceanographic Research Papers 51, 1199–1228. https://doi.org/10.1016/j.dsr.2004.05.002

Sweetman, A.K., Sommer, S., Pfannkuche, O., Witte, U., 2009. RETARDED RESPONSE BY MACROFAUNA-SIZE FORAMINIFERA TO PHYTODETRITUS IN A DEEP NORWEGIAN FJORD. The Journal of Foraminiferal Research 39, 15–22. https://doi.org/10.2113/gsjfr.39.1.15

Tikhonova, A., Merenkova, S., Korsun, S., Matul, A., 2019. Image dataset of common benthic foraminiferal taxa in the North Atlantic seafloor surface sediments (59.5°N transect) between the Labrador sea and Faeroe-Shetland sill. Data in Brief 26, 104554. https://doi.org/10.1016/j.dib.2019.104554

Vaquer-Sunyer, R., Duarte, C.M., 2008. Thresholds of hypoxia for marine biodiversity. Proc. Natl. Acad. Sci. U.S.A. 105, 15452–15457. https://doi.org/10.1073/pnas.0803833105

Vénec-Peyré, M.-T., 2002. Les travaux micropaléontologiques d'Alcide d'Orbigny. Comptes Rendus Palevol 1, 449–459. https://doi.org/10.1016/S1631-0683(02)00053-2

Volk, T., Hoffert, M.I., 2013. Ocean Carbon Pumps: Analysis of Relative Strengths and Efficiencies in Ocean-Driven Atmospheric CO 2 Changes, in: Sundquist, E.T., Broecker, W.S. (Eds.), Geophysical Monograph Series. American Geophysical Union, Washington, D. C., pp. 99–110. https://doi.org/10.1029/GM032p0099

Webb, P.B., Berthelot, S., Oudart, P.L., Valenciennes, 1836. Histoire naturelle des Iles Canaries. Béthune, éditeur, Paris. https://doi.org/10.5962/bhl.title.60795

Chapter 2

Barker, S., Diz, P., Vautravers, M.J., Pike, J., Knorr, G., Hall, I.R., Broecker, W.S., 2009. Interhemispheric Atlantic seesaw response during the last deglaciation. Nature 457, 1097–1102. https://doi.org/10.1038/nature07770

Barker, S., Greaves, M., Elderfield, H., 2003. A study of cleaning procedures used for foraminiferal Mg/Ca paleothermometry: MG/CA PALEOTHERMOMETRY. Geochem. Geophys. Geosyst. 4, n/a-n/a. https://doi.org/10.1029/2003GC000559

Barragán-Montilla, S., Johnstone, H.J.H., Mulitza, S., Pälike, H., 2023a. Bottom water temperatures (raw and processed including confidence intervals) calculated using Mg/Ca ratios of endobenthic Uvigerina spp. from the last 50.000 years from site GeoB9508-5 off NW Africa. https://doi.org/10.1594/PANGAEA.950494

Barragán-Montilla, S., Johnstone, H.J.H., Mulitza, S., Pälike, H., 2023b. Processed stable isotope (carbon and oxygen) data from epibenthic Cibicidoides spp., including confidence intervals from the last 50.000 years from site GeoB9508-5 off NW Africa. https://doi.org/10.1594/PANGAEA.950502

Bereiter, B., Shackleton, S., Baggenstos, D., Kawamura, K., Severinghaus, J., 2018. Mean global ocean temperatures during the last glacial transition. Nature 553, 39–44. https://doi.org/10.1038/nature25152

Blaauw, M., Christen, J.A., 2011. Flexible paleoclimate age-depth models using an autoregressive gamma process. Bayesian Anal. 6, 457–474. https://doi.org/10.1214/ba/1339616472

Boé, J., Hall, A., Qu, X., 2009. Deep ocean heat uptake as a major source of spread in transient climate change simulations. Geophysical Research Letters 36, 2009GL040845. https://doi.org/10.1029/2009GL040845

Böhm, E., Lippold, J., Gutjahr, M., Frank, M., Blaser, P., Antz, B., Fohlmeister, J., Frank, N., Andersen, M.B., Deininger, M., 2015. Strong and deep Atlantic meridional overturning circulation during the last glacial cycle. Nature 517, 73–76. https://doi.org/10.1038/nature14059

Bouimetarhan, I., Groeneveld, J., Dupont, L., Zonneveld, K., 2013. Low- to high-productivity pattern within Heinrich Stadial 1: Inferences from dinoflagellate cyst records off Senegal. Global and Planetary Change 106, 64–76. https://doi.org/10.1016/j.gloplacha.2013.03.007

Brady, E.C., Otto-Bliesner, B.L., 2011. The role of meltwater-induced subsurface ocean warming in regulating the Atlantic meridional overturning in glacial climate simulations. Clim Dyn 37, 1517–1532. https://doi.org/10.1007/s00382-010-0925-9

Broccoli, A.J., Dahl, K.A., Stouffer, R.J., 2006. Response of the ITCZ to Northern Hemisphere cooling. Geophysical Research Letters 33, 2005GL024546. https://doi.org/10.1029/2005GL024546

Buckley, M.W., Marshall, J., 2016. Observations, inferences, and mechanisms of the Atlantic Meridional Overturning Circulation: A review. Reviews of Geophysics 54, 5–63. https://doi.org/10.1002/2015RG000493

Buizert, C., Schmittner, A., 2015. Southern Ocean control of glacial AMOC stability and Dansgaard-Oeschger interstadial duration: SOUTHERN OCEAN CONTROL ON DO DURATION. Paleoceanography 30, 1595–1612. https://doi.org/10.1002/2015PA002795

Butzin, M., Köhler, P., Lohmann, G., 2017. Marine radiocarbon reservoir age simulations for the past 50,000 years. Geophysical Research Letters 44, 8473–8480. https://doi.org/10.1002/2017GL074688

Caesar, L., McCarthy, G.D., Thornalley, D.J.R., Cahill, N., Rahmstorf, S., 2022. Reply to: Atlantic circulation change still uncertain. Nat. Geosci. 15, 168–170. https://doi.org/10.1038/s41561-022-00897-3

Caesar, L., McCarthy, G.D., Thornalley, D.J.R., Cahill, N., Rahmstorf, S., 2021. Current Atlantic Meridional Overturning Circulation weakest in last millennium. Nat. Geosci. 14, 118–120. https://doi.org/10.1038/s41561-021-00699-z

Calvin, K., Dasgupta, D., Krinner, G., Mukherji, A., Thorne, P.W., Trisos, C., Romero, J., Aldunce, P., Barrett, K., Blanco, G., Cheung, W.W.L., Connors, S., Denton, F., Diongue-Niang, A., Dodman, D., Garschagen, M., Geden, O., Hayward, B., Jones, C., Jotzo, F., Krug, T., Lasco, R., Lee, Y.-Y., Masson-Delmotte, V., Meinshausen, M., Mintenbeck, K., Mokssit, A., Otto, F.E.L., Pathak, M., Pirani, A., Poloczanska, E., Pörtner, H.-O., Revi, A., Roberts, D.C., Roy, J., Ruane, A.C., Skea, J., Shukla, P.R., Slade, R., Slangen, A., Sokona, Y., Sörensson, A.A., Tignor, M., Van Vuuren, D., Wei, Y.-M., Winkler, H., Zhai, P., Zommers, Z., Hourcade, J.-C., Johnson, F.X., Pachauri, S., Simpson, N.P., Singh, C., Thomas, A., Totin, E., Arias, P., Bustamante, M., Elgizouli, I., Flato, G., Howden, M., Méndez-Vallejo, C., Pereira, J.J., Pichs-Madruga, R., Rose, S.K., Saheb, Y., Sánchez Rodríguez, R., Ürge-Vorsatz, D., Xiao, C., Yassaa, N., Alegría, A., Armour, K., Bednar-Friedl, B., Blok, K., Cissé, G., Dentener, F., Eriksen, S., Fischer, E., Garner, G., Guivarch, C., Haasnoot, M., Hansen, G., Hauser, M., Hawkins, E., Hermans, T., Kopp, R., Leprince-Ringuet, N., Lewis, J., Ley, D., Ludden, C., Niamir, L., Nicholls, Z., Some, S., Szopa, S., Trewin, B., Van Der Wijst, K.-I., Winter, G., Witting, M., Birt, A., Ha, M., Romero, J., Kim, J., Haites, E.F., Jung, Y., Stavins, R., Birt, A., Ha, M., Orendain, D.J.A., Ignon, L., Park, S., Park, Y., Reisinger, A., Cammaramo, D., Fischlin, A., Fuglestvedt, J.S., Hansen, G., Ludden, C., Masson-Delmotte, V., Matthews, J.B.R., Mintenbeck, K., Pirani, A., Poloczanska, E., Leprince-Ringuet, N., Péan, C., 2023. IPCC, 2023: Climate Change 2023: Synthesis Report. Contribution of Working Groups I, II and III to the Sixth Assessment Report of the Intergovernmental Panel on Climate Change [Core Writing Team, H. Lee and J. Romero (eds.)]. IPCC, Geneva, Switzerland. Intergovernmental

Panel on Climate Change (IPCC). https://doi.org/10.59327/IPCC/AR6-9789291691647

Cummins, P.F., Masson, D., Saenko, O.A., 2016. Vertical heat flux in the ocean: Estimates from observations and from a coupled general circulation model. JGR Oceans 121, 3790–3802. https://doi.org/10.1002/2016JC011647

Denton, G.H., Toucanne, S., Putnam, A.E., Barrell, D.J.A., Russell, J.L., 2022. Heinrich summers. Quaternary Science Reviews 295, 107750. https://doi.org/10.1016/j.quascirev.2022.107750

Dima, M., Nichita, D.R., Lohmann, G., Ionita, M., Voiculescu, M., 2021. Early-onset of Atlantic Meridional Overturning Circulation weakening in response to atmospheric CO2 concentration. npj Clim Atmos Sci 4, 27. https://doi.org/10.1038/s41612-021-00182-x

Dupont, L.M., Schlütz, F., Ewah, C.T., Jennerjahn, T.C., Paul, A., Behling, H., 2010. Two-step vegetation response to enhanced precipitation in Northeast Brazil during Heinrich event 1. Global Change Biology 16, 1647–1660. https://doi.org/10.1111/j.1365-2486.2009.02023.x

Eide, M., Olsen, A., Ninnemann, U.S., Johannessen, T., 2017. A global ocean climatology of preindustrial and modern ocean δ 13 C. Global Biogeochemical Cycles 31, 515–534. https://doi.org/10.1002/2016GB005473

EPICA Community Members, 2006. One-to-one coupling of glacial climate variability in Greenland and Antarctica. Nature 444, 195–198. https://doi.org/10.1038/nature05301

Ezat, M.M., Rasmussen, T.L., Groeneveld, J., 2014. Persistent intermediate water warming during cold stadials in the southeastern Nordic seas during the past 65 k.y. Geology 42, 663–666. https://doi.org/10.1130/G35579.1

Gherardi, J., Labeyrie, L., Mcmanus, J., Francois, R., Skinner, L., Cortijo, E., 2005. Evidence from the Northeastern Atlantic basin for variability in the rate of the meridional overturning circulation through the last deglaciation. Earth and Planetary Science Letters 240, 710–723. https://doi.org/10.1016/j.epsl.2005.09.061

Gherardi, J. -M., Labeyrie, L., Nave, S., Francois, R., McManus, J.F., Cortijo, E., 2009. Glacial-interglacial circulation changes inferred from 231 Pa/ 230 Th sedimentary record in the North Atlantic region. Paleoceanography 24, 2008PA001696. https://doi.org/10.1029/2008PA001696

Greaves, M., Barker, S., Daunt, C., Elderfield, H., 2005. Accuracy, standardization, and interlaboratory calibration standards for foraminiferal Mg/Ca thermometry. Geochem Geophys Geosyst 6, 2004GC000790. https://doi.org/10.1029/2004GC000790

Hasenfratz, A.P., Schiebel, R., Thornalley, D.J.R., Schönfeld, J., Jaccard, S.L., Martínez-García, A., Holbourn, A., Jennings, A.E., Kuhnt, W., Lear, C.H., Marchitto, T.M., Quillmann, U., Rosenthal, Y., Yu, J., Haug, G.H., 2017. Mg/Ca-temperature calibration for the benthic foraminifera Melonis barleeanum and Melonis pompilioides. Geochimica et Cosmochimica Acta 217, 365–383. https://doi.org/10.1016/j.gca.2017.08.038

He, C., Liu, Z., Zhu, J., Zhang, J., Gu, S., Otto-Bliesner, B.L., Brady, E., Zhu, C., Jin, Y., Sun, J., 2020. North Atlantic subsurface temperature response controlled by effective freshwater input in “Heinrich” events. Earth and Planetary Science Letters 539, 116247. https://doi.org/10.1016/j.epsl.2020.116247

Heaton, T.J., Köhler, P., Butzin, M., Bard, E., Reimer, R.W., Austin, W.E., Ramsey, C.B., Grootes, P.M., Hughen, K.A., Kromer, B., Reimer, P.J., Adkins, J.F., Burke, A., Cook, M.S., Olsen, J., Skinner, L.C., 2020. Marine20 - the marine radiocarbon age calibration curve (0 - 55,000 cal BP), simulated data for IntCal20. https://doi.org/10.1594/PANGAEA.914500

Henry, L.G., McManus, J.F., Curry, W.B., Roberts, N.L., Piotrowski, A.M., Keigwin, L.D., 2016. North Atlantic ocean circulation and abrupt climate change during the last glaciation. Science 353, 470–474. https://doi.org/10.1126/science.aaf5529

Howe, J.N.W., Piotrowski, A.M., Noble, T.L., Mulitza, S., Chiessi, C.M., Bayon, G., 2016. North Atlantic Deep Water Production during the Last Glacial Maximum. Nat Commun 7, 11765. https://doi.org/10.1038/ncomms11765

Hu, A., Meehl, G.A., Han, W., Otto-Bliestner, B., Abe-Ouchi, A., Rosenbloom, N., 2015. Effects of the Bering Strait closure on AMOC and global climate under different background climates. Progress in Oceanography 132, 174–196. https://doi.org/10.1016/j.pocean.2014.02.004

Intergovernmental Panel On Climate Change (Ipcc), 2023. Climate Change 2022 – Impacts, Adaptation and Vulnerability: Working Group II Contribution to the Sixth Assessment Report of the Intergovernmental Panel on Climate Change, 1st ed. Cambridge University Press. https://doi.org/10.1017/9781009325844

Intergovernmental Panel On Climate Change (Ipcc), 2022. The Ocean and Cryosphere in a Changing Climate: Special Report of the Intergovernmental Panel on Climate Change, 1st ed. Cambridge University Press. https://doi.org/10.1017/9781009157964

IPCC, 2013: Climate Change 2013: The Physical Science Basis. Contribution of Working Group I to the Fifth Assessment Report of the Intergovernmental Panel on Climate Change, Stocker, T.F., D. Qin, G.-K. Plattner, M. Tignor, S.K. Allen, J. Boschung, A. Nauels, Y. Xia, V. Bex and P.M. Midgley (eds.). ed, 2013. . Cambridge University Press, Cambridge, United Kingdom and New York.

Jackson, L.C., Biastoch, A., Buckley, M.W., Desbruyères, D.G., Frajka-Williams, E., Moat, B., Robson, J., 2022. The evolution of the North Atlantic Meridional Overturning Circulation since 1980. Nat Rev Earth Environ 3, 241–254. https://doi.org/10.1038/s43017-022-00263-2

Johnstone, H.J.H., Lee, W., Schulz, M., 2016. Effect of preservation state of planktonic foraminifera tests on the decrease in Mg/Ca due to reductive cleaning and on sample loss during cleaning. Chemical Geology 420, 23–36. https://doi.org/10.1016/j.chemgeo.2015.10.045

Kilbourne, K.H., Wanamaker, A.D., Moffa-Sanchez, P., Reynolds, D.J., Amrhein, D.E., Butler, P.G., Gebbie, G., Goes, M., Jansen, M.F., Little, C.M., Mette, M., Moreno-Chamarro, E., Ortega, P., Otto-Bliesner, B.L., Rossby, T., Scourse, J., Whitney, N.M., 2022. Atlantic circulation change still uncertain. Nat. Geosci. 15, 165–167. https://doi.org/10.1038/s41561-022-00896-4

Knutti, R., Tomassini, L., 2008. Constraints on the transient climate response from observed global temperature and ocean heat uptake. Geophysical Research Letters 35, 2007GL032904. https://doi.org/10.1029/2007GL032904

Köhler, P., Nehrbass-Ahles, C., Schmitt, J., Stocker, T.F., Fischer, H., 2017 A 156 kyr smoothed history of the atmospheric greenhouse gases CO2, CH4, and N2O and their radiative forcing. Earth Syst. Sci. Data 9, 363–387. https://doi.org/10.5194/essd-9-363-2017

Kostov, Y., Armour, K.C., Marshall, J., 2014. Impact of the Atlantic meridional overturning circulation on ocean heat storage and transient climate change. Geophys. Res. Lett. 41, 2108–2116. https://doi.org/10.1002/2013GL058998

Kuhlbrodt, T., Gregory, J.M., 2012. Ocean heat uptake and its consequences for the magnitude of sea level rise and climate change. Geophysical Research Letters 39, 2012GL052952. https://doi.org/10.1029/2012GL052952

Latif, M., Sun, J., Visbeck, M., Hadi Bordbar, M., 2022. Natural variability has dominated Atlantic Meridional Overturning Circulation since 1900. Nat. Clim. Chang. 12, 455–460. https://doi.org/10.1038/s41558-022-01342-4

LeGrande, A.N., Schmidt, G.A., 2006. Global gridded data set of the oxygen isotopic composition in seawater. Geophysical Research Letters 33, 2006GL026011. https://doi.org/10.1029/2006GL026011

Lessa, D., Morard, R., Jonkers, L., Venancio, I.M., Reuter, R., Baumeister, A., Albuquerque, A.L., Kucera, M., 2020. Distribution of planktonic foraminifera in the subtropical South Atlantic: depth hierarchy of controlling factors. Biogeosciences 17, 4313–4342. https://doi.org/10.5194/bg-17-4313-2020

Levitus, S., Antonov, J., Boyer, T., 2005. Warming of the world ocean, 1955–2003. Geophysical Research Letters 32, 2004GL021592. https://doi.org/10.1029/2004GL021592

Levitus, S., Antonov, J.I., Boyer, T.P., Stephens, C., 2000. Warming of the World Ocean. Science 287, 2225–2229. https://doi.org/10.1126/science.287.5461.2225

Li, S., Liu, W., 2022. Deciphering the Migration of the Intertropical Convergence Zone During the Last Deglaciation. Geophysical Research Letters 49, e2022GL098806. https://doi.org/10.1029/2022GL098806

Lippold, J., Mulitza, S., Mollenhauer, G., Weyer, S., Heslop, D., Christl, M., 2012. Boundary scavenging at the East Atlantic margin does not negate use of 231Pa/230Th to trace Atlantic overturning. Earth and Planetary Science Letters 333–334, 317–331. https://doi.org/10.1016/j.epsl.2012.04.005

Liu, W., Fedorov, A.V., Xie, S.-P., Hu, S., 2020. Climate impacts of a weakened Atlantic Meridional Overturning Circulation in a warming climate. Sci. Adv. 6, eaaz4876. https://doi.org/10.1126/sciadv.aaz4876

Lo Giudice Cappelli, E., Holbourn, A., Kuhnt, W., Regenberg, M., 2016. Changes in Timor Strait hydrology and thermocline structure during the past 130 ka. Palaeogeography, Palaeoclimatology, Palaeoecology 462, 112–124. https://doi.org/10.1016/j.palaeo.2016.09.010

Lobelle, D., Beaulieu, C., Livina, V., Sévellec, F., Frajka-Williams, E., 2020. Detectability of an AMOC Decline in Current and Projected Climate Changes. Geophysical Research Letters 47, e2020GL089974. https://doi.org/10.1029/2020GL089974

Locarnini, R.A., Mishonov, A.V., Antonov, J.I., Boyer, T.P., García, H.E., Baranova, O.K., Zweng, M.M., Johnson, D.. R., 2010. World Ocean Atlas 2009, Volume 1: Temperature, edited by: Levitus, S., NOAA Atlas NESDIS, 68, 184 PP.

Marchitto, T.M., Curry, W.B., Lynch-Stieglitz, J., Bryan, S.P., Cobb, K.M., Lund, D.C., 2014. Improved oxygen isotope temperature calibrations for cosmopolitan benthic foraminifera. Geochimica et Cosmochimica Acta 130, 1–11. https://doi.org/10.1016/j.gca.2013.12.034

Marino, G., Rohling, E.J., Rodríguez-Sanz, L., Grant, K.M., Heslop, D., Roberts, A.P., Stanford, J.D., Yu, J., 2015. Bipolar seesaw control on last interglacial sea level. Nature 522, 197–201. https://doi.org/10.1038/nature14499

Marshall, D.P., Zanna, L., 2014. A Conceptual Model of Ocean Heat Uptake under Climate Change. Journal of Climate 27, 8444–8465. https://doi.org/10.1175/JCLI-D-13-00344.1

Max, L., Nürnberg, D., Chiessi, C.M., Lenz, M.M., Mulitza, S., 2022. Subsurface ocean warming preceded Heinrich Events. Nat Commun 13, 4217. https://doi.org/10.1038/s41467-022-31754-x

McManus, J.F., Francois, R., Gherardi, J.-M., Keigwin, L.D., Brown-Leger, S., 2004. Collapse and rapid resumption of Atlantic meridional circulation linked to deglacial climate changes. Nature 428, 834–837. https://doi.org/10.1038/nature02494

Meckler, A.N., Sigman, D.M., Gibson, K.A., François, R., Martínez-García, A., Jaccard, S.L., Röhl, U., Peterson, L.C., Tiedemann, R., Haug, G.H., 2013. Deglacial pulses of deep-ocean silicate into the subtropical North Atlantic Ocean. Nature 495, 495–498. https://doi.org/10.1038/nature12006

Ménot, G., Bard, E., Rostek, F., Weijers, J.W.H., Hopmans, E.C., Schouten, S., Damsté, J.S.S., 2006. Early Reactivation of European Rivers During the Last Deglaciation. Science 313, 1623–1625. https://doi.org/10.1126/science.1130511

Mulitza, S., Bouimetarhan, I., Bruening, M., Freesemann, A., Gussone, N., Filipsson, H.L., Heil, G., Hessler, S., Jaeschke, A., Johnstone, H.J.H., Klann, M., Klein, F., Kuester, K., Maerz, C., McGregor, H., Minning, M., Mueller, H., Ochsenhirt, W.-T., Paul, A., Pokorna, M., Schewe, F., Schulz, M., Steinloechner, J., Stuut, J.-B., Tjallingii, R., von Dobeneck, T., Wiesmaier, S., Zabel, M., Zonneveld, C., 2005. Report and preliminary results of METEOR Cruise M65/1, Dakar - Dakar, 11.06. - 1.07.2005.

Mulitza, S., Chiessi, C.M., Schefuß, E., Lippold, J., Wichmann, D., Antz, B., Mackensen, A., Paul, A., Prange, M., Rehfeld, K., Werner, M., Bickert, T., Frank, N., Kuhnert, H., Lynch-Stieglitz, J., Portilho-Ramos, R.C., Sawakuchi, A.O., Schulz, M., Schwenk, T., Tiedemann, R., Vahlenkamp, M., Zhang, Y., 2017. Synchronous and proportional deglacial changes in Atlantic meridional overturning and northeast Brazilian precipitation. Paleoceanography 32, 622–633. https://doi.org/10.1002/2017PA003084

Mulitza, S., Prange, M., Stuut, J.-B., Zabel, M., von Dobeneck, T., Itambi, A.C., Nizou, J., Schulz, M., Wefer, G., 2008. Sahel megadroughts triggered by glacial slowdowns of Atlantic meridional overturning. Paleoceanography 23. https://doi.org/10.1029/2008PA001637

Muschitiello, F., D'Andrea, W.J., Schmittner, A., Heaton, T.J., Balascio, N.L., deRoberts, N., Caffee, M.W., Woodruff, T.E., Welten, K.C., Skinner, L.C., Simon, M.H., Dokken, T.M., 2019. Deep-water circulation changes lead North Atlantic climate during deglaciation. Nat Commun 10, 1272. https://doi.org/10.1038/s41467-019-09237-3

Ng, H.C., Robinson, L.F., McManus, J.F., Mohamed, K.J., Jacobel, A.W., Ivanovic, R.F., Gregoire, L.J., Chen, T., 2018. Coherent deglacial changes in western Atlantic Ocean circulation. Nat Commun 9, 2947. https://doi.org/10.1038/s41467-018-05312-3

Niedermeyer, E.M., Prange, M., Mulitza, S., Mollenhauer, G., Schefuß, E., Schulz, M., 2009. Extratropical forcing of Sahel aridity during Heinrich stadials. Geophysical Research Letters 36, 2009GL039687. https://doi.org/10.1029/2009GL039687

Oppo, D.W., Curry, W.B., McManus, J.F., 2015. What do benthic δ 13 C and δ 18 O data tell us about Atlantic circulation during Heinrich Stadial 1? Paleoceanography 30, 353–368. https://doi.org/10.1002/2014PA002667

Osman, M.B., Tierney, J.E., Zhu, J., Tardif, R., Hakim, G.J., King, J., Poulsen, C.J., 2021. Globally resolved surface temperatures since the Last Glacial Maximum. Nature 599, 239–244. https://doi.org/10.1038/s41586-021-03984-4

Poggemann, D. -W., Nürnberg, D., Hathorne, E.C., Frank, M., Rath, W., Reißig, S., Bahr, A., 2018. Deglacial Heat Uptake by the Southern Ocean and Rapid Northward Redistribution Via Antarctic Intermediate Water. Paleoceanog and Paleoclimatol 33, 1292–1305. https://doi.org/10.1029/2017PA003284

Rahmstorf, S., Box, J.E., Feulner, G., Mann, M.E., Robinson, A., Rutherford, S., Schaffernicht, E.J., 2015. Exceptional twentieth-century slowdown in Atlantic

Ocean overturning circulation. Nature Clim Change 5, 475–480. https://doi.org/10.1038/nclimate2554

Rebotim, A., Voelker, A.H.L., Jonkers, L., Waniek, J.J., Meggers, H., Schiebel, R., Fraile, I., Schulz, M., Kucera, M., 2017. Factors controlling the depth habitat of planktonic foraminifera in the subtropical eastern North Atlantic. Biogeosciences 14, 827–859. https://doi.org/10.5194/bg-14-827-2017

Reimer, P.J., Austin, W.E.N., Bard, E., Bayliss, A., Blackwell, P.G., Bronk Ramsey, C., Butzin, M., Cheng, H., Edwards, R.L., Friedrich, M., Grootes, P.M., Guilderson, T.P., Hajdas, I., Heaton, T.J., Hogg, A.G., Hughen, K.A., Kromer, B., Manning, S.W., Muscheler, R., Palmer, J.G., Pearson, C., Van Der Plicht, J., Reimer, R.W., Richards, D.A., Scott, E.M., Southon, J.R., Turney, C.S.M., Wacker, L., Adolphi, F., Büntgen, U., Capano, M., Fahrni, S.M., Fogtmann-Schulz, A., Friedrich, R., Köhler, P., Kudsk, S., Miyake, F., Olsen, J., Reinig, F., Sakamoto, M., Sookdeo, A., Talamo, S., 2020. The IntCal20 Northern Hemisphere Radiocarbon Age Calibration Curve (0–55 cal kBP). Radiocarbon 62, 725–757. https://doi.org/10.1017/RDC.2020.41

Roberts, J., Gottschalk, J., Skinner, L.C., Peck, V.L., Kender, S., Elderfield, H., Waelbroeck, C., Vázquez Riveiros, N., Hodell, D.A., 2016. Evolution of South Atlantic density and chemical stratification across the last deglaciation. Proc. Natl. Acad. Sci. U.S.A. 113, 514–519. https://doi.org/10.1073/pnas.1511252113

Robson, J., Sutton, R.T., Archibald, A., Cooper, F., Christensen, M., Gray, L.J., Holliday, N.P., Macintosh, C., McMillan, M., Moat, B., Russo, M., Tilling, R., Carslaw, K., Desbruyères, D., Embury, O., Feltham, D.L., Grosvenor, D.P., Josey, S., King, B., Lewis, A., McCarthy, G.D., Merchant, C., New, A.L., O'Reilly, C.H., Osprey, S.M., Read, K., Scaife, A., Shepherd, A., Sinha, B., Smeed, D., Smith, D., Ridout, A., Woollings, T., Yang, M., 2018. Recent multivariate changes in the North Atlantic climate system, with a focus on 2005–2016. Intl Journal of Climatology 38, 5050–5076. https://doi.org/10.1002/joc.5815

Rühlemann, C., Mulitza, S., Lohmann, G., Paul, A., Prange, M., Wefer, G., 2004. Intermediate depth warming in the tropical Atlantic related to weakened thermohaline circulation: Combining paleoclimate data and modeling results for the

last deglaciation. Paleoceanography 19, 2003PA000948. https://doi.org/10.1029/2003PA000948

Rühlemann, C., Mulitza, S., Müller, P.J., Wefer, G., Zahn, R., 1999. Warming of the tropical Atlantic Ocean and slowdown of thermohaline circulation during the last deglaciation. Nature 402, 511–514. https://doi.org/10.1038/990069

Schleussner, C.-F., Levermann, A., Meinshausen, M., 2014. Probabilistic projections of the Atlantic overturning. Climatic Change 127, 579–586. https://doi.org/10.1007/s10584-014-1265-2

Shackleton, N.J., 1994. Attainment of isotopic equilibrium between ocean water and the benthonic foraminiferal genus Uvigerina: Isotopic changes in the ocean during the last glacial. Centre National de la Recherche Scientifique Colloques Internationaux 219, 203–209.

Stirpe, C.R., Allen, K.A., Sikes, E.L., Zhou, X., Rosenthal, Y., Cruz-Uribe, A.M., Brooks, H.L., 2021. The Mg/Ca proxy for temperature: A Uvigerina core-top study in the Southwest Pacific. Geochimica et Cosmochimica Acta 309, 299–312. https://doi.org/10.1016/j.gca.2021.06.015

Streeter, S.S., Shackleton, N.J., 1979. Paleocirculation of the Deep North Atlantic: 150,000-Year Record of Benthic Foraminifera and Oxygen-18. Science 203, 168–171. https://doi.org/10.1126/science.203.4376.168

Talley, L., 2013. Closure of the Global Overturning Circulation Through the Indian, Pacific, and Southern Oceans: Schematics and Transports. oceanog 26, 80–97. https://doi.org/10.5670/oceanog.2013.07

Talley, L.D., Reid, J.L., Robbins, P.E., 2003. Data-Based Meridional Overturning Streamfunctions for the Global Ocean. J. Climate 16, 3213–3226. https://doi.org/10.1175/1520-0442(2003)016<3213:DMOSFT>2.0.CO;2

Toucanne, S., Soulet, G., Freslon, N., Silva Jacinto, R., Dennielou, B., Zaragosi, S., Eynaud, F., Bourillet, J.-F., Bayon, G., 2015. Millennial-scale fluctuations of the European Ice Sheet at the end of the last glacial, and their potential impact on

global climate. Quaternary Science Reviews 123, 113–133. https://doi.org/10.1016/j.quascirev.2015.06.010

Völpel, R., Mulitza, S., Paul, A., Lynch-Stieglitz, J., Schulz, M., 2019. Water Mass Versus Sea Level Effects on Benthic Foraminiferal Oxygen Isotope Ratios in the Atlantic Ocean During the LGM. Paleoceanog and Paleoclimatol 34, 98–121. https://doi.org/10.1029/2018PA003359

Waelbroeck, C., Duplessy, J.-C., Michel, E., Labeyrie, L., Paillard, D., Duprat, J., 2001. The timing of the last deglaciation in North Atlantic climate records. Nature 412, 724–727. https://doi.org/10.1038/35089060

Weijer, W., Cheng, W., Garuba, O.A., Hu, A., Nadiga, B.T., 2020. CMIP6 Models Predict Significant 21st Century Decline of the Atlantic Meridional Overturning Circulation. Geophysical Research Letters 47, e2019GL086075. https://doi.org/10.1029/2019GL086075

Weldeab, S., Arce, A., Kasten, S., 2016. Mg/Ca- Δ CO 3 pore water 2 − – temperature calibration for Globobulimina spp.: A sensitive paleothermometer for deep-sea temperature reconstruction. Earth and Planetary Science Letters 438, 95–102. https://doi.org/10.1016/j.epsl.2016.01.009

Yu, J., Elderfield, H., 2008. Mg/Ca in the benthic foraminifera Cibicidoides wuellerstorfi and Cibicidoides mundulus: Temperature versus carbonate ion saturation. Earth and Planetary Science Letters 276, 129–139. https://doi.org/10.1016/j.epsl.2008.09.015

Yu, J., Elderfield, H., Jin, Z., Tomascak, P., Rohling, E.J., 2014. Controls on Sr/Ca in benthic foraminifera and implications for seawater Sr/Ca during the late Pleistocene. Quaternary Science Reviews 98, 1–6. https://doi.org/10.1016/j.quascirev.2014.05.018

Zahn, R., Winn, K., Sarnthein, M., 1986. Benthic foraminiferal δ13C and accumulation rates of organic carbon: Uvigerina Peregrina group and Cibicidoides Wuellerstorfi. Paleoceanography 1, 27–42. https://doi.org/10.1029/PA001i001p00027

Zarriess, M., Johnstone, H., Prange, M., Steph, S., Groeneveld, J., Mulitza, S., Mackensen, A., 2011. Bipolar seesaw in the northeastern tropical Atlantic during Heinrich stadials: BIPOLAR SEESAW IN THE TROPICAL ATLANTIC. Geophys. Res. Lett. 38, n/a-n/a. https://doi.org/10.1029/2010GL046070

Zhang, J., Liu, Z., Brady, E.C., Oppo, D.W., Clark, P.U., Jahn, A., Marcott, S.A., Lindsay, K., 2017. Asynchronous warming and δ 18 O evolution of deep Atlantic water masses during the last deglaciation. Proc. Natl. Acad. Sci. U.S.A. 114, 11075–11080. https://doi.org/10.1073/pnas.1704512114

Zhang, R., Sutton, R., Danabasoglu, G., Kwon, Y., Marsh, R., Yeager, S.G., Amrhein, D.E., Little, C.M., 2019. A Review of the Role of the Atlantic Meridional Overturning Circulation in Atlantic Multidecadal Variability and Associated Climate Impacts. Reviews of Geophysics 57, 316–375. https://doi.org/10.1029/2019RG000644

Chapter 3

Altenbach, A. V., Bernhard, J. M., and Seckbach, J. (Eds.): Anoxia: Evidence for Eukaryote Survival and Paleontological Strategies, Springer Netherlands, Dordrecht, https://doi.org/10.1007/978-94-007-1896-8, 2012.

Bard, E., Rostek, F., Turon, J.-L., and Gendreau, S.: Hydrological Impact of Heinrich Events in the Subtropical Northeast Atlantic, Science, 289, 1321–1324, https://doi.org/10.1126/science.289.5483.1321, 2000.

Bernhard, J. M. and Sen Gupta, B. K.: Foraminifera of oxygen-depleted environments, in: Modern Foraminifera, Springer, Dordrecht, 201–2016, 1999.

Blaauw, M. and Christen, J. A.: Flexible paleoclimate age-depth models using an autoregressive gamma process, Bayesian Anal., 6, 457–474, https://doi.org/10.1214/ba/1339616472, 2011.

Böhm, E., Lippold, J., Gutjahr, M., Frank, M., Blaser, P., Antz, B., Fohlmeister, J., Frank, N., Andersen, M. B., and Deininger, M.: Strong and deep Atlantic meridional overturning circulation during the last glacial cycle, Nature, 517, 73–76, https://doi.org/10.1038/nature14059, 2015.

Boyer, T. P., García, H. E., Locarnini, R. A., Zweng, M. M., Alexey, V., Reagan, J. R., Weathers, K. A., Baranova, O. K., Paver, C. R., Seidov, Dan, and Smolyar, I. V.: World Ocean Atlas 2018. [Annual Data, 1.00 Degree all years]., 2018.

Bradtmiller, L. I., McGee, D., Awalt, M., Evers, J., Yerxa, H., Kinsley, C. W., and deMenocal, P. B.: Changes in biological productivity along the northwest African margin over the past 20,000 years: AFRICAN MARGIN PALEOPRODUCTIVITY, Paleoceanography, 31, 185–202, https://doi.org/10.1002/2015PA002862, 2016.

Brandt, P., Hormann, V., Körtzinger, A., Visbeck, M., Krahmann, G., Stramma, L., Lumpkin, R., and Schmid, C.: Changes in the Ventilation of the Oxygen Minimum Zone of the Tropical North Atlantic, Journal of Physical Oceanography, 40, 1784–1801, https://doi.org/10.1175/2010JPO4301.1, 2010.

Brandt, P., Bange, H. W., Banyte, D., Dengler, M., Didwischus, S.-H., Fischer, T., Greatbatch, R. J., Hahn, J., Kanzow, T., Karstensen, J., Körtzinger, A., Krahmann, G., Schmidtko, S., Stramma, L., Tanhua, T., and Visbeck, M.: On the role of circulation and mixing in the ventilation of oxygen minimum zones with a focus on the eastern tropical North Atlantic, Biogeosciences, 12, 489–512, https://doi.org/10.5194/bg-12-489-2015, 2015.

Broecker, W. S. and Maier-Reimer, E.: The influence of air and sea exchange on the carbon isotope distribution in the sea, Global Biogeochemical Cycles, 6, 315–320, https://doi.org/10.1029/92GB01672, 1992.

Bruno, J. F., Bates, A. E., Cacciapaglia, C., Pike, E. P., Amstrup, S. C., Van Hooidonk, R., Henson, S. A., and Aronson, R. B.: Climate change threatens the world's marine protected areas, Nature Clim Change, 8, 499–503, https://doi.org/10.1038/s41558-018-0149-2, 2018.

Caesar, L., Rahmstorf, S., Robinson, A., Feulner, G., and Saba, V.: Observed fingerprint of a weakening Atlantic Ocean overturning circulation, Nature, 556, 191–196, https://doi.org/10.1038/s41586-018-0006-5, 2018.

Calvin, K., Dasgupta, D., Krinner, G., Mukherji, A., Thorne, P. W., Trisos, C., Romero, J., Aldunce, P., Barrett, K., Blanco, G., Cheung, W. W. L., Connors, S.,

Denton, F., Diongue-Niang, A., Dodman, D., Garschagen, M., Geden, O., Hayward, B., Jones, C., Jotzo, F., Krug, T., Lasco, R., Lee, Y.-Y., Masson-Delmotte, V., Meinshausen, M., Mintenbeck, K., Mokssit, A., Otto, F. E. L., Pathak, M., Pirani, A., Poloczanska, E., Pörtner, H.-O., Revi, A., Roberts, D. C., Roy, J., Ruane, A. C., Skea, J., Shukla, P. R., Slade, R., Slangen, A., Sokona, Y., Sörensson, A. A., Tignor, M., Van Vuuren, D., Wei, Y.-M., Winkler, H., Zhai, P., Zommers, Z., Hourcade, J.-C., Johnson, F. X., Pachauri, S., Simpson, N. P., Singh, C., Thomas, A., Totin, E., Arias, P., Bustamante, M., Elgizouli, I., Flato, G., Howden, M., Méndez-Vallejo, C., Pereira, J. J., Pichs-Madruga, R., Rose, S. K., Saheb, Y., Sánchez Rodríguez, R., Ürge-Vorsatz, D., Xiao, C., Yassaa, N., Alegría, A., Armour, K., Bednar-Friedl, B., Blok, K., Cissé, G., Dentener, F., Eriksen, S., Fischer, E., Garner, G., Guivarch, C., Haasnoot, M., Hansen, G., Hauser, M., Hawkins, E., Hermans, T., Kopp, R., Leprince-Ringuet, N., Lewis, J., Ley, D., Ludden, C., Niamir, L., Nicholls, Z., Some, S., Szopa, S., Trewin, B., Van Der Wijst, K.-I., Winter, G., Witting, M., Birt, A., Ha, M., et al.: IPCC, 2023: Climate Change 2023: Synthesis Report. Contribution of Working Groups I, II and III to the Sixth Assessment Report of the Intergovernmental Panel on Climate Change [Core Writing Team, H. Lee and J. Romero (eds.)]. IPCC, Geneva, Switzerland., Intergovernmental Panel on Climate Change (IPCC), https://doi.org/10.59327/IPCC/AR6-9789291691647, 2023.

Erdem, Z., Schönfeld, J., Rathburn, A. E., Pérez, M.-E., Cardich, J., and Glock, N.: Bottom-water deoxygenation at the Peruvian margin during the last deglaciation recorded by benthic foraminifera, Biogeosciences, 17, 3165–3182, https://doi.org/10.5194/bg-17-3165-2020, 2020.

García, H. E., Weathers, K. A., Paver, C. R., Smolyar, I. V., Boyer, T. P., Locarnini, R. A., Zweng, M. M., Mishonov, A. V., Baranova, O. K., Seidov, Dan, and Reagan, J. R.: World Ocean Atlas 2018, Volume 3: Dissolved Oxygen, Apparent Oxygen Utilization, and Oxygen Saturation. A. Mishonov Technical Ed., 2019.

Gherardi, J., Labeyrie, L., Mcmanus, J., Francois, R., Skinner, L., and Cortijo, E.: Evidence from the Northeastern Atlantic basin for variability in the rate of the meridional overturning circulation through the last deglaciation, Earth and Planetary Science Letters, 240, 710–723, https://doi.org/10.1016/j.epsl.2005.09.061, 2005.

Gilbert, D.: Oceans lose oxygen, Nature, 542, 303–304, https://doi.org/10.1038/542303a, 2017.

Gilly, W. F., Beman, J. M., Litvin, S. Y., and Robison, B. H.: Oceanographic and Biological Effects of Shoaling of the Oxygen Minimum Zone, Annu. Rev. Mar. Sci., 5, 393–420, https://doi.org/10.1146/annurev-marine-120710-100849, 2013.

Gooday, A. J., Levin, L. A., Linke, P., and Heeger, T.: The Role of Benthic Foraminifera in Deep-Sea Food Webs and Carbon Cycling, in: Deep-Sea Food Chains and the Global Carbon Cycle, edited by: Rowe, G. T. and Pariente, V., Springer Netherlands, Dordrecht, 63–91, https://doi.org/10.1007/978-94-011-2452-2_5, 1992.

Hanz, U., Wienberg, C., Hebbeln, D., Duineveld, G., Lavaleye, M., Juva, K., Dullo, W.-C., Freiwald, A., Tamborrino, L., Reichart, G.-J., Flögel, S., and Mienis, F.: Environmental factors influencing benthic communities in the oxygen minimum zones on the Angolan and Namibian margins, Biogeosciences, 16, 4337–4356, https://doi.org/10.5194/bg-16-4337-2019, 2019.

Heaton, T. J., Köhler, P., Butzin, M., Bard, E., Reimer, R. W., Austin, W. E. N., Bronk Ramsey, C., Grootes, P. M., Hughen, K. A., Kromer, B., Reimer, P. J., Adkins, J., Burke, A., Cook, M. S., Olsen, J., and Skinner, L. C.: Marine20—The Marine Radiocarbon Age Calibration Curve (0–55,000 cal BP), Radiocarbon, 62, 779–820, https://doi.org/10.1017/RDC.2020.68, 2020.

Hodell, D. A., Nicholl, J. A., Bontognali, T. R. R., Danino, S., Dorador, J., Dowdeswell, J. A., Einsle, J., Kuhlmann, H., Martrat, B., Mleneck-Vautravers, M. J., Rodríguez-Tovar, F. J., and Röhl, U.: Anatomy of Heinrich Layer 1 and its role in the last deglaciation: HEINRICH EVENT 1, Paleoceanography, 32, 284–303, https://doi.org/10.1002/2016PA003028, 2017.

Holbourn, A. E. L. and Henderson, A. S.: Atlas of benthic foraminifera, Natural History Museum, Chichester, West Sussex ; Hoboken, NJ, 2013.

Huang, E., Mulitza, S., Paul, A., Groeneveld, J., Steinke, S., and Schulz, M.: Response of eastern tropical Atlantic central waters to Atlantic meridional overturning circulation changes during the Last Glacial Maximum and Heinrich Stadial 1,

Paleoceanography, 27, 2012PA002294, https://doi.org/10.1029/2012PA002294, 2012.

Huang, J., Wan, S., Li, A., and Li, T.: Two-phase structure of tropical hydroclimate during Heinrich Stadial 1 and its global implications, Quaternary Science Reviews, 222, 105900, https://doi.org/10.1016/j.quascirev.2019.105900, 2019.

Jones, R. W. and Brady, H. B.: The Challenger foraminifera, Oxford University Press, Oxford ; New York, 149 pp., 1994.

Jorissen, F. J., De Stigter, H. C., and Widmark, J. G. V.: A conceptual model explaining benthic foraminiferal microhabitats, Marine Micropaleontology, 26, 3–15, https://doi.org/10.1016/0377-8398(95)00047-X, 1995.

Kaiho, K.: Benthic foraminiferal dissolved-oxygen index and dissolved-oxygen levels in the modern ocean, Geol, 22, 719, https://doi.org/10.1130/0091-7613(1994)022<0719:BFDOIA>2.3.CO;2, 1994.

Karstensen, J., Stramma, L., and Visbeck, M.: Oxygen minimum zones in the eastern tropical Atlantic and Pacific oceans, Progress in Oceanography, 77, 331–350, https://doi.org/10.1016/j.pocean.2007.05.009, 2008.

Keffer, T.: The Ventilation of the World's Oceans: Maps of the Potential vorticity Field, J. Phys. Oceanogr., 15, 509–523, https://doi.org/10.1175/1520-0485(1985)015<0509:TVOTWO>2.0.CO;2, 1985.

Key, R. M., Olsen, J., van Heuven, S., Lauvset, S. K., Velo, A., Lin, X., Schirnick, C., Kozyr, A., Tanhua, T., Hoppema, M., Jutterström, S., Steinfeldt, R., Jeansson, E., Ishii, M., Perez, F. F., and Suzuki, T.: Global Ocean Data Analysis Project, Version 2 (GLODAPv2), https://doi.org/10.3334/CDIAC/OTG. NDP093_GLODAPv2, 2015.

Kranner, M., Harzhauser, M., Beer, C., Auer, G., and Piller, W. E.: OPEN Calculating dissolved, Scientific Reports, 2022.

Kurian, S., Kessarkar, P. M., Purnachandra Rao, V., Reshma, K., Sarkar, A., Pattan, J. N., and Naqvi, S. W. A.: Controls on organic matter distribution in oxygen

minimum zone sediments from the continental slope off western India, Journal of Marine Systems, 207, 103118, https://doi.org/10.1016/j.jmarsys.2018.09.003, 2020.

Lauvset, S. K., Key, R. M., Olsen, A., van Heuven, S., Velo, A., Lin, X., Schirnick, C., Kozyr, A., Tanhua, T., Hoppema, M., Jutterström, S., Steinfeldt, R., Jeansson, E., Ishii, M., Perez, F. F., Suzuki, T., and Watelet, S.: A new global interior ocean mapped climatology: the 1◦ × 1◦ GLODAP version 2, 2016.

Liu, M. and Tanhua, T.: Water masses in the Atlantic Ocean: characteristics and distributions, Ocean Sci., 17, 463–486, https://doi.org/10.5194/os-17-463-2021, 2021.

Liu, W., Fedorov, A. V., Xie, S.-P., and Hu, S.: Climate impacts of a weakened Atlantic Meridional Overturning Circulation in a warming climate, Sci. Adv., 6, eaaz4876, https://doi.org/10.1126/sciadv.aaz4876, 2020.

Loeblich Jr, A. R. and Tappan, H.: Foraminiferal Genera and Their Classification, Springer, New York, NY, 2015.

McCartney, M. S. and Talley, L. D.: The Subpolar Mode Water of the North Atlantic Ocean, J. Phys. Oceanogr., 12, 1169–1188, https://doi.org/10.1175/1520-0485(1982)012<1169:TSMWOT>2.0.CO;2, 1982.

McGee, D., Moreno-Chamarro, E., Green, B., Marshall, J., Galbraith, E., and Bradtmiller, L.: Hemispherically asymmetric trade wind changes as signatures of past ITCZ shifts, Quaternary Science Reviews, 180, 214–228, https://doi.org/10.1016/j.quascirev.2017.11.020, 2018.

McManus, J. F., Francois, R., Gherardi, J.-M., Keigwin, L. D., and Brown-Leger, S.: Collapse and rapid resumption of Atlantic meridional circulation linked to deglacial climate changes, Nature, 428, 834–837, https://doi.org/10.1038/nature02494, 2004.

Moffitt, S. E., Moffitt, R. A., Sauthoff, W., Davis, C. V., Hewett, K., and Hill, T. M.: Paleoceanographic Insights on Recent Oxygen Minimum Zone Expansion: Lessons for Modern Oceanography, PLoS ONE, 10, e0115246, https://doi.org/10.1371/journal.pone.0115246, 2015.

Mollenhauer, G., Grotheer, H., Gentz, T., Bonk, E., and Hefter, J.: Standard operation procedures and performance of the MICADAS radiocarbon laboratory at Alfred Wegener Institute (AWI), Germany, Nuclear Instruments and Methods in Physics Research Section B: Beam Interactions with Materials and Atoms, 496, 45–51, https://doi.org/10.1016/j.nimb.2021.03.016, 2021.

Moore, W. S.: Review of the geosecs project, Nuclear Instruments and Methods in Physics Research, 223, 459–465, https://doi.org/10.1016/0167-5087(84)90692-6, 1984.

Morkhoven, F. P. C. M. van, Berggren, W. A., and Edwards, A. S.: Cenozoic cosmopolitan deep-water benthic foraminifera, Elf Aquitaine, Pau, 421 pp., 1986.

Mulitza, S., Bouimetarhan, I., Bruening, M., Freesemann, A., Gussone, N., Filipsson, H. L., Heil, G., Hessler, S., Jaeschke, A., Johnstone, H. J. H., Klann, M., Klein, F., Kuester, K., Maerz, C., McGregor, H., Minning, M., Mueller, H., Ochsenhirt, W.-T., Paul, A., Pokorna, M., Schewe, F., Schulz, M., Steinloechner, J., Stuut, J.-B., Tjallingii, R., von Dobeneck, T., Wiesmaier, S., Zabel, M., and Zonneveld, C.: Report and preliminary results of METEOR Cruise M65/1, Dakar - Dakar, 11.06. - 1.07.2005., 2005.

Mulitza, S., Prange, M., Stuut, J., Zabel, M., Von Dobeneck, T., Itambi, A. C., Nizou, J., Schulz, M., and Wefer, G.: Sahel megadroughts triggered by glacial slowdowns of Atlantic meridional overturning, Paleoceanography, 23, 2008PA001637, https://doi.org/10.1029/2008PA001637, 2008.

Murray, J. W.: Ecology and palaeoecology of benthic foraminifera, Longman scientific and technical copublished in the United States with John Wiley and sons, Essex New York, 1991.

Murray, J. W.: Ecology and Applications of Benthic Foraminifera, 1st ed., Cambridge University Press, https://doi.org/10.1017/CBO9780511535529, 2006.

Ng, H. C., Robinson, L. F., McManus, J. F., Mohamed, K. J., Jacobel, A. W., Ivanovic, R. F., Gregoire, L. J., and Chen, T.: Coherent deglacial changes in western

Atlantic Ocean circulation, Nat Commun, 9, 2947, https://doi.org/10.1038/s41467-018-05312-3, 2018.

Novello, V. F., Cruz, F. W., Vuille, M., Stríkis, N. M., Edwards, R. L., Cheng, H., Emerick, S., De Paula, M. S., Li, X., Barreto, E. D. S., Karmann, I., and Santos, R. V.: A high-resolution history of the South American Monsoon from Last Glacial Maximum to the Holocene, Sci Rep, 7, 44267, https://doi.org/10.1038/srep44267, 2017.

Oliver, K. I. C., Hoogakker, B. A. A., Crowhurst, S., Henderson, G. M., Rickaby, R. E. M., Edwards, N. R., and Elderfield, H.: A synthesis of marine sediment core δ13C data over the last 150 000 years, Clim. Past, 6, 645–673, https://doi.org/10.5194/cp-6-645-2010, 2010.

Pauly, D. and Dimarchopoulou, D.: Introduction: Fishes in a warming and deoxygenating world, Environ Biol Fish, 105, 1261–1267, https://doi.org/10.1007/s10641-022-01357-y, 2022.

Pelegrí, J. L. and Peña-Izquierdo, J.: Eastern boundary currents off North-West Africa, in: Oceanographic and biological features in the Canary Current Large Marine Ecosystem, 81–92, 2015.

Pinho, T. M. L., Chiessi, C. M., Portilho-Ramos, R. C., Campos, M. C., Crivellari, S., Nascimento, R. A., Albuquerque, A. L. S., Bahr, A., and Mulitza, S.: Meridional changes in the South Atlantic Subtropical Gyre during Heinrich Stadials, Sci Rep, 11, 9419, https://doi.org/10.1038/s41598-021-88817-0, 2021.

Poole, R. and Tomczak, M.: Optimum multiparameter analysis of the water mass structure in the Atlantic Ocean thermocline, Deep Sea Research Part I: Oceanographic Research Papers, 46, 1895–1921, https://doi.org/10.1016/S0967-0637(99)00025-4, 1999.

Portilho-Ramos, R. C., Chiessi, C. M., Zhang, Y., Mulitza, S., Kucera, M., Siccha, M., Prange, M., and Paul, A.: Coupling of equatorial Atlantic surface stratification to glacial shifts in the tropical rainbelt, Sci Rep, 7, 1561, https://doi.org/10.1038/s41598-017-01629-z, 2017.

Pörtner, H.-O., Bock, C., and Mark, F. C.: Oxygen- and capacity-limited thermal tolerance: bridging ecology and physiology, Journal of Experimental Biology, 220, 2685–2696, https://doi.org/10.1242/jeb.134585, 2017.

Qiu, W., Zhang, X., Jiang, X., Hu, H.-M., Ma, L., Xiao, H., Cai, B., and Shen, C.-C.: Double-plunge structure of the East Asian summer monsoon during Heinrich stadial 1 recorded in Xianyun Cave, southeastern China, Quaternary Science Reviews, 282, 107442, https://doi.org/10.1016/j.quascirev.2022.107442, 2022.

Reißig, S., Nürnberg, D., Bahr, A., Poggemann, D. -W., and Hoffmann, J.: Southward Displacement of the North Atlantic Subtropical Gyre Circulation System During North Atlantic Cold Spells, Paleoceanog and Paleoclimatol, 34, 866–885, https://doi.org/10.1029/2018PA003376, 2019.

Repschläger, J., Weinelt, M., Kinkel, H., Andersen, N., Garbe-Schönberg, D., and Schwab, C.: Response of the subtropical North Atlantic surface hydrography on deglacial and Holocene AMOC changes, Paleoceanography, 30, 456–476, https://doi.org/10.1002/2014PA002637, 2015.

Rühlemann, C., Mulitza, S., Müller, P. J., Wefer, G., and Zahn, R.: Warming of the tropical Atlantic Ocean and slowdown of thermohaline circulation during the last deglaciation, Nature, 402, 511–514, https://doi.org/10.1038/990069, 1999.

Schlitzer, R.: Ocean Data View, , odv.awi.de, 2023.

Schmidtko, S., Stramma, L., and Visbeck, M.: Decline in global oceanic oxygen content during the past five decades, Nature, 542, 335–339, https://doi.org/10.1038/nature21399, 2017.

Schmittner, A., Bostock, H. C., Cartapanis, O., Curry, W. B., Filipsson, H. L., Galbraith, E. D., Gottschalk, J., Herguera, J. C., Hoogakker, B., Jaccard, S. L., Lisiecki, L. E., Lund, D. C., Martínez-Méndez, G., Lynch-Stieglitz, J., Mackensen, A., Michel, E., Mix, A. C., Oppo, D. W., Peterson, C. D., Repschläger, J., Sikes, E. L., Spero, H. J., and Waelbroeck, C.: Calibration of the carbon isotope composition (δ 13 C) of benthic foraminifera, Paleoceanography, 32, 512–530, https://doi.org/10.1002/2016PA003072, 2017.

Sen Gupta, B. K.: Introduction to modern Foraminifera, in: Modern Foraminifera, Springer, Dordrecht, 3–6, 1999.

Shakun, J. D. and Carlson, A. E.: A global perspective on Last Glacial Maximum to Holocene climate change, Quaternary Science Reviews, 29, 1801–1816, https://doi.org/10.1016/j.quascirev.2010.03.016, 2010.

Sharon, Belanger, C., Du, J., and Mix, A.: Reconstructing Paleo-oxygenation for the Last 54,000 Years in the Gulf of Alaska Using Cross-validated Benthic Foraminiferal and Geochemical Records, Paleoceanog and Paleoclimatol, 36, e2020PA003986, https://doi.org/10.1029/2020PA003986, 2021.

Skinner, L. C., Freeman, E., Hodell, D., Waelbroeck, C., Vazquez Riveiros, N., and Scrivner, A. E.: Atlantic Ocean Ventilation Changes Across the Last Deglaciation and Their Carbon Cycle Implications, Paleoceanog and Paleoclimatol, 36, e2020PA004074, https://doi.org/10.1029/2020PA004074, 2021.

Slowey, N. C. and Curry, W. B.: Enhanced ventilation of the North Atlantic subtropical gyre thermocline during the last glaciation, Nature, 358, 665–668, https://doi.org/10.1038/358665a0, 1992.

Southward, A. J.: Advances in marine biology, Academic, San Diego, Calif. London, 2003.

Stramma, L., Johnson, G. C., Sprintall, J., and Mohrholz, V.: Expanding Oxygen-Minimum Zones in the Tropical Oceans, 320, 655–658, https://doi.org/10.1126/science.1153847, 2008.

Stramma, L., Prince, E. D., Schmidtko, S., Luo, J., Hoolihan, J. P., Visbeck, M., Wallace, D. W. R., Brandt, P., and Körtzinger, A.: Expansion of oxygen minimum zones may reduce available habitat for tropical pelagic fishes, Nature Clim Change, 2, 33–37, https://doi.org/10.1038/nclimate1304, 2012.

Tetard, M., Licari, L., and Beaufort, L.: Oxygen history off Baja California over the last 80 kyr: A new foraminiferal-based record: Oxygen History in the California Margin, Paleoceanography, 32, 246–264, https://doi.org/10.1002/2016PA003034, 2017.

Tomczak, M. and Godfrey, J. S.: Regional oceanography: an introduction, 1st ed., Pergamon, Oxford, England ; New York, 422 pp., 1994.

Völpel, R., Mulitza, S., Paul, A., Lynch-Stieglitz, J., and Schulz, M.: Water Mass Versus Sea Level Effects on Benthic Foraminiferal Oxygen Isotope Ratios in the Atlantic Ocean During the LGM, Paleoceanog and Paleoclimatol, 34, 98–121, https://doi.org/10.1029/2018PA003359, 2019.

Weijer, W., Cheng, W., Garuba, O. A., Hu, A., and Nadiga, B. T.: CMIP6 Models Predict Significant 21st Century Decline of the Atlantic Meridional Overturning Circulation, Geophysical Research Letters, 47, e2019GL086075, https://doi.org/10.1029/2019GL086075, 2020.

Wyrtki, K.: The oxygen minima in relation to ocean circulation, Deep Sea Research and Oceanographic Abstracts, 9, 11–23, https://doi.org/10.1016/0011-7471(62)90243-7, 1962.

Zarriess, M. and Mackensen, A.: The tropical rainbelt and productivity changes off northwest Africa: A 31,000-year high-resolution record, Marine Micropaleontology, 76, 76–91, https://doi.org/10.1016/j.marmicro.2010.06.001, 2010.

Zhang, J., Gilbert, D., Gooday, A. J., Levin, L., Naqvi, S. W. A., Middelburg, J. J., Scranton, M., Ekau, W., Peña, A., Dewitte, B., Oguz, T., Monteiro, P. M. S., Urban, E., Rabalais, N. N., Ittekkot, V., Kemp, W. M., Ulloa, O., Elmgren, R., Escobar-Briones, E., and Van Der Plas, A. K.: Natural and human-induced hypoxia and consequences for coastal areas: synthesis and future development, Biogeosciences, 7, 1443–1467, https://doi.org/10.5194/bg-7-1443-2010, 2010.

Zhang, R., Sutton, R., Danabasoglu, G., Kwon, Y., Marsh, R., Yeager, S. G., Amrhein, D. E., and Little, C. M.: A Review of the Role of the Atlantic Meridional Overturning Circulation in Atlantic Multidecadal Variability and Associated Climate Impacts, Reviews of Geophysics, 57, 316–375, https://doi.org/10.1029/2019RG000644, 2019.

Zweng, M. M., Reagan, J. R., Seidov, Dan, Boyer, T. P., Locarnini, R. A., García, H. E., Mishonov, A. V., Baranova, O. K., Weathers, K. A., Paver, C. R., and

Smolyar, I. V.: World Ocean Atlas 2018, Volume 2: Salinity. A. Mishonov Technical Ed., 2019.

Chapter 4

Barker, S., Greaves, M., Elderfield, H., 2003. A study of cleaning procedures used for foraminiferal Mg/Ca paleothermometry: MG/CA PALEOTHERMOMETRY. Geochem. Geophys. Geosyst. 4, n/a-n/a. https://doi.org/10.1029/2003GC000559

Barragán-Montilla, S., Johnstone, H., Mulitza, S., Macaya, D., Pälike, H., 2024. Enhanced ventilation of Eastern North Atlantic Oxygen Minimum Zone with deglacial slowdown of Meridional Overturning. https://doi.org/10.21203/rs.3.rs-4083170/v1

Bartels-Jónsdóttir, H.B., Knudsen, K.L., Abrantes, F., Lebreiro, S., Eiríksson, J., 2006. Climate variability during the last 2000 years in the Tagus Prodelta, western Iberian Margin: Benthic foraminifera and stable isotopes. Marine Micropaleontology 59, 83–103. https://doi.org/10.1016/j.marmicro.2006.01.002

Blaauw, M., Christen, J.A., 2011. Flexible paleoclimate age-depth models using an autoregressive gamma process. Bayesian Anal. 6, 457–474. https://doi.org/10.1214/ba/1339616472

Boyer, T.P., García, H.E., Locarnini, R.A., Zweng, M.M., Alexey, V., Reagan, J.R., Weathers, K.A., Baranova, O.K., Paver, C.R., Seidov, Dan, Smolyar, I.V., 2018. World Ocean Atlas 2018. [Annual Data, 1.00 Degree all years].

Brinkmann, I., Barras, C., Jilbert, T., Paul, K.M., Somogyi, A., Ni, S., Schweizer, M., Bernhard, J.M., Filipsson, H.L., 2023. Benthic Foraminiferal Mn/Ca as Low-Oxygen Proxy in Fjord Sediments. Global Biogeochemical Cycles 37, e2023GB007690. https://doi.org/10.1029/2023GB007690

Calvin, K., Dasgupta, D., Krinner, G., Mukherji, A., Thorne, P.W., Trisos, C., Romero, J., Aldunce, P., Barrett, K., Blanco, G., Cheung, W.W.L., Connors, S., Denton, F., Diongue-Niang, A., Dodman, D., Garschagen, M., Geden, O., Hayward, B., Jones, C., Jotzo, F., Krug, T., Lasco, R., Lee, Y.-Y., Masson-Delmotte, V., Meinshausen, M., Mintenbeck, K., Mokssit, A., Otto, F.E.L., Pathak, M., Pirani, A., Poloczanska, E., Pörtner, H.-O., Revi, A., Roberts, D.C., Roy, J., Ruane, A.C., Skea,

J., Shukla, P.R., Slade, R., Slangen, A., Sokona, Y., Sörensson, A.A., Tignor, M., Van Vuuren, D., Wei, Y.-M., Winkler, H., Zhai, P., Zommers, Z., Hourcade, J.-C., Johnson, F.X., Pachauri, S., Simpson, N.P., Singh, C., Thomas, A., Totin, E., Arias, P., Bustamante, M., Elgizouli, I., Flato, G., Howden, M., Méndez-Vallejo, C., Pereira, J.J., Pichs-Madruga, R., Rose, S.K., Saheb, Y., Sánchez Rodríguez, R., Ürge-Vorsatz, D., Xiao, C., Yassaa, N., Alegría, A., Armour, K., Bednar-Friedl, B., Blok, K., Cissé, G., Dentener, F., Eriksen, S., Fischer, E., Garner, G., Guivarch, C., Haasnoot, M., Hansen, G., Hauser, M., Hawkins, E., Hermans, T., Kopp, R., Leprince-Ringuet, N., Lewis, J., Ley, D., Ludden, C., Niamir, L., Nicholls, Z., Some, S., Szopa, S., Trewin, B., Van Der Wijst, K.-I., Winter, G., Witting, M., Birt, A., Ha, M., Romero, J., Kim, J., Haites, E.F., Jung, Y., Stavins, R., Birt, A., Ha, M., Orendain, D.J.A., Ignon, L., Park, S., Park, Y., Reisinger, A., Cammaramo, D., Fischlin, A., Fuglestvedt, J.S., Hansen, G., Ludden, C., Masson-Delmotte, V., Matthews, J.B.R., Mintenbeck, K., Pirani, A., Poloczanska, E., Leprince-Ringuet, N., Péan, C., 2023. IPCC, 2023: Climate Change 2023: Synthesis Report. Contribution of Working Groups I, II and III to the Sixth Assessment Report of the Intergovernmental Panel on Climate Change [Core Writing Team, H. Lee and J. Romero (eds.)]. IPCC, Geneva, Switzerland. Intergovernmental Panel on Climate Change (IPCC). https://doi.org/10.59327/IPCC/AR6-9789291691647

Caralp, M.H., 1989. Size and morphology of the benthic foraminifer Melonis barleeanum; relationships with marine organic matter. The Journal of Foraminiferal Research 19, 235–245. https://doi.org/10.2113/gsjfr.19.3.235

Corliss, B.H., 1985. foraminifera within deep-sea sediments 314.

Corliss, B.H., Emerson, S., 1990. Distribution of rose bengal stained deep-sea benthic foraminifera from the Nova Scotian continental margin and Gulf of Maine. Deep Sea Research Part A. Oceanographic Research Papers 37, 381–400. https://doi.org/10.1016/0198-0149(90)90015-N

Cummins, P.F., Masson, D., Saenko, O.A., 2016. Vertical heat flux in the ocean: Estimates from observations and from a coupled general circulation model. JGR Oceans 121, 3790–3802. https://doi.org/10.1002/2016JC011647

Elderfield, H., Greaves, M., Barker, S., Hall, I.R., Tripati, A., Ferretti, P., Crowhurst, S., Booth, L., Daunt, C., 2010. A record of bottom water temperature and seawater δ18O for the Southern Ocean over the past 440kyr based on Mg/Ca of benthic foraminiferal Uvigerina spp. Quaternary Science Reviews 29, 160–169. https://doi.org/10.1016/j.quascirev.2009.07.013

Filipsson, H.L., Romero, O.E., Stuut, J.W., Donner, B., 2011. Relationships between primary productivity and bottom-water oxygenation off northwest Africa during the last deglaciation. J Quaternary Science 26, 448–456. https://doi.org/10.1002/jqs.1473

Fontanier, C., Jorissen, F.J., Chaillou, G., Anschutz, P., Grémare, A., Griveaud, C., 2005. Live foraminiferal faunas from a 2800m deep lower canyon station from the Bay of Biscay: Faunal response to focusing of refractory organic matter. Deep Sea Research Part I: Oceanographic Research Papers 52, 1189–1227. https://doi.org/10.1016/j.dsr.2005.01.006

Fontanier, C., Jorissen, F.J., Licari, L., Alexandre, A., Anschutz, P., Carbonel, P., 2002. Live benthic foraminiferal faunas from the Bay of Biscay: faunal density, composition, and microhabitats. Deep Sea Research Part I: Oceanographic Research Papers 49, 751–785. https://doi.org/10.1016/S0967-0637(01)00078-4

Geslin, E., Heinz, P., Jorissen, F., Hemleben, Ch., 2004. Migratory responses of deep-sea benthic foraminifera to variable oxygen conditions: laboratory investigations. Marine Micropaleontology 53, 227–243. https://doi.org/10.1016/j.marmicro.2004.05.010

Greaves, M., Barker, S., Daunt, C., Elderfield, H., 2005. Accuracy, standardization, and interlaboratory calibration standards for foraminiferal Mg/Ca thermometry. Geochem Geophys Geosyst 6, 2004GC000790. https://doi.org/10.1029/2004GC000790

Griveaud, C., Jorissen, F., Anschutz, P., 2010. Spatial variability of live benthic foraminiferal faunas on the Portuguese margin 56, 297–322.

Groeneveld, J., Filipsson, H.L., 2013. Mg/Ca and Mn/Ca ratios in benthic foraminifera: the potential to reconstruct past variations in temperature and hypoxia in shelf regions. Biogeosciences 10, 5125–5138. https://doi.org/10.5194/bg-10-5125-2013

Hasenfratz, A.P., Schiebel, R., Thornalley, D.J.R., Schönfeld, J., Jaccard, S.L., Martínez-García, A., Holbourn, A., Jennings, A.E., Kuhnt, W., Lear, C.H., Marchitto, T.M., Quillmann, U., Rosenthal, Y., Yu, J., Haug, G.H., 2017. Mg/Ca-temperature calibration for the benthic foraminifera Melonis barleeanum and Melonis pompilioides. Geochimica et Cosmochimica Acta 217, 365–383. https://doi.org/10.1016/j.gca.2017.08.038

Heaton, T.J., Köhler, P., Butzin, M., Bard, E., Reimer, R.W., Austin, W.E.N., Bronk Ramsey, C., Grootes, P.M., Hughen, K.A., Kromer, B., Reimer, P.J., Adkins, J., Burke, A., Cook, M.S., Olsen, J., Skinner, L.C., 2020. Marine20—The Marine Radiocarbon Age Calibration Curve (0–55,000 cal BP). Radiocarbon 62, 779–820. https://doi.org/10.1017/RDC.2020.68

Jansen, J.H.F., De Lange, G.J., van Bennekom, A.J., 1990. (Pale)oceanography and geochemistry of the Angola Basin (South Atlantic Ocean) : cruise report R.V. Tyro 30 September-19 November 11–65.

Johnstone, H.J.H., Steinke, S., Kuhnert, H., Bickert, T., Pälike, H., Mohtadi, M., 2016. Automated cleaning of foraminifera shells before Mg/Ca analysis using a pipette robot. Geochem Geophys Geosyst 17, 3502–3511. https://doi.org/10.1002/2016GC006422

Jorissen, F.J., 1999. Benthic foraminiferal microhabitats below the sediment-water interface, in: Modern Foraminifera. Springer Netherlands, Dordrecht, pp. 161–179. https://doi.org/10.1007/0-306-48104-9_10

Jorissen, F.J., De Stigter, H.C., Widmark, J.G.V., 1995. A conceptual model explaining benthic foraminiferal microhabitats. Marine Micropaleontology 26, 3–15. https://doi.org/10.1016/0377-8398(95)00047-X

Koho, K.A., De Nooijer, L.J., Fontanier, C., Toyofuku, T., Oguri, K., Kitazato, H., Reichart, G.-J., 2017. Benthic foraminiferal Mn / Ca ratios reflect microhabitat preferences. Biogeosciences 14, 3067–3082. https://doi.org/10.5194/bg-14-3067-2017

Koho, K.A., De Nooijer, L.J., Reichart, G.J., 2015. Combining benthic foraminiferal ecology and shell Mn/Ca to deconvolve past bottom water oxygenation and paleoproductivity. Geochimica et Cosmochimica Acta 165, 294–306. https://doi.org/10.1016/j.gca.2015.06.003

Koho, K.A., Piña-Ochoa, E., 2012. Benthic Foraminifera: Inhabitants of Low-Oxygen Environments, in: Altenbach, A.V., Bernhard, J.M., Seckbach, J. (Eds.), Anoxia, Cellular Origin, Life in Extreme Habitats and Astrobiology. Springer Netherlands, Dordrecht, pp. 249–285. https://doi.org/10.1007/978-94-007-1896-8_14

Koho, K.A., Piña-Ochoa, E., Geslin, E., Risgaard-Petersen, N., 2011. Vertical migration, nitrate uptake and denitrification: survival mechanisms of foraminifers (Globobulimina turgida) under low oxygen conditions: Survival mechanisms of foraminifers. FEMS Microbiology Ecology 75, 273–283. https://doi.org/10.1111/j.1574-6941.2010.01010.x

Kostov, Y., Armour, K.C., Marshall, J., 2014. Impact of the Atlantic meridional overturning circulation on ocean heat storage and transient climate change. Geophys. Res. Lett. 41, 2108–2116. https://doi.org/10.1002/2013GL058998

Kristjánsdóttir, G.B., Lea, D.W., Jennings, A.E., Pak, D.K., Belanger, C., 2007. New spatial Mg/Ca-temperature calibrations for three Arctic, benthic foraminifera and reconstruction of north Iceland shelf temperature for the past 4000 years: Mg/Ca-TEMPERATURE CALIBRATIONS. Geochem. Geophys. Geosyst. 8, n/a-n/a. https://doi.org/10.1029/2006GC001425

Lauvset, S.K., Lange, N., Tanhua, T., Bittig, H.C., Olsen, A., Kozyr, A., Alin, S., Álvarez, M., Azetsu-Scott, K., Barbero, L., Becker, S., Brown, P.J., Carter, B.R., Da Cunha, L.C., Feely, R.A., Hoppema, M., Humphreys, M.P., Ishii, M., Jeansson, E., Jiang, L.-Q., Jones, S.D., Lo Monaco, C., Murata, A., Müller, J.D., Pérez, F.F., Pfeil, B., Schirnick, C., Steinfeldt, R., Suzuki, T., Tilbrook, B., Ulfsbo, A., Velo, A., Woosley,

R.J., Key, R.M., 2022. GLODAPv2.2022: the latest version of the global interior ocean biogeochemical data product. Earth Syst. Sci. Data 14, 5543–5572. https://doi.org/10.5194/essd-14-5543-2022

Lear, C.H., Rosenthal, Y., Slowey, N., 2002. Benthic foraminiferal Mg/Ca-paleothermometry: a revised core-top calibration. Geochimica et Cosmochimica Acta 66, 3375–3387. https://doi.org/10.1016/S0016-7037(02)00941-9

Levitus, S., 2005. Warming of the world ocean, 1955–2003. Geophys. Res. Lett. 32, L02604. https://doi.org/10.1029/2004GL021592

Levitus, S., Antonov, J.I., Boyer, T.P., Stephens, C., 2000. Warming of the World Ocean 287.

Linke, P., Lutze, G.F., 1993. Microhabitat preferences of benthic foraminifera—a static concept or a dynamic adaptation to optimize food acquisition? Marine Micropaleontology 20, 215–234. https://doi.org/10.1016/0377-8398(93)90034-U

Liu, W., Fedorov, A.V., Xie, S.-P., Hu, S., 2020. Climate impacts of a weakened Atlantic Meridional Overturning Circulation in a warming climate. Sci. Adv. 6, eaaz4876. https://doi.org/10.1126/sciadv.aaz4876

Lueker, T.J., Dickson, A.G., Keeling, C.D., 2000. Ocean pCO2 calculated from dissolved inorganic carbon, alkalinity, and equations for K1 and K2: validation based on laboratory measurements of CO2 in gas and seawater at equilibrium. Marine Chemistry 70, 105–119. https://doi.org/10.1016/S0304-4203(00)00022-0

Marcott, S.A., Clark, P.U., Padman, L., Klinkhammer, G.P., Springer, S.R., Liu, Z., Otto-Bliesner, B.L., Carlson, A.E., Ungerer, A., Padman, J., He, F., Cheng, J., Schmittner, A., 2011. Ice-shelf collapse from subsurface warming as a trigger for Heinrich events. Proc. Natl. Acad. Sci. U.S.A. 108, 13415–13419. https://doi.org/10.1073/pnas.1104772108

Marshall, D.P., Zanna, L., 2014. A Conceptual Model of Ocean Heat Uptake under Climate Change. Journal of Climate 27, 8444–8465. https://doi.org/10.1175/JCLI-D-13-00344.1

Mojtahid, M., Hennekam, R., De Nooijer, L., Reichart, G.-J., Jorissen, F., Boer, W., Le Houedec, S., De Lange, G.J., 2019. Evaluation and application of foraminiferal element/calcium ratios: Assessing riverine fluxes and environmental conditions during sapropel S1 in the Southeastern Mediterranean. Marine Micropaleontology 153, 101783. https://doi.org/10.1016/j.marmicro.2019.101783

Mojtahid, M., Jorissen, F., Lansard, B., Fontanier, C., 2010. MICROHABITAT SELECTION OF BENTHIC FORAMINIFERA IN SEDIMENTS OFF THE RHONE RIVER MOUTH (NW MEDITERRANEAN). The Journal of Foraminiferal Research 40, 231–246. https://doi.org/10.2113/gsjfr.40.3.231

Mollenhauer, G., Grotheer, H., Gentz, T., Bonk, E., Hefter, J., 2021. Standard operation procedures and performance of the MICADAS radiocarbon laboratory at Alfred Wegener Institute (AWI), Germany. Nuclear Instruments and Methods in Physics Research Section B: Beam Interactions with Materials and Atoms 496, 45–51. https://doi.org/10.1016/j.nimb.2021.03.016

Mulitza, S., Bouimetarhan, I., Bruening, M., Freesemann, A., Gussone, N., Filipsson, H.L., Heil, G., Hessler, S., Jaeschke, A., Johnstone, H.J.H., Klann, M., Klein, F., Kuester, K., Maerz, C., McGregor, H., Minning, M., Mueller, H., Ochsenhirt, W.-T., Paul, A., Pokorna, M., Schewe, F., Schulz, M., Steinloechner, J., Stuut, J.-B., Tjallingii, R., von Dobeneck, T., Wiesmaier, S., Zabel, M., Zonneveld, C., 2005. Report and preliminary results of METEOR Cruise M65/1, Dakar - Dakar, 11.06. - 1.07.2005.

Ní Fhlaithearta, S., Fontanier, C., Jorissen, F., Mouret, A., Dueñas-Bohórquez, A., Anschutz, P., Fricker, M.B., Günther, D., De Lange, G.J., Reichart, G.-J., 2018. Manganese incorporation in living (stained) benthic foraminiferal shells: a bathymetric and in-sediment study in the Gulf of Lions (NW Mediterranean). Biogeosciences 15, 6315–6328. https://doi.org/10.5194/bg-15-6315-2018

Okansen, J., Simpson, G., Blanchet, F., Kindt, R., Legendre, P., Minchin, P., O'Hara, R., Solymos, P., Stevens, M., Szoecs, E., Wagner, H., Barbour, M., Bedward, M., Bolker, B., Borcard, D., Carvalho, G., Chirico, M., De Caceres, M., Durand, S., Evangelista, H., FitzJohn, R., Friendly, M., Furneaux, B., Hannigan, G., Hill, M., Lahti, L., McGlinn, D., Ouellette, M., Ribeiro Cunha, E., Smith, T., Stier, A., Ter Braak, C.,

Weedon, J., 2022. _vegan: Community Ecology Package_. R package version 2.6-4, <https://CRAN.R-project.org/package=vegan>.

Oppo, D.W., Curry, W.B., McManus, J.F., 2015. What do benthic δ 13 C and δ 18 O data tell us about Atlantic circulation during Heinrich Stadial 1? Paleoceanography 30, 353–368. https://doi.org/10.1002/2014PA002667

Oppo, D.W., Lu, W., Huang, K. -F., Umling, N.E., Guo, W., Yu, J., Curry, W.B., Marchitto, T.M., Wang, S., 2023. Deglacial Temperature and Carbonate Saturation State Variability in the Tropical Atlantic at Antarctic Intermediate Water Depths. Paleoceanog and Paleoclimatol 38, e2023PA004674. https://doi.org/10.1029/2023PA004674

Poggemann, D. -W., Nürnberg, D., Hathorne, E.C., Frank, M., Rath, W., Reißig, S., Bahr, A., 2018. Deglacial Heat Uptake by the Southern Ocean and Rapid Northward Redistribution Via Antarctic Intermediate Water. Paleoceanog and Paleoclimatol 33, 1292–1305. https://doi.org/10.1029/2017PA003284

Robbins, L.L., Hansen, M.E., Kleypas, J.A., Meylan, S.C., 2010. CO2calc – A user-friendly seawater carbon calculator for Windows, Max OS X, and iOS (iPhone).

Roberts, J., Gottschalk, J., Skinner, L.C., Peck, V.L., Kender, S., Elderfield, H., Waelbroeck, C., Vázquez Riveiros, N., Hodell, D.A., 2016. Evolution of South Atlantic density and chemical stratification across the last deglaciation. Proc. Natl. Acad. Sci. U.S.A. 113, 514–519. https://doi.org/10.1073/pnas.1511252113

Romero, O.E., Kim, J., Donner, B., 2008. Submillennial-to-millennial variability of diatom production off Mauritania, NW Africa, during the last glacial cycle. Paleoceanography 23, 2008PA001601. https://doi.org/10.1029/2008PA001601

Rosenthal, Y., Lear, C.H., Oppo, D.W., Linsley, B.K., 2006. Temperature and carbonate ion effects on Mg/Ca and Sr/Ca ratios in benthic foraminifera: Aragonitic species Hoeglundina elegans. Paleoceanography 21, 2005PA001158. https://doi.org/10.1029/2005PA001158

Sælen, G., Kristensen, D.K., Westerlund, S., Jansen, E., 2010. Sr/Ca in Calcitic Tests of Benthic Foraminifera - A Potential Water-Depth Proxy? TOGEOJ 3, 90–97. https://doi.org/10.2174/1874262900903010090

Schefuß, E., Versteegh, G.J.M., Jansen, J.H.F., Sinninghe Damsté, J.S., 2004. Lipid biomarkers as major source and preservation indicators in SE Atlantic surface sediments. Deep Sea Research Part I: Oceanographic Research Papers 51, 1199–1228. https://doi.org/10.1016/j.dsr.2004.05.002

Schlitzer, R., 2023. Ocean Data View, , odv.awi.de.

Schmittner, A., Bostock, H.C., Cartapanis, O., Curry, W.B., Filipsson, H.L., Galbraith, E.D., Gottschalk, J., Herguera, J.C., Hoogakker, B., Jaccard, S.L., Lisiecki, L.E., Lund, D.C., Martínez-Méndez, G., Lynch-Stieglitz, J., Mackensen, A., Michel, E., Mix, A.C., Oppo, D.W., Peterson, C.D., Repschläger, J., Sikes, E.L., Spero, H.J., Waelbroeck, C., 2017. Calibration of the carbon isotope composition (δ 13 C) of benthic foraminifera. Paleoceanography 32, 512–530. https://doi.org/10.1002/2016PA003072

Shackleton, N.J., 1994. Attainment of isotopic equilibrium between ocean water and the benthonic foraminiferal genus Uvigerina: Isotopic changes in the ocean during the last glacial. Centre National de la Recherche Scientifique Colloques Internationaux 219, 203–209.

Skinner, L.C., Shackleton, N.J., Elderfield, H., 2003. Millennial-scale variability of deep-water temperature and δ 18 O dw indicating deep-water source variations in the Northeast Atlantic, 0–34 cal. ka BP. Geochem Geophys Geosyst 4, 2003GC000585. https://doi.org/10.1029/2003GC000585

Stirpe, C.R., Allen, K.A., Sikes, E.L., Zhou, X., Rosenthal, Y., Cruz-Uribe, A.M., Brooks, H.L., 2021. The Mg/Ca proxy for temperature: A Uvigerina core-top study in the Southwest Pacific. Geochimica et Cosmochimica Acta 309, 299–312. https://doi.org/10.1016/j.gca.2021.06.015

Völpel, R., Mulitza, S., Paul, A., Lynch-Stieglitz, J., Schulz, M., 2019. Water Mass Versus Sea Level Effects on Benthic Foraminiferal Oxygen Isotope Ratios in the

Atlantic Ocean During the LGM. Paleoceanog and Paleoclimatol 34, 98–121. https://doi.org/10.1029/2018PA003359

Von Schuckmann, K., Minière, A., Gues, F., Cuesta-Valero, F.J., Kirchengast, G., Adusumilli, S., Straneo, F., Ablain, M., Allan, R.P., Barker, P.M., Beltrami, H., Blazquez, A., Boyer, T., Cheng, L., Church, J., Desbruyeres, D., Dolman, H., Domingues, C.M., García-García, A., Giglio, D., Gilson, J.E., Gorfer, M., Haimberger, L., Hakuba, M.Z., Hendricks, S., Hosoda, S., Johnson, G.C., Killick, R., King, B., Kolodziejczyk, N., Korosov, A., Krinner, G., Kuusela, M., Landerer, F.W., Langer, M., Lavergne, T., Lawrence, I., Li, Y., Lyman, J., Marti, F., Marzeion, B., Mayer, M., MacDougall, A.H., McDougall, T., Monselesan, D.P., Nitzbon, J., Otosaka, I., Peng, J., Purkey, S., Roemmich, D., Sato, Kanako, Sato, Katsunari, Savita, A., Schweiger, A., Shepherd, A., Seneviratne, S.I., Simons, L., Slater, D.A., Slater, T., Steiner, A.K., Suga, T., Szekely, T., Thiery, W., Timmermans, M.-L., Vanderkelen, I., Wjiffels, S.E., Wu, T., Zemp, M., 2023. Heat stored in the Earth system 1960–2020: where does the energy go? Earth Syst. Sci. Data 15, 1675–1709. https://doi.org/10.5194/essd-15-1675-2023

Waelbroeck, C., Duplessy, J.-C., Michel, E., Labeyrie, L., Paillard, D., Duprat, J., 2001. The timing of the last deglaciation in North Atlantic climate records. Nature 412, 724–727. https://doi.org/10.1038/35089060

Weldeab, S., Arce, A., Kasten, S., 2016. Mg/Ca- Δ CO 3 pore water 2 − – temperature calibration for Globobulimina spp.: A sensitive paleothermometer for deep-sea temperature reconstruction. Earth and Planetary Science Letters 438, 95–102. https://doi.org/10.1016/j.epsl.2016.01.009

Yu, J., Elderfield, H., 2008. Mg/Ca in the benthic foraminifera Cibicidoides wuellerstorfi and Cibicidoides mundulus: Temperature versus carbonate ion saturation. Earth and Planetary Science Letters 276, 129–139. https://doi.org/10.1016/j.epsl.2008.09.015

Zhang, J., Liu, Z., Brady, E.C., Oppo, D.W., Clark, P.U., Jahn, A., Marcott, S.A., Lindsay, K., 2017. Asynchronous warming and δ 18 O evolution of deep Atlantic water masses during the last deglaciation. Proc. Natl. Acad. Sci. U.S.A. 114, 11075–11080. https://doi.org/10.1073/pnas.1704512114

Chapter 5

Barker, S., Greaves, M., Elderfield, H., 2003. A study of cleaning procedures used for foraminiferal Mg/Ca paleothermometry. Geochemistry, Geophysics, Geosystems 4. https://doi.org/10.1029/2003GC000559

Barragán-Montilla, S., Johnstone, H., Mulitza, S., Macaya, D., Pälike, H., 2024. Enhanced ventilation of Eastern North Atlantic Oxygen Minimum Zone with deglacial slowdown of Meridional Overturning. https://doi.org/10.21203/rs.3.rs-4083170/v1

Barragán-Montilla, S., Mulitza, S., Johnstone, H.J.H., Pälike, H., 2023. Stagnant North Atlantic Deep Water Heat Uptake With Reduced Atlantic Meridional Overturning Circulation During the Last Deglaciation. Paleoceanography and Paleoclimatology 38, e2022PA004575. https://doi.org/10.1029/2022PA004575

Blaauw, M., Christen, J.A., 2011. Flexible paleoclimate age-depth models using an autoregressive gamma process. Bayesian Anal. 6, 457–474. https://doi.org/10.1214/ba/1339616472

Böhm, E., Lippold, J., Gutjahr, M., Frank, M., Blaser, P., Antz, B., Fohlmeister, J., Frank, N., Andersen, M.B., Deininger, M., 2015. Strong and deep Atlantic meridional overturning circulation during the last glacial cycle. Nature 517, 73–76. https://doi.org/10.1038/nature14059

Boyer, T.P., García, H.E., Locarnini, R.A., Zweng, M.M., Alexey, V., Reagan, J.R., Weathers, K.A., Baranova, O.K., Paver, C.R., Seidov, Dan, Smolyar, I.V., 2018. World Ocean Atlas 2018. [Annual Data, 1.00 Degree all years].

Came, R.E., Curry, W.B., Oppo, D.W., Broccoli, A.J., Stouffer, R.J., Lynch-Stieglitz, J., 2007. North Atlantic intermediate depth variability during the Younger Dryas: Evidence from benthic foraminiferal Mg/Ca and the GFDL R30 Coupled Climate Model, in: Schmittner, A., Chiang, J.C.H., Hemming, S.R. (Eds.), Geophysical Monograph Series. American Geophysical Union, Washington, D. C., pp. 247–263. https://doi.org/10.1029/173GM16

Cummins, P.F., Masson, D., Saenko, O.A., 2016. Vertical heat flux in the ocean: Estimates from observations and from a coupled general circulation model. JGR Oceans 121, 3790–3802. https://doi.org/10.1002/2016JC011647

El Bani Altuna, N., Ezat, M.M., Greaves, M., Rasmussen, T.L., 2021. Millennial-Scale Changes in Bottom Water Temperature and Water Mass Exchange Through the Fram Strait 79°N, 63-13 ka. Paleoceanog and Paleoclimatol 36, e2020PA004061. https://doi.org/10.1029/2020PA004061

El Bani Altuna, Naima, Rasmussen, T.L., Ezat, M.M., Vadakkepuliyambatta, S., Groeneveld, J., Greaves, M., 2021. Deglacial bottom water warming intensified Arctic methane seepage in the NW Barents Sea. Commun Earth Environ 2, 188. https://doi.org/10.1038/s43247-021-00264-x

Elder, H., 2000. Past temperature and d18O of surface ocean waters inferred from foraminiferal Mg/Ca ratios 405.

Elderfield, H., Greaves, M., Barker, S., Hall, I.R., Tripati, A., Ferretti, P., Crowhurst, S., Booth, L., Daunt, C., 2010. A record of bottom water temperature and seawater δ18O for the Southern Ocean over the past 440kyr based on Mg/Ca of benthic foraminiferal Uvigerina spp. Quaternary Science Reviews 29, 160–169. https://doi.org/10.1016/j.quascirev.2009.07.013

Ezat, M.M., Rasmussen, T.L., Groeneveld, J., 2014. Persistent intermediate water warming during cold stadials in the southeastern Nordic seas during the past 65 k.y. Geology 42, 663–666. https://doi.org/10.1130/G35579.1

García, H.E., Weathers, K.A., Paver, C.R., Smolyar, I.V., Boyer, T.P., Locarnini, R.A., Zweng, M.M., Mishonov, A.V., Baranova, O.K., Seidov, Dan, Reagan, J.R., 2019. World Ocean Atlas 2018, Volume 3: Dissolved Oxygen, Apparent Oxygen Utilization, and Oxygen Saturation. A. Mishonov Technical Ed.

Gherardi, J., Labeyrie, L., Mcmanus, J., Francois, R., Skinner, L., Cortijo, E., 2005. Evidence from the Northeastern Atlantic basin for variability in the rate of the meridional overturning circulation through the last deglaciation. Earth and Planetary Science Letters 240, 710–723. https://doi.org/10.1016/j.epsl.2005.09.061

Greaves, M., Barker, S., Daunt, C., Elderfield, H., 2005. Accuracy, standardization, and interlaboratory calibration standards for foraminiferal Mg/Ca thermometry. Geochem Geophys Geosyst 6, 2004GC000790. https://doi.org/10.1029/2004GC000790

Gu, S., Liu, Z., Zhang, J., Rempfer, J., Joos, F., Oppo, D.W., 2017. Coherent Response of Antarctic Intermediate Water and Atlantic Meridional Overturning Circulation During the Last Deglaciation: Reconciling Contrasting Neodymium Isotope Reconstructions From the Tropical Atlantic. Paleoceanography 32, 1036–1053. https://doi.org/10.1002/2017PA003092

Hasenfratz, A.P., Schiebel, R., Thornalley, D.J.R., Schönfeld, J., Jaccard, S.L., Martínez-García, A., Holbourn, A., Jennings, A.E., Kuhnt, W., Lear, C.H., Marchitto, T.M., Quillmann, U., Rosenthal, Y., Yu, J., Haug, G.H., 2017. Mg/Ca-temperature calibration for the benthic foraminifera Melonis barleeanum and Melonis pompilioides. Geochimica et Cosmochimica Acta 217, 365–383. https://doi.org/10.1016/j.gca.2017.08.038

He, C., Liu, Z., Zhu, J., Zhang, J., Gu, S., Otto-Bliesner, B.L., Brady, E., Zhu, C., Jin, Y., Sun, J., 2020. North Atlantic subsurface temperature response controlled by effective freshwater input in “Heinrich” events. Earth and Planetary Science Letters 539, 116247. https://doi.org/10.1016/j.epsl.2020.116247

Heaton, T.J., Köhler, P., Butzin, M., Bard, E., Reimer, R.W., Austin, W.E., Ramsey, C.B., Grootes, P.M., Hughen, K.A., Kromer, B., Reimer, P.J., Adkins, J.F., Burke, A., Cook, M.S., Olsen, J., Skinner, L.C., 2020. Marine20 - the marine radiocarbon age calibration curve (0 - 55,000 cal BP), simulated data for IntCal20. https://doi.org/10.1594/PANGAEA.914500

Howe, J.N.W., Piotrowski, A.M., Noble, T.L., Mulitza, S., Chiessi, C.M., Bayon, G., 2016. North Atlantic Deep Water Production during the Last Glacial Maximum. Nat Commun 7, 11765. https://doi.org/10.1038/ncomms11765

Huang, E., Mulitza, S., Paul, A., Groeneveld, J., Steinke, S., Schulz, M., 2012. Response of eastern tropical Atlantic central waters to Atlantic meridional overturning

circulation changes during the Last Glacial Maximum and Heinrich Stadial 1. Paleoceanography 27, 2012PA002294. https://doi.org/10.1029/2012PA002294

Huang, K.-F., Oppo, D.W., Curry, W.B., 2014. Decreased influence of Antarctic intermediate water in the tropical Atlantic during North Atlantic cold events. Earth and Planetary Science Letters 389, 200–208. https://doi.org/10.1016/j.epsl.2013.12.037

Intergovernmental Panel On Climate Change (Ipcc), 2023. Climate Change 2022 – Impacts, Adaptation and Vulnerability: Working Group II Contribution to the Sixth Assessment Report of the Intergovernmental Panel on Climate Change, 1st ed. Cambridge University Press. https://doi.org/10.1017/9781009325844

Johnstone, H.J.H., Lee, W., Schulz, M., 2016. Effect of preservation state of planktonic foraminifera tests on the decrease in Mg/Ca due to reductive cleaning and on sample loss during cleaning. Chemical Geology 420, 23–36. https://doi.org/10.1016/j.chemgeo.2015.10.045

Köhler, P., Nehrbass-Ahles, C., Schmitt, J., Stocker, T.F., Fischer, H., 2017. A 156 kyr smoothed history of the atmospheric greenhouse gases CO2, CH4, and N2O and their radiative forcing. Earth Syst. Sci. Data 9, 363–387. https://doi.org/10.5194/essd-9-363-2017

Kostov, Y., Armour, K.C., Marshall, J., 2014. Impact of the Atlantic meridional overturning circulation on ocean heat storage and transient climate change. Geophys. Res. Lett. 41, 2108–2116. https://doi.org/10.1002/2013GL058998

Kristjánsdóttir, G.B., Lea, D.W., Jennings, A.E., Pak, D.K., Belanger, C., 2007. New spatial Mg/Ca-temperature calibrations for three Arctic, benthic foraminifera and reconstruction of north Iceland shelf temperature for the past 4000 years: Mg/Ca-TEMPERATURE CALIBRATIONS. Geochem. Geophys. Geosyst. 8, n/a-n/a. https://doi.org/10.1029/2006GC001425

Lauvset, S.K., Lange, N., Tanhua, T., Bittig, H.C., Olsen, A., Kozyr, A., Alin, S., Álvarez, M., Azetsu-Scott, K., Barbero, L., Becker, S., Brown, P.J., Carter, B.R., Da Cunha, L.C., Feely, R.A., Hoppema, M., Humphreys, M.P., Ishii, M., Jeansson, E., Jiang, L.-Q., Jones, S.D., Lo Monaco, C., Murata, A., Müller, J.D., Pérez, F.F., Pfeil,

B., Schirnick, C., Steinfeldt, R., Suzuki, T., Tilbrook, B., Ulfsbo, A., Velo, A., Woosley, R.J., Key, R.M., 2022. GLODAPv2.2022: the latest version of the global interior ocean biogeochemical data product. Earth Syst. Sci. Data 14, 5543–5572. https://doi.org/10.5194/essd-14-5543-2022

LeGrande, A.N., Schmidt, G.A., 2006. Global gridded data set of the oxygen isotopic composition in seawater. Geophysical Research Letters 33, 2006GL026011. https://doi.org/10.1029/2006GL026011

Levitus, S., Antonov, J., Boyer, T., 2005. Warming of the world ocean, 1955–2003. Geophysical Research Letters 32, 2004GL021592. https://doi.org/10.1029/2004GL021592

Levitus, S., Antonov, J.I., Boyer, T.P., Stephens, C., 2000. Warming of the World Ocean 287.

Liu, W., Fedorov, A.V., Xie, S.-P., Hu, S., 2020. Climate impacts of a weakened Atlantic Meridional Overturning Circulation in a warming climate. Sci. Adv. 6, eaaz4876. https://doi.org/10.1126/sciadv.aaz4876

Liu, Z., Otto-Bliesner, B.L., He, F., Brady, E.C., Tomas, R., Clark, P.U., Carlson, A.E., Lynch-Stieglitz, J., Curry, W., Brook, E., Erickson, D., Jacob, R., Kutzbach, J., Cheng, J., 2009. Transient Simulation of Last Deglaciation with a New Mechanism for Bølling-Allerød Warming. Science 325, 310–314. https://doi.org/10.1126/science.1171041

Lynch-Stieglitz, J., Schmidt, M.W., Gene Henry, L., Curry, W.B., Skinner, L.C., Mulitza, S., Zhang, R., Chang, P., 2014. Muted change in Atlantic overturning circulation over some glacial-aged Heinrich events. Nature Geosci 7, 144–150. https://doi.org/10.1038/ngeo2045

Marcott, S.A., Clark, P.U., Padman, L., Klinkhammer, G.P., Springer, S.R., Liu, Z., Otto-Bliesner, B.L., Carlson, A.E., Ungerer, A., Padman, J., He, F., Cheng, J., Schmittner, A., 2011. Ice-shelf collapse from subsurface warming as a trigger for Heinrich events. Proc. Natl. Acad. Sci. U.S.A. 108, 13415–13419. https://doi.org/10.1073/pnas.1104772108

Marshall, D.P., Zanna, L., 2014. A Conceptual Model of Ocean Heat Uptake under Climate Change. Journal of Climate 27, 8444–8465. https://doi.org/10.1175/JCLI-D-13-00344.1

Martin, P.A., Lea, D.W., Rosenthal, Y., Shackleton, N.J., Sarnthein, M., Papenfuss, T., 2002. Quaternary deep sea temperature histories derived from benthic foraminiferal Mg/Ca. Earth and Planetary Science Letters 198, 193–209. https://doi.org/10.1016/S0012-821X(02)00472-7

Max, L., Nürnberg, D., Chiessi, C.M., Lenz, M.M., Mulitza, S., 2022. Subsurface ocean warming preceded Heinrich Events. Nat Commun 13, 4217. https://doi.org/10.1038/s41467-022-31754-x

McManus, J.F., Francois, R., Gherardi, J.-M., Keigwin, L.D., Brown-Leger, S., 2004. Collapse and rapid resumption of Atlantic meridional circulation linked to deglacial climate changes. Nature 428, 834–837. https://doi.org/10.1038/nature02494

Mecking, J.V., Drijfhout, S.S., 2023. The decrease in ocean heat transport in response to global warming. Nat. Clim. Chang. 13, 1229–1236. https://doi.org/10.1038/s41558-023-01829-8

Mollenhauer, G., Grotheer, H., Gentz, T., Bonk, E., Hefter, J., 2021. Standard operation procedures and performance of the MICADAS radiocarbon laboratory at Alfred Wegener Institute (AWI), Germany. Nuclear Instruments and Methods in Physics Research Section B: Beam Interactions with Materials and Atoms 496, 45–51. https://doi.org/10.1016/j.nimb.2021.03.016

Mulitza, S., Bouimetarhan, I., Bruening, M., Freesemann, A., Gussone, N., Filipsson, H.L., Heil, G., Hessler, S., Jaeschke, A., Johnstone, H.J.H., Klann, M., Klein, F., Kuester, K., Maerz, C., McGregor, H., Minning, M., Mueller, H., Ochsenhirt, W.-T., Paul, A., Pokorna, M., Schewe, F., Schulz, M., Steinloechner, J., Stuut, J.-B., Tjallingii, R., von Dobeneck, T., Wiesmaier, S., Zabel, M., Zonneveld, C., 2005. Report and preliminary results of METEOR Cruise M65/1, Dakar - Dakar, 11.06. - 1.07.2005.

Ng, H.C., Robinson, L.F., McManus, J.F., Mohamed, K.J., Jacobel, A.W., Ivanovic, R.F., Gregoire, L.J., Chen, T., 2018. Coherent deglacial changes in western

Atlantic Ocean circulation. Nat Commun 9, 2947. https://doi.org/10.1038/s41467-018-05312-3

Oppo, D.W., Curry, W.B., McManus, J.F., 2015. What do benthic δ13C and δ18O data tell us about Atlantic circulation during Heinrich Stadial 1? Paleoceanography 30, 353–368. https://doi.org/10.1002/2014PA002667

Oppo, D.W., Lu, W., Huang, K. -F., Umling, N.E., Guo, W., Yu, J., Curry, W.B., Marchitto, T.M., Wang, S., 2023. Deglacial Temperature and Carbonate Saturation State Variability in the Tropical Atlantic at Antarctic Intermediate Water Depths. Paleoceanog and Paleoclimatol 38, e2023PA004674. https://doi.org/10.1029/2023PA004674

Osman, M.B., Tierney, J.E., Zhu, J., Tardif, R., Hakim, G.J., King, J., Poulsen, C.J., 2021. Globally resolved surface temperatures since the Last Glacial Maximum. Nature 599, 239–244. https://doi.org/10.1038/s41586-021-03984-4

Poggemann, D. -W., Nürnberg, D., Hathorne, E.C., Frank, M., Rath, W., Reißig, S., Bahr, A., 2018. Deglacial Heat Uptake by the Southern Ocean and Rapid Northward Redistribution Via Antarctic Intermediate Water. Paleoceanog and Paleoclimatol 33, 1292–1305. https://doi.org/10.1029/2017PA003284

Reißig, S., Nürnberg, D., Bahr, A., Poggemann, D. -W., Hoffmann, J., 2019. Southward Displacement of the North Atlantic Subtropical Gyre Circulation System During North Atlantic Cold Spells. Paleoceanog and Paleoclimatol 34, 866–885. https://doi.org/10.1029/2018PA003376

Roberts, J., Gottschalk, J., Skinner, L.C., Peck, V.L., Kender, S., Elderfield, H., Waelbroeck, C., Vázquez Riveiros, N., Hodell, D.A., 2016. Evolution of South Atlantic density and chemical stratification across the last deglaciation. Proceedings of the National Academy of Sciences 113, 514–519. https://doi.org/10.1073/pnas.1511252113

Rühlemann, C., Mulitza, S., Lohmann, G., Paul, A., Prange, M., Wefer, G., 2004. Intermediate depth warming in the tropical Atlantic related to weakened thermohaline circulation: Combining paleoclimate data and modeling results for the

last deglaciation. Paleoceanography 19, 2003PA000948. https://doi.org/10.1029/2003PA000948

Schlitzer, R., 2023. Ocean Data View, , odv.awi.de.

Schmidt, M.W., Chang, P., Hertzberg, J.E., Them, T.R., Ji, L., Otto-Bliesner, B.L., 2012. Impact of abrupt deglacial climate change on tropical Atlantic subsurface temperatures. Proc. Natl. Acad. Sci. U.S.A. 109, 14348–14352. https://doi.org/10.1073/pnas.1207806109

Shackleton, N.J., 1994. Attainment of isotopic equilibrium between ocean water and the benthonic foraminiferal genus Uvigerina: Isotopic changes in the ocean during the last glacial. Centre National de la Recherche Scientifique Colloques Internationaux 219, 203–209.

Skinner, L.C., Shackleton, N.J., Elderfield, H., 2003. Millennial-scale variability of deep-water temperature and δ 18 O dw indicating deep-water source variations in the Northeast Atlantic, 0–34 cal. ka BP. Geochem Geophys Geosyst 4, 2003GC000585. https://doi.org/10.1029/2003GC000585

Tallobre, C., Giresse, P., Bassetti, M.-A., Loncke, L., Bayon, G., Buscail, R., Tudryn, A., Zaragosi, S., 2019. Formation and evolution of glauconite in the Demerara Contourite depositional system related to NADW circulation changes during late Quaternary (French Guiana). Journal of South American Earth Sciences 92, 167–183. https://doi.org/10.1016/j.jsames.2019.03.011

Valley, S., Lynch-Stieglitz, J., Marchitto, T.M., 2017. Timing of Deglacial AMOC Variability From a High-Resolution Seawater Cadmium Reconstruction. Paleoceanography 32, 1195–1203. https://doi.org/10.1002/2017PA003099

Völpel, R., Mulitza, S., Paul, A., Lynch-Stieglitz, J., Schulz, M., 2019. Water Mass Versus Sea Level Effects on Benthic Foraminiferal Oxygen Isotope Ratios in the Atlantic Ocean During the LGM. Paleoceanog and Paleoclimatol 34, 98–121. https://doi.org/10.1029/2018PA003359

Von Schuckmann, K., Minière, A., Gues, F., Cuesta-Valero, F.J., Kirchengast, G., Adusumilli, S., Straneo, F., Ablain, M., Allan, R.P., Barker, P.M., Beltrami, H.,

Blazquez, A., Boyer, T., Cheng, L., Church, J., Desbruyeres, D., Dolman, H., Domingues, C.M., García-García, A., Giglio, D., Gilson, J.E., Gorfer, M., Haimberger, L., Hakuba, M.Z., Hendricks, S., Hosoda, S., Johnson, G.C., Killick, R., King, B., Kolodziejczyk, N., Korosov, A., Krinner, G., Kuusela, M., Landerer, F.W., Langer, M., Lavergne, T., Lawrence, I., Li, Y., Lyman, J., Marti, F., Marzeion, B., Mayer, M., MacDougall, A.H., McDougall, T., Monselesan, D.P., Nitzbon, J., Otosaka, I., Peng, J., Purkey, S., Roemmich, D., Sato, Kanako, Sato, Katsunari, Savita, A., Schweiger, A., Shepherd, A., Seneviratne, S.I., Simons, L., Slater, D.A., Slater, T., Steiner, A.K., Suga, T., Szekely, T., Thiery, W., Timmermans, M.-L., Vanderkelen, I., Wjiffels, S.E., Wu, T., Zemp, M., 2023. Heat stored in the Earth system 1960–2020: where does the energy go? Earth Syst. Sci. Data 15, 1675–1709. https://doi.org/10.5194/essd-15-1675-2023

Waelbroeck, C., Duplessy, J.-C., Michel, E., Labeyrie, L., Paillard, D., Duprat, J., 2001. The timing of the last deglaciation in North Atlantic climate records. Nature 412, 724–727. https://doi.org/10.1038/35089060

Weldeab, S., Friedrich, T., Timmermann, A., Schneider, R.R., 2016. Strong middepth warming and weak radiocarbon imprints in the equatorial Atlantic during Heinrich 1 and Younger Dryas. Paleoceanography 31, 1070–1082. https://doi.org/10.1002/2016PA002957

Xie, R.C., Marcantonio, F., Schmidt, M.W., 2012. Deglacial variability of Antarctic Intermediate Water penetration into the North Atlantic from authigenic neodymium isotope ratios. Paleoceanography 27, 2012PA002337. https://doi.org/10.1029/2012PA002337

Yu, J., Elderfield, H., 2008. Mg/Ca in the benthic foraminifera Cibicidoides wuellerstorfi and Cibicidoides mundulus: Temperature versus carbonate ion saturation. Earth and Planetary Science Letters 276, 129–139. https://doi.org/10.1016/j.epsl.2008.09.015

Zhang, J., Liu, Z., Brady, E.C., Oppo, D.W., Clark, P.U., Jahn, A., Marcott, S.A., Lindsay, K., 2017. Asynchronous warming and δ 18 O evolution of deep Atlantic water masses during the last deglaciation. Proc. Natl. Acad. Sci. U.S.A. 114, 11075–11080. https://doi.org/10.1073/pnas.1704512114

Final Conclusions and Remarks

Böhm, E., Lippold, J., Gutjahr, M., Frank, M., Blaser, P., Antz, B., Fohlmeister, J., Frank, N., Andersen, M.B., Deininger, M., 2015. Strong and deep Atlantic meridional overturning circulation during the last glacial cycle. Nature 517, 73–76. https://doi.org/10.1038/nature14059

Came, R.E., Curry, W.B., Oppo, D.W., Broccoli, A.J., Stouffer, R.J., Lynch-Stieglitz, J., 2007. North Atlantic intermediate depth variability during the Younger Dryas: Evidence from benthic foraminiferal Mg/Ca and the GFDL R30 Coupled Climate Model, in: Schmittner, A., Chiang, J.C.H., Hemming, S.R. (Eds.), Geophysical Monograph Series. American Geophysical Union, Washington, D. C., pp. 247–263. https://doi.org/10.1029/173GM16

Caralp, M.H., 1989. Size and morphology of the benthic foraminifer Melonis barleeanum; relationships with marine organic matter. The Journal of Foraminiferal Research 19, 235–245. https://doi.org/10.2113/gsjfr.19.3.235

Haake, F.W., 1980. Benthische Foraminiferen in Oberflächen-Sedimenten und Kernen des Ostatlantiks vor Senegal/Gambia (Westafrika).

Jorissen, F.J., Wittling, I., Peypouquet, J.P., Rabouille, C., Relexans, J.C., 1998. Live benthic foraminiferal faunas off Cape Blanc, NW-Africa: Community structure and microhabitats. Deep Sea Research Part I: Oceanographic Research Papers 45, 2157–2188. https://doi.org/10.1016/S0967-0637(98)00056-9

Linke, P., Lutze, G.F., 1993. Microhabitat preferences of benthic foraminifera—a static concept or a dynamic adaptation to optimize food acquisition? Marine Micropaleontology 20, 215–234. https://doi.org/10.1016/0377-8398(93)90034-U

Lutze, G.F., Coulbourn, W.T., n.d. RECENT BENTHIC FORAMINIFERA FROM THE CONTINENTAL MARGIN OF NORTHWEST AFRICA: COMMUNITY STRUCTURE AND DISTRIBUTION.

McManus, J.F., Francois, R., Gherardi, J.-M., Keigwin, L.D., Brown-Leger, S., 2004. Collapse and rapid resumption of Atlantic meridional circulation linked to deglacial climate changes. Nature 428, 834–837. https://doi.org/10.1038/nature02494

Oppo, D.W., Lu, W., Huang, K. -F., Umling, N.E., Guo, W., Yu, J., Curry, W.B., Marchitto, T.M., Wang, S., 2023. Deglacial Temperature and Carbonate Saturation State Variability in the Tropical Atlantic at Antarctic Intermediate Water Depths. Paleoceanog and Paleoclimatol 38, e2023PA004674. https://doi.org/10.1029/2023PA004674

Poggemann, D. -W., Nürnberg, D., Hathorne, E.C., Frank, M., Rath, W., Reißig, S., Bahr, A., 2018. Deglacial Heat Uptake by the Southern Ocean and Rapid Northward Redistribution Via Antarctic Intermediate Water. Paleoceanog and Paleoclimatol 33, 1292–1305. https://doi.org/10.1029/2017PA003284

Rühlemann, C., Mulitza, S., Lohmann, G., Paul, A., Prange, M., Wefer, G., 2004. Intermediate depth warming in the tropical Atlantic related to weakened thermohaline circulation: Combining paleoclimate data and modeling results for the last deglaciation. Paleoceanography 19, 2003PA000948. https://doi.org/10.1029/2003PA000948

Weldeab, S., Friedrich, T., Timmermann, A., Schneider, R.R., 2016. Strong middepth warming and weak radiocarbon imprints in the equatorial Atlantic during Heinrich 1 and Younger Dryas. Paleoceanography 31, 1070–1082. https://doi.org/10.1002/2016PA002957

Appendix 1 – Congress Abstracts

PhD Days GLOMAR – June 2022 (Bremen, Germany) - POSTER

Changing intermediate water conditions off NW Africa during the last deglaciation

Barragán-Montilla, Sofía[1]; Mulitza, Stefan [1]: Johnstone, Heather J. H.[1]; Pälike, Heiko[1]
[1]MARUM – Center for Marine Environmental Sciences, University of Bremen
*Corresponding author: sobarraganmo@gmail.com

The modern Atlantic Meridional Overturning Circulation (AMOC) plays a key role in global climate balance by redistributing the heat absorbed by the ocean, thus pacing global warming. However, climatic models suggest a potential AMOC slowdown during the 21st century, making it relevant to understand the impact such an event will suppose on global warming in the future. Since the end of the Last Glacial Maximum 19 kyrs BP, changes in the strength of AMOC have been registered in the geological record, offering the possibility to directly study this phenomenon. More specifically, AMOC was nearly shutdown during the Heinrich Stadial 1 (HS1; 17.5 – 14.8 kyrs BP) and an important decline is registered during the Younger Dryas (YD: 12.8 – 11.5 kyrs BP). In this study, we analyse benthic foraminifera distribution and geochemical proxies from core GeoB9512-5 (790 m depth) of north-western Africa. This multiproxy dataset covers the last 30 kyrs, allowing us to observe how ocean heat-uptake and redistribution were affected by AMOC slowdown. The results suggest poor ventilation of bottom waters in times of reduced AMOC, leading to intense warming and heat-uptake stagnation from the HS1 through the Bølling–Allerød period into the YD, at the same time benthic foraminifera register a decrease in dissolved oxygen concentration. This points to a reduced capacity of the ocean to store heat at intermediate depths at the same time heat redistribution decreased. Such a response suggests that a potential slowdown of AMOC in the future can lead to enhanced global warming and ocean deoxygenation.

MARUM Cluster Retreat 2022 (Bremen, Germany) – POSTER

DEGLACIAL CHANGES IN INTERMEDIATE WATER VENTILATION OF NW AFRICA

S. Barragán-Montilla, S. Mulitza, H. J. H. Johnstone, H. Pälike

What if the heat redistribution from the North Atlantic stopped? Climatic models show that a potential slowdown of the Atlantic Meridional Overturning Circulation (AMOC) in the 21st century can have serious implications for global warming if ocean heat uptake decreases.

Funded by DFG Deutsche Forschungsgemeinschaft German Research Foundation
marum Zentrum für Marine Umweltwissenschaften Universität Bremen
University of Bremen
GLOMAR Bremen International Graduate School for Marine Sciences

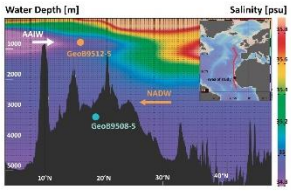

THE CORES (1)

Benthic foraminifera were extracted from sites GeoB9512-5 (790 m water depth) and GeoB9508-5 (2.384 m WD) from the Mauritanian shelf.

We used sediments from the top 5,5 m of GeoB9512-5 and 3,8 m of GeoB9508-5 deposited in the last deglacial cycle (27 kyrs to present).

The age model was estimated with Bacon in R, from 16 radiocarbon dates of planktic foraminifera for GeoB9512-5 and 11 for GeoB9508-5.

BENTHIC FORAMINIFERA: DEEPWATER RECORDERS (2)

These unicellular microscopic organisms live on the seafloor and produce a test in "chemical equilibrium" with the sorrounding water. By extracting this chemical print we can estimate how deep ***bottom water* (BW)** properties have change through time.

This research uses **(1)** $\delta^{13}C$ to reconstruct BW ventilation **(2)** $\delta^{18}O$ to estimate salinity along with **(3)** ***Bottom Water Temperatures* (BWT)** calculated from Mg/Ca ratios and **(4)** Benthic Foraminifera taxonomical and quantitative analyses to observe paleoecological changes.

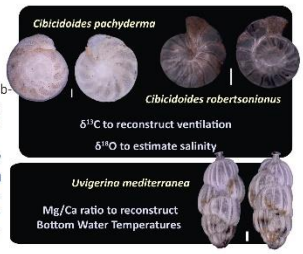

BOTTOM WATER WARMING IN TIMES OF REDUCED VENTILATION (4)

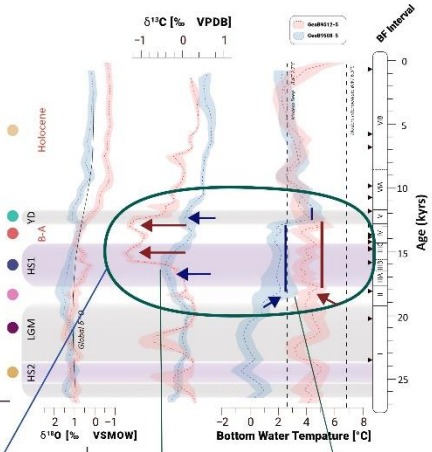

$\delta^{13}C$ from HS1 and B-A show decreased ventilation due to AMOC slowdown. Lighter $\delta^{13}C$ on core GeoB9512-5 is potentially also influenced by higher trophic level conditions.

BWT changes are more intese in deep settings: in times of reduced AMOC, heatuptake decreases and becomes stagnated for 5.4 kyrs in the HS1 and 2.5 kyrs in the YD.

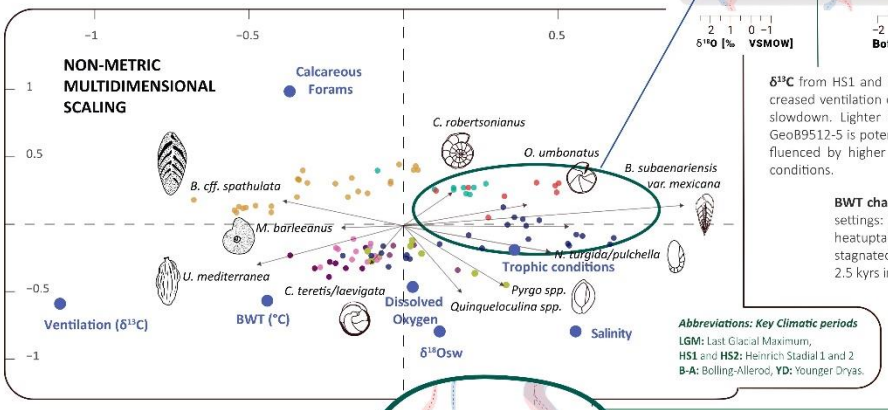

Abbreviations: Key Climatic periods
LGM: Last Glacial Maximum,
HS1 and **HS2:** Heinrich Stadial 1 and 2
B-A: Bolling-Allerod, **YD:** Younger Dryas.

PALEOECOLOGY GeoB9512-5 (3)

Benthic foraminifera distribution is controlled by BW environmental parameters influenced by major climate shifts in the Northern hemisphere:

- Moderate diversity occurs in times of eutrophia and low oxygenation during warmer periods (post-LGM, B-A, upper Holocene) and the midlle of the HS1
- High diversity characterized colder periods (LGM, HS1, and YD) when BW were mesotrophic and better oxygenated.
- Salinity was relatively higher before the Holocene.

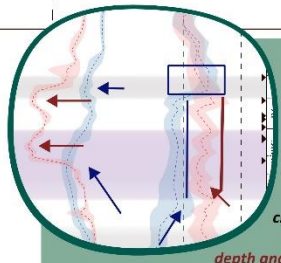

WHAT DID WE FIND? (5)

Reduced ventilation from the HS1- YD related to AMOC slowdown coincide with BWT decrease at intermediate depths suggesting heat is no longer being stored here since the end of the LGM. Effects at deep waters are more enhanced and in an AMOC slowdown scenario like the predicted for the 2st century (similar to the YD), ***heat uptake decreases and stops for 2.4 kyrs in times of reduced ventilation.***

Our results show that AMOC has the potential to set the depth and rate at which heat is stored in the Ocean, and a slowdown can decrease ocean heat uptake contributing to global warming.

@Alleblack
sofiabm93

ACKNOWLEDGEMENTS

This research is funded by the "Deutsche Forschungsgemeinschaft" (DFG) through the Cluster of Excellence "The Ocean Floor – Earth's Uncharted Interface" at MARUM Institute. Sample material has been provided by the GeoB Core Repository at the MARUM, Stable Isotope measurements were carried out at the MARUM Stable Isotope Laboratory, and Mg/Ca measurements were made by Heather J. H. Johnstone from the Paleoceanography Group of the MARUM Institute. Radiocarbon dating was runned by the MICADAS (Mini Carbon Dating System) Laboratory from the Alfred Wegener Institute in Bremerhaven. Microfossil images were taken at the Microscopy Laboratory at MARUM. This research is also supported by GLOMAR – Bremen International Graduate School for Marine Sciences, University of Bremen. The first author would like to thank the GeoLatinas organization for their support and feedback.

ICP14: 14th International Conference on Paleoceanography – August 2022 (Bergen, Norway) -POSTER

Deglacial changes in intermediate water ventilation off NW Africa

Barragán-Montilla, Sofía[1]; Mulitza, Stefan [1]; Johnstone, Heather J. H.[1]; Pälike, Heiko[1]

[1]MARUM – Center for Marine Environmental Sciences, University of Bremen
*Corresponding author: sobarraganmo@gmail.com

A multiproxy approach using benthic foraminifera assemblages, Mg/Ca ratios and stable isotope measurements, suggests that decreased ventilation during the Heinrich Stadial 1 in times of reduced Atlantic Meridional Overturning Circulation led to a cooling of intermediate waters in the Northeastern Atlantic. The records come from site GeoB9512-5 (790 m water depth), and Mg/Ca measurements in *Uvigerina mediterranea* indicate paleotemperatures of 3.8°C, 0.6°C lower than those observed during the Last Glacial Maximum. This was followed by a warming event (to 4.3°C) from the terminal part of the late Heinrich Stadial 1 (15.7 ka BP) that persisted for approximately 1.3 ka.

Intensely reduced ventilation during Heinrich Stadial 1 is interpreted from $\delta^{13}C$ measured in *Cibicidoides* sp. and is associated with eutrophic conditions represented by increased abundances of infaunal foraminifera like *U. mediterranea* and *Bolivina subaenariensis.* Subsequently, bottom water temperatures drop below 3.5°C during the Younger Dryas, at the same time ventilation was shortly reduced and conditions became mesotrophic, as shown by abundant *Melonis barleeanus* and *Cibicidoides robertsonianus*. This cooling was followed by relative temperature stability (3.1 °C on average) over the last ~10 ka, when bottom water ventilation improved as Atlantic Meridional Overturning Circulation increased. These results illustrate the impact of changing Atlantic Meridional Overturning Circulation on intermediate water properties and sets an important precedent for future studies of ocean circulation - climate dynamics in the eastern North Atlantic

EGU General Assembly April, 2023 (Vienna, Austria *Online*) – ORAL PRESENTATIONS

EGU23-2109 – Session SSP1.5
https://doi.org/10.5194/egusphere-egu23-2109

Response of benthic foraminiferal assemblages off NW Africa to climate change during the past 27.000 years

Barragán-Montilla, Sofía[1]; Mulitza, Stefan [1]: Johnstone, Heather J. H.[1]; Pälike, Heiko[1]

[1]MARUM – Center for Marine Environmental Sciences, University of Bremen
*Corresponding author: sobarraganmo@gmail.com

Benthic foraminifera (BF) typically constitute around 50% of the eukaryotic biomass of seafloor environments and are excellent recorders of bottom water environmental and geochemical changes in the past. In the last 27.000 years, major climatic oscillations including the Heinrich Stadial 1 (HS1), Bølling–Allerød (B-A) and Younger Dryas (YD) shaped the climate of a big part of the northern hemisphere. Although the response of the ocean surface to these events is well documented, information about the response of benthic ecosystems is still limited.

To better understand how BF responded to major climatic shifts in the last 27.000 years, we analyzed the benthic foraminifera content from core GeoB9512-5 (15°29.90'N/17°56.88'W, 793 m water depth) off NW Africa. Our high-resolution sediment record covers the last 27.000 years of the eastern North Atlantic, including the Heinrich Stadial 2 (HS2), Last Glacial Maximum (LGM), HS1, B-A and YD.

Taxonomic and quantitative analyses were used to reconstruct changes in bottom water oxygenation and organic matter fluxes and show that BF assemblages shifted in coincidence with the major climatic periods documented for the North Atlantic. After the LGM, Bottom water salinity, oxygenation and quantity/quality of organic matter played a major role in BF distribution and are linked to transient changes in BF diversity in the last 27.000 years.

The LGM showed no major diversity changes for thousands of years, while BF distribution shifted rapidly during HS1, B-A and YD. Low-diversity intervals during the HS1, B-A and the last 6.000 years are typically dominated by stress species in times of oxygen decrease and high organic matter content at bottom waters. These short intervals (typically lasting 500-1300 years) are commonly intercalated by low-duration high-diversity periods, associated with higher bottom water oxygenation and relatively lower organic matter content. Additionally, relatively abundant porcelaneous BF during HS1, LGM and HS1 indicate relatively higher salinity than the observed in the last 14.000 years.

Our results show that BF at intermediate depths at the NE Atlantic off NW Africa are strongly influenced by changes in bottom water paleoenvironmental conditions potentially linked to major climatic events. Bottom water oxygenation played a major role in BF diversity, observed by alternating low-diversity periods in times of low oxic conditions and high-diversity intervals in high oxic bottom waters. At the same time, bottom water salinity favored porcelaneous BF distribution during LGM and HS1 times and increasing hyaline-calcareous BF show decreased salinity in this part of the NE Atlantic after the end of the HS1.

How to cite: Barragán-Montilla, S., Mulitza, S., Johnstone, H. J., and Pälike, H.: Response of benthic foraminiferal assemblages off NW Africa to climate change during the past 27.000 years, EGU General Assembly 2023, Vienna, Austria, 24–28 Apr 2023, EGU23-2109, https://doi.org/10.5194/egusphere-egu23-2109, 2023.

EGU23-5172, Session EOS1.1
https://doi.org/10.5194/egusphere-egu23-5172

GeoLatinas: bringing down the language barrier to increase Latin American representation and democratize science communication in Earth and Planetary Sciences

Sofía Barragán-Montilla[1,2], Daniela Navarro-Perez[1,3,4], Adriana Guatame-Garcia[1,5], Dariana Isamel Avila-Velasquez[1,6], Grisel Jimenez Soto[1,7], and Rocio Paola Caballero-Gill[1,8]

[1]GeoLatinas – Latinas in Earth and Planetary Sciences
[2]MARUM –Center for Marine Environmental Sciences, University of Bremen, Bremen, Germany
[3]School of Earth and Environment, University of Leeds, UK
[4]Chemical Engineering Department, Universidad de Magallanes, Chile
[5]Department of Geological Sciences and Geological Engineering, Queen's University, Kingston, ON, Canada
[6]IIAMA - Institute of Water and Environmental Engineering, Universitat Politècnica de València, Spain
[7]Centre for Subsurface Imaging, Institute of Hydrocarbon Recovery, Universiti Teknologi PETRONAS, Malaysia
[8]Department of Atmospheric, Oceanic and Earth Sciences, George Mason University, VA, USA

GeoLatinas is a member-driven organization that inspires, embraces and empowers Latinas to thrive in Earth and Planetary Sciences (E&PS) by creating initiatives to address and overcome career progression barriers for the representation of the Latin American community. The GeoLatinas' **Voice your needs** survey, conducted in English and Spanish, showed in 2020 that many respondents in our community (42%) found language barrier as one of the most pressing issues.

Perceiving English as the main communication language in the science community creates a barrier for non-native English speakers, hindering their inclusion and representation. Bilingual education in Latin American schools is uncommon. The high cost of learning and obtaining proof of English proficiency, results in limited access to higher education. The English barrier is also a challenge when publishing in indexed journals or presenting research at international events. Consequently, education and employment opportunities for aspiring scientists and professionals decrease.

GeoLatinas transforms the language barrier into an opportunity by communicating in English, Spanish, and Portuguese, thus contributing to a diverse E&PS community. Specifically, we continuously develop strategies to overcome language-related issues like: (1) English as a requirement for inclusion and recognition in the science community; (2) lack of access to opportunities for Non-English speaking experts and non-experts; and (3) limited recognition of Latin American scientists' work.

Initiatives addressing the first issue include ***Conversando con GeoLatinas*** (Chatting with GeoLatinas), a space to improve English and Spanish conversational skills; **Dry Runs & Peer Review***,* a comprehensive database of native English, Spanish and Portuguese-speaking reviewers, allowing members to receive feedback on written and oral pieces; and **GeoSeminars,** where leaders of *GeoLatinas por Mexico* host presentations in Spanish and English, with diverse experts sharing their knowledge with a broader community online. Lastly, collaborations with *Nature Reviews Earth and Environment* help our members publish short scientific articles in English, and Spanish or Portuguese. Regarding the second issue, the **GeoLatinas Blog** gives members and invited experts a platform to share their research and thoughts on diverse topics in blogs available in our three languages. In addition, GeoLatinas has fostered partnerships for specific translations to Spanish, such as Eos.org short science articles (with science communication production entity *Planeteando*); and also to English, like the booklet *GEAS: Women who study the Earth* (with the ENGIE project). Confronting the third issue, the GeoLatinas' social-media based initiative **Friday Feature in Geo** has broadcasted over 160 profiles highlighting the work and contributions of Latinas in E&PS across all career stages. Together with the **GeoLatinas around the world** podcast in Spanish and Portuguese, we inspire and inform new generations, sharing funding opportunities and experiences from latinx scholars.

As a multicultural organization, we see strength in our differences and leverage them diversifying the E&PS. Together, we nurture our multilingual communication skills and use them as high-value traits for the scientific community. By embracing our heritage and communicating science in our native languages, GeoLatinas brings down the language barrier, democratizes science communication and increases Latin American representation in science.

How to cite: Barragán-Montilla, S., Navarro-Perez, D., Guatame-Garcia, A., Avila-Velasquez, D. I., Jimenez Soto, G., and Caballero-Gill, R. P.: GeoLatinas: bringing down the language barrier to increase Latin American representation and democratize science communication in Earth and Planetary Sciences, EGU General Assembly 2023, Vienna, Austria, 23–28 Apr 2023, EGU23-5172, https://doi.org/10.5194/egusphere-egu23-5172, 2023.

Paper in Review at Community Science Journal: **GeoTraductores: a Collaborative Initiative Democratizing Science Communication in Latin America.**

Daniela Navarro-Perez (University of Leeds) (corr-auth)
Anthony Ramírez-Salazar (Universidad Nacional Autónoma de México)
Sofía Barragán-Montilla (University of Bremen)
Mariela Garcia Arredondo (University of Massachusetts Amherst)
Nelmary Rodríguez Sepúlveda (University of California)
Oriana Venturi Herrera (IFP School)
Angelique Rosa Marín (University of South Florida)
Mónica Alejandra Gómez Correa (Universität Hamburg)
Caryl-Sue Micalizio (AGU)
Bernardo A. Bastien-Olvera (University of California San Diego)

MARUM Cluster Retreat June, 2023 (Bremen, Germany) - POSTER

ENVIRONMENTAL CONTROLS ON BENTHIC FORAMINIFERA Mg/Ca: RECONSTRUCTING DEGLACIAL BOTTOM WATER TEMPERATURES IN THE NE ATLANTIC

S. Barragán-Montilla, S. Mulitza, H. J. H. Johnstone, H. Pälike

Benthic Foraminifera Mg/Ca is a widely used proxy to reconstruct Bottom Water Temperatures (BWT) of the past. As Uvigerina is the most employed species in the deep N Atlantic ocean, challenges arise when paleodepth and other paleoenvironmental changes limit this species occurrence. Here we explore other benthic foraminifera as potential paleothermometers of the NE Atlantic to observe how other environmental parameters affect Mg uptake inducing error in paleotemperature reconstructions.

Funded by DFG Deutsche Forschungsgemeinschaft German ResearchFoundation
marum Zentrum für Marine Umweltwissenschaften Universität Bremen
University of Bremen
GLOMAR Bremen International Graduate School for Marine Sciences

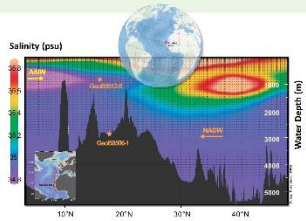

(1) THE CORES

Benthic foraminifera were extracted from sites GeoB9512-5 (9512, 790 m water depth) and GeoB9506-1 (9506, 2.956 m WD) off the Senegal coast.

We used sediments from the top 5,5 m of GeoB9512-5 and 2,6 m of GeoB9506-1 deposited during the last deglacial cycle (27 kyrs to present).

For the age model, 16 radiocarbon dates of planktic foraminifera for 9512 and 12 for 9506 were processed using Bacon in RStudio.

(2) BENTHIC FORAMINIFERA: DEEPWATER RECORDERS

These unicellular microscopic organisms live on the seafloor and produce a test in "chemical equilibrium" with the surrounding water. By extracting this chemical print we can estimate how deep bottom water (BW) properties have change through time.

This research uses (1) $\delta^{13}C$ to reconstruct BW ventilation (2) $\delta^{18}O$ to estimate salinity along with (3) Bottom Water Temperatures (BWT) calculated from Mg/Ca ratios and (4) Benthic Foraminifera taxonomical and quantitative analyses to observe paleoenviromental changes.

(3) PALEOECOLOGY

Benthic foraminifera distribution is controlled by BW environmental parameters mainly oxygen and nutrient variability.

At intermediate waters (9512) benthic foraminifera assemblages were highly variable, and change in coincidence with the key climatic periods from the last 28 kyrs, seen as alternating High Oxic - Low Oxic periods with trophic levels transient shifts.

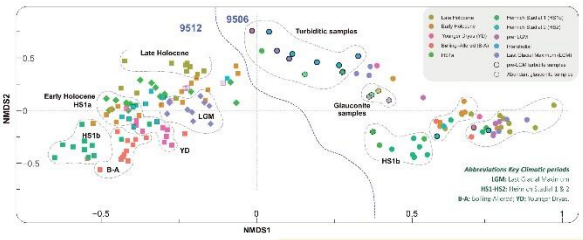

Deeper waters (9506) are characterized by strong mesotrophic-eutrophic conditions and persistent low-oxic BW environments (only High oxic from 4.6 – 9.3 Kyrs). No major changes is seen in the assemblage composition, being *U. peregrina* the dominant species.

(4) BENTHIC FORAMINIFERA Mg/Ca from site 9512

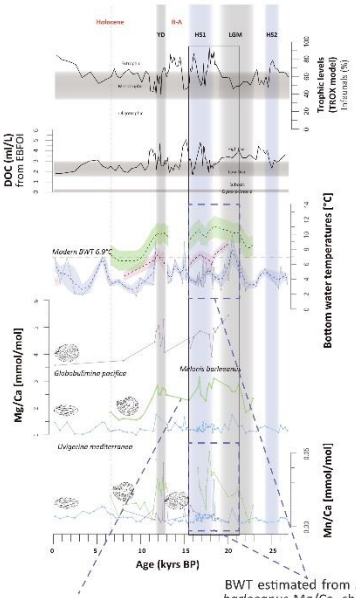

BWT offset increase between *M. barleeanus* and *U. mediterranea* coincides with increasing Mn/Ca a proxy commonly used for benthic Foraminifera microhabitat depth.

BWT estimated from *M. barleeanus* Mg/Ca, show similar trends at the start of LGM and after the YD. The second part of the LGM and HS1 show different trends and larger offset compared to *U. mediterranea* BWT.

(5) WHAT DID WE FIND?

For site 9506, BWT from *M. barleeanus* and *U. peregrina* are similar. In addition, Mn/Ca from both species show similar trends--> no significant microhabitat migration is observed.

This suggests that Mg/Ca uptake of *M. barleeanus* **on site 9512** ***can be linked to microhabitat depth migration as a response to bottom water oxygen variability during the LGM and HS1.***

Also important to note: although BWT on site 9506 from both species is in the same range, *M. barleeanus* BWT during the LGM and HS1 show a 1°C **warming,** while *Uvigerina* BWT show up to a 6°C **cooling** in the LGM and 2°C variability during the HS1.

Our results leave 2 questions: (1) Did environmental conditions during the LGM and HS1 affected M. barleeanus microhabitat depth in the NE Atlantic? and if so, does this affect other Benthic Foraminifera and the trace element signal in their tests?

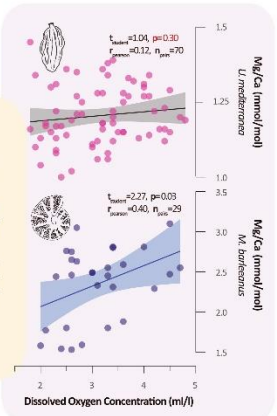

@Alleblack
sofiabm93
scicoforams.com

ACKNOWLEDGEMENTS

This research is funded by the "Deutsche Forschungsgemeinschaft" (DFG) through the Cluster of Excellence "The Ocean Floor – Earth's Uncharted Interface" at MARUM Institute.Sample material has been provided by the GeoB Core Repository at the MARUM, Stable Isotope measurements were carried out at the MARUM Stable Isotope Laboratory, Radiocarbon dating was runned by the MICADAS (Mini Carbon Dating System) Laboratory from the Alfred Wegener Institute in Bremerhaven. Microfossil images were taken at the Microscopy Laboratory at MARUM. This research is also supported by GLOMAR – Bremen International Graduate School for Marine Sciences, University of Bremen. The first author thanks the GeoLatinas organization for their support and feedback.

If you have any questions or comments you can get in touch via email at sbarraganmontilla@marum.de

International Symposium on Foraminifera FORAMS, June 2023 (Perugia, Italy) – **Awarded Best Student Oral Presentation**

Benthic foraminiferal palaeothermometry in deglacial sediments off NW Africa: how accurately is Mg/Ca recording bottom water temperature changes in the past?

Barragán-Montilla, Sofía[1]; Johnstone, Heather J. H.[1]; Mulitza, Stefan 1; Pälike, Heiko[1]

[1]MARUM – Center for Marine Environmental Sciences, University of Bremen
*Corresponding author: sobarraganmo@gmail.com

The need to reconstruct deep water temperatures to understand the role of ocean circulation in the climate system has drawn growing interest in using Mg/Ca of benthic foraminifera as a paleotemperature proxy. There are now several bottom water temperature (BWT) records published for timescales of thousands to millions of years. Many of these records are based on the common deep-sea infaunal foraminifera genus *Uvigerina,* with numerous core top calibrations from different areas of the Atlantic and Pacific oceans.

However, low recovery and poor preservation of this genus in shallower sites, or specific environmental conditions in the geological record that limit the occurrence of *Uvigerina,* make it necessary to investigate other species groups as potential bottom water paleothermometers. Intermediate to deep infaunal foraminifera like *Cassidulina* spp., *Nonion* spp., *Globobulimina* spp., and *Melonis barleeanus* have been used in paleotemperature reconstructions of the (mainly western) North Atlantic and the Nordic seas.

Benthic foraminifera Mg/Ca is sensitive not just to temperature, but also to other environmental parameters and parallel records may isolate confounding factors. In this research we tested the potential of Mg/Ca ratios of common intermediate infaunal *Melonis barleeanus* and deep infaunal *Globobulimina turgida* from site GeoB9512-5 (water depth 794 m) in the tropical East Atlantic, to reconstruct BWT changes at intermediate depths during the last deglaciation. In the process, we evaluated the possible correlation of other paleoenvironmental factors affecting Mg/Ca uptake from these species that could influence paleotemperature reconstructions.

The comparison of Mg/Ca ratios and BWT estimates from *Melonis barleeanus* and *Globobulimina turgida* with *Uvigerina mediterranea* records, show that *M. barleeanus* does not record the same Mg/Ca-based paleotemperatures as *U. mediterranea* and *G. turgida*, furthermore no fixed offset can be calculated. Our Mn/Ca data suggests, that as *U. mediterranea* and *G. turgida*, remain at relatively constant depths in the sediment, *M. barleeanus* seem to have migrated vertically due to bottom water oxygenation and trophic levels variability**, potentially affecting Mg uptake during calcification**. Moreover, a strong correlation between Mn/Ca and Mg/Ca from *M. barleanus* and low correlation of these two parameters in *U. mediterranea* supports our findings. This suggests that *M. barleeanus* is not a suitable species for paleotemperature reconstructions in the NE Atlantic and highlights the importance of local Mg/Ca calibrations and multi-species measurements in paleoceanographic studies.

EGU General Assembly April 2024 (Vienna, Austria) – ORAL PRESENTATIONS

Session SSP4.1
https://doi.org/10.5194/egusphere-egu24-3023

Deglacial North Eastern Atlantic Oxygen Minimum Zone changes registered by Benthic foraminifera

Sofía Barragán Montilla[1] and Dharma A. Reyes Macaya[1,2,3]

[1]University of Bremen, MARUM, FB5, Bremen, Germany (sobarraganmo@gmail.com)
[2]Lyell Centre, Heriot-Watt University, Edinburgh, UK
[3]Millennium Nucleus UPWELL, Concepcion, Chile

The eastern north Atlantic hosts a volumetrically important oxygen minimum zone (OMZ) influenced by the subtropical ocean circulation in the area and the upwelling off NW Africa. Ocean warming related to the increase in greenhouse gases and coastal eutrophication due to anthropogenic activity, leads to ocean deoxygenation and OMZs expansion. This makes relevant to study of the north Atlantic middle depth variability analogs in past climate change scenarios, to understand the future of the north Atlantic OMZ. During this study, we used benthic foraminifera from site GeoB9512-5 (793 m water depth) off NW Africa to reconstruct the bottom water oxygen concentration changes in the north Atlantic OMZ during the last 27,000 years. This high-resolution record registered an enhanced OMZ during the Bølling–Allerød (B-A) and Holocene that declined during the Heinrich Stadial 1 (HS1) and Younger Dryas (YD). These shifts are related to changes in bottom water ventilation and organic matter concentrations during the last deglaciation. Low benthic foraminifera diversity is synchronous with the oxygen decline of the B-A and Holocene, and benthic foraminifera assemblages show relevant changes consistent with these oxygenation shifts seen in our site. We provide new evidence of potential north Atlantic OMZ expansion in times of reduced bottom water ventilation during the B-A and Holocene times. These changes were driven by the shifts in the subtropical circulation during the last deglaciation registered in previous studies, and are relevant for understanding the

future of OMZs in a climate change scenario and its possible consequences for marine biodiversity.

How to cite: Barragán Montilla, S. and Reyes Macaya, D. A.: Deglacial North Eastern Atlantic Oxygen Minimum Zone changes registered by Benthic foraminifera, EGU General Assembly 2024, Vienna, Austria, 14–19 Apr 2024, EGU24-3023, https://doi.org/10.5194/egusphere-egu24-3023, 2024.

Session EOS1.8

https://doi.org/10.5194/egusphere-egu24-15895

GeoTraductores: one translation at a time

Daniela Navarro-Perez[1,2,3], Anthony Ramírez-Salazar[4,5], **Sofía Barragán-Montilla**[6,2], Mariela Garcia Arredondo[7,2], Caryl-Sue Micalizio[8], Angelique Rosa Marín[9,2], and María Alejandra Gómez Correa[10,2]

[1]University of Leeds, School of Earth and Environment, Leeds, United Kingdom of Great Britain.
[2]GeoLatinas - Latinas in Earth and Planetary Sciences.
[3]Departamento de Ingenieria Quimica, Universidad de Magallanes, Chile.
[4]Instituto de Geología, Universidad Nacional Autónoma de México, Mexico City, Mexico.
[5]Estudios Planeteando, Mexico City, Mexico.
[6]MARUM –Center for Marine Environmental Sciences, University of Bremen, Bremen, Germany.
[7]School of Earth & Sustainability and Stockbridge School of Agriculture, University of Massachusetts Amherst, USA.
[8]Eos, AGU, Washington, D.C., USA.
[9]College of Marine Science, University of South Florida, Saint Petersburg, Florida, USA.
[10]Faculty of Mathematics, Informatics and Natural Sciences, Universität Hamburg, Hamburg, Germany.

GeoTraductores, a collaborative initiative involving Eos.org, GeoLatinas, and Planeteando, aims to overcome the language barrier in climate change and Earth science communication within Spanish-speaking communities. To accomplish this, science articles from Eos.org have been translated into Spanish by approximately 40 volunteers as part of the Eos en Español project. Around 85% of our team comprises Latin women, who have translated over 150 articles, contributing to expanding the Spanish-speaking audience of Eos.org and solidifying the initiative's success. This strategic translation effort not only enhances accessibility but also promotes the

representation of Latin American Early Careers Scientists, many of whom reside and work in predominantly English-speaking countries.

Since 2020, the GeoTraductores initiative has been co-led by (1) members of the non-profit organization GeoLatinas dedicated to embracing, empowering, and inspiring Latinas in Earth and Planetary Sciences; (2) Planeteando, a Mexican scientific and social outreach project in Earth and Environmental Sciences; and (3) Eos.org, the science news magazine published by AGU. Each party plays a distinct role in the initiative: (1) volunteer recruitment of translators is handled by GeoLatinas and Planeteando, (2) proofreading and editing of the translated articles is mainly led by Planeteando, and (3) the articles and platforms to make the final Spanish translation available are provided by Eos.org. In a broader effort, all involved collaborators utilize their social media platforms to make this bilingual content more accessible to a wider readership.

Throughout this initiative, the GeoTraductores volunteers benefit by improving their English and translation skills, gaining visibility on social media, and making an altruistic contribution to the Latin American general public. Collaborators also benefit from engaging and gaining a wider audience to communicate science, as they foster the capacity building of volunteers, promoting a science communication co-production, and boosting each other. Overall, GeoTraductores is forging a pathway to democratize science, particularly in Latin America. Through establishing and strengthening a network of expert bilingual science communicators, this initiative addresses historical language barriers that impede the accessibility and dissemination of scientific information to the general public. By empowering volunteers and embracing diversity, GeoTraductores paves the way for expanding multilingual spaces within Earth and Planetary sciences one translation at a time.

How to cite: Navarro-Perez, D., Ramírez-Salazar, A., Barragán-Montilla, S., Garcia Arredondo, M., Micalizio, C.-S., Rosa Marín, A., and Gómez Correa, M. A.: GeoTraductores: one translation at a time, EGU General Assembly 2024, Vienna, Austria, 14–19 Apr 2024, EGU24-15895, https://doi.org/10.5194/egusphere-egu24-15895, 2024.

Session SSP4.1
EGU24-7569, updated on 08 Mar 2024
https://doi.org/10.5194/egusphere-egu24-7569

Early Initiation of Tasman Leakage and the formation of modern Indian Ocean circulation

Jing Lyu[1], Sofia Barragán Montilla[2], Or Bialik[1], Beth Christensen[3], Gerald Auer[4], Anta-Clarisse Sarr[5,6], and David De Vleeschouwer[1]

[1]Institute of Geology and Paleontology, University Münster, Germany (j.lyu@uni-muenster.de)
[2]MARUM–Center for Marine Environmental Sciences, University of Bremen, Bremen, Germany
[3]Department of Environmental Science, School of Earth and Environment, Rowan University, Glassboro, NJ, USA
[4]Institute of Earth Sciences (Geology and Paleontology), University of Graz, Graz, Austria
[5]Department of Earth Sciences, University of Oregon Eugene, USA
[6]Univ. Grenoble Alpes, Univ. Savoie Mont Blanc, CNRS, IRD, Univ. Gustave Eiffel, ISTerre, 38000 Grenoble, France

The exchange of water between the Pacific and Indian Oceans is important in regulating planetary climate. North of Australia, this exchange plays a key role in regulating the Indo-Pacific Warm Pool with far-reaching effects via Indonesian Throughflow (ITF). The exchange south of Australia is far less understood, and much of the exchange occurs at intermediate depths through Tasman Leakage (TL). Here, we investigate Ocean Drilling Program (ODP) Site 752 which was drilled on Broken Ridge. The Site is located within the path of TL, and thus, can provide a paleoceanographic history of TL. Benthic foraminiferal (BF) assemblage is a useful tool to reconstruct paleoceanographic patterns. At ODP Site 752, BF assemblages vary over time but at no point exhibit evidence of extreme stress or oxygen deficiency. Benthic foraminiferal diversity measured with the Fischer Alpha diversity index remains between 5 and 10, indicating moderate diversity throughout the last 9 million years. Furthermore, the high abundance of epiphytic species *Cibicidoides wuellerstorfi* and *Lobatula lobatula* likely reflects a high current energy environment over Broken Ridge during this time. Based on our comprehensive benthic foraminiferal assemblage study, we suggest that the driving factor behind the benthic ecological changes on Broken Ridge since the Late Miocene has been TL intensity, distinguished by its

kinetic energy. In addition, we present a ~13 Myr neodymium (Nd) isotopic record, suggesting that TL onset likely occurred sometime in the late Middle Miocene, advecting isotopically older Pacific-sourced waters into the Indian Ocean. The latter findings challenge the previously presumed onset of TL at ~7 Ma and indicate a much earlier initiation of TL between 14 – 10 Ma, that intensified during the Late Miocene when the modern-like TL was established.

How to cite: Lyu, J., Barragán Montilla, S., Bialik, O., Christensen, B., Auer, G., Sarr, A.-C., and De Vleeschouwer, D.: Early Initiation of Tasman Leakage and the formation of modern Indian Ocean circulation, EGU General Assembly 2024, Vienna, Austria, 14–19 Apr 2024, EGU24-7569, https://doi.org/10.5194/egusphere-egu24-7569, 2024.

The Micropaleontological Society (TMS)-Cushman Foundation of Foraminiferal Research (CFFR) Spring Meeting, May 2024 (Cologne, Germany) – **Awarded Best Poser Presentation**

Accelerated Subtropical Gyre in times of Atlantic Meridional Overturning Circulation oxygenated the eastern tropical North Atlantic Oxygen Minimum Zone during the last deglaciation: evidence from benthic foraminifera

Sofía Barragán Montilla[1,2]

[1]University of Bremen, MARUM, FB5, Bremen, Germany (sobarraganmo@gmail.com)
[2]GeoLatinas – Latinas in Earth and Planetary Sciences

Atlantic Meridional Overturning Circulation (AMOC) is projected to slow down over the 21st century, making it necessary to understand its relationship with ocean circulation processes that influence global climate. During the last deglaciation, AMOC slowdown resulted in decreased ventilation of the deep Atlantic. However, the response of the intermediate and subsurface circulation processes remains poorly understood. This gap in our knowledge introduces important challenges in climatic models, which in turn are unable to reproduce the mean shape and known trends of Atlantic Oxygen Minimum Zones. This is the case of the suboxic eastern Tropical North Atlantic Oxygen Minimum one (ETNA-OMZ) off the NW African margin. In this study, we used benthic foraminifera detailed taxonomy and quantitative analyses to reconstruct the oxygen concentrations changes of site GeoB9512-5 (793 m water depth) from the low oxic margin of the ETNA-OMZ. This new record registered oxygen changes in the last 27.000 years with an average age resolution of 270 years. We find that in times of reduced AMOC, in the Heinrich Stadial 1 (first between 17.5 and 16.4 ka BP; and then between 15.5 – 14.8 ka BP) and in the Younger Dryas-early Holocene (12.2 – 10.9 ka BP), the low oxic end of ETNA-OMZ became high oxic. Our findings suggest that during this time, the subtropical gyre circulation in the north Atlantic accelerated with steeper temperature gradients related to AMOC slowdown. This accelerated circulation provided more ventilated waters, bringing more oxygen at intermediate depths and oxygenating ETNA-OMZ. Our results provide new valuable information about subsurface circulation relationship to AMOC changes and puts forward evidence on the impact in Atlantic OMZs.

Appendix 1.1 – Recent Benthic from surface samples of the eastern tropical Atlantic

GeoB9512-4 (15.33, - 17.36; 787 m water depth)

1. *Bolivina* cff. *spathulata* (Williamson, 1858)
2. *Chilostomella oolina* Schwager, 1878
3. *Globobulimina turgida* (Bailey, 1851)
4. *Uvigerina peregrina* Cushman, 1923
5. *Glandulina ovula* d'Orbigny, 1846
6. *Vaginulina spinigera* Brady, 1881
7. *Vaginulina spinigera* Brady, 1881
8. *Vaginulina spinigera* Brady, 1881
9. *Valvulineria bradyana* (Fornasini, 1900)
10. *Cassidulina teretis* Tappan, 1951
11. *Planulina arimenensis* d'Orbigny, 1826
12. *Saracenaria italica* Defrance, 1824

GeoB9508-4 (15.49, - 17.95; 2,393 m water depth)

13. *Nodosaria cff. vertabralis* (Batsch, 1791)
14. *Uvigerina peregrina* Cushman, 1923
15. *Cibicidoides wuellerstorfi* (Schwager, 1866)
16. *Cibicidoides robertsonianus* (Brady, 1881)
17. *Cassidulina teretis* Tappan, 1951
18. *Valvulineria bradyana* (Fornasini, 1900)
19. *Hoeglundina elegans* (d'Orbigny, 1826)
20. *Melonis pompilioides* (Fichtel & Moll, 1798)
21. *Pyrgo murrhine* (Schwager, 1866)
22. *Melonis barleeanus* (Williamson, 1858)


9512-4
1a
1b
2a
2b
3a
3b
4a
4b
5a
5b
6a
6b
7a
7b
8a
8b
9a
9b
10a
10b
11a
11b
12a
12b
9508-4
13a
13b
14a
14b
15a
15b
15c
16a
16b
16c
17a
17b
18a
18b
18c
19a
19b
19c
20a
20b
20c
21a
21b
22a
22b
22c

GeoB9532-1 (8.95, - 14.89; 1,234 m water depth)

1. *Trifarina angulosa* (Williamson, 1858)
2. *Uvigerina peregrina* Cushman, 1923
3. *Globobulimina affinis* (d'Orbigny, 1839)
4. *Amphycoryna scalaris* (Batsch, 1791)
5. *Hanzawaia boueana* (d'Orbigny, 1846)
6. *Planorbulina* sp. d'Orbigny, 1826
7. *Spiroloculina depressa* d'Orbigny, 1826

GeoB9533-3 (8.92, - 14.91; 384 m water depth)

8. *Trifarina angulosa* (large) (Williamson, 1858)
9. *Amphycoryna scalaris* (Batsch, 1791)
10. *Bulimina aculeata* d'Orbigny, 1826
11. *Lenticulina iota* (Cushman, 1923)
12. *Cancris auriculus* (Fichtel & Moll, 1798)
13. *Ehrenbergina trigona* Goës, 1896
14. *Melonis barleeanus* (Williamson, 1858)
15. *Hoeglundina elegans* (d'Orbigny, 1826)

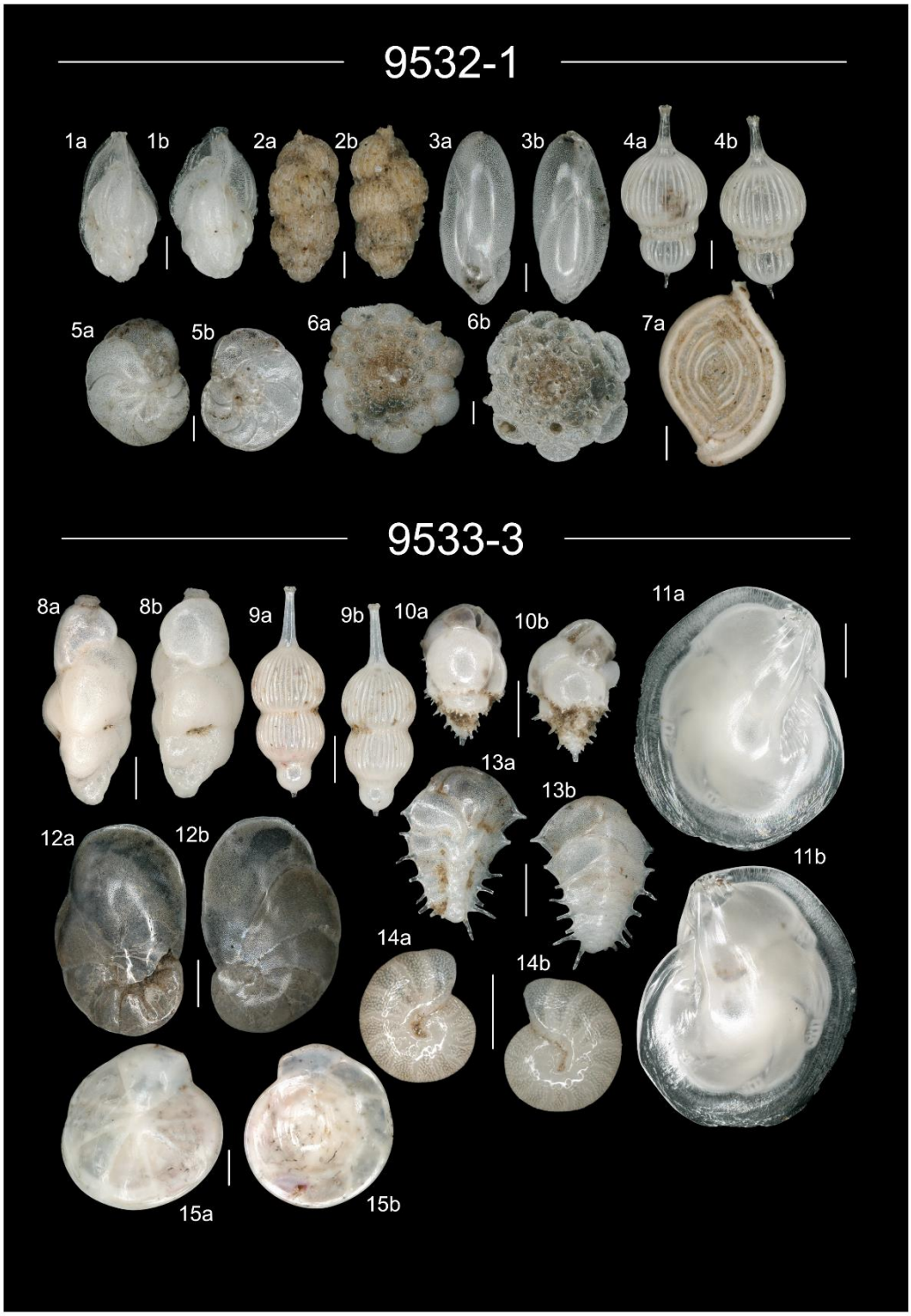
9532-1
1a
1b
2a
2b
3a
3b
4a
4b
5a
5b
6a
6b
7a
9533-3
8a
8b
9a
9b
10a
10b
11a
13a
13b
12a
12b
11b
14a
14b
15a
15b

GeoB9535-5 (8.87, - 14.96; 666 m water depth)

1. *Martinottiella communis* (d'Orbigny, 1846)
2. *Eggerella bradyi* (Cushman, 1911)
3. *Bulimina aculeata* d'Orbigny, 1826
4. *Bulimina striata* d'Orbigny in Guérin-Méneville, 1832
5. *Reophax* cff. *pilulifer* Brady, 1884
16. *Uvigerina* cff. *peregrina* Cushman, 1923
6. *Ceratobulimina contraria* (Reuss, 1851) †
7. *Heterolepa bradyi* (Trauth, 1918)

GeoB9529-1 (9.35, - 17.36; 1,234 m water depth)

8. *Rhizammina* cff. *algaeformis* Brady, 1879
9. *Rhizammina* cff. *algaeformis* Brady, 1879
10. *Rhizammina* cff. *algaeformis* Brady, 1879
11. *Rhizammina* cff. *algaeformis* Brady, 1879
12. *Rhizammina* cff. *algaeformis* Brady, 1879
13. *Rhizammina* cff. *algaeformis* Brady, 1879
14. *Rhizammina* cff. *algaeformis* Brady, 1879
15. *Rhizammina* cff. *algaeformis* Brady, 1879
16. *Rhizammina* cff. *algaeformis* Brady, 1879
17. *Uvigerina hispida* Schwager, 1866
18. *Uvigerina proboscidea* Schwager, 1866
19. *Uvigerina proboscidea* Schwager, 1866
20. *Melonis barleeanus* (Williamson, 1858)
21. *Pullenia bulloides* (d'Orbigny, 1846)
22. *Ceratobulimina contraria* (Reuss, 1851) †
23. *Osangularia culter* (Parker and Jones, 1865)
24. *Pullenia quinuqeloba* (Reuss, 1851)

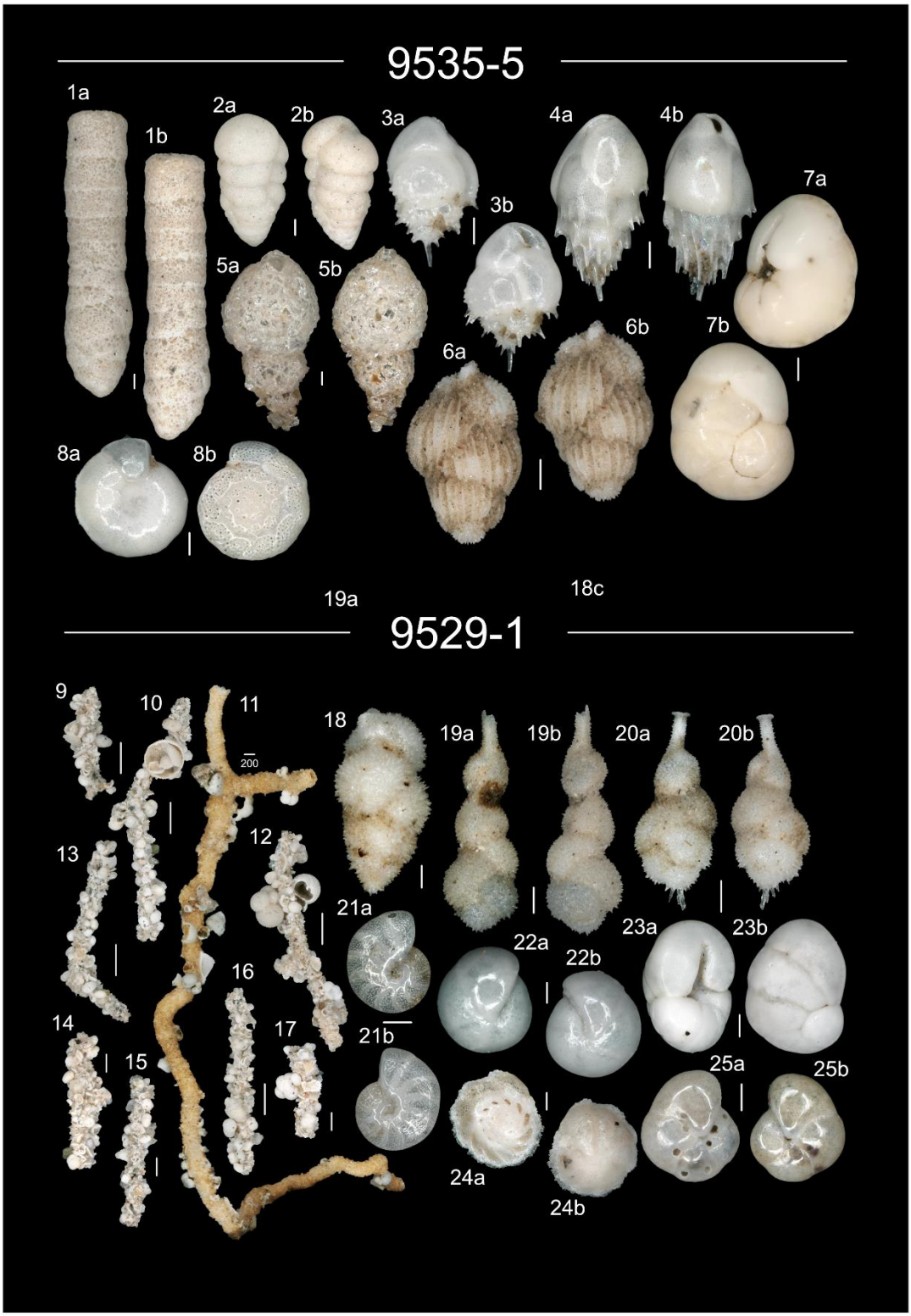
9535-5
1a
1b
2a
2b
3a
3b
4a
4b
5a
5b
6a
6b
7a
7b
8a
8b
19a
18c
9529-1
9
10
11
200
12
13
14
15
16
17
18
19a
19b
20a
20b
21a
21b
22a
22b
23a
23b
24a
24b
25a
25b

T89-16 (-5.70, 11.23; 826 m water depth)

1. *Virgulina subsquamosa* Egger, 1857
2. *Virgulina subsquamosa* Egger, 1857
3. *Saracenaria* sp. (d'Orbigny, 1846)
4. *Uvigerina* cff. *hispida* Schwager, 1866
5. *Rutherfordoides rotundatus* (Parr, 18950)
6. *Cibicidoides pachyderma* (Rzehak, 1886)
7. *Valvulineria bradyana* (Fornasini, 1900)
8. *Sphaeroidina bulloides* d'Orbigny, 1826
9. *Oridorsalis umbonatus* (Reuss, 1851)

T89-14 (-3.51, 9.69; 868 m water depth)

10. *Haplophragmium cff. fontinense* Reuss, 1860
11. *Karreriella bradyi* (Cushman, 1911)
12. *Uvigerina* cff. *peregrina* Cushman, 1923
13. *Globobulimina turgida* (Bailey, 1851)
14. *Globobulmina affinis* (d'Orbigny, 1839)
15. *Bulimina striata* d'Orbigny in Guérin-Méneville, 1832 –
16. *Chilostomella ovoidea* Reuss, 1850
17. *Virgulina subsquamosa* Egger, 1857
18. *Sphaeroidina bulloides* d'Orbigny in Deshayes,
19. *Valvulineria bradyana* (Fornasini, 1900)
20. *Melonis barleeanus* (Williamson, 1858)
21. *Cibicidoides pachyderma* (Rzehak, 1886)
22. *Cibicidoides robertsonianus* (Brady, 1881)

T89-12 (-5.2, 7.97; 4,068 m water depth)

23. *Cyclammina trullissata* (Brady, 1879)
24. *Buzasina galeata* (Brady, 1881)
25. *Eratidus foliaceus* (Brady, 1881)
26. *Ammodiscus incertus* (d'Orbigny, 1839)
27. *Haplophragmoides canariensis* (d'Orbigny, 1839)
28. *Lagenammina* sp. (Cushman, 1944)
29. *Eratidus foliaceus* (Brady, 1881)
30. *Ammoglobigerina globigeriniformis* (Parker and Jones, 1865)

31. *Haplophragmoides latidorsatus* (Bornemann, 1855)

32. *Lagenammina* sp. (Cushman, 1944)

33. *Ammodiscus incertus* (d'Orbigny, 1839)

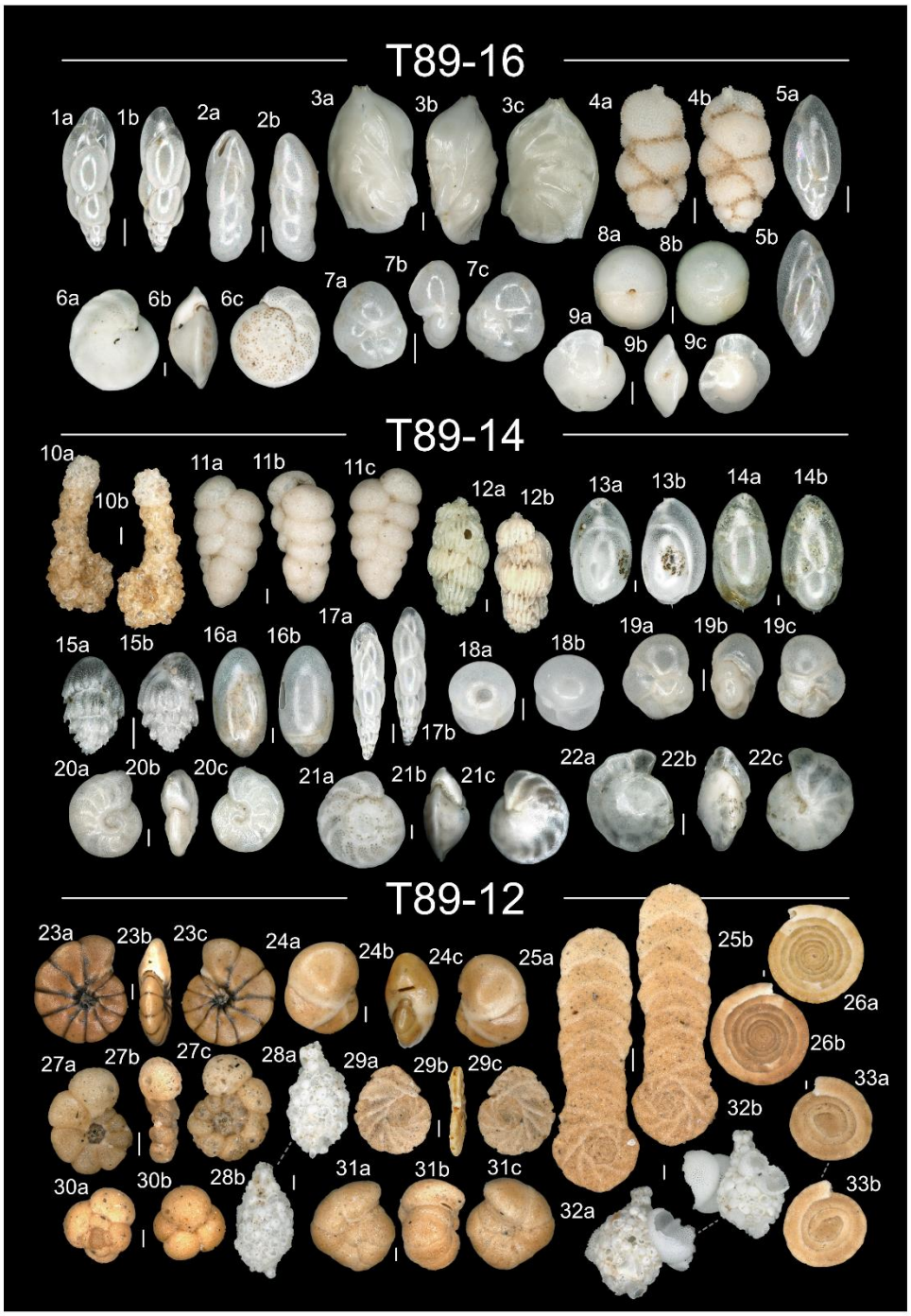

T89-22 (-7.1, 12.06; 200 m water depth)

1. *Textularia* sp. Defrance, 1824
2. *Textularia hystrix* Jones, 1994
3. *Bulimina striata* d'Orbigny in Guérin-Méneville, 1832
4. *Bulimina marginata* d'Orbigny, 1826
5. *Bolivina* sp. 1
6. *Uvigerina peregrina* Cushman, 1923
7. *Amphycoryna scalaris* (Batsch, 1791)
8. *Trifarina angulosa* (large) (Williamson, 1858)
9. *Cassidulina laevigata* d'Orbigny, 1826
10. *Lenticulina* cff. *cushmani* (Galloway & Wissler, 1927)
11. *Hoeglundina elegans* (d'Orbigny, 1826)

T89-21 (-7.3, 11.99; 490 m water depth)

12. *Liebusella intermedia* (van den Broeck, 1876)
13. *Ehrenbergina trigona* Goës, 1896
14. *Bulimina aculeata* d'Orbigny, 1826
15. *Chilostomella oolina* Schwager, 1878
16. *Bolivina* sp. 1
17. *Bolivina* cff. *spathulata* (Williamson, 1858)
18. *Rectuvigerina* cff. *elongatastriata* (Colom, 1952)
19. *Bolivina subaenariensis* var. *mexicana* Cushman, 1922
20. *Planulina ariminensis* d'Orbigny, 1826
21. *Spiroloculina depressa* d'Orbigny, 1826
22. *Cancris auriculus* (Fichtel & Moll, 1798)

T89-23 (-8.51, 12.10; 796 m water depth)

23. *Fursenkoina complanate* (Egger, 1893)
24. *Bolivina* sp. 1
25. *Bulimina striata* d'Orbigny in Guérin-Méneville, 1832
26. *Bulimina marginata* d'Orbigny, 1826
27. *Bolivina subaenariensis* var. *mexicana* Cushman, 1922


T89-22
1a
1b
2a
2b
3a
3b
4a
4b
5a
5b
6a
6b
7a
7b
8a
8b
9a
9b
10a
10b
11a
11b
T89-21
12
13a
13b
14a
14b
15a
15b
16a
16b
17a
17b
18a
18b
19a
19b
20a
20b
21a
21b
22a
22b
T89-23
23a
23b
24a
24b
25a
25b
26a
26b
27a
27b

T89-25 (-9.36, 10.44; 4,164 m water depth)

1. *Eratidus foliaceus* (Brady, 1881)
2. *Eratidus foliaceus* (Brady, 1881)
3. *Haplophragmium cff. fontinense* (Brady, 1881)
4. *Haplophragmium cff. fontinense* (Brady, 1881)
5. *Buzasina galeata* (Brady, 1881)
6. *Reophax* sp. Montfort, 1808
7. *Amphycoryna scalaris* (Batsch, 1791)
8. *Ammoglobigerina globigeriniformis* (Parker and Jones, 1865)
9. *Lagenammina* sp. (Cushman, 1944)
10. *Lenticulina* cff. *Cushmani* (Galloway & Wissler, 1927)
11. *Hormosina globulifera* Brady, 1879
12. *Haplophragmoides latidorsatus* (d'Orbigny, 1839)

T89-11 (-4.31, 6.45; 4,627 m water depth)

13. *Lagenammina arenulata* (Skinner, 1961)
14. *Lagenammina arenulata* (Skinner, 1961)
15. *Melonis pompilioides* (Fitchell and Moll, 1798)
16. *Pullenia bulloides* (d'Orbigny, 1846)
17. *Reophax* sp. Montfort, 1808
18. *Pyrgo murrhine* (Schwager, 1866)
19. *Pulenia quinqueloba* (Reuss, 1851)
20. *Epistominella exigua* (Brady, 1884)

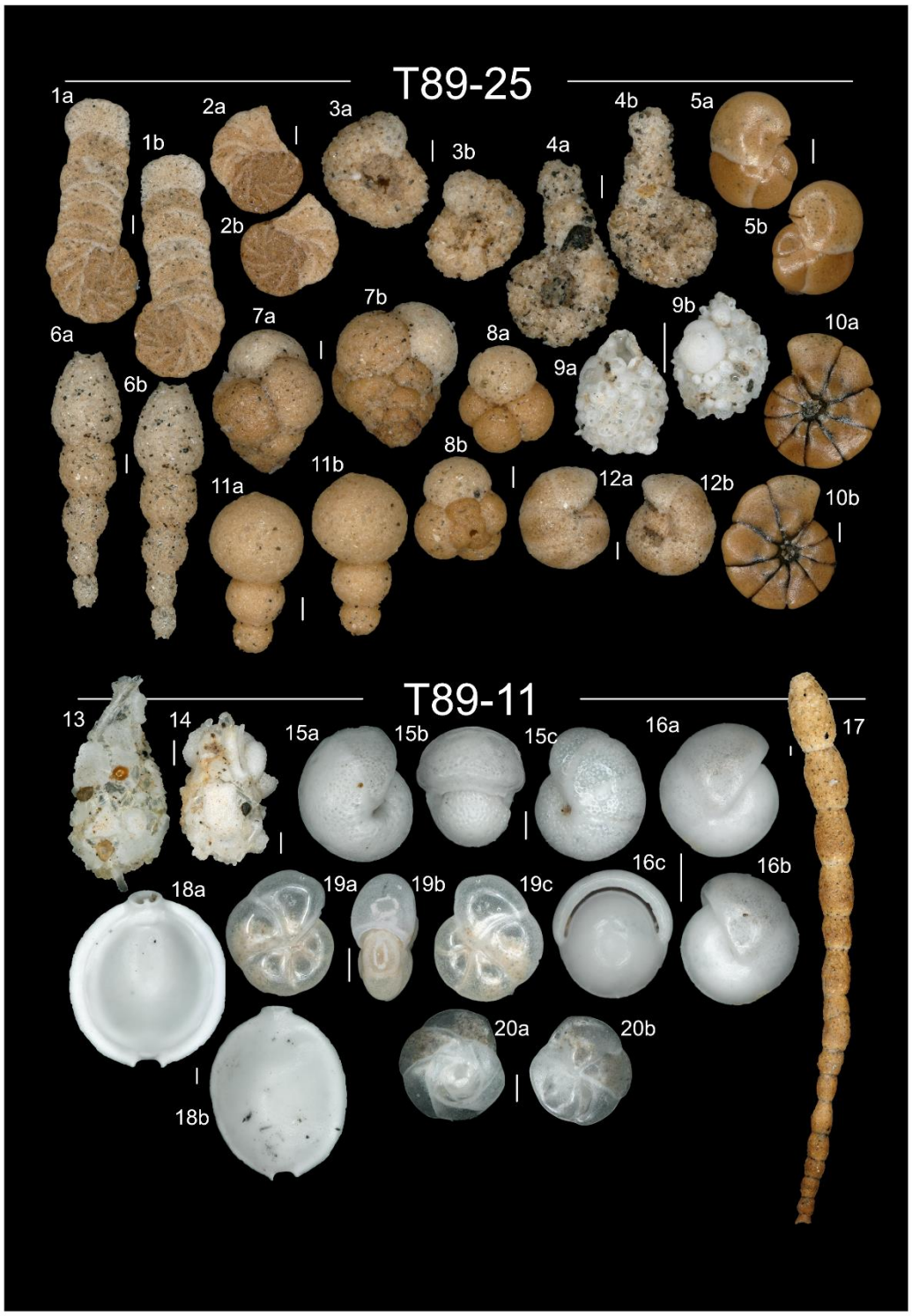
T89-25
1a
1b
2a
2b
3a
3b
4a
4b
5a
5b
6a
6b
7a
7b
8a
8b
9a
9b
10a
10b
11a
11b
12a
12b
T89-11
13
14
15a
15b
15c
16a
16b
16c
17
18a
18b
19a
19b
19c
20a
20b

Appendix 2.1 – Benthic Foraminifera interpretation Chapter 2

Paleoenvironmental inferences based on GeoB9512-5 Benthic Foraminifera

From the 34,340 hand-picked benthic foraminifera specimens, taxonomic analysis allowed to identify 71 genera and 120 species. The downcore paleoenvironmental interpretations are based on benthic foraminifera diversity changes (e.g. Murray 1991, 2006), and benthic foraminifera intervals (BFI) were identified based on Fisher Alpha Index (FAI) variability (Figure 1a). Each BFI is in turn characterized by changes in the benthic foraminifera assemblages (Figure 1) as a response to variations in bottom water oxygenation, organic matter content, and salinity.

Abundance of specific morpho-Microhabitat groups of benthic foraminifera are used to reconstruct changes in bottom water organic matter content, based on the TROX model (Jorissen et al. 1995). High abundance of infaunal foraminifera (Figure 1h) indicates higher fluxes of organic matters to bottom water environments. Relative abundances of this group > 66% is related to Eutrophic environments, while percentages of less than 33% indicate Oligotrophic environments (Jorissen et al., 1995).

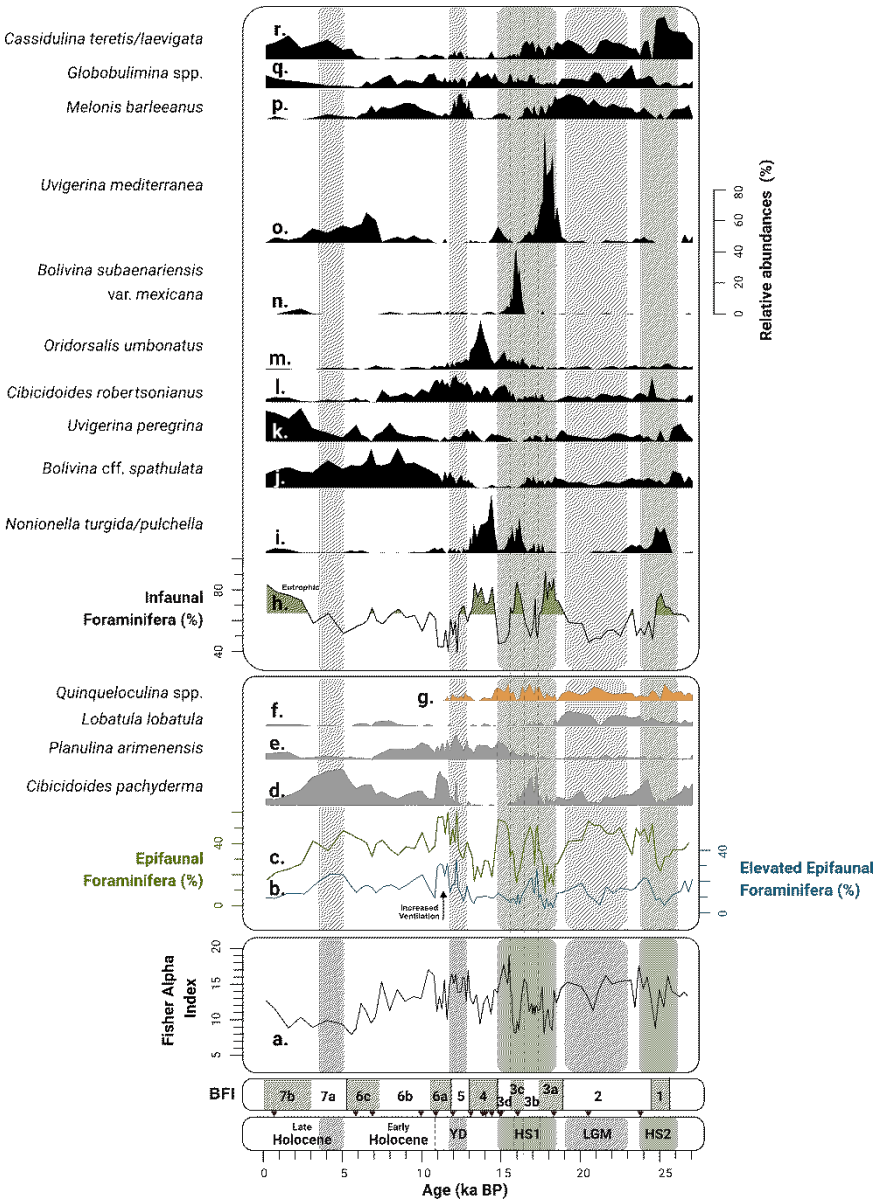

Figure 1. *GeoB9512-5 downcore benthic foraminifera diversity, intervals, and relative abundances of the most relevant species and groups.* **a.** Benthic Foraminifera diversity measured with the Fisher Alpha Index; Percentage of **b.** Elevated Epifaunal foraminifera and **c.** Epifaunal foraminifera; **d-g.** Relative abundances of the most representative epifaunal species; **h.** Percentage of Infaunal foraminifera; **i-r.** Relative abundances of the most representative infaunal species. **Key Climate events:** Heinrich Stadial 2 (HS2); Last Glacial Maximum (LGM); Heinrich Stadial 1 (HS1); Bølling–Allerød (B-A); Younger Dryas (YD). Triangles in the age axis indicate radiocarbon ages.

Diversity measured with the FAI (Figure 1a) was moderate to high (7.9 -19) and decreased during the last 5 kyrs of the Holocene. Diversity and benthic foraminifera distribution changes allowed the identification of 7 BFI and 9 subintervals (Figure 1), that mostly coincide with the key climatic periods in our site. Higher diversity (Figure 1a) was registered from pre-LGM times to the end of the LGM (FAI > 14, 27.1 - 19

kyrs), HS1 (FAI >12.4, 17.5 - 16.4 kyrs; and FAI >15.6m 14.8 - 15.7 kyrs), and YD (FAI > 15, 11.9 - 12.9 kyrs). Each interval represents specific environmental conditions, characterized by an alternation of low oxic - high oxic conditions (Figure 2d) inferred from the Enhanced Benthic Foraminifera Oxygen Index (EBFOI).

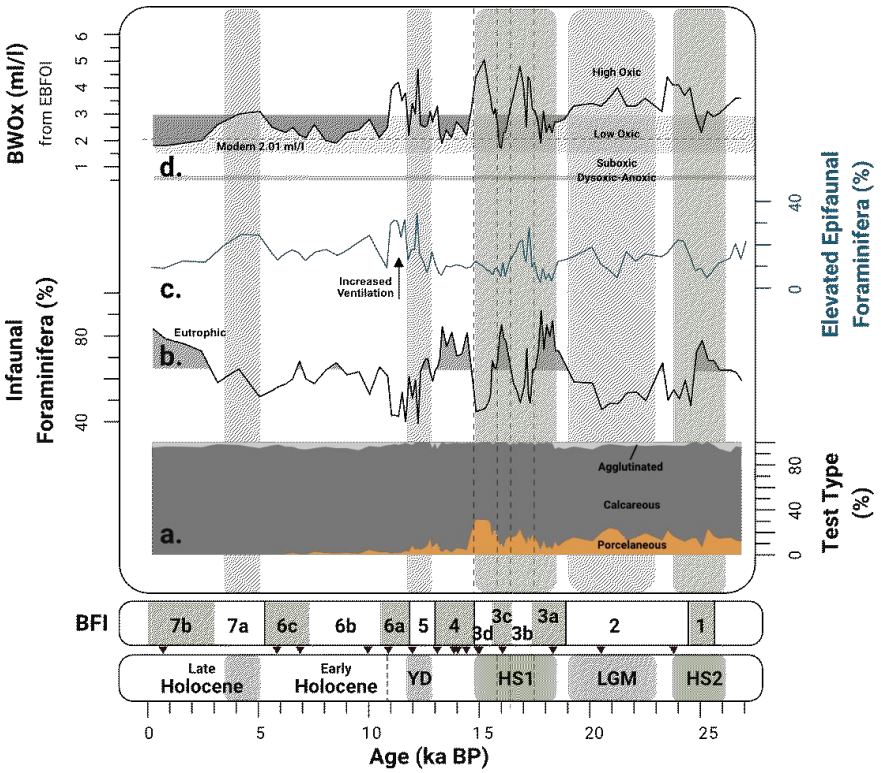

Figure 2. *GeoB9512-5 downcore benthic foraminifera paleoenvironmental proxies.* **a.** Benthic Foraminifera test types; **b.** Relative abundances of **b.** infaunal and **c.** elevated epifaunal foraminifera; **d.** Bottom Water Oxygenation (BWOx) calculated with the Enhanced Benthic Foraminifera Oxygen Index (EBFOI). **Key Climate events:** Heinrich Stadial 2 (HS2); Last Glacial Maximum (LGM); Heinrich Stadial 1 (HS1); Bølling–Allerød (B-A); Younger Dryas (YD). Triangles in the age axis indicate radiocarbon ages.

Non-metric multidimensional scaling (NMDS) analyses made on RStudio using the Bray–Curtis similarity index. We used the raw counts of the most abundant species (>5 %), from a data frame where taxonomical units were grouped into a single variable (Supplementary Information 6.3). The variables were normalized with the Hellinger method. The NMDS is an ordination method that allows to simplify large multivariate data, combining all variables into fewer dimensions to facilitate interpretation. These analyses allow to observe how the studied samples are distributed based on their

benthic foraminifera species distribution, therefore grouping samples with similar paleoenvironmental conditions.

The NMDS of GeoB9512-5 most abundant benthic foraminifera (Figure 3), shows groups similar to the BFIs differentiation. Furthermore, the groups correspond to the key climatic periods of the last 27 kyrs (LGM, HS1, B-A, YD, early Holocene – Holocene Climatic Optimum - and the late Holocene), and our records show that this distribution is related to the transient changes of oxic conditions (Figure 3d) and variations in the type of organic matter (Figure 3b) at bottom waters in the tropical eastern Atlantic. Salinity also played a key role in benthic ecosystems, and samples grouped in negative NMDS2 values are characterized by an abundant content of porcelaneous foraminifera (Figure 2a; orange in Figure 3b), a group used as qualitative indicator of salinity changes in bottom waters (e.g. Murray et al., 2006). These groups contain mostly samples from LGM to HS1 of GeoB9512-5 (Figure 3a) hinting at more saline conditions (Supplementary Figure 1b) compared to the Holocene.

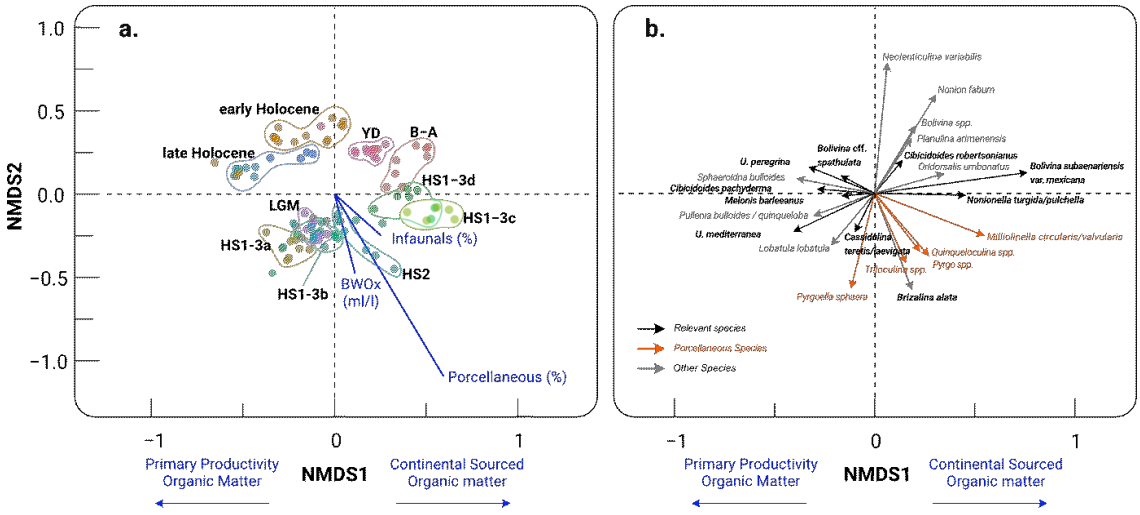

Figure 3. *Non-metric multidimensional scaling NMDS of the main benthic foraminifera species from cores GeoB9512-5 in the NE Atlantic.* **a.** Distribution of the analysed samples from core GeoB9512-5 in relation to the most abundant benthic foraminifera identified in this study, with the environmental fit of oxygen, organic matter (infaunal) and salinity (porcelaneous) proxies in this study (blue lines and text in the plot); **b.** Distribution in the NMDS of the most representative Benthic foraminifera. **Key Climate events:** Heinrich Stadial 2 (HS2); Last Glacial Maximum (LGM); Heinrich Stadial 1 (HS1); Bølling–Allerød (B-A); Younger Dryas (YD).

Bottom water oxygenation has relevant contributions in both axes. The low oxic intervals identified from our data show positive NMDS1 values (B-A and Holocene), while high oxic intervals are mostly located in the negative NMDS1 (LGM and HS1), except for the YD period. The lack of an exclusive oxygen control is explained by the different benthic foraminifera assemblages identified in each climatic period (Figure 1). These assemblages are influenced by the type of organic matter available on the seafloor and to a lesser extent by the amount. In general, the infaunal foraminifera percentages (Figure 1h, Figure 2b) suggest moderate to high organic matter content throughout the whole section with highest concentrations registered in HS2, BFI 3a and 3c of the HS1, B-A and the late Holocene (2.6 – 0.2 kyrs).

The high oxic periods identified here coincide (Figure 2d) with the higher relative abundance of epifaunal (Figure 1c), more specifically elevated epifaunal foraminifera (Figure 1b and Figure 2c), that represent times of enhanced circulation and ventilation (e.g. Schönfeld et al., 2002). On the other hand, the low oxic intervals are consistent with a decrease in epifaunal foraminifera, as bottom water circulation is limited. The moderate to high organic matter content in our site is strongly related to primary productivity that results from the enhanced upwelling that characterizes the region (e. g. Pelegrí and Peña-Izquierdo, 2015). However, altered organic matter from continental runoff also influenced benthic ecosystems in our site, and the changes in the proportion of these different types of organic matter is consistent with the rapid changes in the benthic foraminifera assemblages.

Species like *Nonionella turgida* (Figure 1i) and porcelaneous *Quinqueloculina* spp. (Figure 1g) are closely related to river input areas in the mediterranean (Mojtahid et al. 2010a) and are also abundant in prodelta environments of Portugal (Bartels-Jónsdóttir et al., 2006). In GeoB9512-5 *N. turgida* peaks of abundance occur in the HS2 (Figure 1i), BFI 3c and part of 3d of HS1 and in the B-A (Figure 4e), hinting at episodes dominated by a continental-sourced organic matter. In addition, the relatively high abundance of *Quinqueloculina* spp. from pre-LGM times until the end of the HS1 and to a lesser extent during the YD (Figure 1g), also suggests a predominant organic matter from continental sources. However, the abundance of this porcelaneous can also be due to the higher salinities, or even to unusually high carbonate state (Reymond et al., 2014).

The remaining abundant infaunal species, concentrated in the LGM, BFIs 3a, 3b and 3c of HS1 and the YD (Figure 1h-r), are consistent with high surface productivity related to upwelling activity. Particularly, *C. laevigata* is found as an assemblage with other bolivinids in the South Atlantic as characteristic of almost all-year upwelling (Mackensen et al. 1995), and it is known to rapidly reproduce in environments with abundant fresh organic matter input (Mojtahid et al. 2010b). This species is abundant in our site during the beginning of the HS2, LGM, BFI 3b of HS1 and in the late Holocene (Figure 1r). Furthermore, relatively higher epifaunal foraminifera (Figure 1c-g), considered to feed on fresher organic matter from primary productivity are also abundant in these intervals.

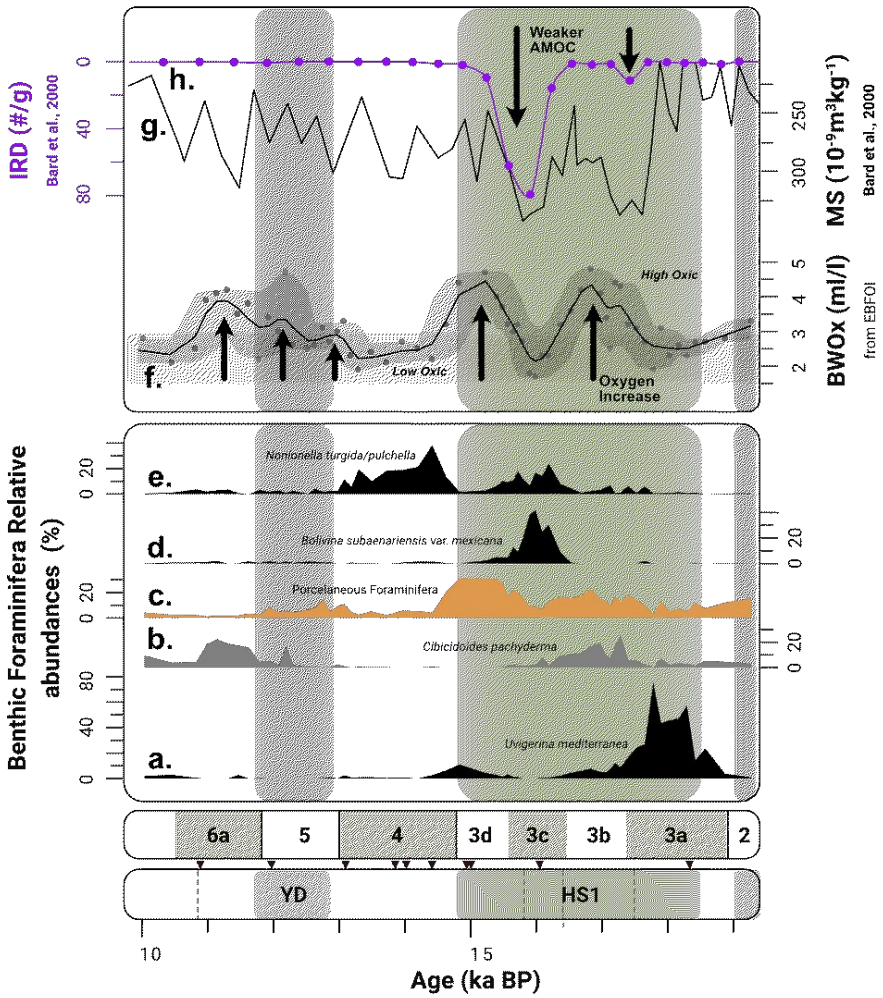

Figure 4. *Heinrich Stadial 1 to Bølling–Allerød representative benthic foraminifera from site GeoB9512-5.* **a-e.** Representative benthic Foraminifera species of intervals 2 – 6c; **f.** Bottom Water Oxygenation (BWOx) calculated with the Enhanced Benthic Foraminifera Oxygen Index (EBFOI); **g.** Magnetic Susceptibility (MS) and **h.** Ice-rafted detritus (IRD) from site SU8118 (37.76 N, 10.18 W; Bard et al.,

2000). **Key Climate events:** Heinrich Stadial 2 (HS2); Last Glacial Maximum (LGM); Heinrich Stadial 1 (HS1); Bølling–Allerød (B-A); Younger Dryas (YD).

The end of the LGM is sharply marked by the peak in abundance of *U. mediterranea* (Figure 1o), a shallow infaunal foraminifera that feeds on labile organic matter in relatively oxygenated environments (Fontanier et al., 2002). In our site, this species occurs in the low oxic BFI 3a of the HS1 (Figure 2a). During the BFI 3c of HS1, *B. subaenariensis mexicana* becomes a dominant species (Figure 1n, Figure 4d) that is common in turbiditic environments (Duros et al., 2017) and that prefers pulsed organic matter fluxes (Hess and Jorissen, 2009; Mojtahid et al. 2010b). It is also known as an early colonizer of disturbed environments that bring organic matter to the seafloor (Hess and Kuhnt,1996; Hess et al., 2001, 2005). This could represent one of the abrupt changes of the HS1 (Bard et al., 2000) consistent with a transient AMOC decline (our peak coincides with an IRD and MS peak in Figure 4g-h). Furthermore, this is synchronous with the *N. turgida* increase (Figure 4e) compatible with increased organic matter from continental sources.

During the YD peak in abundance of *C. pachyderma* (Figure 1d, Figure 4b) and in less extent of shallow infaunal *C. robertsonianus* (Figure 1l) is compatible with fresh organic matter from surface productivity and well-ventilated conditions (high elevated epifauna Figure 1b, Figure 2c). This is also registered for BFI 3b of the HS1 and in the Holocene between 5 and 3.1 kyrs, all intervals corresponding to high oxic intervals (Figure 2d).

The late Holocene is a relatively homogeneous period and is characterized by abundant *B. cff. Spathulata* (Figure 1j), a species typical of the Oxygen Minimum Zone of the red Sea in the Indian Ocean (Murray, 2006). This species is considered highly tolerant to stressed environments and has been observed to withstand anthropogenic driven pollution (Dimisa et al., 2018). In the late Holocene (from 5.5 ka BP) species like *U. peregrina*, *U. mediterranea* and *C. teretis*/*laevigata* became abundant hinting to more stable upwelling activity in the area.

References

Bartels-Jónsdóttir, H.B., Knudsen, K.L., Abrantes, F., Lebreiro, S., Eiríksson, J., 2006. Climate variability during the last 2000 years in the Tagus Prodelta, western Iberian Margin: Benthic foraminifera and stable isotopes. Marine Micropaleontology 59, 83–103. https://doi.org/10.1016/j.marmicro.2006.01.002

Duros, P., Silva Jacinto, R., Dennielou, B., Schmidt, S., Martinez Lamas, R., Gautier, E., Roubi, A., Gayet, N., 2017. Benthic foraminiferal response to sedimentary disturbance in the Capbreton canyon (Bay of Biscay, NE Atlantic). Deep Sea Research Part I: Oceanographic Research Papers 120, 61–75. https://doi.org/10.1016/j.dsr.2016.11.012

Fontanier, C., Jorissen, F.J., Licari, L., Alexandre, A., Anschutz, P., Carbonel, P., 2002. Live benthic foraminiferal faunas from the Bay of Biscay: faunal density, composition, and microhabitats. Deep Sea Research Part I: Oceanographic Research Papers 49, 751–785. https://doi.org/10.1016/S0967-0637(01)00078-4

Hess, S., 2005. BENTHIC FORAMINIFERAL RECOVERY AFTER RECENT TURBIDITE DEPOSITION IN CAP BRETON CANYON, BAY OF BISCAY. The Journal of Foraminiferal Research 35, 114–129. https://doi.org/10.2113/35.2.114

Hess, S., Jorissen, F.J., 2009. Distribution patterns of living benthic foraminifera from Cap Breton canyon, Bay of Biscay: Faunal response to sediment instability. Deep Sea Research Part I: Oceanographic Research Papers 56, 1555–1578. https://doi.org/10.1016/j.dsr.2009.04.003

Hess, S., Kuhnt, W., 1996. Deep-sea benthic foraminiferal recolonization of the 1991 Mt. Pinatubo ash layer in the South China Sea. Marine Micropaleontology 28, 171–197. https://doi.org/10.1016/0377-8398(95)00080-1

Hess, S., Kuhnt, W., Hill, S., Kaminski, M.A., Holbourn, A., De Leon, M., 2001. Monitoring the recolonization of the Mt Pinatubo 1991 ash layer by benthic foraminifera. Marine Micropaleontology 43, 119–142. https://doi.org/10.1016/S0377-8398(01)00025-1

Jorissen, F.J., De Stigter, H.C., Widmark, J.G.V., 1995. A conceptual model explaining benthic foraminiferal microhabitats. Marine Micropaleontology 26, 3–15. https://doi.org/10.1016/0377-8398(95)00047-X

Mackensen, A., Schmiedl, G., Harloff, J., Giese, M., 1995. Deep-Sea Foraminifera in the South Atlantic Ocean: Ecology and Assemblage Generation. Micropaleontology 41, 342. https://doi.org/10.2307/1485808

Mojtahid, Meryem, Griveaud, C., Fontanier, C., Anschutz, P., Jorissen, F.J., 2010. Live benthic foraminiferal faunas along a bathymetrical transect (140–4800m) in the Bay of Biscay (NE Atlantic). Revue de Micropaléontologie 53, 139–162. https://doi.org/10.1016/j.revmic.2010.01.002

Mojtahid, M., Jorissen, F., Lansard, B., Fontanier, C., 2010. MICROHABITAT SELECTION OF BENTHIC FORAMINIFERA IN SEDIMENTS OFF THE RHONE RIVER MOUTH (NW MEDITERRANEAN). The Journal of Foraminiferal Research 40, 231–246. https://doi.org/10.2113/gsjfr.40.3.231

Murray, J.W., 2006. Ecology and Applications of Benthic Foraminifera, 1st ed. Cambridge University Press. https://doi.org/10.1017/CBO9780511535529

Murray, J.W., 1991. Ecology and palaeoecology of benthic foraminifera. Longman scientific and technical copublished in the United States with John Wiley and sons, Essex New York.

Pelegrí, J.L., Peña-Izquierdo, J., 2015. Eastern boundary currents off North-West Africa, in: Oceanographic and Biological Features in the Canary Current Large Marine Ecosystem, IOC Technical Serie. pp. 81–92.

Reymond, C.E., Mateu-Vicens, G., Westphal, H., 2014. Foraminiferal assemblages from a transitional tropical upwelling zone in the Golfe d'Arguin, Mauritania. Estuarine, Coastal and Shelf Science 148, 70–84. https://doi.org/10.1016/j.ecss.2014.05.034

Schönfeld, J., 2002. A new benthic foraminiferal proxy for near-bottom current velocities in the Gulf of Cadiz, northeastern Atlantic Ocean. Deep Sea Research Part

I: Oceanographic Research Papers 49, 1853–1875. https://doi.org/10.1016/S0967-0637(02)00088-2

Appendix 2.2 – GeoB9512-5 Benthic foraminifera digital microscope images

Plate 1

Scale bar 100 µm

1. *Karreriella bradyi* (Cushman, 1911) – 187.5 cm
2. *Sigmoilopsis schlumbergeri* (Silvestri, 1904) – 432.5 cm
3. *Sigmoilopsis schlumbergeri* (Silvestri, 1904) – 452.5 cm
4. *Sigmoilopsis schlumbergeri* (Silvestri, 1904) – 532.5 cm
5. *Reophax* spp. – 262.5 cm
6. *Haplophragmoides* spp. – 262.5 cm
7. *Martinottiella communis* (d'Orbigny, 1846) – 262.5 cm
8. *Martinottiella communis* (d'Orbigny, 1846) – 262.5 cm
9. *Triloculina trigonula* (Lamarck, 1804) – 442.5 cm
10. *Pyrgo williamsoni* (Silvestri, 1923) – 447.5 cm
11. *Pyrgo williamsoni* (Silvestri, 1923) – 417.5 cm
12. *Pyrgo williamsoni* (Silvestri, 1923) – 387.5 cm
13. *Pyrgo comata* (Brady, 1881) – 397.5 cm
14. *Pyrgo comata* (Brady, 1881) – 222.5 cm
15. *Pyrgo depressa* (d'Orbigny, 1826) – 247.5 cm
16. *Pyrgo depressa* (d'Orbigny, 1826) – 252.5 cm
17. *Spiroloculina depressa* d'Orbigny, 1826 – 112.5
18. *Quinqueloculina seminulum* (Linnaeus, 1758) – 227.5 cm
19. *Quinqueloculina seminulum* (Linnaeus, 1758) – 232.5 cm
20. *Quinqueloculina seminulum* (Linnaeus, 1758) – 247.5 cm
21. *Quinqueloculina suborbicularis* d'Orbigny in Fornasini, 1905 – 247.5 cm
22. *Triloculina trigonula* (Lamarck, 1804) – 220 cm
23. *Lagena semistriata* Williamson, 1848 – 267.5 cm
24. *Cushmanina* sp. – 272.5 cm
25. *Lagena semistriata* Williamson, 1848 – 167.5 cm
26. *Lagena* cff. *sulcata* (Walker & Jacob, 1798) – 202.5 cm
27. *Lagena* cff. *sulcata* (Walker & Jacob, 1798) – 152.5 cm
28. *Lagena striata* (d'Orbigny, 1839) – 152.5 cm
29. *Lagena sulcata* (Walker & Jacob, 1798) – 212.5 cm
30. *Cushmanina* sp. – 167.5 cm

Plate 1

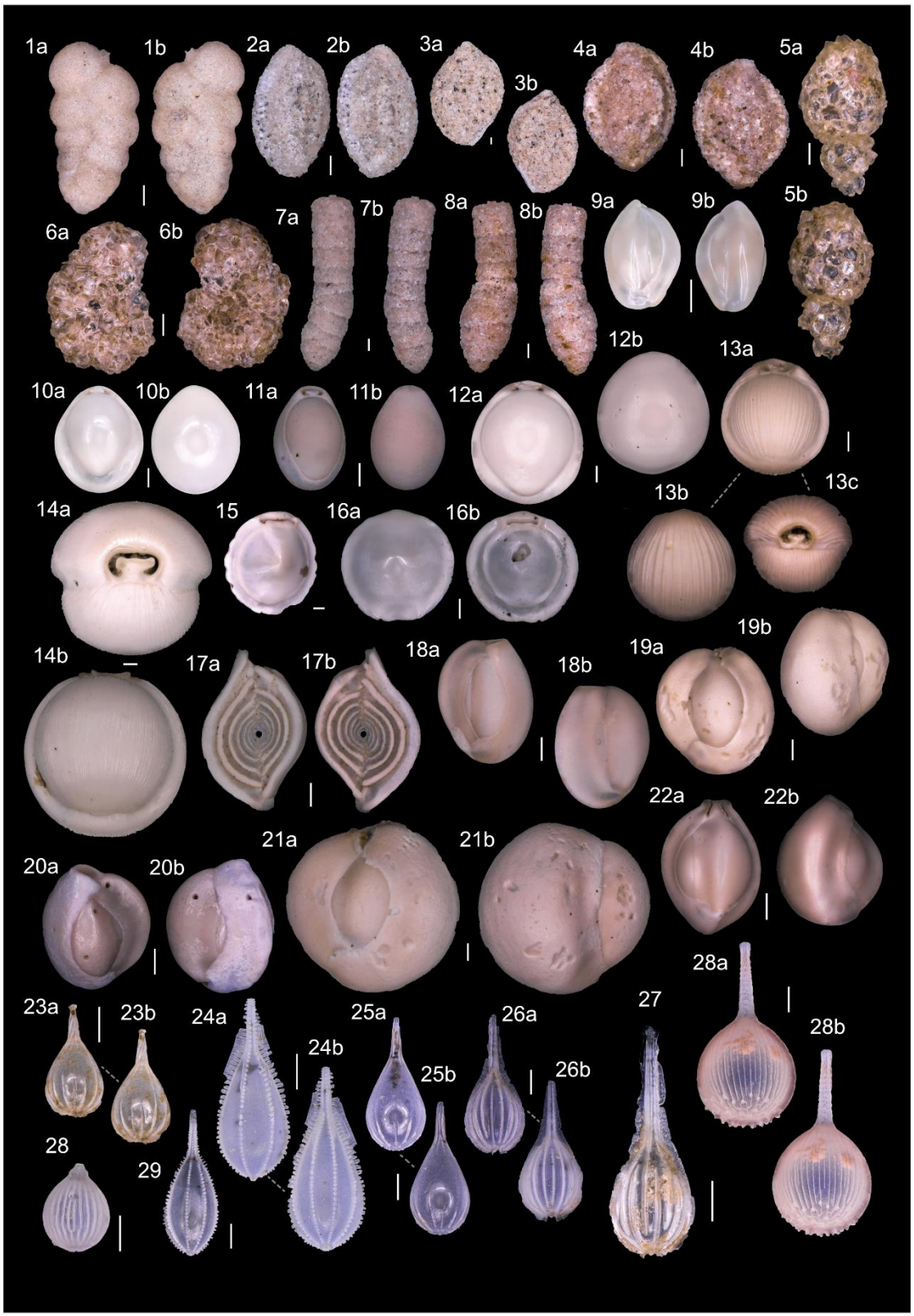
1a
1b
2a
2b
3a
3b
4a
4b
5a
5b
6a
6b
7a
7b
8a
8b
9a
9b
10a
10b
11a
11b
12a
12b
13a
13b
13c
14a
14b
15
16a
16b
17a
17b
18a
18b
19a
19b
20a
20b
21a
21b
22a
22b
23a
23b
24a
24b
25a
25b
26a
26b
27
28a
28b
28
29

Plate 2

Scale bar 100 µm

1. *Hyalinonetrion gracillimum* (Seguenza, 1862) – 267.5 cm
2. *Grigelis pyrula* (d'Orbigny, 1826) – 262.5 cm
3. *Hyalinonetrion gracillimum* (Seguenza, 1862) – 302.5 cm
4. *Amphicoryna scalaris* (Batsch, 1791) – 312.5 cm
5. *Amphicoryna scalaris* (Batsch, 1791) – 92.5 cm
6. *Uvigerina mediterranea* Hofker, 1932 – 62.5 cm
7. *Uvigerina mediterranea* Hofker, 1932 – 382.5 cm
8. *Uvigerina mediterranea* Hofker, 1932 – 382.5 cm
9. *Bulimina striata* d'Orbigny in Guérin-Méneville, 1832 – 472.5 cm
10. *Uvigerina peregrina* Cushman, 1923 – 2.5 cm
11. *Uvigerina hispida* Schwager, 1866 – 97.5 cm
12. *Bolivina* cff. *spathulata* (Williamson, 1858) – 27.5 cm
13. *Rectuvigerina* cff. *elongatastriata* (Colom, 1952) – 2.5 cm
14. *Bulimina aculeata* d'Orbigny, 1826 – 37.5 cm
15. *Bulimina marginata* d'Orbigny, 1826 – 17.5 cm
16. *Bolivina subaenariensis* var. *mexicana* Cushman, 1922 – 282.5 cm
17. *Bolivina* cff. *spathulata* (Williamson, 1858) – 27.5 cm
18. *Bolivina subaenariensis* var. *mexicana* Cushman, 1922 – 292.5 cm
19. *Bolivina subaenariensis* var. *mexicana* Cushman, 1922 – 277.5 cm
20. *Bolivina* cff. *spathulata* (Williamson, 1858) – 17.5 cm
21. *Globobulimina turgida* (Bailey, 1851) – 72.5 cm
22. *Globobulimina pacifica* Cushman, 1927 – 62.5 cm
23. *Chilostomella oolina* Schwager, 1878 – 82.5 cm
24. *Globobulimina turgida* (Bailey, 1851) – 212.5 cm
25. *Globobulimina turgida* (Bailey, 1851) – 217.5 cm
26. *Globobulimina turgida* (Bailey, 1851) – 257.5 cm
27. *Chilostomella oolina* Schwager, 1878 – 217.5 cm
28. *Glandulina ovula* d'Orbigny, 1846 – 212.5 cm
29. *Fissurina* sp. 1 – 117.5 cm
30. *Fissurina* cff. *staphyllearia* Schwager, 1866 – 117.5 cm
31. *Fissurina* cff. *staphyllearia* Schwager, 1866 – 177.5 cm
32. *Robertinoides bradyi* (Cushman & Parker, 1936) – 437.5 cm
33. *Fursenkoina bradyi* (Cushman, 1922) – 247.5 cm
34. *Fursenkoina bradyi* (Cushman, 1922) – 262.5 cm
35. *Fursenkoina bradyi* (Cushman, 1922) – 262.5 cm
36. *Fursenkoina bradyi* (Cushman, 1922) – 92.5 cm
37. *Nonionella* cff. *pulchella* Hada, 1931 – 102.5 cm

Plate 2

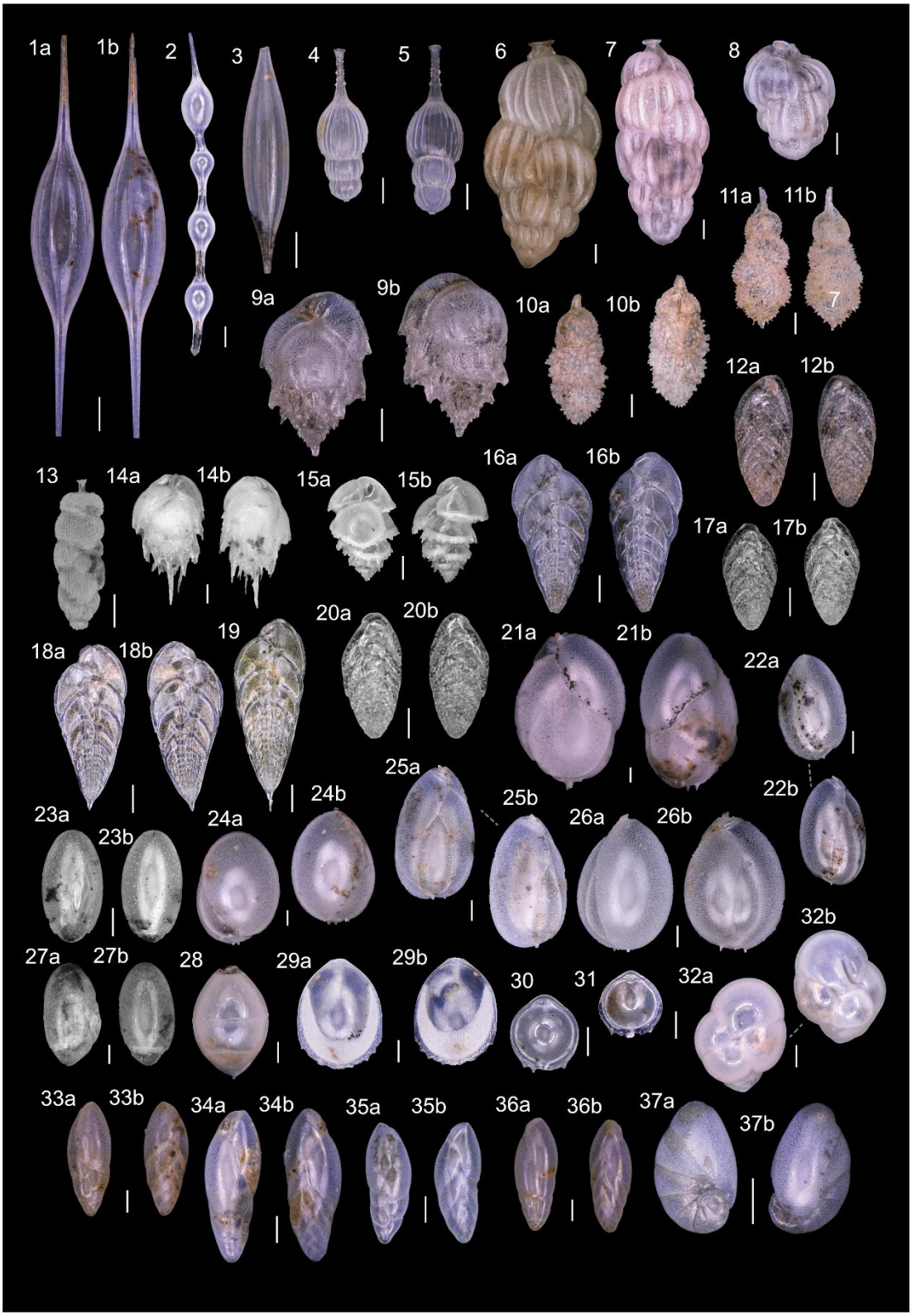
1a
1b
2
3
4
5
6
7
8
11a
11b
7
9a
9b
10a
10b
12a
12b
13
14a
14b
15a
15b
16a
16b
17a
17b
18a
18b
19
20a
20b
21a
21b
22a
22b
23a
23b
24a
24b
25a
25b
26a
26b
27a
27b
28
29a
29b
30
31
32a
32b
33a
33b
34a
34b
35a
35b
36a
36b
37a
37b

Plate 3

Scale bar 100 µm

1. *Nonion* cff. *fabum* (Fichtel & Moll, 1798) – 102.5 cm
2. *Nonion* cff. *fabum* (Fichtel & Moll, 1798) – 192.5 cm
3. *Nonionella* cff. *pulchella* Hada, 1931 – 187.5 cm
4. *Cancris auriculus* (Fichtel & Moll, 1798) – 447.5 cm
5. *Cancris auriculus* (Fichtel & Moll, 1798) – 462.5 cm
6. *Nonion* cff. *fabum* (Fichtel & Moll, 1798) – 207.5 cm
7. *Cancris auriculus* (Fichtel & Moll, 1798) – 57.5 cm
8. *Sphaeroidina bulloides* d'Orbigny in Deshayes, 1832 – 22.5 cm
9. *Neolenticulina variabilis* (Reuss, 1850) – 242.5 cm
10. *Sphaeroidina bulloides* d'Orbigny in Deshayes, 1832 – 42.5 cm
11. *Neolenticulina variabilis* (Reuss, 1850) – 212.5 cm
12. *Oridorsalis umbonatus* (Reuss, 1851) – 127.5 cm
13. *Oridorsalis umbonatus* (Reuss, 1851) – 147.5 cm
14. *Cassidulina laevigata* d'Orbigny, 1826 – 27.5 cm
15. *Cassidulina laevigata* d'Orbigny, 1826 – 27.5 cm
16. *Hanzawaia boueana* (d'Orbigny, 1846) – 97.5 cm
17. *Hanzawaia boueana* (d'Orbigny, 1846) – 132.5 cm
18. *Cibicidoides wuellerstorfi* (Schwager, 1866) – 87.5 cm
19. *Planulina ariminensis* d'Orbigny, 1826 - 92.5 cm
20. *Planulina ariminensis* d'Orbigny, 1826 - 72.5 cm
21. *Cibicidoides robertsonianus* (Brady, 1881) – 102.5 cm
22. *Lenticulina iota* (Cushman, 1923) – 232.5 cm
23. *Hyalinea balthica* (Schröter, 1783) – 482.5 cm
24. *Melonis barleeanus* (Williamson, 1858) – 457.5 cm
25. *Pullenia bulloides* (d'Orbigny, 1846) – 132.5 cm

Plate 3

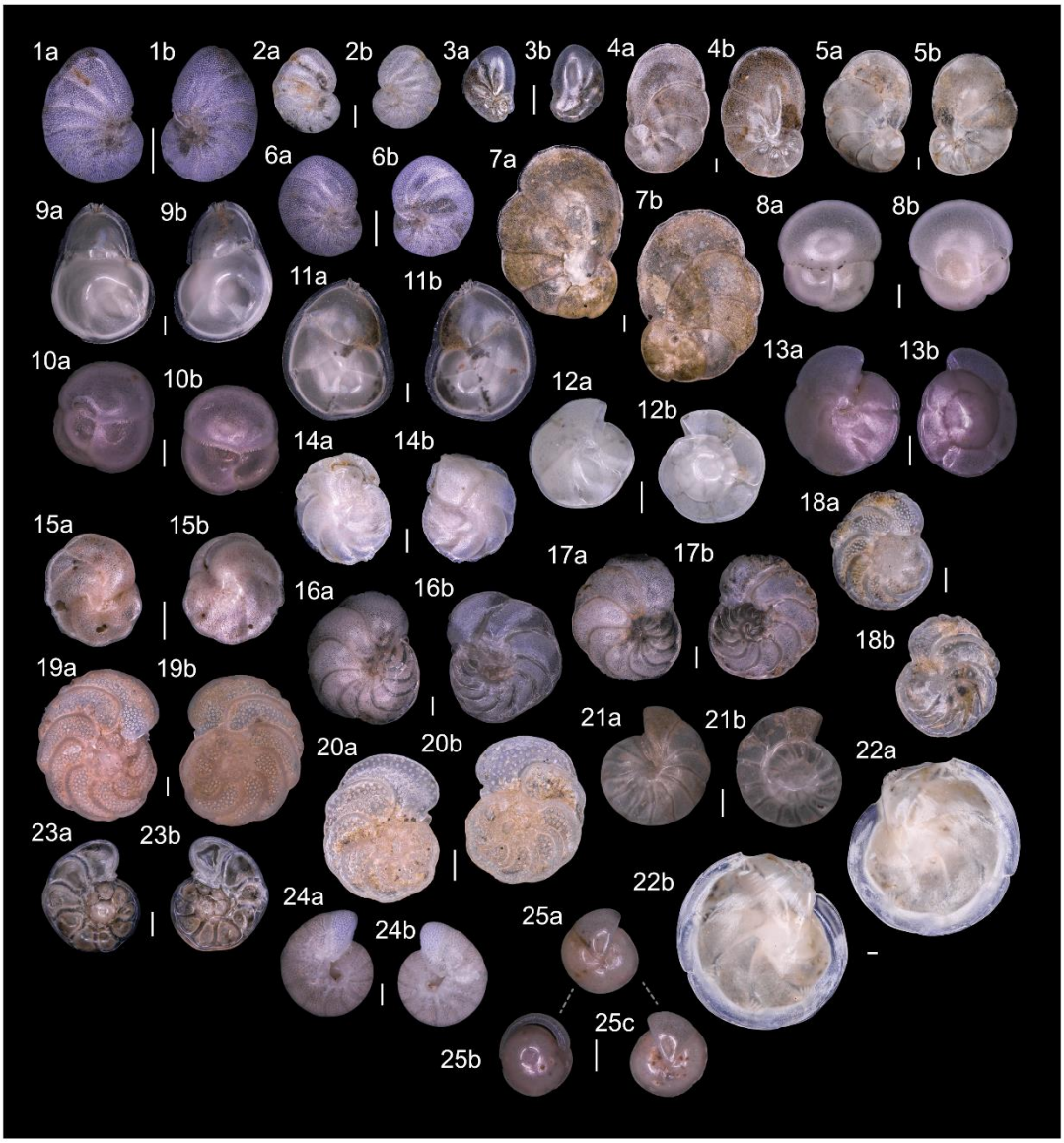
1a
1b
2a
2b
3a
3b
4a
4b
5a
5b
6a
6b
7a
7b
8a
8b
9a
9b
11a
11b
10a
10b
12a
12b
13a
13b
14a
14b
15a
15b
16a
16b
17a
17b
18a
18b
19a
19b
20a
20b
21a
21b
22a
22b
23a
23b
24a
24b
25a
25b
25c

Appendix 3.1 – Supplementary Information Chapter 3

Supplementary information 4

GeoB9512-5 downcore bottom water temperatures (BWT) during the last deglaciation, estimated from *Melonis barleeanus* Mg/Ca in the temperature calibration of Kristjándóttir et al. (2007) and equations 5 and 6 in this study.

Depth [cm]	Median Age [kyrs]	Mg/Ca [mmol/mol]	Melonis BWT [deg C] (Kristjándóttir et al., 2007)	Melonis BWT [deg C] (This Study Eq. 4)	Melonis BWT [deg C] (This Study Eq. 5)
52.5	6.5	1.82	7.23	9.50	8.56
67.5	7.5	1.55	6.44	8.16	7.75
72.5	8.0	1.60	6.40	8.11	7.87
87.5	9.5	1.56	6.43	8.16	7.77
92.5	10.0	1.61	6.70	8.62	7.99
97.5	10.4	1.79	7.32	9.67	8.69
117.5	11.3	2.32	9.36	13.09	10.52
127	11.6	2.80	10.20	14.52	11.88
137.5	11.9	2.83	10.34	14.73	12.28
142.5	12.1	2.52	10.14	14.35	11.89
147.5	12.2	2.58	10.04	14.20	11.80
152.5	12.3	2.49	10.07	14.26	12.01
157.5	12.4	2.67	10.16	14.44	12.35
162.5	12.5	2.79	10.25	14.58	12.57
167.5	12.6	2.71	10.27	14.61	12.61
177.5	12.9	2.66	10.09	14.30	12.27
182.5	13.0	2.52	9.94	14.03	12.04
192.5	13.2	2.47	9.72	13.65	11.83
257.5	15.6	2.29	9.16	12.77	10.61
317.5	16.6	2.77	10.59	15.16	12.40
327.5	16.7	3.13	10.62	15.20	12.33
337.5	16.9	2.50	10.14	14.37	11.47
372.5	17.5	2.35	9.74	13.72	11.51
377.5	17.6	2.68	10.08	14.28	12.12
387.5	17.9	2.92	10.60	15.15	13.06

397.5	18.2	2.78	10.78	15.46	13.45
407.5	18.4	3.08	11.15	16.08	14.14
422.5	19.2	3.37	11.64	16.93	14.84
432.5	20.1	2.84	10.69	15.32	12.96
437.5	20.5	2.58	10.18	14.48	12.06
442.5	20.9	2.62	10.14	14.41	11.87
447.5	21.2	2.84	10.20	14.46	11.93
452.5	21.6	2.48	9.31	12.97	10.76
457.5	22.1	1.82	8.34	11.35	9.44
462.5	22.5	1.90	8.09	10.94	9.05
467.5	22.9	2.34	8.43	11.52	9.50

Supplementary information 5

Regression tests for M. barleeanus and Uvigerina peregrina Mn/Ca vs. paleo-oxygenation from GeoB9512-5. Dissolved Oxygen Concentration record edited from Barragán-Montilla et al., in review).

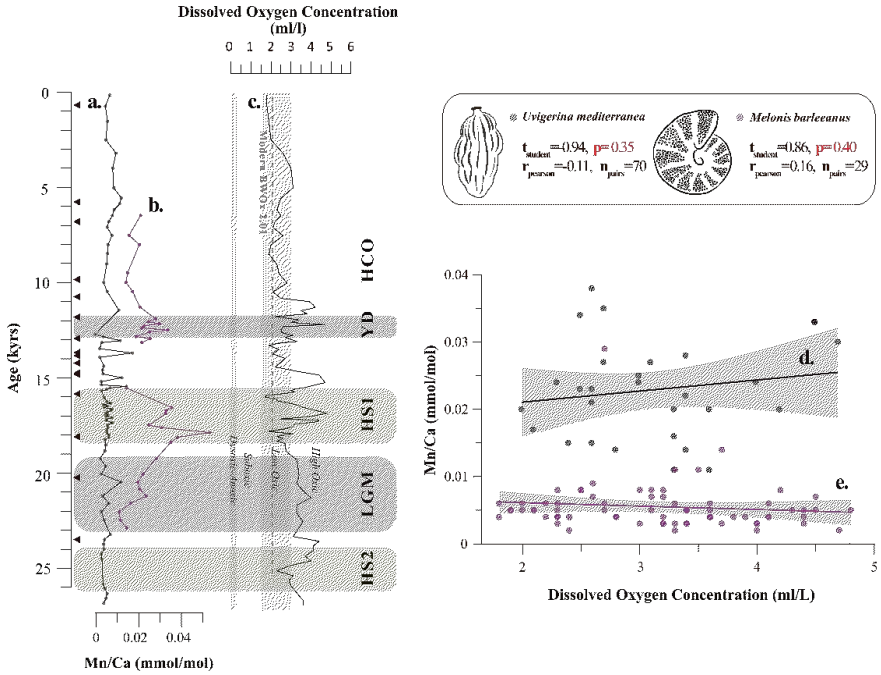

Supplementary information 6

Scanning Electron Microscope (SEM) images of *M. barleeanus* before cleaning protocol (a) and after cleaning (b-e).

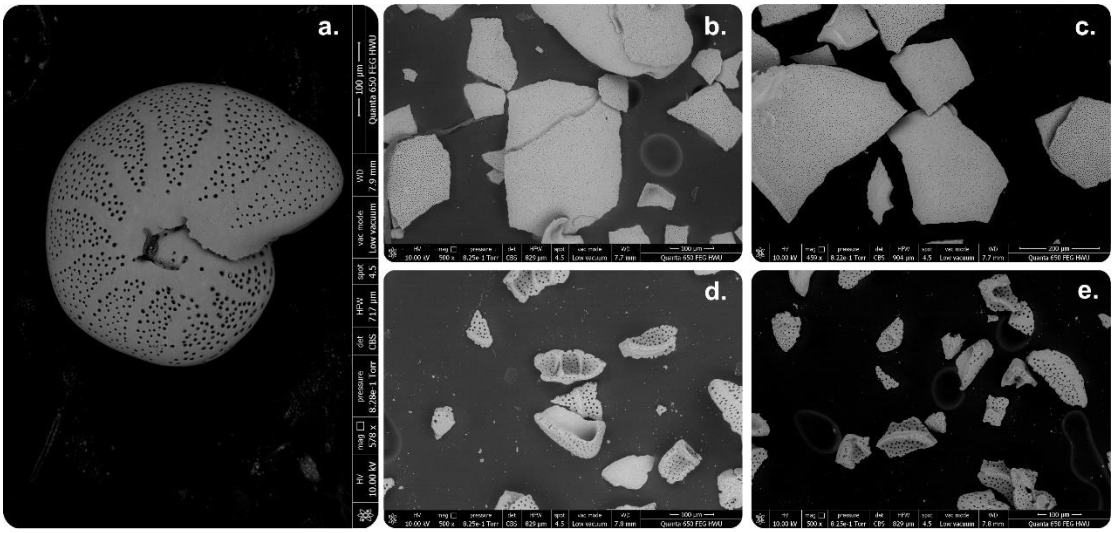
a.
b.
c.
d.
e.

Appendix 6 – Eastern tropical North Atlantic Benthic Foraminifera response to paleoceanographic changes during the last deglaciation

Sofía Barragán-Montilla[1]

[1]MARUM – University of Bremen, Germany
Correspondence to: Sofía Barragán Montilla (sbarraganmontilla@marum.de)

Abstract

During the last deglaciation, climate change induced profound environmental modifications well recorded in Atlantic Ocean sedimentary records, however, its effect on benthic ecosystems is limited. Here, we present a high-resolution taxonomy/quantitative analysis of eastern tropical North Atlantic benthic foraminifera from gravity core GeoB9506-1 (2,956 m water depth) and already published GeoB9512-5 (793 m water depth) off NW Africa. Our results show that in the last 27,000 years, bottom water oxygenation (BWOx) and food availability shaped benthic foraminifera diversity. At intermediate depths (GeoB9512-5), transient diversity drops are linked to intervals of low BWOx during the Holocene, probably related to intensification of the eastern tropical Atlantic Oxygen Minimum Zone during times of stronger Atlantic Meridional Overturning Circulation. In contrast, low-oxic environments during the deglaciation, observed in deep waters (GeoB9506-1) contain a high-diversity of stress species, and abundant infaunal foraminifera in eutrophic environmentssuggesting increased oxygen consumption via carbon respiration as well as limited oxygen supply. We show that benthic foraminifera are more sensitive to paleoceanographic-linked paleoenvironmental changes at intermediate depths, where assemblages show resilience to abrupt changes, while at deeper settings, paleoenvironmental changes led to a decrease in diversity.

Introduction

Marine biodiversity from plankton, corals, benthic invertebrates, and other vertebrates is affected by the changes in ocean temperature and oxygenation related to climate change (Poloczanska et al., 2013; Moffitt et al., 2015a), in benthic ecosystems, around

50% of the eukaryotic biomass correspond to benthic foraminifera (Gooday, 2001), that also represent one of the most diverse groups of hard-shelled microorganisms in today's oceans (Sen Gupta, 2002). Their distribution and diversity depend (mainly) on nutrient availability and oxygenation (Jorissen et al., 1995). Benthic foraminifera species who thrive in environmental stressed conditions like limited oxygen (Altenbach et al., 2012; Bernhard and Sen Gupta, 1999; Kaiho, 1994; Kranner et al., 2022; Southward et al., 2006), are known as opportunistic or stress species. In contrast, other benthic foraminifera are better adapted to oxygenated environments, and others prefer fresh organic matter. Such well documented environmental preferences, make this microfossil group excellent tools to investigate changes in bottom water environments and their link to major climatic events in the fossil record (Alegret et al., 2021; Gooday et al. 1992; Gooday et al., 2020; Murray, 2006; Schmiedl et al., 2023).

Detailed taxonomic/quantitative analyses of benthic foraminifera can be used to estimate bottom water dissolved oxygen concentrations (Kaiho, 1994; Kranner et al., 2022), an ecologically and climatically relevant element that strongly controls diversity in modern oceans (Vaquer-Sunyer and Duarte, 2008). Bottom water oxygenation (BWOx) depends on factors like deep-ocean ventilation, circulation, or carbon consumption (e.g. Brandt et al., 2015; Jaccard et al., 2016; Moffit et al., 2015b). Moreover, oxygen consumption can be used to observe the strength of the biological carbon pump that uptakes carbon and prevents its release to the atmosphere (Volk and Hoffert, 1985; Reichle, 2023). On the other hand, infaunal benthic foraminifera who live buried in the sediment can be are used to reconstruct variations in quantity/type of food (Gooday et al., 1992; Jorissen et al., 1995; Sweetman et al., 2009) also relevant for the carbon pump. This underlines the importance of a deeper understanding of bottom water paleoenvironmental changes and its relation to benthic diversity and climate change.

Here we present new, high-resolution records from site GeoB9506-1 (2,956 m water depth) of the eastern tropical North Atlantic, contrasted with benthic foraminifera records of intermediate site GeoB9512-5 (794m water depth). These records register benthic foraminifera diversity and distribution changes since the Last Glacial Maximum (LGM), related to major paleoceanographic changes in a climate change scenario.

Changes in BWOx and trophic levels in the last 27 kyrs were reconstructed from integrated benthic foraminifera taxonomic/quantitative analyses (results from GeoB9512-5 are reported in Barragán-Montilla et al., in review – Chapter 2, Appendix 2.1), that coupled with diversity calculations show different diversification trends to paleoceanographic-driven environmental fluctuations at intermediate and deep settings.

Benthic foraminifera diversity and distribution in GeoB9512-5 was linked to transient environmental changes of the eastern tropical North Atlantic Oxygen Minimum Zone (ETNA-OMZ) as the Atlantic Meridional Overturning Circulation (AMOC) strengthchanged (Barragán-Montilla et al., in review), and lower diversity occurred with reduced BWOx and increased organic matter concentration. The response at deeper setting is different, as relatively stable low oxic conditions during the LGM and most of the deglaciation led to a diverse benthic foraminifera assemblage mainly dominated by stress and infaunal species. A shift to more oxic conditions in the Holocene supposed a decrease in benthic foraminifera diversity in site GeoB9506-1, showing a low adaptation response to abrupt changes.

Our data shows that although paleoceanographic shifts effects on benthic foraminifera was stronger at intermediate depths in the eastern tropical North Atlantic, diversification was seemingly higher as the observed in deeper settings, suggesting the impact of climate change could have a stronger impact on eastern tropical North Atlantic deep ecosystems.

Methods

2.1 Core Location and materials

Sediments from core GeoB9506-1 (Chapter 5) were recovered in the NE Atlantic (Figure 1) off NW Africa (Multiza et al., 2005). This site (2,956 m water depth) is located in the North Atlantic Deep Water (NADW), with bottom water temperatures (BWT) of 2.7°C and dissolved oxygen concentration (BWOx) of 5.3 ml/l (Lauvset et al., 2022).

Samples were collected in the GeoB core repository laboratories and were washed for micropaleontological analyses as described by Barragán-Montilla et al. (in review).

The sediments were washed with deionized water through a 63 µm sieve and then dried at temperatures of around 45°C in an oven for less than 24 hours. Lastly, the resulting dry sediments were sieved to obtain fractions of 63, 125, 150 and 250 µm each one stored in labelled glass vials. Benthic foraminifera for taxonomy and quantitative analyses were extracted from the coarser fractions (> 150 µm).

A total of 64 sediments samples were retrieved between 0 and 260 cm core depth from GeoB9506-1, with an average age resolution of 0.44 kyrs (Chapter 5). These sediments are from the lower bathyal zone, with a turbiditic event (202.5 to 217.5 cm) seen as a course more porous level (Multiza et al., 2005; Chapter 5), inferred as a contourite level based on the glauconite content observed during the micropaleontological analyses, including planktic and benthic foraminifera filled with dark to light green glauconite (Supplementary Information 6.1 – Glauconitic Foraminifera).

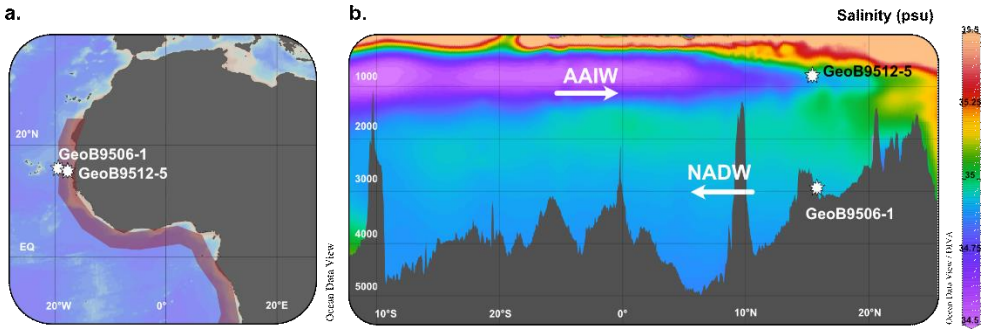

Figure 1. Geographic and hydrographic location of the studied in the eastern tropical North Atlantic off NW Africa*;* **a. Geographic location of** gravity cores GeoB9512-5 (15°20'13.20''N/17°22'1.20''W, 793 m water depth) and GeoB9506-1 (15°36'36.00''/18°21'0.60''W, 2,956 m water depth); **b. Oceanographic situation and water depth of the studied sites,** with the modern oceanographic water masses Arctic Intermediate Water (AAIW) and North Atlantic Deep Water (NADW). Plotted using Ocen Data View (Schlitzer, Reiner, Ocean Data View, https://odv.awi.de, 2022) and GLODAP version 2 (Lauvset et al., 2022).

2.2 Benthic foraminifera taxonomy and quantitative analyses

Paleoenvironmental and diversity results and interpretation are based on taxonomical and quantitative analyses of at least 200 -250 BF from 100 samples from core GeoB9512-5 (Barragán-Montilla et al., in review – Chapter 3) and 64 from core

GeoB9506-1. Benthic foraminifera were morphologically separated, and the taxonomical identification was made to a specific level when possible. Genera were determined following Loeblich and Tappan (1987), while species were identified based on multiple references (e.g. Jones and Brady, 1994; Holbourn et al., 2013; van Morkhoven et al., 1986). The updated taxonomy was revised using the online database WoRMS. Benthic foraminifera were photographed at the Microscopy Laboratory at the MARUM Institute, with a Keyence VHX 6000 digital microscope with a motorized stage (Appendix 3.2, Supplementary Information 6.1).

2.3 Paleoenvironmental and Paleoceanographic reconstruction

Downcore paleoenvironmental interpretations are based on benthic foraminifera diversity changes (e.g. Murray 1991, 2006). Benthic foraminifera intervals (BFI) were identified based on Fisher Alpha Index variability, each one characterized by changes in the benthic foraminifera assemblages as a response to variations in bottom water oxygenation, trophic conditions, and salinity. For site GeoB9512-5, we used the age model published by (Barragán-Montilla et al., in review), while for site GeoB9506-1 the ages correspond to the reported in Chapter 5.

Bottom water oxygenation was estimated using the most recent approach by Kranner et al. (2022), using an Enhanced Benthic Foraminifera Oxygen Index (EBFOI) to better estimate Dissolve Oxygen Concentration (BWOx) in past marine deposits. These results were also contrasted with the distribution of stress species (species better adapted to oxygen depleted environments like *Bulimina, Bolivina, Uvigerina, Cassidulina, Melonis, Fissurina, Globobobulimna;* Southward et al., 2006) to assess the accuracy of our bottom water oxygen reconstructions. Inferences on organic matter content at bottom waters is based on the abundance of specific morpho-Microhabitat groups of benthic foraminifera using the TROX model (Jorissen et al. 1995). This model predicts the amount of organic matter based on the percentage of infaunal foraminifera, and high abundance of this group is related to high organic matter at bottom water environments. Relative abundances of this microhabitat group over 66% are linked to Eutrophic environments (high organic matter), while relative abundances of less than 33% can be linked to Oligotrophic conditions (less organic matter, Jorissen et al., 1995).

Results and Discussion

3.1 Benthic Foraminifera during the last deglaciation in the NE Atlantic

A total of 39.591 BF specimens were hand- picked from 164 samples from gravity cores GeoB9512-5 (Barragán-Montilla et al., in review) and GeoB9506-1. The taxonomic analyses from the microfossil material allowed the identification of 100 genus and 156 species. The following interpretations are based on the quantitative analyses of benthic foraminifera counts per sample and were made separately for each core. Only the data frames containing all species with relative abundance's higher than 5% in at least one sample are considered. Abundant species here are considered as taxonomical units with average percentages > 10 % per interval, while accessory species are considered with average percentages between 5 – 10%.

3.1.1 Transient diversity and distribution changes during the last deglaciation at intermediate depths

A detailed description of the benthic foraminifera diversity and distribution from site GeoB9512-5 is included in Appendix 3.1 Overall diversity was moderate to high (7.9 - 19 Fisher Alpha index) and decreased during last 5 kyrs of the Holocene (Figure 2). The BF assemblages were predominantly calcareous (on average over 87% of the relative abundance, Supplementary Information 6.2). However, porcelaneous foraminifera represented on average more than 15 % of the assemblage from 27 – 15.8 kyrs with a peak in abundance during the beginning of the B-A period (average 25.7 %), followed by a decrease under 3 % in the last 14.4 kyrs. Diversity variability was analyzed with the Fisher Alpha Index (FAI), showing 7 intervals and 9 subintervals characterized by changes in benthic foraminifera distribution (Figure 2). The benthic foraminifera intervals (BFI), coincide with the key climatic periods recorded in core GeoB9512-5 (Figure 2 age axis), showing that changes of this microfossil group distribution were controlled by variations in bottom water conditions driven by paleoceanographic shifts (Barragán-Montilla et al., in review).

The end of the LGM was marked by a drop in diversity and a peak in abundance of shallow infaunal *Uvigerina mediterranea* (Figure 2) into the HS1 (**BFI-3,** FAI 8 -19). During this period diversity changed in 4 phases: a high diversity phase (**BFI-3a,** FAI ~ 9.5) dominated by *U. mediterranea*; a low diversity phase (**BFI-3b,** FAI ~ 12.5), with

abundant *C. pachyderma* and *U. mediterranea;* another low diversity interval (**BFI-3c,** FAI ~ 9.7) dominated by *Bolivina subaenariensis* var. *Mexicana* and *N. turgida*/*pulchella*; and finally a high diversity interval (**BFI-3d,** FAI ~ 15.6), characterized by an homogeneous association with abundant *N. turgida*/*pulchella, Cibicidoides robertsonianus*, *Quinqueloculina* spp., *Planulina ariminensis, Milliolinella circularis*/*valvularis, Oridorsalis umbonatus, Chilostomella oolina* and *Globobulima* spp. (Figure 2).

During the B-A, benthic foraminifera shifted to a *N. turgida*/*pulchella – O. umbonatus* dominated assemblage as diversity increased (**BFI-4,** FAI 9.4 -14.3). This diversification persisted during the YD (**BFI 5**, FAI 12.6 – 16.9) as species like *C. robertsonianus, P. arimennesis* and *M. barleeanus* were more representative (Figure 2). However, a transient shift into progressively decreasing BF diversity at the beginning of the Holocene is seen first from 11.6 to 10.9 kyrs (**BFI 6a**, FAI ~ 12.3) with abundant *C. pachyderma* and *C. robertsonianus*, followed by abundant *Bolivina* cff. *spathulata* (**BFI 6a**, FAI ~ 13.7), into the last part of the early Holocene (10.8 – 5 ka BP) were the latter species increased as diversity dropped (**BFI 6c**, FAI ~ 9.9) and *Sphaeroidina bulloides, C. pachyderma,* and *U. mediterranea* also become abundant (Figure 3). During the last part of the Holocene diversity remained low (**BFI 7a**, FAI ~ 9.4; **BFI 7b**, FAI ~ 10.9), characterized by abundant species like *C. pachyderma, U. peregrina, S. bulloides, B.* cff. *spathulata* and *C. teretis*/*laevigata*.

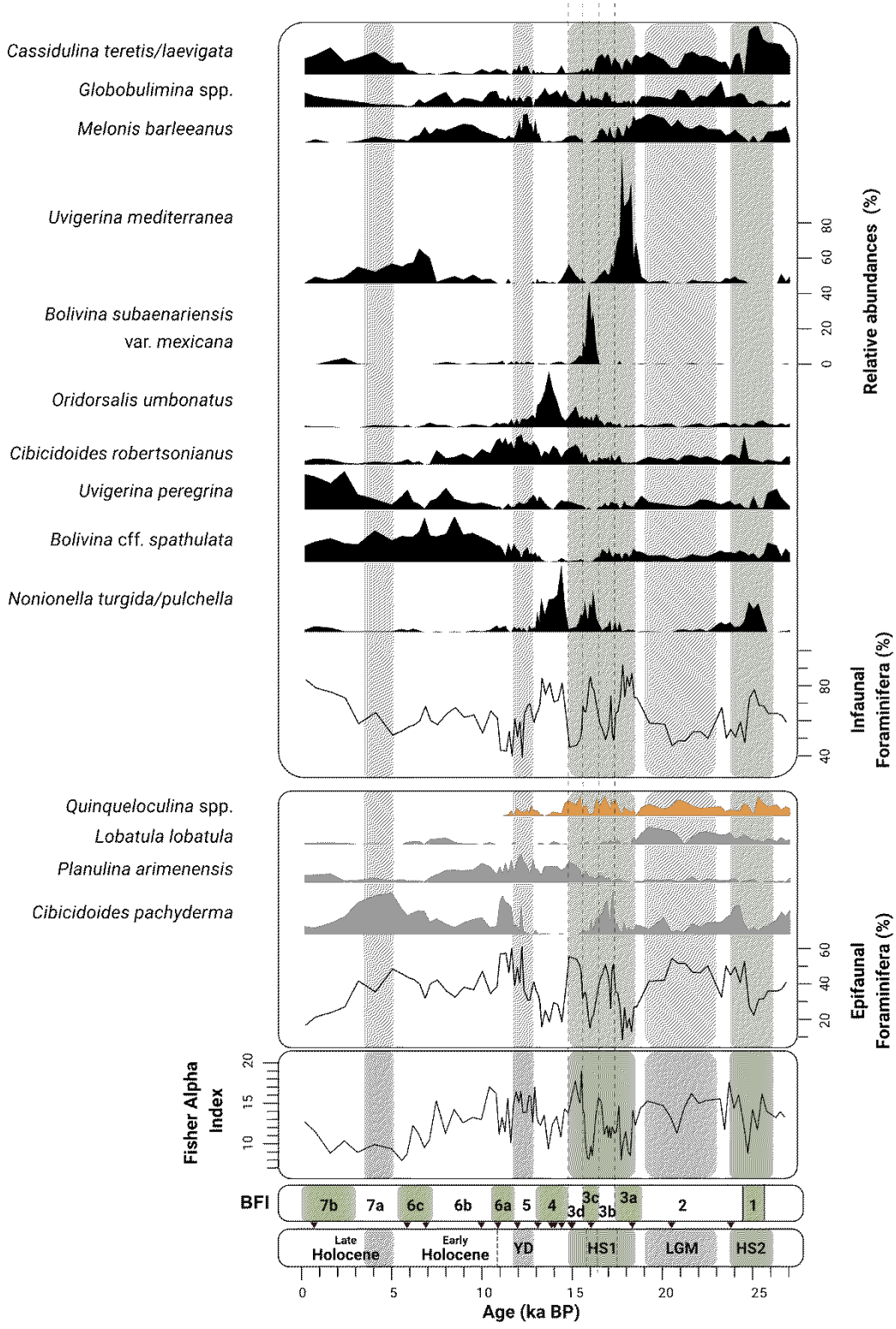

Figure 2. Downcore GeoB9512-5 benthic foraminifera diversity (Fisher Alpha Index) and most abundant species modified from Appendix 3. Filled grey curves are epifaunal foraminifera and filled black curves correspond to infaunal foraminifera; orange filled curves correspond to porcelaneous foraminifera. **Key Climate events:** Heinrich Stadial 2 (HS2); Last Glacial Maximum (LGM); Heinrich Stadial 1 (HS1); Bølling–Allerød (B-A); Younger Dryas (YD). Triangles in the age axis indicate points of radiocarbon ages.

3.1.2 Benthic Foraminifera in NE Atlantic deep-sea environments

At deep-sea environments (GeoB9506-1), 86 genera and 133 species were identified. Diversity was moderate to high (6.9 – 20.3 Fisher Alpha index, Figure 3). Changes in the assemblages were not so abrupt in GeoB9506-1 and 8 intervals and 7 subintervals are identified by FAI variability (Figure 3). The benthic foraminifera assemblages were mostly calcareous (Supplementary Information 6.3, however peaks in porcelaneous foraminifera (~ 33%) were observed during the HS1 (BFI-5b, 17.5 – 17 ka BP), and to less extent during the LGM (~ 12%; BFI-4b, 20.5 – 18.8 ka BP). In addition, at the end of the Holocene (BFI-8b, 17.5 – 17 ka BP), agglutinated foraminifera increased (~ 18.4%), and between 1.5 - 0.6 ka BP benthic foraminifera recovery was visibly lower.

Benthic foraminifera distribution in this site is mostly dominated by *U. peregrina* and changes in relative abundance of less dominant stress species like *C. teretis*/*laevigata*, *Melonis barleeanus*/*pompiloides* were used to differentiate sub-intervals (Figure 3). Additionally, the contourite level of Subinterval 2b (described in Chapter 5) was characterized by the presence of potentially reworked *U. mediterranea* from shallower environments.

The record starts with **BFI-1**, a diverse assemblage interval (FAI 9.2 – 13.7) dominated by *U. peregrina, C. teretis*/*laevigata*, *M. barleeanus, U. peregrina* and *C. wuellerstorfi* (Figure 3). The second interval, still in pre-LGM times, saw an increase in diversity (**BFI 2**, FAI ~ 15.3) as dominant species are *U. peregrina* and *C. teretis*/*laevigata.* The HS2 is mostly represented by a contourite interval, with abundant glauconite and foraminifera glauconitic fillings, therefore interpretations from this interval will not be discussed. During the LGM, two subintervals were identified. The first one, a high diversity period (**BFI 4a**, FAI ~ 15.5) with a large increase of *C. teretis*/*laevigata* abundance, while *U. peregrina* remains abundant (Figure 3). The second subinterval was less abundant (**BFI 4b**, FAI ~ 9.11), and dominated by *M. barleeanus*, *Epistominella exigua* and *U. peregrina.* The HS1 is divided into three subintervals, characterized by an alternation of high -low -high diversity (Figure 3). The first one (**BFI 5a**, FAI ~ 15.6), dominated by *C. teretis*/*laevigata* and to less extent by *U. peregrina*; the second one (**BFI 5b**, FAI ~ 8.4), dominated by *Quinqueloculina* spp., and *M. barleeanus* and *C. teretis*/*laevigata*, also characterized by the lowest

percentages of *U. peregrina*; and the third one (**BFI 5b**, FAI ~ 13.8) dominated by *C. teretis/laevigata, M. barleeanus* and *U. peregrina.*

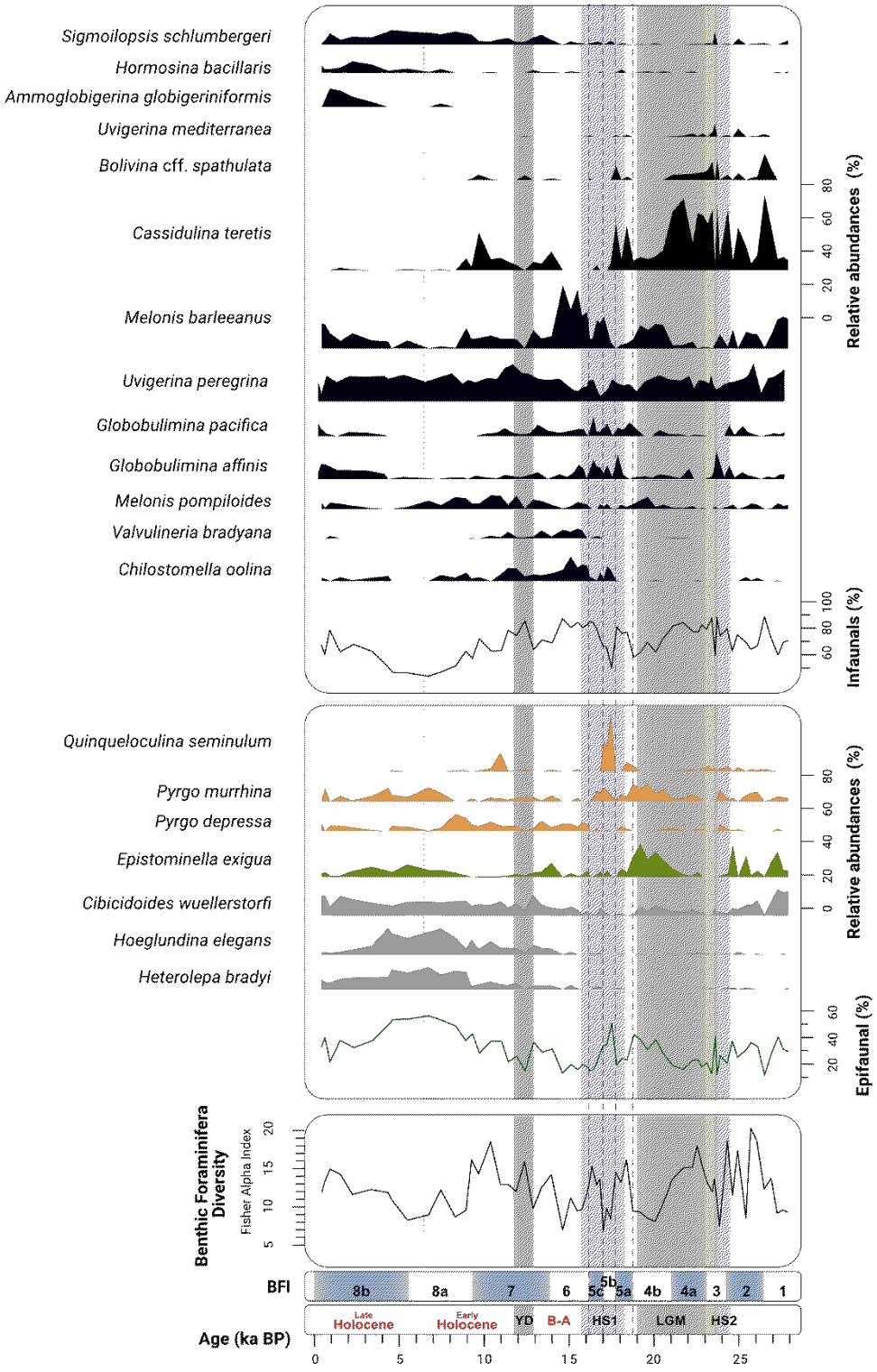

Figure 3. Downcore GeoB9506-1 benthic foraminifera diversity (Fisher Alpha Index) and most abundant species. Filled grey curves are epifaunal foraminifera and filled black curves correspond to infaunal foraminifera; orange filled curves correspond to porcelaneous foraminifera; green filled curve

corresponds to phytodetrital species. **Key Climate events:** Heinrich Stadial 2 (HS2); Last Glacial Maximum (LGM); Heinrich Stadial 1 (HS1); Bølling–Allerød (B-A); Younger Dryas (YD). Triangles in the age axis indicate points of radiocarbon ages.

During the B-A, diversity decreased (**BFI 6**, FAI ~ 10.5) as *M. barleeanus* reaches the highest percentages of this core (Figure 3), and other species like *Chilostomella oolina* and *U. peregrina* are abundant. For the YD and beginning of the Holocene (**BFI 6**, FAI ~ 10.5), *U. peregrina, M. barleenaus* and *C. teretis*/*laevigata* represent the benthic foraminifera association, followed by a drop in diversity (**BFI 8a**, FAI ~ 8.5), when the assemblage shifted to be dominated by *U. peregrina*, *Heterolepa bradyi* and *Hoeglundina elegans*. In the last part of the Holocene diversity increased (**BFI 8a**, FAI ~ 12.7), and the assemblage became more heterogenous with abundant *U. peregrina,* and accessory species *M. barleeanus, C. wuellerstorfi, H. bradyi, H. elegans* and *Globobulimina* spp. (Figure 3).

3.2 Paleoenvironmental implications: Benthic Foraminifera and geochemical proxies

Benthic foraminifera distribution in the eastern tropical North Atlantic was mainly controlled by bottom water oxygenation, trophic conditions, and salinity during the last deglaciation. These paleoenvironmental parameters were reconstructed for both cores using a multiproxy approach.

3.2.1 Glacial-deglacial high salinity in the intermediate tropical eastern North Atlantic

As described in Chapter 5 $\delta^{18}O_{sw}$ (Figure 4a) has a similar trend to the global $\delta^{18}O$ change related to ice effect (Waelbrock et al., 2001) in both sites. A detailed analysis of the sea water $\delta^{18}O$ changes is described in Chapter 5 (Section 3.1.1). In site GeoB9512-5, higher $\delta^{18}O_{SW}$ and salinity observed from the HS2 into the YD (Figure 4a-b), coincides with increasing relative abundance of porcelaneous foraminifera (Figure 4c). These proxies are compatible with relatively higher bottom water salinity during this time interval, that decreased closer to modern values in the last 11.7 kyrs.

At site GeoB9506-1, $\delta^{18}O_{sw}$ and salinity (Figure 5a-b) reconstructions show relatively stable trends throughout the study interval, with some transient increases at the beginning of the LGM and during the Holocene (Figure 5b). Porcelaneous foraminifera

also remained relatively stable script for a peak in abundance during the HS1 (Figure 3c), absent in the geochemical record, suggesting such peak was controlled by other parameters.

In contrast deep waters were more saline that intermediate waters in the tropical eastern North Atlantic (gray areas in Figure 6c-d) during most of the last 27 kyrs, except for the HS1, LGM and the upper part of the YD (red areas in Figure 6c-d), suggesting that at intermediate depths very saline central waters were present at our site (Chapter 5 – section 3.5). the higher salinities from site GeoB9506-1 are consistent with the location of this site in the North Atlantic Deep Water during times of strong AMOC (Chapter 5 – section 3.5)

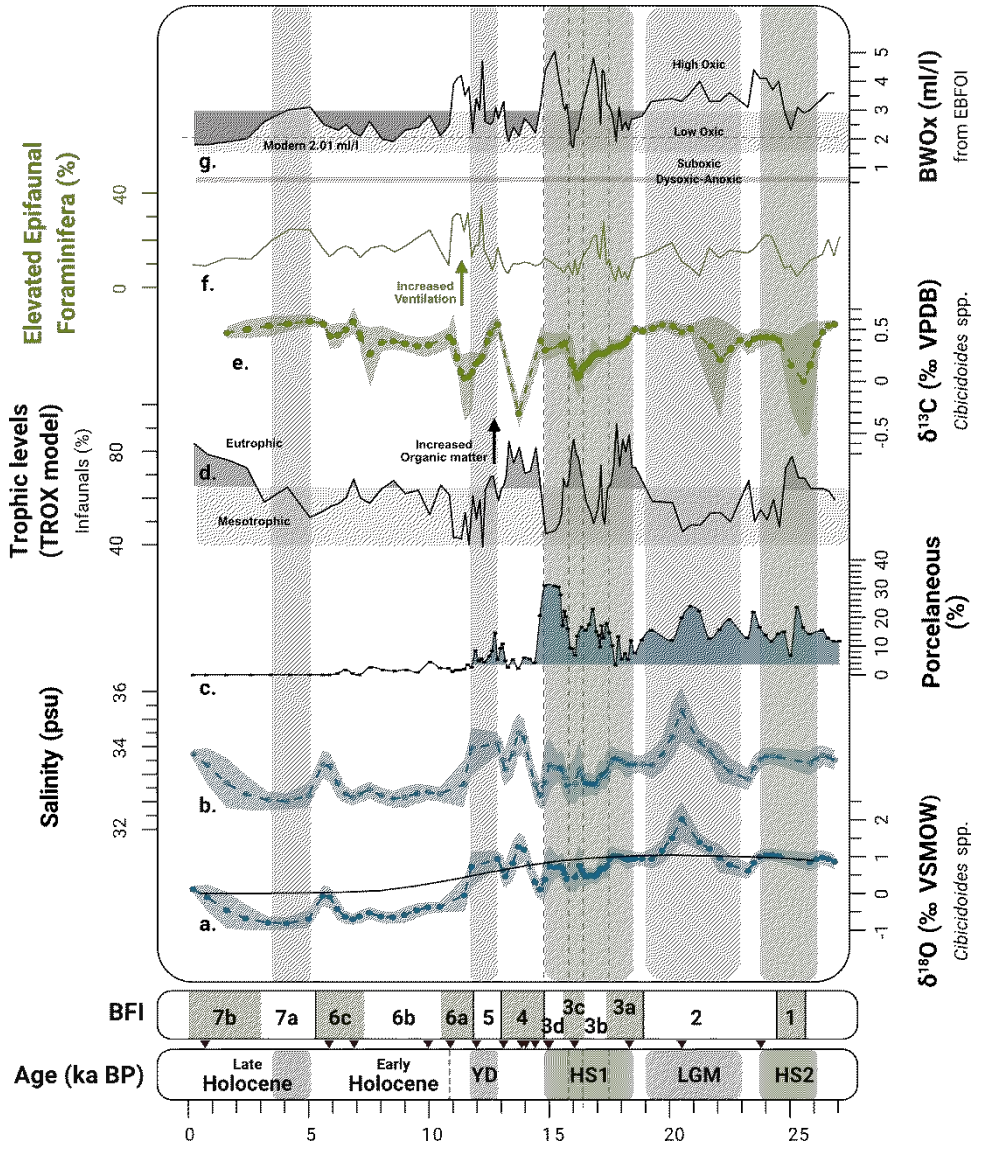

Figure 4. Downcore GeoB9512-5 benthic foraminifera geochemical and taxonomic/quantitative proxies. a. $\delta^{18}O_{sw}$ modified from Chapter 5; **b**. Salinity estimated in Chapter 5; **c.** Porcelaneous foraminifera relative abundances; **d.** TROX model described by the relative abundance of infaunal foraminifera; **e.** *Cibicidoides spp.* $\delta^{13}C$ modified from Chapter 5; **f.** Relative abundances of elevated epifaunal foraminifera; **g.** Bottom Water Oxygen reconstruction from Barragán-Montilla et al. (in review – Chapter 3). Shaded areas in stable isotope records show the 95% confidence interval. **Key Climate events:** Heinrich Stadial 2 (HS2); Last Glacial Maximum (LGM); Heinrich Stadial 1 (HS1); Bølling–Allerød (B-A); Younger Dryas (YD). Triangles in the age axis indicate points of radiocarbon ages.

3.2.2 Intermediate depth trophic conditions and bottom water ventilation

Mesotrophic to eutrophic environments were seen from data of GeoB9512-5 (Figure 4d). Strong mesotrophic conditions (infaunal foraminifera ~ 62.6 %) during HS2 (BFI-1), were followed by a drop during the LGM (BFI-2) when conditions remained mesotrophic (infaunal foraminifera ~ 57.4 %). Increasing organic matter fluxes at the end of the LGM and start of the HS1 (BFI-3a), as eutrophic conditions (infaunal foraminifera ~ 83.2 %) favored the peak in abundance of infaunal *U. mediterranea* (Figure 3). During the HS1 period, trophic conditions shifted to mesotrophic (infaunal foraminifera ~ 59.6 %) in BFI-3b, and to eutrophic during BFI-4b (infaunal foraminifera ~ 75.9 %). These rapid variations were also observed in the benthic foraminifera assemblages as described in section 3.1.1.

For the B-A warming period (BFI-4), Bottom water conditions became eutrophic (infaunal foraminifera ~ 73.5 %), and the subsequent YD (BFI-5) saw a decrease in organic matter fluxes leading to mesotrophic environments (infaunal foraminifera ~ 59.6 %). During the start of the Holocene (BFI-6a), trophic levels decreased (infaunal foraminifera ~ 44.5 %) and increasing trophic levels during the early Holocene (BFI-6b), led to stronger mesotrophic conditions (infaunal foraminifera ~ 61.5%). Mesotrophic conditions persisted in the rest of the early Holocene (BFI-6c, infaunal foraminifera ~ 58 %) and in the late Holocene (BFI-7a, infaunal foraminifera ~ 61.4 %). In the last part of the Holocene (BFI-7b) bottom water conditions became eutrophic (infaunal foraminifera ~ 77%).

The abundance of elevated epifaunal foraminifera (Figure 4f), regarded is high current velocities indicators (e.g. Schönfeld, 2002), shows GoeB9512-5 had two episodes of

increased ventilation in the HS1 and (BFI-3b) and in the YD to beginning of the Holocene (BFI5 – 6a). This agrees with the BWOx record of Barragán-Montilla et al. (in review), which shows periods of increased ventilation that drove higher oxygenation period in the low oxic margin of the eastern tropical North Atlantic Oxygen Minimum Zone, also during BFI-3d in the HS1.

The stable carbon isotope record from GeoB9512-5 (Figure 4e), shows trends that partially agree with the trophic level reconstruction from benthic foraminifera analysis (Figure 4d). A detailed description of this record can be found in Chapter 5 (section 3.1.1). In general, $\delta^{13}C$ was between -0.06 to 0.73 ‰, and remained relatively stable during HS2 -LGM. A decrease is observed during the first part of the HS1 (BFI3a-3b), and rapidly increases during the last part (BFI3d). Data in the B-A is limited, and a single point suggests a decrease. Between the end of the B-A and beginning of the YD, $\delta^{13}C$ increased followed by a decrease trend toward the start of the Holocene. From the base of the Holocene, $\delta^{13}C$ increases from 10.99 to 7.50 kyrs and stabilizes to average 0.5 ‰ in the last 7 kyrs.

From our records, we can infer those changes in the carbon isotope signal of *Cibicidoides* spp. in GeoB9512-5 (Figure 4e) were linked to variation in organic matter concentration at benthic ecosystems (Figure 4d). Decreasing $\delta^{13}C$ in the HS1 and during a part of the HS1 (BFI-3a and 3c) occurs in eutrophic bottom water environments, as increasing $\delta^{13}C$ during BFI-3d coincides with a decrease in infaunal foraminifera content (mesotrophic conditions). In addition, predominant mesotrophic conditions partially coincide with higher $\delta^{13}C$ in the Holocene. However, a ventilation signal can also be present in the $\delta^{13}C$ record, making the interpretation of this proxy less accurate.

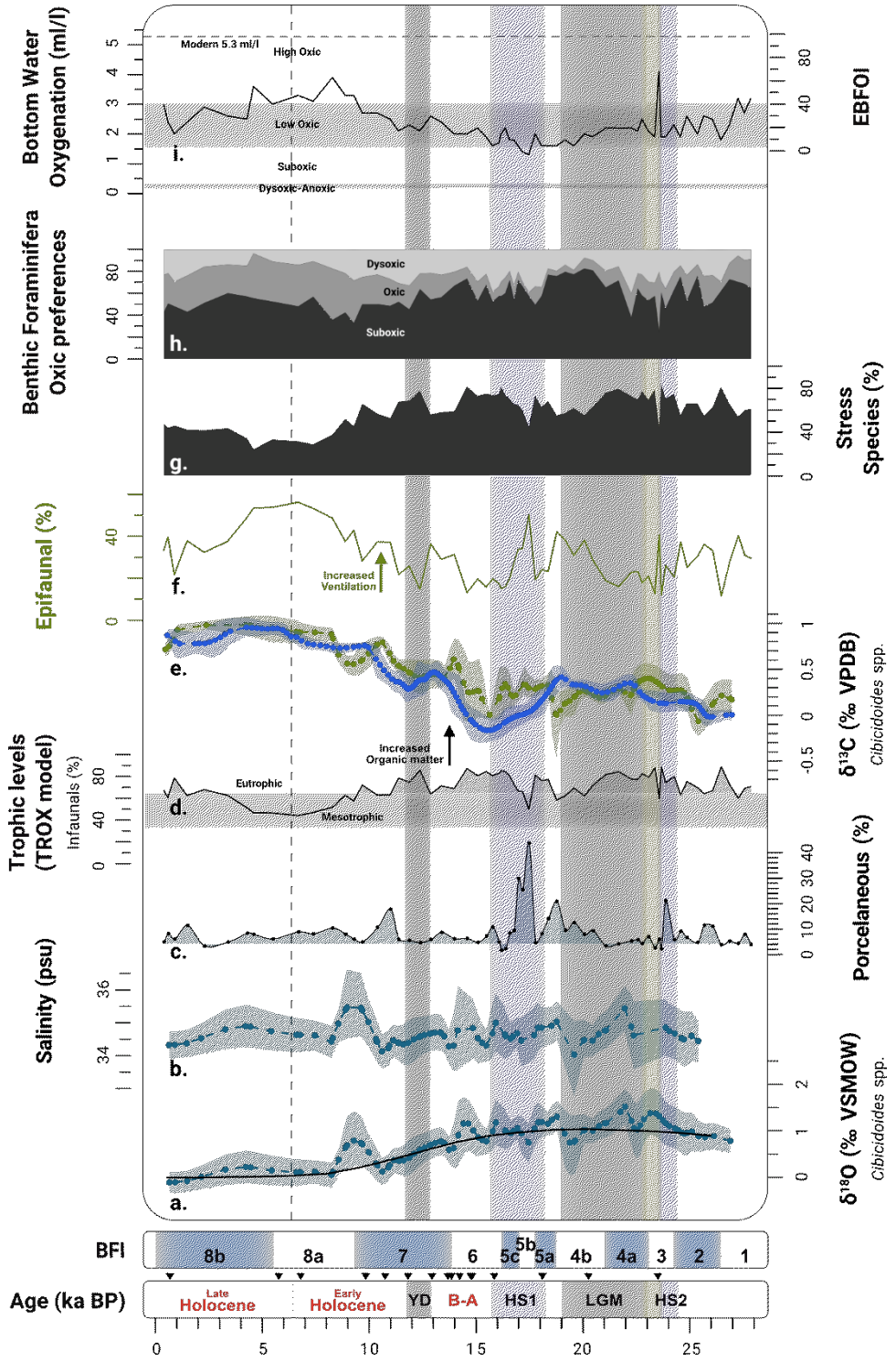

Figure 5. Downcore GeoB9506-1 benthic foraminifera geochemical and taxonomic/quantitative proxies. a. $\delta^{18}O_{sw}$ modified from Chapter 5; **b**. Salinity estimated in Chapter 5; **c.** Porcelaneous foraminifera relative abundances; **d.** TROX model described by the relative abundance of infaunal foraminifera; **e.** *Cibicidoides wuellerstorfi* $\delta^{13}C$ modified from Chapter 5, GeoB9508-5 *Cibicidoides wuellerstorfi* $\delta^{13}C$ modified from (Barragán-Montilla et al., 2023); **f.** Relative abundances of epifaunal foraminifera; **g.** Relative abundances of stress species; **h.** percentage proportion of benthic foraminifera oxygen preferences used in the Enhanced Benthic Foraminifera Oxygen Index (EBFOI), to estimate **i.**

Bottom Water Oxygen dissolved oxygen (ml/l). Shaded areas in stable isotope records show the 95% confidence interval. **Key Climate events:** Heinrich Stadial 2 (HS2); Last Glacial Maximum (LGM); Heinrich Stadial 1 (HS1); Bølling–Allerød (B-A); Younger Dryas (YD). Triangles in the age axis indicate points of radiocarbon ages.

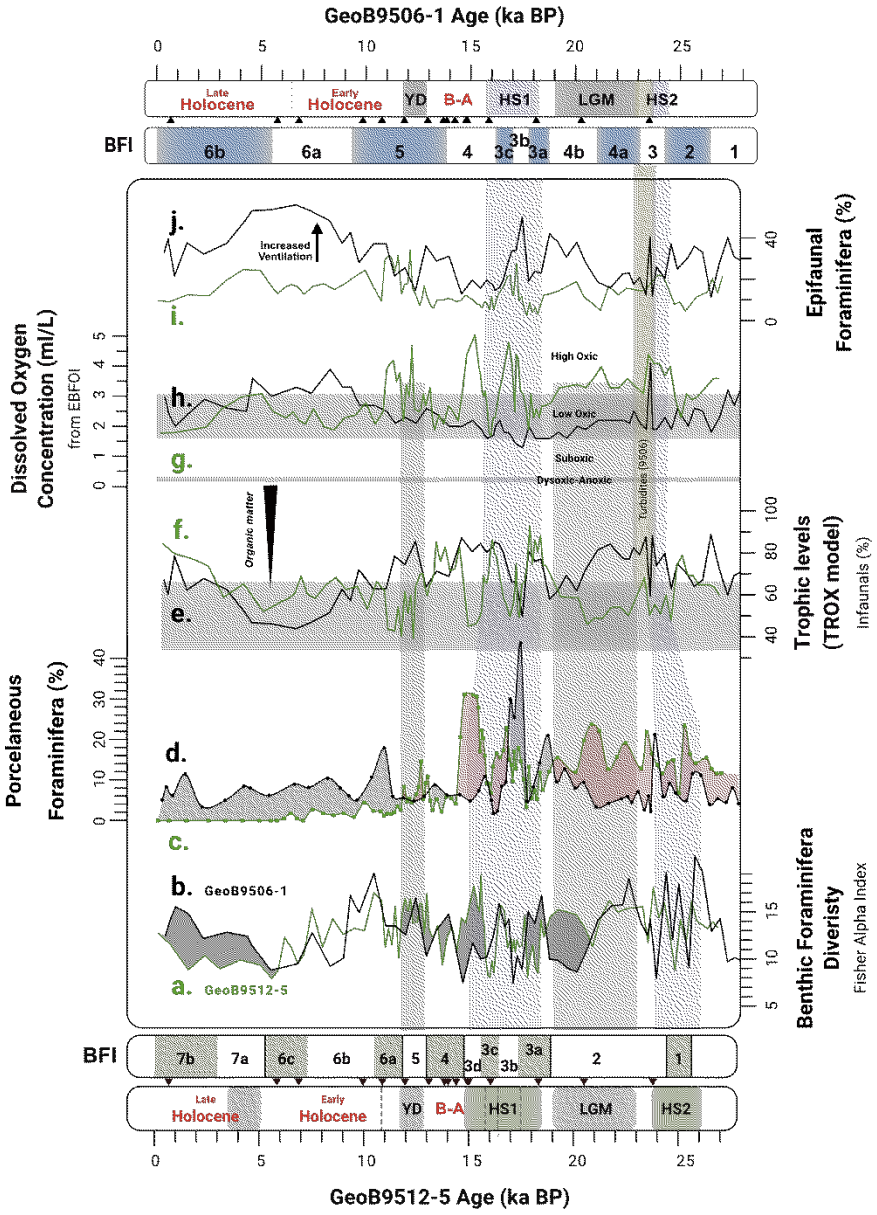

Figure 6. Comparison between downcore GeoB9506-1 (black curves) and GeoB9512-5 (green curves) benthic foraminifera diversity and taxonomic/quantitative proxies. a- b. Benthic foraminifera diversity measured with the Fisher Alpha Index; **c – d.** Porcelaneous foraminifera relative abundances; **e - f.** TROX model described by the relative abundance of infaunal foraminifera (GeoB9512-5 record modified from Appendix 3.1); **g - h.** Dissolved oxygen concentrations (ml/l) estimated using the Enhanced Benthic Foraminifera Oxygen Index (EBFOI); **i – j.** relative abundances of epifaunal foraminifera. GeoB9512-5 data modified from Appendix 3.1. **Key Climate events:** Heinrich

Stadial 2 (HS2); Last Glacial Maximum (LGM); Heinrich Stadial 1 (HS1); Bølling–Allerød (B-A); Younger Dryas (YD). Triangles in the age axis indicate points of radiocarbon ages.

3.2.3 Deep NE Atlantic trophic conditions, carbon isotopes and bottom water ventilation

Trophic levels at bottom waters in site GeoB9506-1 core were relatively more stable (Figure 5d). During pre-LGM times (BFI-1) benthic environments were eutrophic (infaunal foraminifera ~72.1 %) and remain this way throughout most of the studied section, except for BFI-8a when decrease of infaunal foraminifera (~50.2 %). Peaks of infaunal foraminifera (> 80 %) occurred in the LGM (BFI-4a), end of the HS1 (BFI-5c) and B-A (BFI-6).

Epifaunal foraminifera (Figure 5f) were on average < 30 %, and consistently higher toward the end of the LGM, part of the B-A and throughout the Holocene. The carbon isotope signal from *Cibicidoides wuellerstorfi* in core GeoB9506-1 (green curve, Figure 5e) described in detail in Chapter 5 (section 3.1.2) and showed values between -0.07 and 0.98 ‰ in the last 27 kyrs. Trends were similar to the observed in site GeoB9508-5 (blue curve in Figure 5e, modified from Barragán-Montilla et al., 2023), suggesting it shows ventilation changes related to Atlantic Meridional Overturing Circulation (AMOC). A decline in AMOC during the HS1 and YD has been suggested by sedimentary proxies (Böhm et al., 2015; Gherardi et al., 2005; McManus et al., 2004; Ng et al., 2018; Valley et al., 2017), compatible with a drop in $\delta^{13}C$ of site GeoB9508-5 (blue curve in Figure 5e), also observed in GeoB9506-1 (green curve, Figure 5e). In contrast, AMOC resumption during the B-A and Holocene is synchronous with an increase in GeoB9506-1 and GeoB9508-5 $\delta^{13}C$ suggesting enhanced ventilation during this time.

Different to the observed relationship between trophic fluctuations and BF $\delta^{13}C$ in GeoB9512-5, core GeoB9506-1 shows a clear bottom water ventilation effect in the carbon isotope signal (Figure 5e-f), consistent with changes in AMOC strength, also compatible with increasing organic matter concentrations at bottom waters (Figure 5d). Strong eutrophic bottom water environments during pre-LGM to YD times are linked to relatively lower $\delta^{13}C$ records, and as environments become progressively

mesotrophic with less nutrient content, $\delta^{13}C$ of *Cibicidoides wuellerstorfi* starts to increase. Furthermore, the presence of phytodetritus species *Epistominella exigua* (Gooday et al., 1993; Thomas et al., 1995), shows a peak in primary productivity during the LGM. However, high surface productivity can be inferred from most of this site, as *U. peregrina* is abundant through most of this interval (Figure 3), and is a species associated to high organic matter from surface productivity (Zarriess and Mackensen, 2010). Other species also abundant in GeoB9506-1 that are associated with this type of organic matter include *Melonis barleeanus* and *Cassidulina* spp. (Zarriess and Mackensen, 2010).

A detailed description of the changes in organic matter regimes inferred from GeoB9512-5 benthic foraminifera can be found in Appendix 3.1. In general, this site was influenced by organic matter from continental and marine sources. During HS2, BFI 3c and part of 3d of HS1 and in the B-A, increase of *Nonionella turgida*/*pulchella* (Figure 2) is associated to continental-sourced organic matter (Bartels-Jónsdóttir et al., 2006; Mojtahid et al. 2010a). During the LGM, BFIs 3a, 3b and 3c of HS1 and the YD (Figure 4), high surface productivity was inferred, potentially related to upwelling. Species like *C. laevigata* are regarded as an indicator of all-year upwelling (Mackensen et al. 1995), as it reproduces rapidly in environments with abundant fresh organic matter (Mojtahid et al. 2010b). Transient peaks of *U. mediterranea* at the end of the LGM and *B. subaenariensis* var. *Mexicana* in BFI 3c of HS1 (Figure 2), indicate respectively times of labile organic matter input (Fontanier et al., 2002), and turbiditic environments (Duros et al., 2017; Hess and Kuhnt,1996; Hess et al., 2001, 2005) with pulsed organic matter fluxes (Hess and Jorissen, 2009; Mojtahid et al. 2010b). These abrupt and short changes during HS1 are temporally consistent with a transient AMOC decline (Bard et al., 2000). Furthermore, *B. subaenariensis* var. *Mexicana* peaks occurs with *N. turgida* increase (Figure 2) in agreement with increased continental-sourced organic matter.

3.2.4 Bottom oxygen conditions: from eastern tropical North Atlantic Oxygen minimum zone dynamics in the upper Atlantic to stable oxygen conditions at deeper depths

A detailed description of GeoB9512-5 oxygen reconstruction can be found in Chapter 3 (Barragán-Montilla et al., in review). The bottom water oxygen variations interpreted

from the EBFOI in this site (Figures 4g and 6g), are linked to changes in the eastern tropical North Atlantic Oxygen Minimum Zone associated to variations in subsurface ventilation. High oxic periods in the HS1 and YD occur in times of AMOC slowdown (Böhm et al., 2015; Gherardi et al., 2005; McManus et al., 2004; Ng et al., 2018; Valley et al., 2017), and are related to increase ventilation in the upper Atlantic due to an accelerated subtropical cell driven by stronger winds as sea surface temperature gradients increased (Barragán-Montilla et al., in review).

The paleo-oxygenation record at site GeoB9506-1, shows a different trend (Figures 5i and 6h). Oxygen conditions were predominantly low-oxic from pre-LGM times (26.9 kyrs) into the start of the Holocene (9.7 kyrs), from where oxygen increased until modern times. The record starts with high-oxic conditions from 27.9 to 27.3 kyrs, rapidly dropping to low-oxic environments (average 2.3 ml/l BWOx) that persisted into the LGM (26.9 – 21.1 kyrs). BWOx values dropped to < 2 ml/l from 20.5 to 15.5 kyrs (LGM to HS1) recording minimum values (1.3 – 1.4 ml/l) around 17.5 – 17.2 kyrs. Low-oxic environments (on average 2.3 ml/l) continued until the beginning of the Holocene, interrupted by an increase in BWOx (> 3 ml/l) from 9.3 to 4.6 kyrs. The last 4.3 kyrs are seen as a return to low-oxic conditions with average BWOx of 2.5 ml/l. Overall, high stress species content (Figure 5g) agree with these observations. The average stress species abundance of 65.9 % from the deglacial low-oxic conditions observed, dropped to average 35.5 % during the Holocene high-oxic interval, while average 42 % is recorded for the last 4.3 kyrs.

The mechanisms driving oxygen availability at the deeper site seem to be more influenced by organic matter content than circulation changes, at least during the LGM and subsequent deglaciation (Figure 5d and 6e). Large changes in productivity have been recorded off west Africa through the deglaciation (Zarries and Mackensen, 2010; Bradtmiller et al., 2016). Abundance of organic matter in the benthic foraminifera could have increased oxygen consumption in eutrophic environments (e.g. Brandt et al., 2015; Jaccard et al., 2016), therefore explaining the low oxic and even suboxic (BFI-3b) conditions seen in our palo-oxygenation record.

In addition, increasing oxygen in the Holocene, is synchronous with AMOC resumption after the end of the YD, also observed in the increasing elevated epifaunal foraminifera (Figures 5f and 6j), suggesting that oxygen increase during this time was most likely linked to increase ocean circulation.

Conclusions

Benthic foraminifera distribution at the intermediate (GeoB9512-5) and deep (GeoB9506-1) eastern tropical North Atlantic, is visibly influenced by the changes in the paleoenvironmental conditions at benthic ecosystems related to major paleoceanographic shifts that shaped global climate in the last 27,000 years.

At intermediate depths, the eastern tropical North Atlantic Oxygen Minimum Zone dynamics related to subsurface circulation changes in times of AMOC strength shifts played an important role in the oxygen conditions that controlled benthic foraminifera assemblages in site GeoB9512-5. In addition, a clear imprint on the changes in type of organic matter was also observed by the peaks in abundance of species like *Nonionella turgida*/*pulchella* that prefer continental sourced organic matter, or *Cassidulina teretis*/*laevigata* who feeds preferentially on fresh high productivity organic matter, also linked to primary productivity enhanced by upwelling off NW Africa (e.g. Romero et al., 2008). Diversity remained relatively high in the last 27,000 years, and although abrupt drops are recorded in times lower oxygen concentrations (Figure 6a), diversity increased rapidly with increasing oxygen.

In the deep Atlantic (GeoB9506-1) paleoenvironmental conditions were more stable. A predominantly low oxic LGM and deglaciation period, was represented by diverse assemblages dominated by stress and infaunal species, better adapted to conditions of high organic matter and limited oxygen supply. Low oxic conditions seem to have been mainly driven by increased carbon respiration that enhanced oxygen consumption, however, increase in dissolved oxygen concentration during the Holocene is more compatible with the resumption of the Atlantic Meridional Overturning Circulation after the slowdown period of the YD. This led to an increase in bottom water ventilation in the deep Atlantic, bringing more oxygen to benthic ecosystems. However, lower diversity during this time shows that benthic foraminifera

species were not well adapted to these rapid changes (Figure 6b), suggesting that this type of assemblages are more susceptible to paleoceanographic driven changes.

Resilience of intermediate benthic ecosystems is also seen in diversification rates (DR), calculated with data pairs of consecutive samples from the topmost to lowermost samples. The diversification rates were obtained by extracting the oldest Fisher Alpha Index to the youngest (ΔFisher Alpha) and divided by the number of kyrs between the datapoints (ΔAge). The average diversification rates were calculated for each key climatic period to aid in the interpretation (Table 1). Although average age resolution for GeoB9512-5 (0.247 kyrs) was two times higher than the obtained for GeoB9506-1 (0.437 kyrs), diversification rates from the deeper core are seemingly lower since the Heinrich Stadial 1 into the Holocene, in coincidence with increasing BWOx conditions, while diversification rates are consistently higher in GeoB9512-5 during the HS1 and B-A, in times of transient paleoenvironmental changes, except during the YD when DR are the lowest.

Overall, our results show how even though paleoenvironmental conditions at intermediate benthic ecosystems were heavily influenced by major paleoceanographic changes, benthic foraminifera assemblages remain resilient and adapted rapidly to abrupt changes. On the contrary, the deep eastern tropical North Atlantic diversification rates were lower in times of paleoenvironmental shifts, even when bottom water conditions were more stable in time, showing deep benthic ecosystems are potentially more affected in climate change scenario.

Table 1. Summary of average benthic foraminifera diversification rates in the studied sites for each key climatic period in the eastern Atlantic in the last 28.000 years.

Average Diversification Rates

Climatic interval	GeoB9512-5	GeoB9506-1
Late Holocene	-0.10	-0.34
Early Holocene	1.28	-1.02
Younger Dryas	-4.19	-0.31
Bølling–Allerød	2.01	0.88

Heinrich Stadial 1a	3.17	1.60
Heinrich Stadial 1b	3.35	-3.14
Last Glacial Maximum	-0.22	0.43
Heinrich Stadial 3	0.26	4.29
pre-LGM	0.25	0.73

Acknowledgements

This research was funded by the “Deutsche Forschungsgemeinschaft” (DFG) through the Cluster of Excellence EXC 2077 “The Ocean Floor – Earth’s Uncharted Interface”. The sample material used here was provided by the GeoB Core Repository at the MARUM – Center for Marine Environmental Sciences, University of Bremen, Germany, and samples were washed at the UFT laboratories of the same University by Ishani Rathnayake. This research was supported by GLOMAR – Bremen International Graduate School for Marine Sciences, and by the GeoLatinas organization.

Data availability

Barragán-Montilla, Sofía (in review): Benthic Foraminifera counts off NW Africa during the last deglaciation. PANGAEA, https://doi.org/10.1594/PANGAEA.962951

References

Alegret, L., Arreguín-Rodríguez, G.J., Trasviña-Moreno, C.A., Thomas, E., 2021. Turnover and stability in the deep sea: Benthic foraminifera as tracers of Paleogene global change. Global and Planetary Change 196, 103372. https://doi.org/10.1016/j.gloplacha.2020.103372

Altenbach, A.V., Bernhard, J.M., Seckbach, J. (Eds.), 2012. Anoxia: Evidence for Eukaryote Survival and Paleontological Strategies, Cellular Origin, Life in Extreme Habitats and Astrobiology. Springer Netherlands, Dordrecht. https://doi.org/10.1007/978-94-007-1896-8

Bard, E., Rostek, F., Turon, J.-L., Gendreau, S., 2000. Hydrological Impact of Heinrich Events in the Subtropical Northeast Atlantic. Science 289, 1321–1324. https://doi.org/10.1126/science.289.5483.1321

Barragán-Montilla, S., Johnstone, H., Mulitza, S., Macaya, D., Pälike, H., 2024. Enhanced ventilation of Eastern North Atlantic Oxygen Minimum Zone with deglacial slowdown of Meridional Overturning. https://doi.org/10.21203/rs.3.rs-4083170/v1

Barragán-Montilla, S., Mulitza, S., Johnstone, H.J.H., Pälike, H., 2023. Stagnant North Atlantic Deep Water Heat Uptake With Reduced Atlantic Meridional Overturning Circulation During the Last Deglaciation. Paleoceanography and Paleoclimatology 38, e2022PA004575. https://doi.org/10.1029/2022PA004575

Bartels-Jónsdóttir, H.B., Knudsen, K.L., Abrantes, F., Lebreiro, S., Eiríksson, J., 2006. Climate variability during the last 2000 years in the Tagus Prodelta, western Iberian Margin: Benthic foraminifera and stable isotopes. Marine Micropaleontology 59, 83–103. https://doi.org/10.1016/j.marmicro.2006.01.002

Bernhard, J.M., Sen Gupta, B.K., 1999. Foraminifera of oxygen-depleted environments, in: Modern Foraminifera. Springer Netherlands, Dordrecht, pp. 201–216. https://doi.org/10.1007/0-306-48104-9_12

Böhm, E., Lippold, J., Gutjahr, M., Frank, M., Blaser, P., Antz, B., Fohlmeister, J., Frank, N., Andersen, M.B., Deininger, M., 2015. Strong and deep Atlantic meridional overturning circulation during the last glacial cycle. Nature 517, 73–76. https://doi.org/10.1038/nature14059

Bradtmiller, L. I., McGee, D., Awalt, M., Evers, J., Yerxa, H., Kinsley, C. W., and deMenocal, P. B.: Changes in biological productivity along the northwest African margin over the past 20,000 years: AFRICAN MARGIN PALEOPRODUCTIVITY, Paleoceanography, 31, 185–202, https://doi.org/10.1002/2015PA002862, 2016.

Brandt, P., Bange, H.W., Banyte, D., Dengler, M., Didwischus, S.-H., Fischer, T., Greatbatch, R.J., Hahn, J., Kanzow, T., Karstensen, J., Körtzinger, A., Krahmann, G., Schmidtko, S., Stramma, L., Tanhua, T., Visbeck, M., 2015. On the role of circulation and mixing in the ventilation of oxygen minimum zones with a focus on the eastern tropical North Atlantic. Biogeosciences 12, 489–512. https://doi.org/10.5194/bg-12-489-2015

Duros, P., Silva Jacinto, R., Dennielou, B., Schmidt, S., Martinez Lamas, R., Gautier, E., Roubi, A., Gayet, N., 2017. Benthic foraminiferal response to sedimentary disturbance in the Capbreton canyon (Bay of Biscay, NE Atlantic). Deep Sea Research Part I: Oceanographic Research Papers 120, 61–75. https://doi.org/10.1016/j.dsr.2016.11.012

Fontanier, C., Jorissen, F.J., Licari, L., Alexandre, A., Anschutz, P., Carbonel, P., 2002. Live benthic foraminiferal faunas from the Bay of Biscay: faunal density, composition, and microhabitats. Deep Sea Research Part I: Oceanographic Research Papers 49, 751–785. https://doi.org/10.1016/S0967-0637(01)00078-4

Gherardi, J., Labeyrie, L., Mcmanus, J., Francois, R., Skinner, L., Cortijo, E., 2005. Evidence from the Northeastern Atlantic basin for variability in the rate of the meridional overturning circulation through the last deglaciation. Earth and Planetary Science Letters 240, 710–723. https://doi.org/10.1016/j.epsl.2005.09.061

Gooday, A.J., 2001. Benthic Foraminifera, in: Encyclopedia of Ocean Sciences. Elsevier, pp. 274–286. https://doi.org/10.1006/rwos.2001.0217

Gooday, A.J., 1993. Deep-sea benthic foraminiferal species which exploit phytodetritus: Characteristic features and controls on distribution. Marine Micropaleontology 22, 187–205. https://doi.org/10.1016/0377-8398(93)90043-W

Gooday, A.J., Levin, L.A., Linke, P., Heeger, T., 1992. The Role of Benthic Foraminifera in Deep-Sea Food Webs and Carbon Cycling, in: Rowe, G.T., Pariente, V. (Eds.), Deep-Sea Food Chains and the Global Carbon Cycle. Springer Netherlands, Dordrecht, pp. 63–91. https://doi.org/10.1007/978-94-011-2452-2_5

Gooday, A.J., Schoenle, A., Dolan, J.R., Arndt, H., 2020. Protist diversity and function in the dark ocean – Challenging the paradigms of deep-sea ecology with special emphasis on foraminiferans and naked protists. European Journal of Protistology 75, 125721. https://doi.org/10.1016/j.ejop.2020.125721

Hess, S., 2005. BENTHIC FORAMINIFERAL RECOVERY AFTER RECENT TURBIDITE DEPOSITION IN CAP BRETON CANYON, BAY OF BISCAY. The Journal of Foraminiferal Research 35, 114–129. https://doi.org/10.2113/35.2.114

Hess, S., Jorissen, F.J., 2009. Distribution patterns of living benthic foraminifera from Cap Breton canyon, Bay of Biscay: Faunal response to sediment instability. Deep Sea Research Part I: Oceanographic Research Papers 56, 1555–1578. https://doi.org/10.1016/j.dsr.2009.04.003

Hess, S., Kuhnt, W., 1996. Deep-sea benthic foraminiferal recolonization of the 1991 Mt. Pinatubo ash layer in the South China Sea. Marine Micropaleontology 28, 171–197. https://doi.org/10.1016/0377-8398(95)00080-1

Holbourn, A.E.L., Henderson, A.S., 2013. Atlas of benthic foraminifera. Natural History Museum, Chichester, West Sussex ; Hoboken, NJ.

Jaccard, S.L., Galbraith, E.D., Martínez-García, A., Anderson, R.F., 2016. Covariation of deep Southern Ocean oxygenation and atmospheric CO2 through the last ice age. Nature 530, 207–210. https://doi.org/10.1038/nature16514

Jones, R.W., Brady, H.B., 1994. The Challenger foraminifera. Oxford University Press, Oxford ; New York.

Jorissen, F.J., De Stigter, H.C., Widmark, J.G.V., 1995. A conceptual model explaining benthic foraminiferal microhabitats. Marine Micropaleontology 26, 3–15. https://doi.org/10.1016/0377-8398(95)00047-X

Kaiho, K., 1994. Benthic foraminiferal dissolved-oxygen index and dissolved-oxygen levels in the modern ocean. Geol 22, 719. https://doi.org/10.1130/0091-7613(1994)022<0719:BFDOIA>2.3.CO;2

Kranner, M., Harzhauser, M., Beer, C., Auer, G., Piller, W.E., 2022. Calculating dissolved marine oxygen values based on an enhanced Benthic Foraminifera Oxygen Index. Sci Rep 12, 1376. https://doi.org/10.1038/s41598-022-05295-8

Lauvset, S.K., Lange, N., Tanhua, T., Bittig, H.C., Olsen, A., Kozyr, A., Alin, S., Álvarez, M., Azetsu-Scott, K., Barbero, L., Becker, S., Brown, P.J., Carter, B.R., Da Cunha, L.C., Feely, R.A., Hoppema, M., Humphreys, M.P., Ishii, M., Jeansson, E., Jiang, L.-Q., Jones, S.D., Lo Monaco, C., Murata, A., Müller, J.D., Pérez, F.F., Pfeil, B., Schirnick, C., Steinfeldt, R., Suzuki, T., Tilbrook, B., Ulfsbo, A., Velo, A., Woosley,

R.J., Key, R.M., 2022. GLODAPv2.2022: the latest version of the global interior ocean biogeochemical data product. Earth Syst. Sci. Data 14, 5543–5572. https://doi.org/10.5194/essd-14-5543-2022

Loeblich Jr, A.R., Tappan, H., 2015. Foraminiferal Genera and Their Classification. Springer, New York, NY.

Mackensen, A., Schmiedl, G., Harloff, J., Giese, M., 1995. Deep-Sea Foraminifera in the South Atlantic Ocean: Ecology and Assemblage Generation. Micropaleontology 41, 342. https://doi.org/10.2307/1485808

McManus, J.F., Francois, R., Gherardi, J.-M., Keigwin, L.D., Brown-Leger, S., 2004. Collapse and rapid resumption of Atlantic meridional circulation linked to deglacial climate changes. Nature 428, 834–837. https://doi.org/10.1038/nature02494

Moffitt, S.E., Hill, T.M., Roopnarine, P.D., Kennett, J.P., 2015a. Response of seafloor ecosystems to abrupt global climate change. Proc. Natl. Acad. Sci. U.S.A. 112, 4684–4689. https://doi.org/10.1073/pnas.1417130112

Moffitt, S.E., Moffitt, R.A., Sauthoff, W., Davis, C.V., Hewett, K., Hill, T.M., 2015b. Paleoceanographic Insights on Recent Oxygen Minimum Zone Expansion: Lessons for Modern Oceanography. PLoS ONE 10, e0115246. https://doi.org/10.1371/journal.pone.0115246

Mojtahid, Meryem, Griveaud, C., Fontanier, C., Anschutz, P., Jorissen, F.J., 2010. Live benthic foraminiferal faunas along a bathymetrical transect (140–4800m) in the Bay of Biscay (NE Atlantic). Revue de Micropaléontologie 53, 139–162. https://doi.org/10.1016/j.revmic.2010.01.002

Mojtahid, M., Hennekam, R., De Nooijer, L., Reichart, G.-J., Jorissen, F., Boer, W., Le Houedec, S., De Lange, G.J., 2019. Evaluation and application of foraminiferal element/calcium ratios: Assessing riverine fluxes and environmental conditions during sapropel S1 in the Southeastern Mediterranean. Marine Micropaleontology 153, 101783. https://doi.org/10.1016/j.marmicro.2019.101783

Mojtahid, M., Jorissen, F., Lansard, B., Fontanier, C., 2010. MICROHABITAT SELECTION OF BENTHIC FORAMINIFERA IN SEDIMENTS OFF THE RHONE RIVER MOUTH (NW MEDITERRANEAN). The Journal of Foraminiferal Research 40, 231–246. https://doi.org/10.2113/gsjfr.40.3.231

Mulitza, S., Bouimetarhan, I., Bruening, M., Freesemann, A., Gussone, N., Filipsson, H.L., Heil, G., Hessler, S., Jaeschke, A., Johnstone, H.J.H., Klann, M., Klein, F., Kuester, K., Maerz, C., McGregor, H., Minning, M., Mueller, H., Ochsenhirt, W.-T., Paul, A., Pokorna, M., Schewe, F., Schulz, M., Steinloechner, J., Stuut, J.-B., Tjallingii, R., von Dobeneck, T., Wiesmaier, S., Zabel, M., Zonneveld, C., 2005. Report and preliminary results of METEOR Cruise M65/1, Dakar - Dakar, 11.06. - 1.07.2005.

Murray, J.W., 2006. Ecology and Applications of Benthic Foraminifera, 1st ed. Cambridge University Press. https://doi.org/10.1017/CBO9780511535529

Murray, J.W., 1991. Ecology and palaeoecology of benthic foraminifera. Longman scientific and technical copublished in the United States with John Wiley and sons, Essex New York.

Ng, H.C., Robinson, L.F., McManus, J.F., Mohamed, K.J., Jacobel, A.W., Ivanovic, R.F., Gregoire, L.J., Chen, T., 2018. Coherent deglacial changes in western Atlantic Ocean circulation. Nat Commun 9, 2947. https://doi.org/10.1038/s41467-018-05312-3

Poloczanska, E.S., Brown, C.J., Sydeman, W.J., Kiessling, W., Schoeman, D.S., Moore, P.J., Brander, K., Bruno, J.F., Buckley, L.B., Burrows, M.T., Duarte, C.M., Halpern, B.S., Holding, J., Kappel, C.V., O'Connor, M.I., Pandolfi, J.M., Parmesan, C., Schwing, F., Thompson, S.A., Richardson, A.J., 2013. Global imprint of climate change on marine life. Nature Clim Change 3, 919–925. https://doi.org/10.1038/nclimate1958

Reichle, D.E., 2023. Dynamic properties of the global carbon cycle, in: The Global Carbon Cycle and Climate Change. Elsevier, pp. 355–387. https://doi.org/10.1016/B978-0-443-18775-9.00006-1

Romero, O.E., Kim, J., Donner, B., 2008. Submillennial-to-millennial variability of diatom production off Mauritania, NW Africa, during the last glacial cycle. Paleoceanography 23, 2008PA001601. https://doi.org/10.1029/2008PA001601

Schlitzer, R., 2023. Ocean Data View, , odv.awi.de.

Schmiedl, G., Milker, Y., Mackensen, A., 2023. Climate forcing of regional deep-sea biodiversity documented by benthic foraminifera. Earth-Science Reviews 244, 104540. https://doi.org/10.1016/j.earscirev.2023.104540

Sen Gupta, B.K. (Ed.), 2002. Modern foraminifera, first published in paperback. ed. Kluwer, Dordrecht.

Southward, A.J., Young, C.M., Fuiman, L.A., 2006. Advances In Marine Biology, Advances in Marine Biology. Academic Press, Burlington.

Sweetman, A.K., Sommer, S., Pfannkuche, O., Witte, U., 2009. RETARDED RESPONSE BY MACROFAUNA-SIZE FORAMINIFERA TO PHYTODETRITUS IN A DEEP NORWEGIAN FJORD. The Journal of Foraminiferal Research 39, 15–22. https://doi.org/10.2113/gsjfr.39.1.15

Thomas, E., Booth, L., Maslin, M., Shackleton, N.J., 1995. Northeastern Atlantic benthic foraminifera during the last 45,000 years: Changes in productivity seen from the bottom up. Paleoceanography 10, 545–562. https://doi.org/10.1029/94PA03056

Valley, S., Lynch-Stieglitz, J., Marchitto, T.M., 2017. Timing of Deglacial AMOC Variability From a High-Resolution Seawater Cadmium Reconstruction. Paleoceanography 32, 1195–1203. https://doi.org/10.1002/2017PA003099

van Morkhoven, F.P.C.M., 1988. CENOZOIC COSMOPOLITAN DEEP-WATER BENTHIC FORAMINIFERA. The Journal of Foraminiferal Research 18, 90–91. https://doi.org/10.2113/gsjfr.18.1.90

Vaquer-Sunyer, R., Duarte, C.M., 2008. Thresholds of hypoxia for marine biodiversity. Proc. Natl. Acad. Sci. U.S.A. 105, 15452–15457. https://doi.org/10.1073/pnas.0803833105

Volk, T., Hoffert, M.I., 2013. Ocean Carbon Pumps: Analysis of Relative Strengths and Efficiencies in Ocean-Driven Atmospheric CO 2 Changes, in: Sundquist, E.T., Broecker, W.S. (Eds.), Geophysical Monograph Series. American Geophysical Union, Washington, D. C., pp. 99–110. https://doi.org/10.1029/GM032p0099

Waelbroeck, C., Duplessy, J.-C., Michel, E., Labeyrie, L., Paillard, D., Duprat, J., 2001. The timing of the last deglaciation in North Atlantic climate records. Nature 412, 724–727. https://doi.org/10.1038/35089060

WoRMS Editorial Board, 2024. World Register of Marine Species. Available from https://www.marinespecies.org at VLIZ. Accessed yyyy-mm-dd. https://doi.org/10.14284/170

Zarriess, M., Mackensen, A., 2010. The tropical rainbelt and productivity changes off northwest Africa: A 31,000-year high-resolution record. Marine Micropaleontology 76, 76–91. https://doi.org/10.1016/j.marmicro.2010.06.001

Supplementary Information 6.1 – Benthic Foraminifera Digital Microscope Images from site GeoB9506-1

Plate 1

Scale bar 100 µm

1. *Hormosina bacillaris* (Brady, 1881) – 10 cm
2. *Rhizammina* sp. Brady, 1879 – 10 cm
3. *Rhizammina* sp. Brady, 1879 – 12.5 cm
4. *Karreriella bradyi* (Cushman, 1911) – 12.5 cm
5. *Lagenammina* sp. – 5 cm
6. *Lagenammina* sp. – 7.5 cm
7. *Haplophragmoides* sp. – 2.5 cm
8. *Hormosina bacillaris* (Brady, 1881) – 12.5 cm
9. *Rhizammina algaeformis* Brady, 1879 – 5 cm
10. *Sigmoilopsis schlumbergeri* (Silvestri, 1904) – 28 cm
11. *Chilostomella oolina* Schwager, 1878 – 53 cm
12. *Globobulimina affinis* (d'Orbigny, 1839) – 122.5 cm
13. *Valvulineria bradyana* (Fornasini, 1900) – 97.5 cm
14. *Melonis barleeanus* (Williamson, 1858) – 118 cm
15. *Hoeglundina elegans (*d'Orbigny, 1826) – 17.5 cm
16. *Lobatula lobatula* (Walker & Jacob, 1798) – 38 cm
17. *Cibicidoides wuellerstorfi* (Schwager, 1866) – 58 cm
18. *Melonis pompilioides* (Fichtel & Moll, 1798) – 33 cm
19. *Chilostomella oolina* Schwager, 1878 – 58 cm
20. *Bulimina buchiana* d'Orbigny, 1846 – 188 cm
21. *Heterolepa bradyi* (Trauth, 1918) – 43 cm
22. *Melonis barleeanus* (Williamson, 1858) – 87.5 cm
23. *Hoeglundina elegans (*d'Orbigny, 1826) – 73 cm
24. *Valvulineria bradyana* (Fornasini, 1900) – 87.5 cm
25. *Epistominella exigua* (Brady, 1884) – 158 cm
26. *Globobulimina affinis* (d'Orbigny, 1839) – 122.5 cm
27. *Fursenkoina bradyi* (Cushman, 1922) – 163 cm
28. *Globobulimina affinis* (d'Orbigny, 1839) – 122.5 cm
29. *Globobulimina affinis* (d'Orbigny, 1839) – 122.5 cm
30. *Uvigerina peregrina* Cushman, 1923 – 112.5 cm
31. *Uvigerina peregrina* Cushman, 1923 – 112.5 cm
32. *Uvigerina* spp. – 260 cm
33. *Bulimina buchiana* d'Orbigny, 1846 – 188 cm
34. *Uvigerina hispida* Schwager, 1866 – 215 cm
35. *Trifarina angulosa* (large) – 198 cm
36. *Trifarina angulosa* (Williamson, 1858) – 198 cm

Plate 1

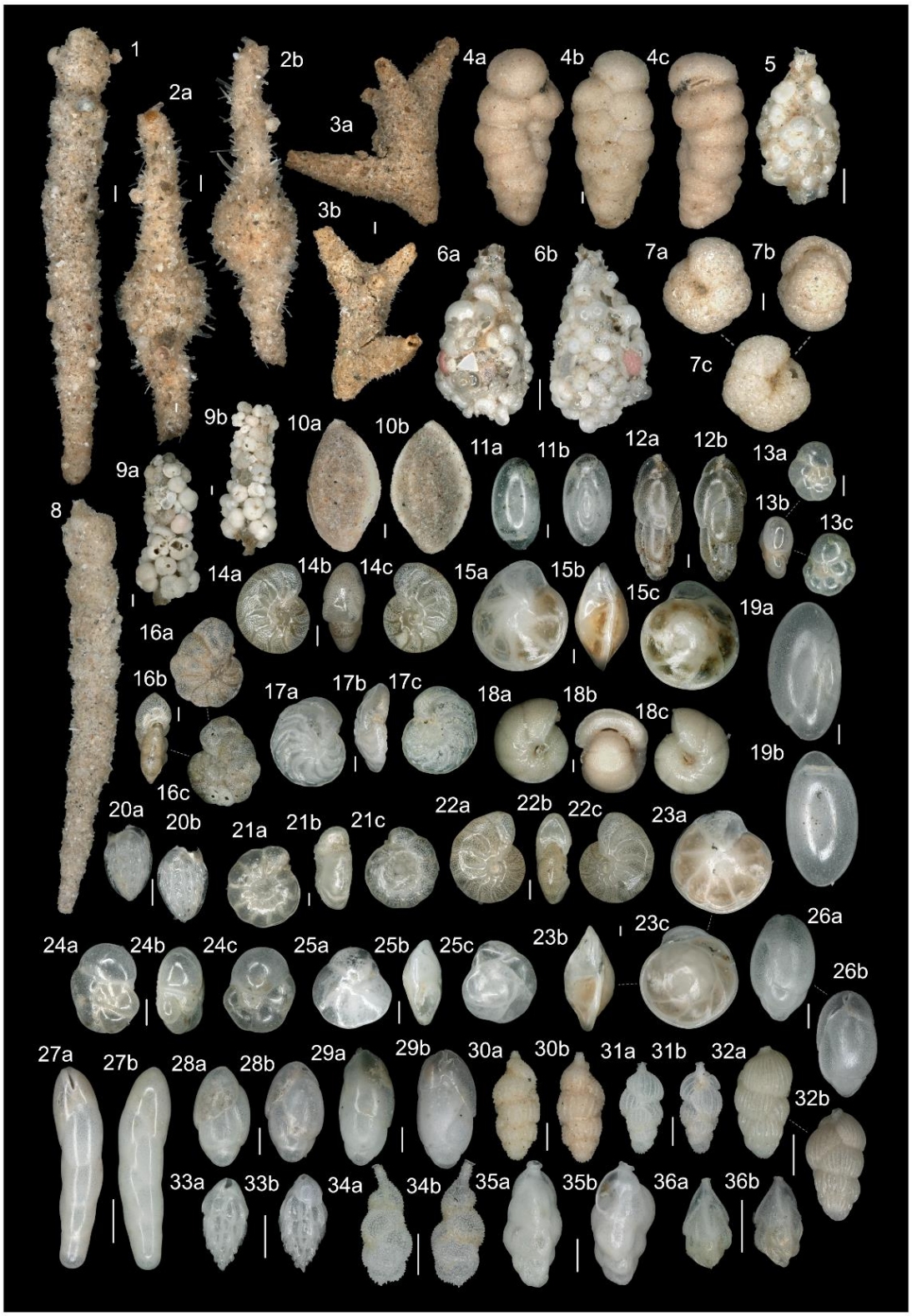
1
2a
2b
3a
3b
4a
4b
4c
5
6a
6b
7a
7b
7c
8
9a
9b
10a
10b
11a
11b
12a
12b
13a
13b
13c
14a
14b
14c
15a
15b
15c
16a
16b
16c
17a
17b
17c
18a
18b
18c
19a
19b
20a
20b
21a
21b
21c
22a
22b
22c
23a
23b
23c
24a
24b
24c
25a
25b
25c
26a
26b
27a
27b
28a
28b
29a
29b
30a
30b
31a
31b
32a
32b
33a
33b
34a
34b
35a
35b
36a
36b

Plate 2

Scale bar 100 µm

1. *Melonis pompilioides* (Fichtel & Moll, 1798) – 48 cm
2. *Melonis barleeanus* (Williamson, 1858) – 163 cm
3. *Pullenia quinqueloba* (Reuss, 1851) – 243 cm
4. *Pullenia bulloides* (d'Orbigny, 1846) – 257.5 cm
5. *Cassidulina laevigata/teretis* – 183 cm
6. *Cassidulina laevigata/teretis* – 188 cm
7. *Lobatula lobatula* (Walker & Jacob, 1798) – 213 cm
8. *Ammonia falsobeccarii* (Rouvillois, 1974) – 215 cm
9. *Cibicidoides wuellerstorfi* (Schwager, 1866) – 28 cm
10. *Elphidium crispum* (Linnaeus, 1758) – 35 cm
11. *Triloculina trigonula* (Lamarck, 1804) – 220 cm
12. *Pyrgo depressa* (d'Orbigny, 1826) – 220 cm
13. *Bulimina striata* d'Orbigny in Guérin-Méneville, 1832 – 215 cm
14. *Bulimina buchiana* d'Orbigny, 1846 – 143 cm
15. *Globobulimina affinis* (d'Orbigny, 1839) – 118 cm
16. *Globobulimina turgida* (Bailey, 1851) – 118 cm
17. *Globobulimina affinis* (d'Orbigny, 1839) – 122.5 cm
18. *Bolivina subaenariensis* var. *mexicana* Cushman, 1922 - 208 cm
19. *Bolivina* cff. *spathulata* (Williamson, 1858) – 143 cm
20. *Uvigerina peregrina* Cushman, 1923 – 73 cm
21. *Uvigerina* spp. – 163 cm
22. *Uvigerina hispida* Schwager, 1866 – 215 cm
23. *Hyalinea balthica* (Schröter, 1783) – 112.5 cm
24. *Planulina ariminensis* d'Orbigny, 1826 - 112.5 cm
25. *Cassidulina laevigata* d'Orbigny, 1826 – 112.5 cm
26. *Epistominella exigua* (Brady, 1884) – 163 cm
27. *Melonis pompilioides* (Fichtel & Moll, 1798) – 168 cm
28. *Melonis barleeanus* (Williamson, 1858) – 118 cm
29. *Spiroloculina depressa* d'Orbigny, 1826 – 112.5
30. *Spiroloculina rotunda* d'Orbigny, 1826 – 188 cm
31. *Pyrgo murrhina* (Schwager, 1866) – 163 cm
32. *Bulimina striata* d'Orbigny in Guérin-Méneville, 1832 - 215
33. *Bulimina marginata* d'Orbigny, 1826 – 198 cm
34. *Bulimina marginata* d'Orbigny, 1826 – 193 cm
35. *Bulimina elegans* d'Orbigny in Parker, Jones & Brady, 1865
36. *Bulimina buchiana* d'Orbigny, 1846 – 188 cm
37. *Bulimina buchiana* d'Orbigny, 1846 – 143 cm
38. *Bolivina subaenariensis* var. *mexicana* Cushman, 1922 - 203 cm
39. *Uvigerina peregrina* Cushman, 1923 – 112.5 cm
40. *Uvigerina peregrina* Cushman, 1923 – 87.5 cm

Plate 2

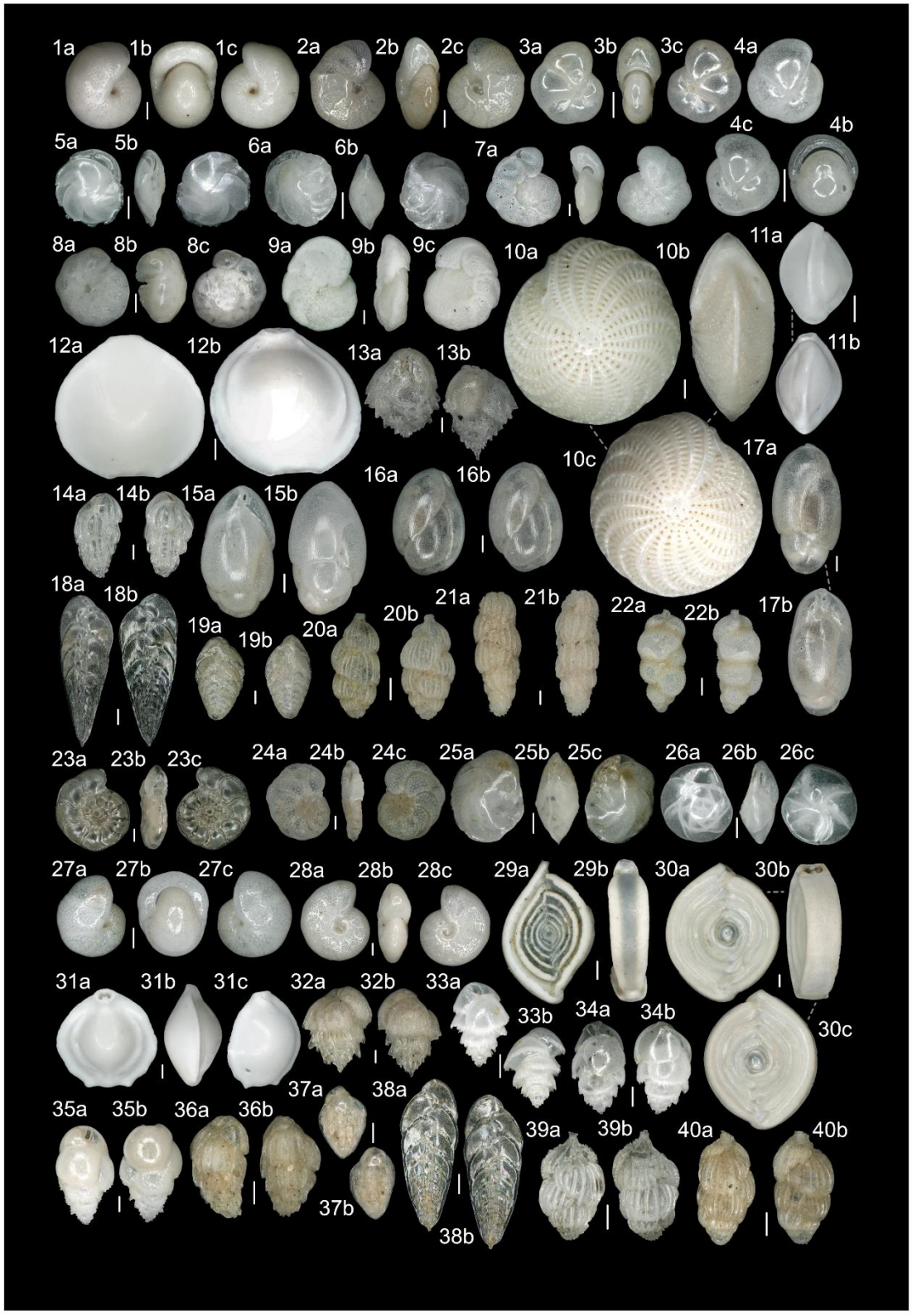
1a 1b 1c 2a 2b 2c 3a 3b 3c 4a
4c 4b
5a 5b 6a 6b 7a
8a 8b 8c 9a 9b 9c 10a 10b 11a
11b
12a 12b 13a 13b
10c 17a
14a 14b 15a 15b 16a 16b
18a 18b 19a 19b 20a 20b 21a 21b 22a 22b 17b
23a 23b 23c 24a 24b 24c 25a 25b 25c 26a 26b 26c
27a 27b 27c 28a 28b 28c 29a 29b 30a 30b
31a 31b 31c 32a 32b 33a 33b 34a 34b 30c
37a 38a
35a 35b 36a 36b 39a 39b 40a 40b
37b 38b

Plate 3

Scale bar 100 µm

1. *Uvigerina mediterranea* Hofker, 1932 – 215 cm
2. *Eubuliminella exilis* (Brady, 1884) = *Bulimina exilis* – 228 cm
3. *Trifarina angulosa* (Williamson, 1858) – 198 cm
4. *Globobulimina affinis* (d'Orbigny, 1839) – 220 cm
5. *Nonionella turgida*/*pulchella* – 158 cm
6. *Melonis barleeanus* (Williamson, 1858) – 163 cm
7. *Cassidulina teretis* Tappan, 1951 – 153 cm
8. *Sphaeroidina bulloides* d'Orbigny in Deshayes, 1832 – 260 cm
9. *Ammonia falsobeccarii* (Rouvillois, 1974) – 215 cm
10. *Hyalinea balthica* (Schröter, 1783) – 35 cm
11. *Elphidium crispum* (Linnaeus, 1758) – 203 cm
12. *Cibicidoides pachyderma* (Rzehak, 1886) – 215 cm
13. *Lobatula lobatula* (Walker & Jacob, 1798) – 208 cm
14. *Lobatula lobatula* (Walker & Jacob, 1798) – 213 cm
15. *Quinqueloculina laevigata* d'Orbigny, 1839 – 132.5 cm
16. *Sigmoilopsis schlumbergeri* (Silvestri, 1904) – 73 cm
17. *Melonis pompilioides* (Fichtel & Moll, 1798) – 48 cm
18. *Oridorsalis umbonatus* (Reuss, 1851) – 107.5 cm
19. *Cibicidoides pachyderma* (Rzehak, 1886) – 238 cm
20. *Lobatula lobatula* (Walker & Jacob, 1798) – 143 cm
21. *Uvigerina* cff. *tenuistriata* Reuss, 1870 – 260 cm
22. *Uvigerina peregrina* Cushman, 1923 – 143 cm
23. *Uvigerina peregrina* Cushman, 1923 – 173 cm
24. *Uvigerina peregrina* Cushman, 1923 – 203 cm
25. *Uvigerina peregrina* Cushman, 1923 – 80 cm

Foraminifera filled with glauconite (198 cm, 213 cm and 238 cm)

Scale bar 100 µm

1. *Cassidulina* sp.
2. *Trifarina angulosa* (Williamson, 1858)
3. *Nonionella turgida*/*pulchella*
4. *Bulimina buchiana* d'Orbigny, 1846
5. *Uvigerina peregrina* Cushman, 1923
6. *Elphidium* sp.
7. *Nonionella turgida*/*pulchella*
8. *Nonionella turgida*/*pulchella*
9. *Planulina arimenensis*
10. *Planulina* sp.
11. *Bulimina* sp.
12. *Uvigerina* sp.
13. Bulimina sp.
14. Rotaliids indeterminate
15. *Nonion* sp.

16-22. *Cassidulina* spp.

23. *Elphidium* sp.

24. *Textularia* sp.

25-28. Rotaliid indeterminate

29-42. Globigerinids

Plate 3

Glauconitic Foraminifera

Additional Supplementary Information

For the Additional Supplementary Information scan the QR code to click the link below

SCAN ME

Link: Additional Supplementary Information (Google Drive)

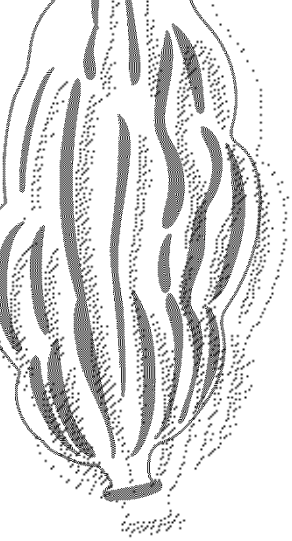

Atlantic Meridional Overturning Circulation slowdown effects on deglacial tropical eastern Atlantic paleoceanography recorded by benthic foraminifera

by Sofía Barragán-Montilla

Bremen, April 2024

marum

University of Bremen